SOME ASPECTS OF THE PROSPECTIVE EXPERIMENTAL USE OF THE STANFORD TWO-MILE ACCELERATOR

W.Chinowsky, J.W.DeWire, D.B.Lichtenberg, G.Masek,
J.J.Murray, M.Perl, M.Schwartz, J.Tinlot, G.Trilling

SLAC REPORT NO. 5
Summer 1962

AEC Contract AT(04-3)-400

STANFORD LINEAR ACCELERATOR CENTER
Stanford University • Stanford, California

DISCLAIMER

SLAC-5
UC-28, Particle Accelerators
and High-Voltage Machines
UC-34, Physics
TID-4500

SOME ASPECTS OF THE PROSPECTIVE EXPERIMENTAL USE OF THE STANFORD TWO-MILE ACCELERATOR

Summer 1962

by

W. Chinowsky, J. W. DeWire, D. B. Lichtenberg, G. Masek,
J. J. Murray, M. Perl, M. Schwartz, J. Tinlot, G. Trilling

Technical Report
Prepared Under
Contract AT(04-3)-400
for the USAEC
San Francisco Operations Office

Printed in USA. Price $3.00. Available from the Office of Technical Services, Department of Commerce, Washington 25, D.C.

PREFACE

The papers in this Report were written by members of a group assembled at the Stanford Linear Accelerator Center (SLAC) at Stanford University during the summer of 1962. Not all of the members of the group were present at the same time, and in some cases work done late in the summer may affect the conclusions of work done earlier.

These papers were written informally and were not intended for journal publication, since much of the work reported is preliminary and speculative. We suggest that anyone who wishes to cite one of these papers in the literature should obtain its author's permission to do so.

Members of the SLAC 1962 Summer Study Group:

W. Chinowsky	Lawrence Radiation Laboratory University of California Berkeley, California
J. W. DeWire	Cornell University Ithaca, New York
D. B. Lichtenberg*	Michigan State University East Lansing, Michigan
G. Masek	University of Washington Seattle, Washington
J. J. Murray	Lawrence Radiation Laboratory University of California Berkeley, California
M. Perl	University of Michigan Ann Arbor, Michigan
M. Schwartz	Columbia University New York, New York
J. Tinlot	University of Rochester Rochester, New York
G. Trilling	Lawrence Radiation Laboratory University of California Berkeley, California

*At SLAC until August 1963.

Robert F. Mozley
January 1963

TABLE OF CONTENTS

PHOTON BEAM FROM PROJECT M ACCELERATOR

by

J. W. DeWire

August, 1962

1. Introduction

The purpose of this report is to discuss some of the problems connected with making and using a photon beam with the M machine, and in particular the use of a monocrystal radiator to obtain a spectrum having sharp discontinuities. The discussion is greatly influenced by conversations with various members of Project M, especially with R. Mozley.

The expected properties of the M accelerator are such that it seems feasible to produce a useful photon beam while using the electron beam for some other purpose, such as the production of beams of secondary particles or neutrinos. An average electron beam current of 30 μa will produce a photon beam of useful intensity in a very thin radiator ($\approx 10^{-4}$ radiation length). If such a radiator is introduced properly into a beam transport system it should have a negligible effect on the electron beam. It should then be possible to do simultaneous experiments on photon-produced reactions and secondary particles. However, it is unlikely that the energy requirements in the two types of experiments will be the same. For studies with secondary-particle beams, the maximum electron energy will certainly be desirable, and little need for variation in this energy should occur. On the other hand, it is possible that photo-reactions will be studied at energies below the maximum, and it will be necessary to vary and carefully control the energy to properly identify the reactions.[1] Both of these requirements can be satisfied by using a monocrystal as the bremsstrahlung radiator in the manner recently demonstrated by Diambrini et al.[2] The discontinuities in the coherent photon spectrum can be moved along the energy scale simply by rotating the crystal with respect to the direction of the electron beam. The drastic departure from the usual bremsstrahlung spectrum

---

[1] A. Silverman, Simultaneous Experiments with the M Accelerator, Report M-284 (SLAC), August, 1961.

[2] Barbiellini, Bologna, Diambrini, and Murtas, Phys. Rev. Lett. 8, 454 (1962).

that is expected for high electron energies may provide a reduced background for many experiments, and the sharp discontinuities in the photon intensity will provide a means for relating measured phenomena to a definite photon energy. However, it is necessary first to look at some of the details of the spectrum from a monocrystal.

2. Properties of the Bremsstrahlung from a Monocrystal

Constructive interference in bremsstrahlung from a monocrystal occurs whenever the momentum transferred to the lattice is normal to a set of lattice planes and has the value

$$q = n \frac{h}{d} \qquad (1)$$

where d is the separation between adjacent planes, and n is an integer. This is exactly the condition for Bragg reflection. The enhancement of the spectrum for values of q satisfying this condition depends on the density of the lattice points in the planes and is also affected by the thermal lattice vibrations. The effect is reduced if the screening radius is much less than the lattice spacing. To obtain large constructive interference one should use a crystal of high density, high Debye temperature, and low Z. The best substance is diamond, with beryllium a possible second choice if monocrystals of beryllium in thin plates can be obtained. Diamond has the higher Debye temperature ($1860^{\circ}K$ compared to $1160^{\circ}K$ for Be) and the higher density. The difference in screening radius is probably not significant, since it varies as $Z^{-1/3}$.

The problem of obtaining a suitable diamond radiator is not trivial. A thickness of 10^{-3} radiation length corresponds to 0.045 gm/cm^2 or 0.013 cm. As we shall see later, it may be desirable to use an even thinner radiator, but this may be difficult. The exposed area should be about one cm^2. If we use an electron current of 30 μa there will be 2.7 watts given up to a diamond of 10^{-3} radiation length. To radiate this power the temperature will rise to about $700^{\circ}K$. As we shall see, it will be desirable to maintain the angular position of the crystal to within 10^{-5}. To do this at such a temperature will be very difficult. Mozley has suggested that for this reason it

may be necessary to use only a small part of an analyzed electron beam, since the resulting photon intensity would still be ample for many experiments.

In order to calculate the interference spectrum, one must express the Bethe-Heitler formula as a function of q, then make the appropriate sum over the various crystal planes. The method has been described by Uberall,[3] who replaced the summation by an integral and as a result obtained only the average behavior and not the detailed interference spectrum. (The sharp structure which he predicts at the upper end of the spectrum is attributable to the longitudinal component of the momentum transfer and has no corresponding effect in ordinary Bragg reflection.) However, Uberall's paper contains the most detailed description of the process. The expression for the summation is given in reference 2 and in a recent paper by Uberall.[4]

Following the notation of Uberall and Diambrini et al. we can write an expression for $p(x)dx$, the probability per radiation length that an electron of energy E radiates a photon of energy $k = xE$ in the interval dx,

$$p(x)dx = \left[p^c(x) + p^i(x)\right] dx \qquad (2)$$

where $p^c(x)$ and $p^i(x)$ refer to the continuous and interference parts of the spectrum.

$$p^c(x) = \frac{1}{4\ell n(183\ Z^{-1/3})} \frac{dx}{x} \left[\left\{1 + (1 - x)^2\right\} \psi_1^c - \frac{2}{3}(1 - x)\, \psi_2^c\right] \qquad (3)$$

---

[3] H. Uberall, Phys. Rev. 103, 1055 (1956).

[4] H. Uberall, Die polarisation der quasi-monochromatischen bremsstrahlung von einem einkristall, Z. fur Naturforschung 17, 332-334 (1962).

$$p^i(x) = \frac{1}{4\ell n(183\ Z^{-1/3})}\ \frac{dx}{x}\left[\left\{1 + (1-x)^2\right\}\ \psi_1^{0*} - \frac{2}{3}(1-x)\ \psi_1^{0*}\right] \quad (4)$$

where the ψ^c's are given by equation (39) in reference 3, and the ψ^{0*}'s by equation (4) in reference 2. All the expressions contain the factor A, which represents the effect of the thermal lattice vibrations and is given by equation (36) in reference 2. It contains the function φ (whose argument is Θ/T, where Θ is the Debye temperature, and T is the temperature in ^oK) which is plotted in Fig. 1. For diamond, A has the following values:

$T(^oK)$	A
0	108
293	126
500	156

The expressions ψ^c depend on δ, the minimum momentum transfer, which can be written

$$\delta = \frac{1}{2E}\ \frac{x}{1-x} \quad (5)$$

in units of mc. For our case $\delta << 1$, and we can evaluate the ψ^c's for $\delta = 0$ since they vary slowly. We get for the continuous spectrum for diamond at 500^oK

$$xp^c(x)dx = 0.81\ \left[\left\{1 + (1-x)^2\right\} - 0.51\ (1-x)\right]\ dx \quad (6)$$

This is not much different from the normal bremsstrahlung spectrum (complete screening),

$$xp(x)dx = \left[1.0\left\{1 + (1-x)^2\right\} - 0.67\ (1-x)\right]\ dx \quad (7)$$

The interference part of the spectrum can be computed for a particular orientation of the crystal using equation (4) in reference 2. Interesting

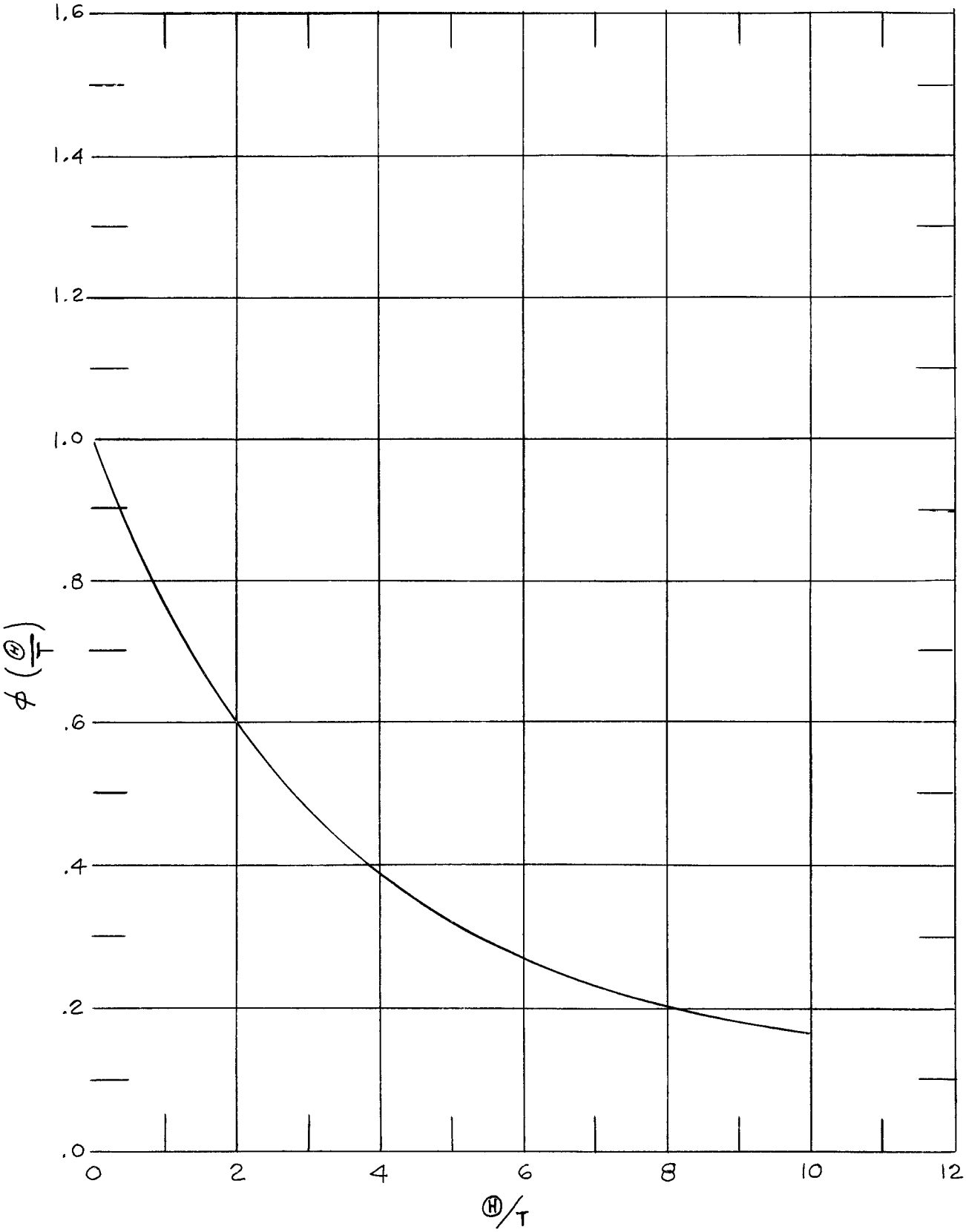

FIG. 1

interference patterns are obtained whenever the electron beam makes a small angle with one of the crystal axes, and the shape of the spectrum depends critically on this angle. A number of cases for an electron beam directed near the (110) axis of diamond at 500°K have been programmed for a computer by C. Moore, and some of the computed spectra are plotted in Figures 2-9. Figures 2-5 are cases in which the electron beam and the (110) and ($1\bar{1}0$) axes lie in the same plane. Figures 6-9 are cases in which the electron beam and the (110) and (001) axes are coplanar.

The spectra are total spectra integrated over the emission angle of the photons. The angular spread of the emitted photons is similar to that for normal bremsstrahlung, but there is a variation in intensity with azimuth that arises from the correlation between the direction of the recoil momentum and the orientation of the plane containing the scattered electron and the photon. Uberall[5] has calculated this effect using his approximation for the crystal structure, but such a calculation has not been done for a real crystal. This effect gives a net linear polarization to the photons. Calculations[4] predict large polarizations where the peaks occur in the spectrum.

The two remarkable features of the spectra are the very large enhancements over the normal bremsstrahlung and the large discontinuities. The latter are the more interesting, since there should be more than enough photon intensity. These discontinuities arise from the fact that the bremsstrahlung cross section increases to a sharp maximum as the longitudinal component of the momentum transfer approaches the minimum δ. Uberall describes the distribution of recoil momenta as a pancake perpendicular to the incident electron momentum and having a sharp plane surface a momentum distance δ from the point of interaction. The peaks in the spectra correspond to conditions under which a line of inverse lattice points lies in the surface of the pancake. The position of a

---

[4]H. Uberall, op. cit.

[5]H. Uberall, Phys. Rev. 107, 223 (1957).

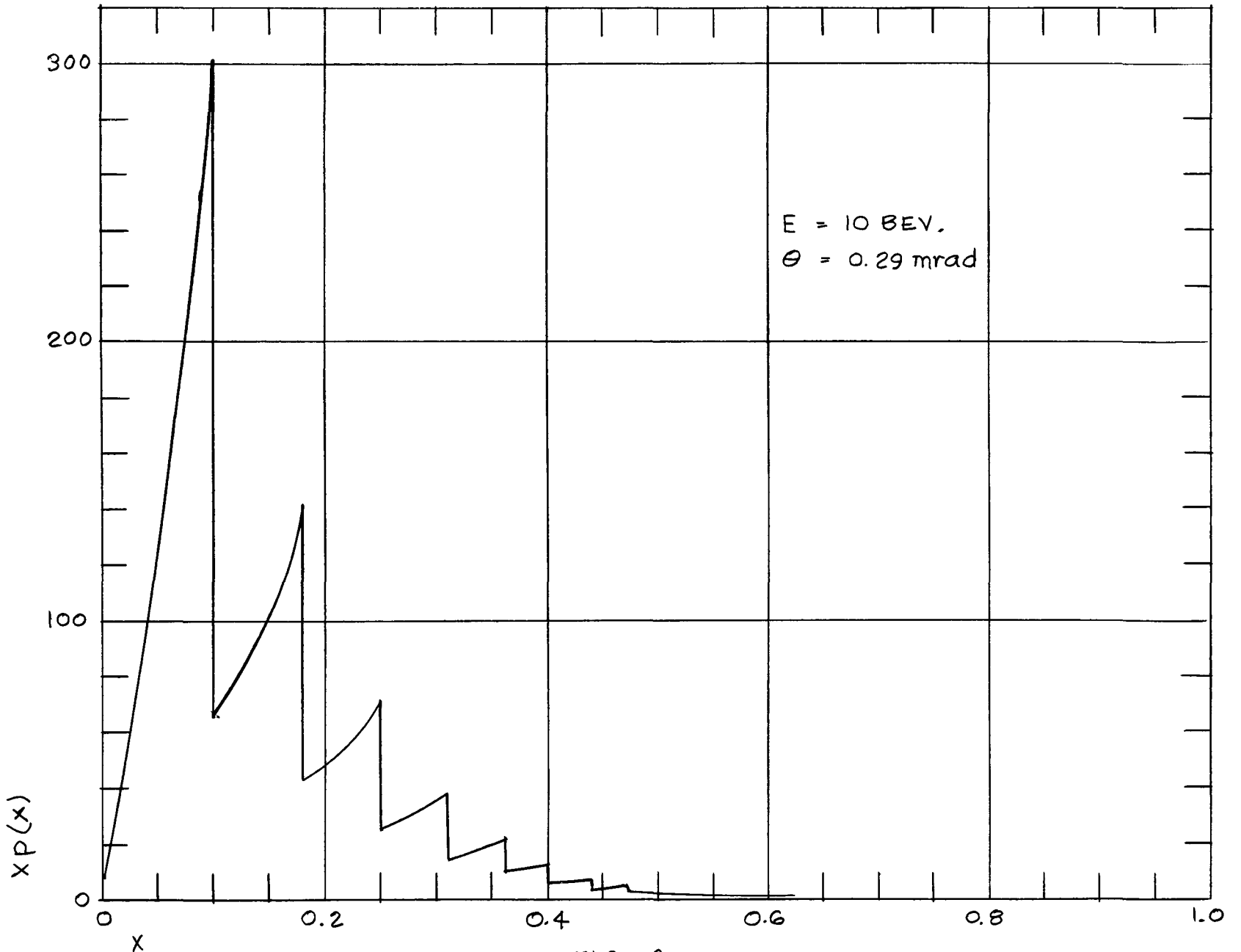

FIG. 2

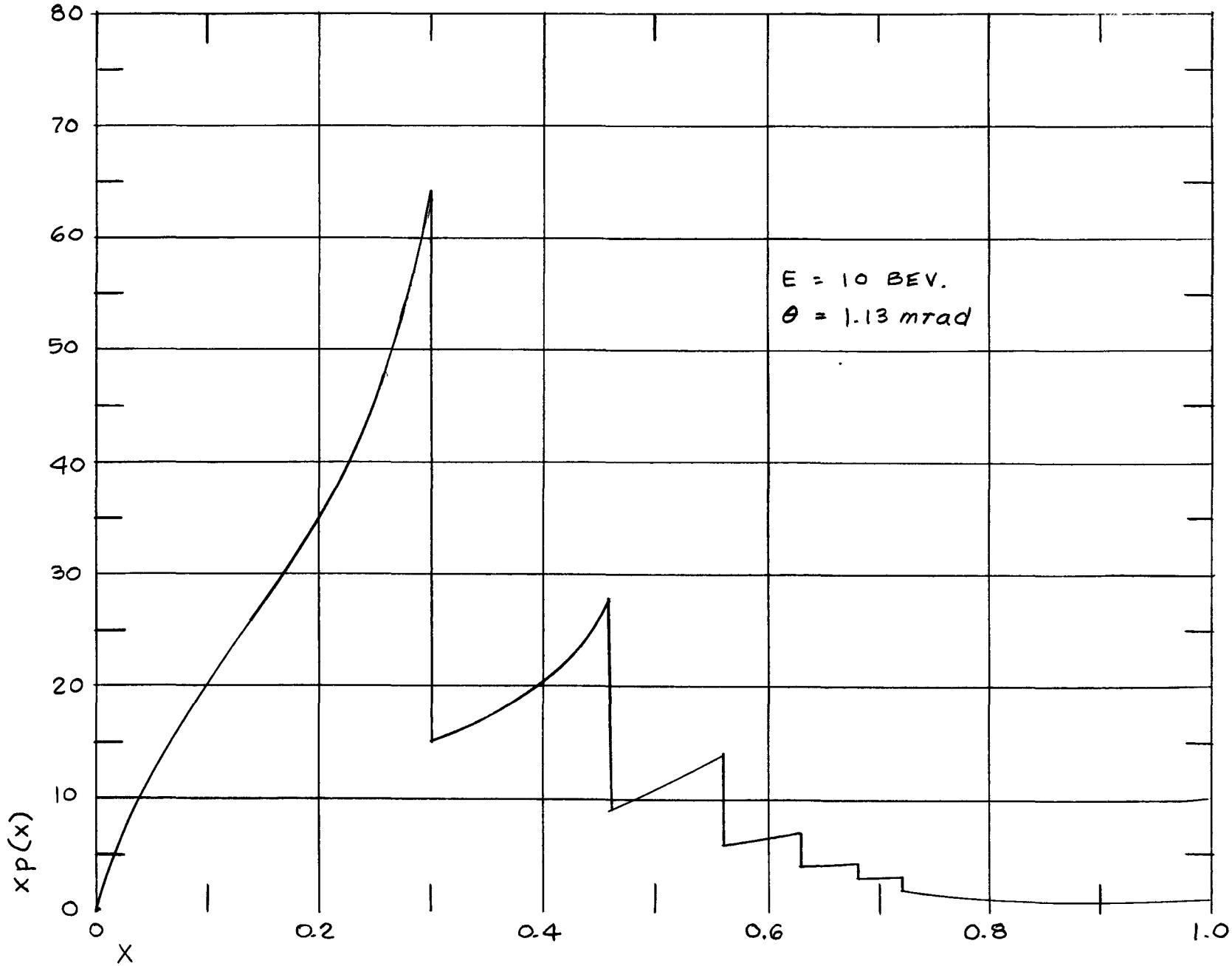

FIG. 3

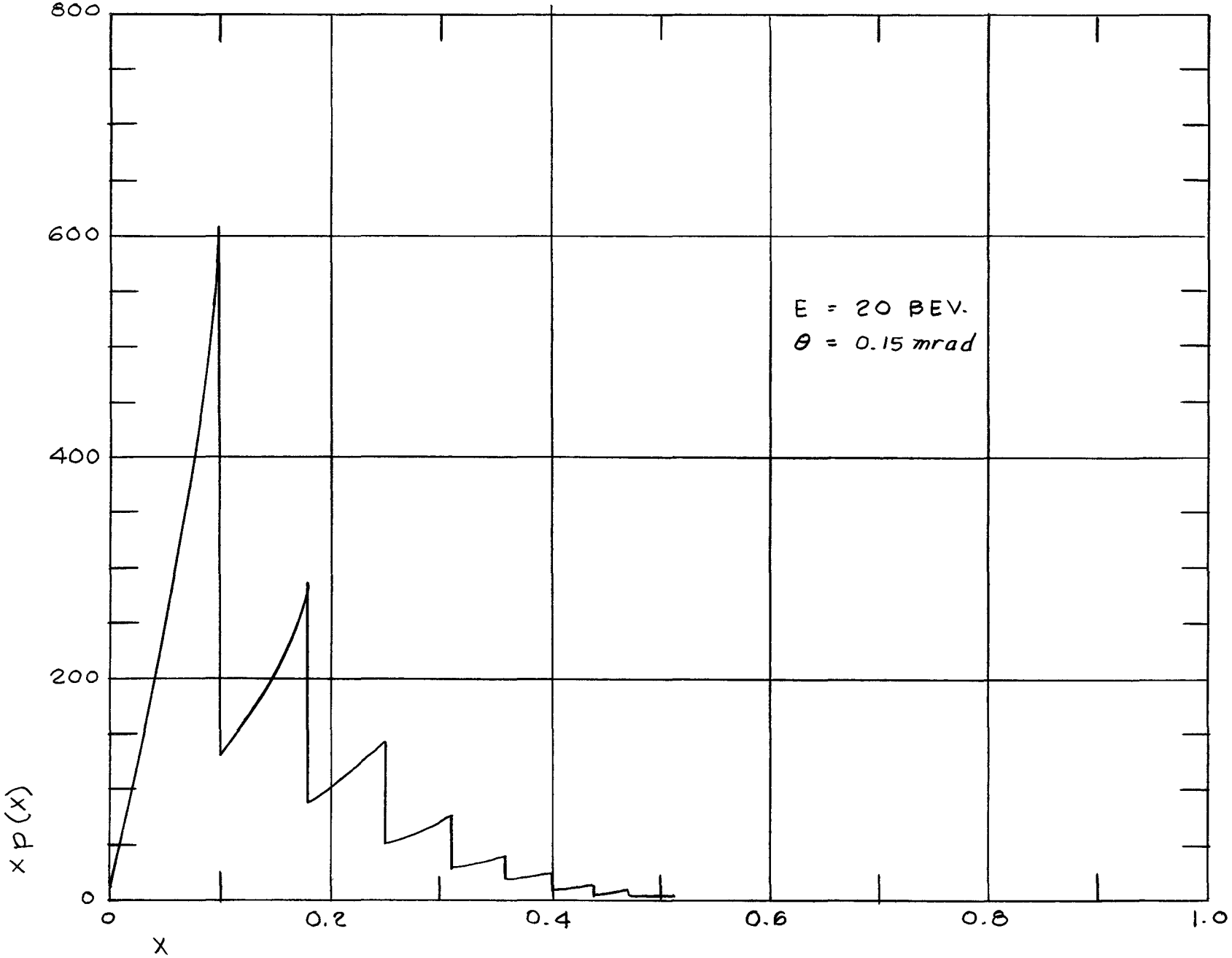

FIG. 4

SLAC-5-A
DeWire

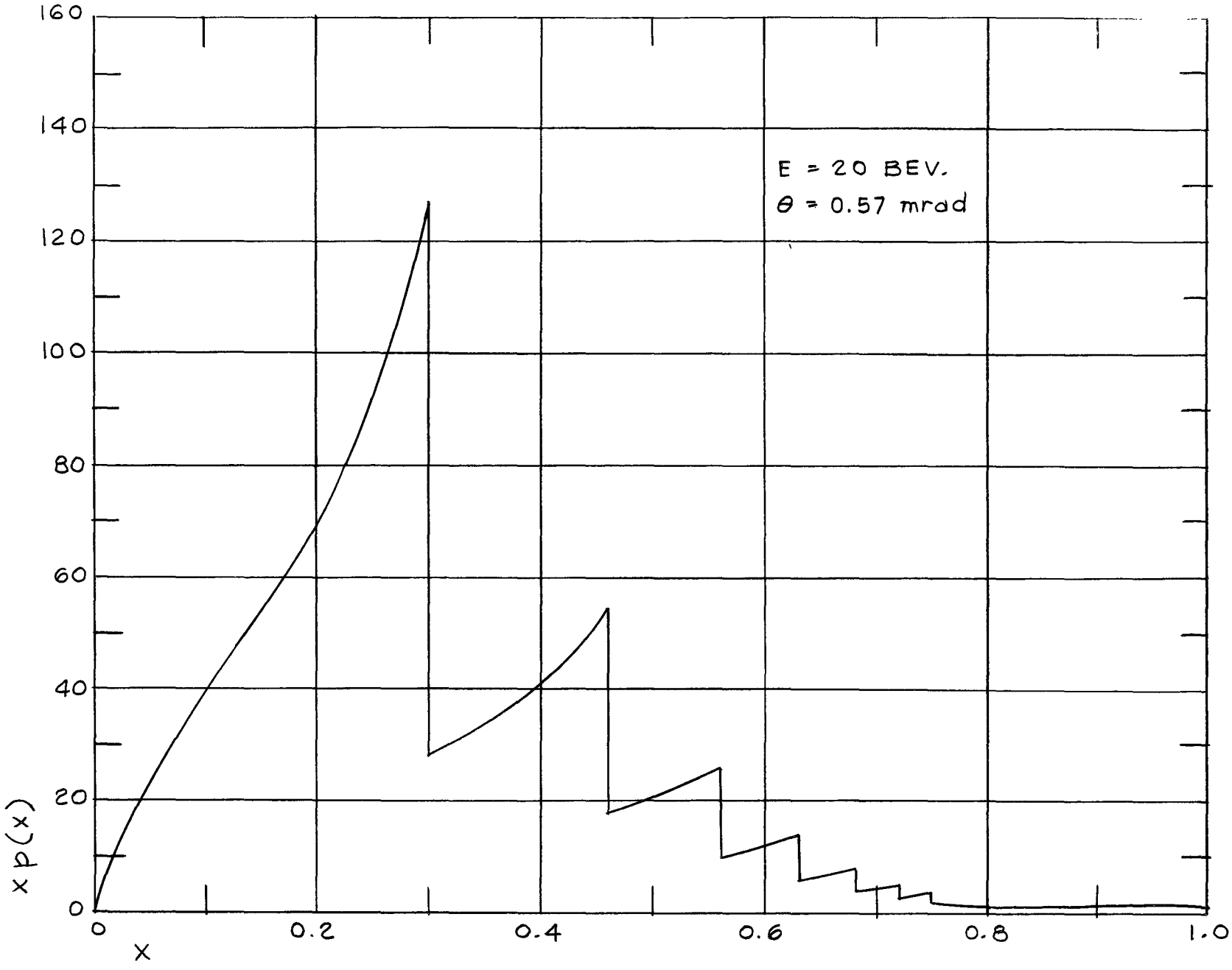
E = 20 BEV.
θ = 0.57 mrad
160
140
120
100
80
60
40
20
0
0
0.2
0.4
0.6
0.8
1.0
X
x p(x) dx

FIG. 5

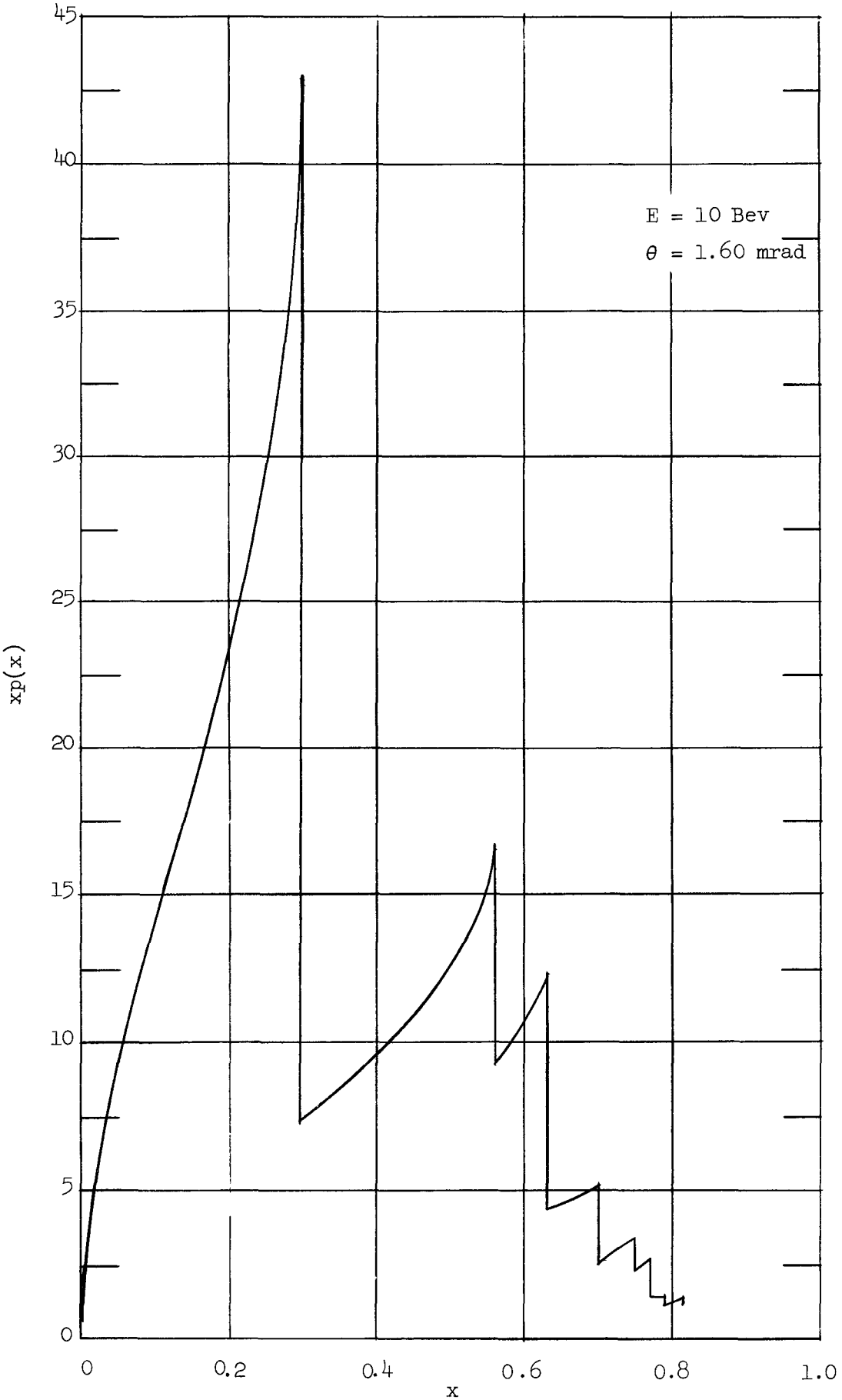

FIG. 6

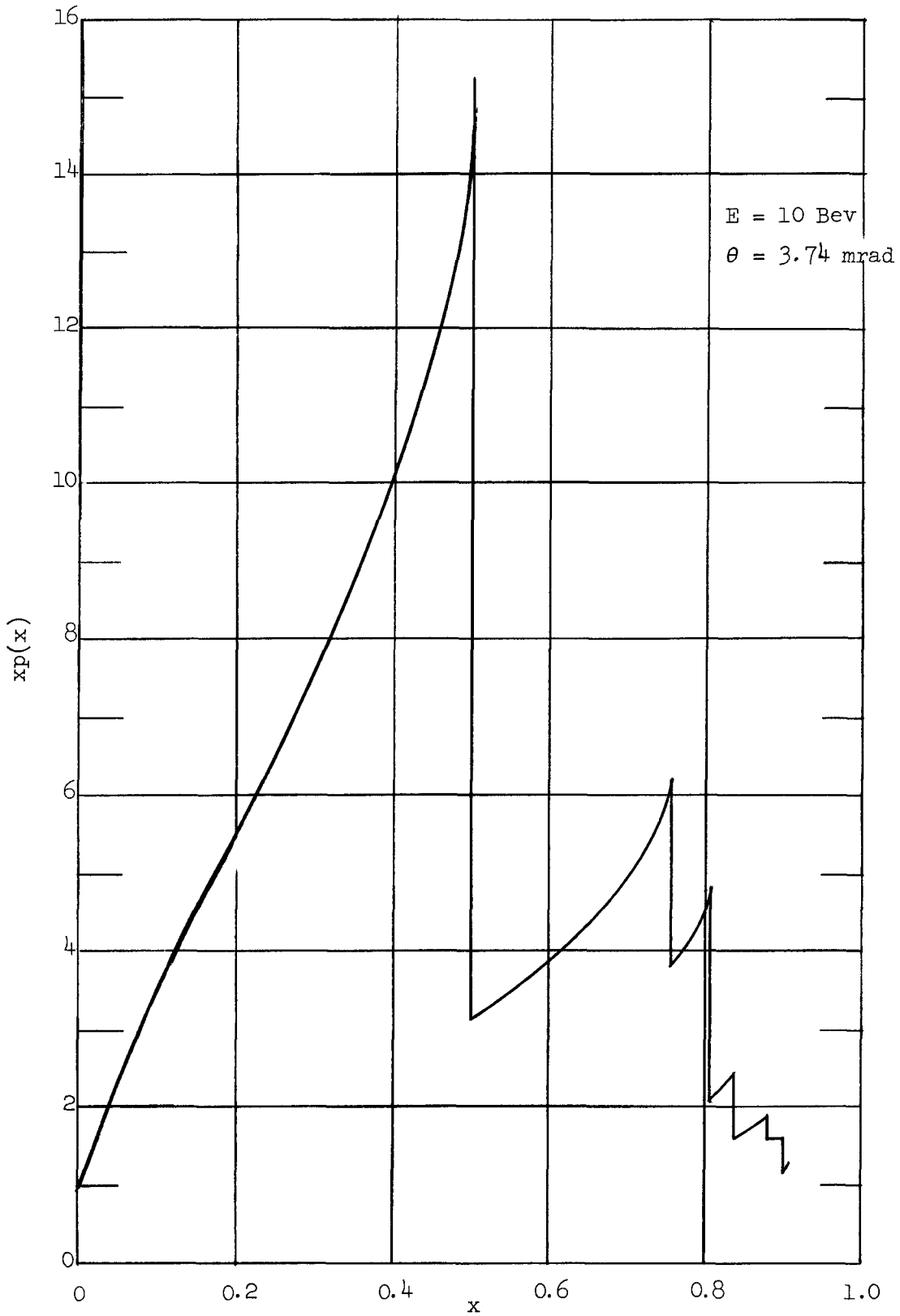

FIG. 7

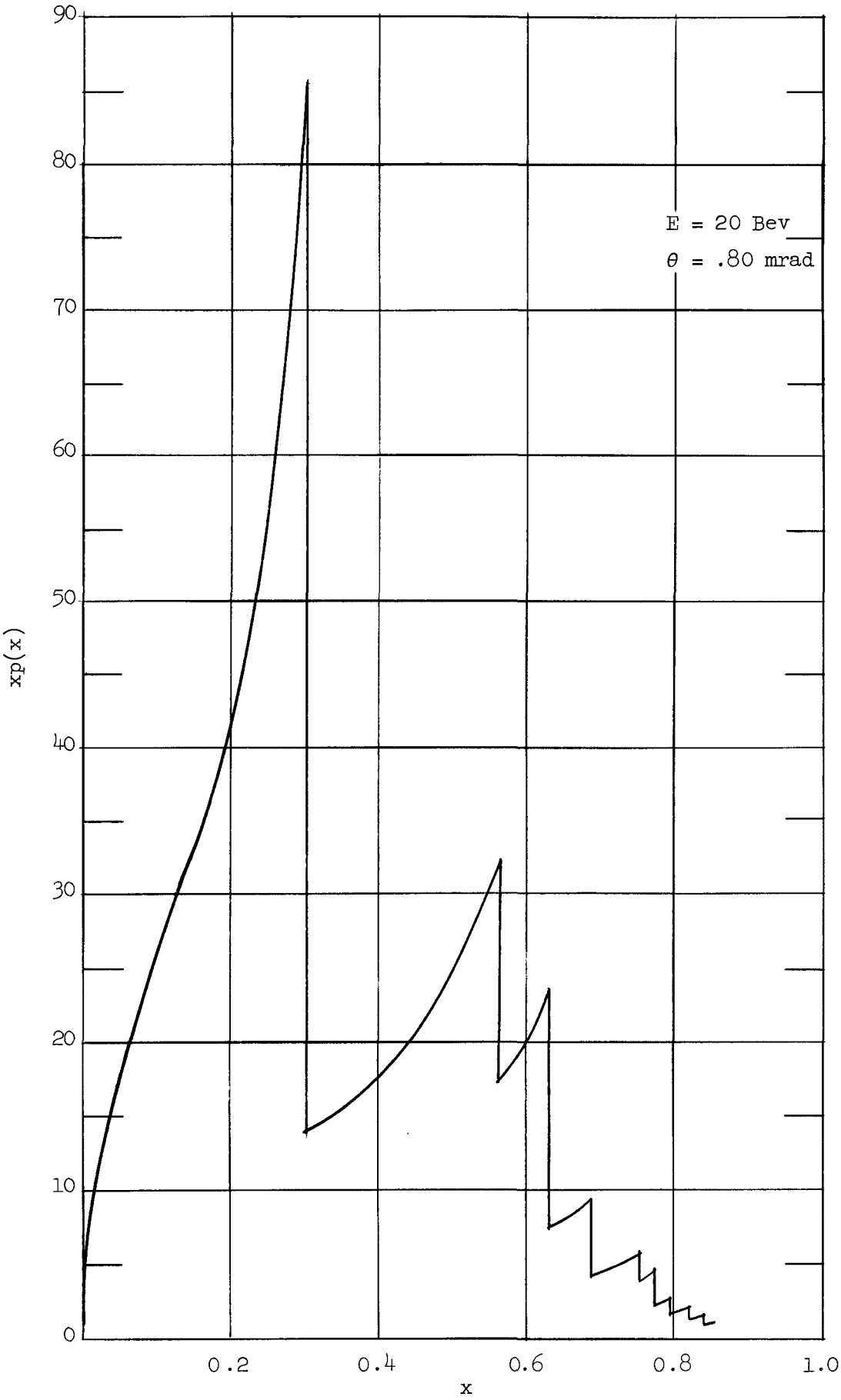

FIG. 8

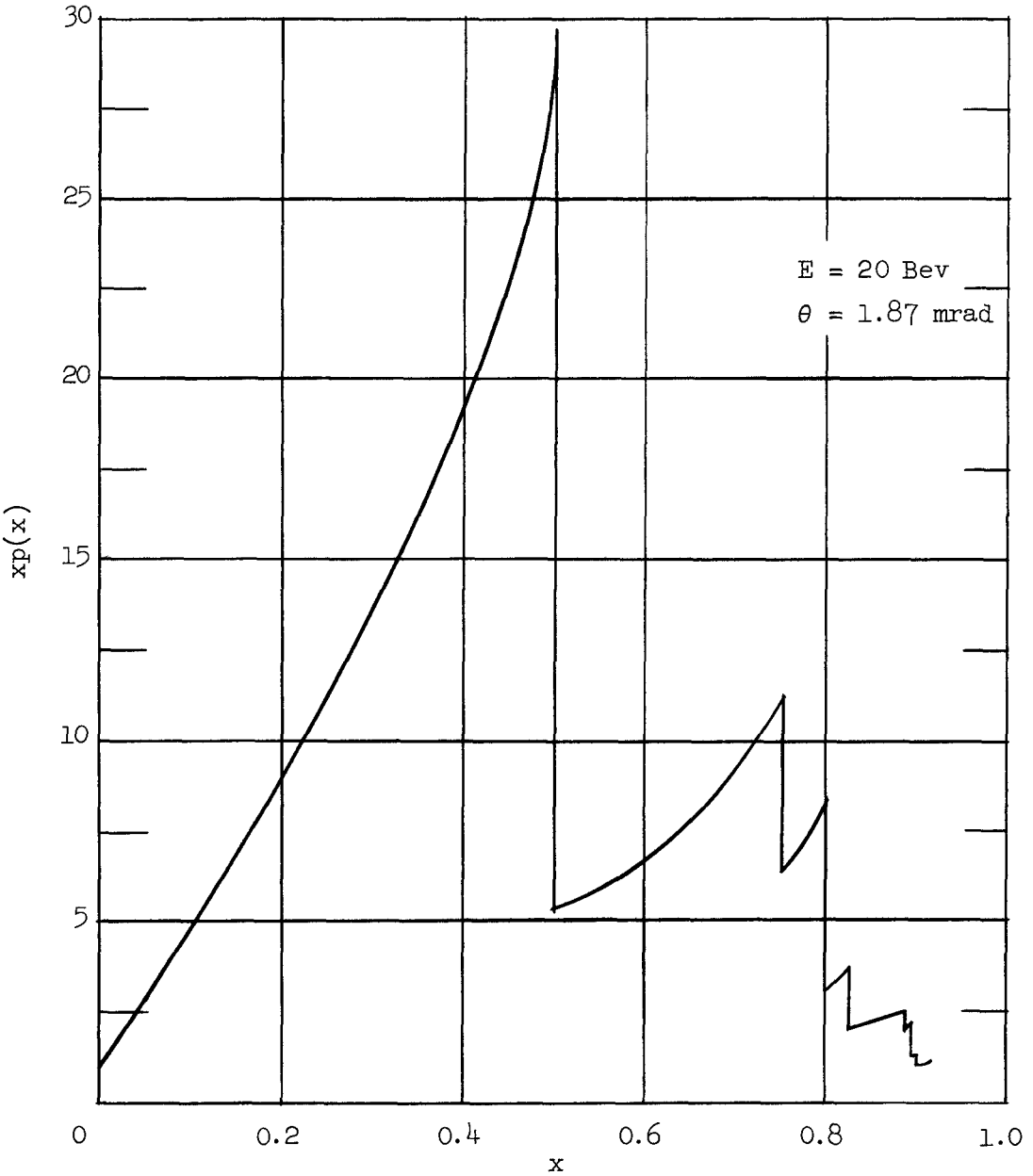

FIG. 9

given peak is determined by

$$\frac{\delta}{\theta} = \text{constant} \tag{8}$$

where the constant describes the position of the row of lattice points. Substituting for δ we obtain

$$\frac{x}{1-x} = \text{constant} \cdot 2E\theta \tag{9}$$

which describes how a given peak will move as θ and E are varied. We note by differentiation

$$\frac{dx}{x} = (1 - x) \left(\frac{dE}{E} + \frac{d\theta}{\theta} \right) \tag{10}$$

so that the relative position of a peak is less influenced by variations in E and θ as x increases. This is important in considering application to experiments.

3. Experimental Considerations

Two aspects of the diamond spectra affect how well the spectra can be used for experiments: the sharpness and stability of the discontinuities, and the background contributed by photons outside the main peak. It seems clear that the situation illustrated by Figures 6-9 is superior from both points of view.

The sharpness and position of a discontinuity are determined by the angular spread and energy of the incident electrons. For many experiments it will be necessary to have $\Delta x/x \leq 0.01$ for the main peak. If k is 5 Bev, then $\Delta k = 50$ Mev, which is less than a pion mass. One can see from Equation (10) that both E and θ must be held to one per cent. For E this is just a question of having a good beam analyzer. For θ we must consider the beam spread, multiple scattering in the radiator, and stability of radiator orientation. It should be possible

to use values of $\theta \geq 10^{-5}$, so one must keep $\Delta\theta \approx 10^{-5}$. Evidently there is some evidence that the angular spread of the beam may be this small. To keep the multiple scattering within this limit one should use a radiator of 10^{-4} radiation length. It should be possible to solve the problem of the mechanical support of the crystal unless heating effects become too severe. It is important to keep in mind that the restriction on θ is reduced by using large values of θ and x.

4. Background

If one looks at some photon-produced reaction and uses a magnet to select the momentum of one of the reaction products, the background counting rate is most severe at forward angles and is produced by electrons from wide-angle pairs and from forward pairs that undergo Coulomb scattering. These electron-counting rates can be computed and compared with the effect to be measured to determine whether an experiment is feasible. It is possible to do this for the spectrum from a diamond radiator for some particular reaction and a specific detection scheme, but for our purposes it is more useful to make a comparison between electron contaminations from a diamond spectrum and from the normal bremsstrahlung spectrum.

As an example, let us assume that we measure some reaction caused by photons of energy $k = 6$ Bev and that we detect one of the products in a magnet set for momentum q. The magnet resolution Δq corresponds to a photon-energy interval Δk. We first consider the situation with a bremsstrahlung spectrum with upper limit $k_{max} \approx 6$ Bev. The spectrum is given by $p(x) = 1/x$, $x = k/k_{max}$. The counting rate from the reaction can be written

$$C_R = R\Delta x\, p(I) = R\Delta x$$

where $\Delta x = \Delta k/k_{max}$, and R is a constant of the geometry, beam intensity, and cross section. The counting rate of electron background

is approximately

$$C_B = B \int_{x_{min}}^{1} \Delta x \; p(x) \; \frac{dx}{x}$$

where $x_{min} = q/k_{max}$. The ratio of these rates becomes

$$C_B/C_R = \left(\frac{B}{R} \; \frac{1}{x_{min}} - 1 \right)$$

We now consider the same experimental geometry but use the spectrum shown in Figure 5, where the first peak falls at $k = 6$ Bev. We approximate this spectrum by

$$p(x) = \frac{126}{.3} = 420 \qquad x < 0.3$$

$$= \frac{65}{x} \left(1 - \frac{x}{0.8} \right) \qquad 0.3 < x < 0.8$$

$$= 0 \qquad x > 0.8$$

We obtain for the counting rates

$$C_R' = R \cdot 420 \, \Delta x$$

$$C_B' = B \, \Delta x \left[\int_{x_{min}}^{0.3} 420 \, \frac{dx}{x} + \int_{0.3}^{0.8} \frac{65}{x^2} \left(1 - \frac{x}{0.8} \right) dx \right]$$

$$= B \, \Delta x \left(420 \, \ell n \, \frac{0.3}{x_{min}} + 56 \right)$$

Using $x_{min} = q/6$ for the normal bremsstrahlung and $x_{min} = q/20$ for the diamond spectrum, we find

$$C_B/C_R = \frac{B}{R}\left(\frac{6}{q} - 1\right)$$

and

$$C_B'/C_R' = \frac{B}{R}\left(\ln\frac{6}{q} + 0.13\right)$$

These ratios are equal for $q = 3.75$ Bev/c and do not show much relative variation with q. Hence we see that the spectrum from diamond produces an electron contamination that is not significantly different from that of the normal bremsstrahlung.

It is likely that the neutron background from the diamond spectrum would be less than that from bremsstrahlung, since the 1/k low-energy rise is greatly reduced.

5. Photon Monitor

The usual methods of monitoring give a measure of the total beam intensity and will not be adequate for work with the diamond spectrum, since it will be necessary to monitor the number of photons close to a discontinuity as well as the total beam intensity. Small variations of the position of the discontinuity could drastically change the number of photons at a particular energy without changing the total intensity. The most obvious monitor is a pair spectrometer. A spectrometer having a resolution of about one per cent would be needed, in order to measure only those photons which contribute to the reaction being studied. The chief limitation on the use of such a spectrometer is the magnitude of the chance-coincidence rate.

In order to get an estimate of this limitation we consider a single-channel symmetrical-pair spectrometer set to count photons at the first peak in Figure 5. We approximate the spectrum as we did in the previous section. We assume 360 beam pulses per second and a pulse width of one microsecond. If we make the further assumption that all counts in the

electron detectors come from the pair target, then the ratio of accidental to true coincidences is

$$\frac{\text{Acc.}}{\text{True}} = 5 \times 10^5 \ \tau \ t_R t_T N$$

where τ is the coincidence resolving time, t_R and t_T are the thicknesses of the diamond radiator and pair target in radiation lengths, and N is the electron beam intensity in electrons per second. If we use $\tau = 10^{-9}$ sec, and t_R and $t_T = 10^{-4}$, we then get 10 percent accidentals for $N = 2 \times 10^{10}$ electrons per sec, which is only 0.01 per cent of the expected beam. Clearly the pair spectrometer could not be used as a continuous monitor but could be used with separate calibration runs at low intensity.

6. Further Study

It would be desirable to study in greater detail the problems involved in using these photon beams from a crystal. More careful calculations on backgrounds using the spectra in Figures 6-9 should be done. The theory of the bremsstrahlung process should be studied, in particular to learn what limitations there are on the sharpness of the discontinuities. It would also be advisable to investigate how much the theory is altered when electronic wave functions appropriate to the crystal are used to calculate the screening.

CONJECTURES ON THE EFFECTS OF REGGE POLES ON DRELL PROCESSES

by

D. B. Lichtenberg

August, 1962

1. Introduction

Drell[1] has calculated cross sections for electromagnetic pair production of high-energy particles using a peripheral model in which one member of the pair interacts strongly with the target particle, while the other escapes. The amplitude for a Drell process contains a pole at an unphysical value of the momentum transfer. It is the purpose of this note to consider possible changes in a Drell production cross section if the pole in the amplitude is a Regge pole.

In elastic scattering, the effect of replacing an ordinary pole by a Regge pole is to reduce the cross section, the magnitude of the reduction depending on how much the actual momentum transfer differs from the value at the pole. In a Drell process, the smaller the mass of the produced particle, the closer the pole is to the physical region, and the smaller will be the effect of processes not considered, including the effect of the possible Regge character of the pole. Thus, as Drell recognized, the peripheral mechanism is most reliable for production of pions, less so for K mesons, and still less for production of anti-protons.

For elastic scattering, the Regge mechanism has been shown to exist in non-relativistic potential theory.[2] The generalization to field theory is based on conjecture, but has received some experimental confirmation. Work has also been done in the non-relativistic case for multichannel processes in which no channel contains more than two particles.[3,4]

---

[1] S. D. Drell, Report M-200-7A, SLAC, Stanford University (1960).

[2] T. Regge, Nuovo Cimento 14, 951 (1959) and 18, 947 (1960).

[3] L. Fonda, L. Radicati, and T. Regge, Ann. Phys. 12, 68 (1961); J. Charap and E. Squires, UCRL-10138.

[4] L. Favella and M. T. Reineri, Nuovo Cimento 23, 617 (1962).

In particular, Favella and Reineri[4] have shown that the poles are confined to a strip along the imaginary axis. If this behavior carries over into field theory with many-body final states, then the effects of Regge poles on the Drell mechanism will be small. However, since it is a long leap from a two-body non-relativistic process to a many-body relativistic one, we shall make different guesses about what happens in the relativistic case. We shall see that, depending on the assumptions, we can obtain cross sections for producing particles of the K-meson mass or greater which differ by two orders of magnitude. The cross section for producing pions is not appreciably affected by the Regge pole hypothesis.

2. Modification of the Drell Formula

Consider the production process shown in Fig. 1.

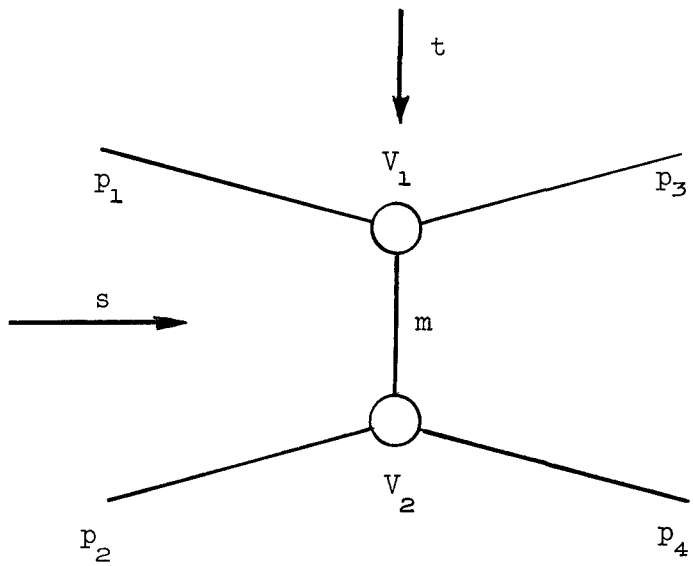

FIG. 1

Our notation is that in the s-channel, $s = (p_1 + p_2)^2$ is the square of the total center-of-mass energy, and $t = (p_1 - p_3)^2$ is the square of the four-momentum transfer. Similarly, in the t-channel, t is the square of the energy, and s is the square of the momentum transfer.

[4] L. Favella and M. T. Reineri, op. cit.

If the exchanged particle in Fig. 1 has spin ℓ, then the amplitude A_t in the t-channel contains (for the other particles spinless) the factor $A_t \propto P_\ell \left|\cos \theta_t\right| / \left|t - m^2\right|$, where θ_t is the center-of-mass scattering angle. The s-channel amplitude A_s contains the same factor, except that $\cos \theta_t$ is no longer in the physical region.

In elastic scattering, the conjecture is to make the replacements[5]

$$P_\ell\left|\cos \theta_t\right| \rightarrow \left|s/s_o\right|^{\alpha(t)} \tag{1}$$

$$t - m^2 \rightarrow c(t) \sin \pi \alpha(t) \tag{2}$$

where α and c are functions of t, and s_o is an arbitrary constant. A necessary (but not sufficient) condition for making the replacement (1) is that in the region of the s-channel under consideration

$$\left|\cos \theta_t\right| \gg 1 \tag{3}$$

In elastic scattering this condition is automatically satisfied for $s \gg t$ and $s \gg M^2$, where M is the largest mass entering the problem. In a production process it is not necessarily true that $\left|\cos \theta_t\right| \gg 1$ even if s is large and t is small.

Inspection of $\cos \theta_t$ for a production process with an incident photon indicates that condition (3) is not satisfied at $\theta_s = 0$ at any energy. Therefore, it is not justified to make the replacement (1) in the amplitude. Furthermore, in a Drell process (see Fig. 2 below), particle number 4 is in fact a collection of particles with variable internal energy M_4. Therefore s and t are not the only invariants of the problem.

---

[5]S. Frautschi, M. Gell-Mann, and F. Zachariasen, Phys. Rev. 126, 2204 (1962).

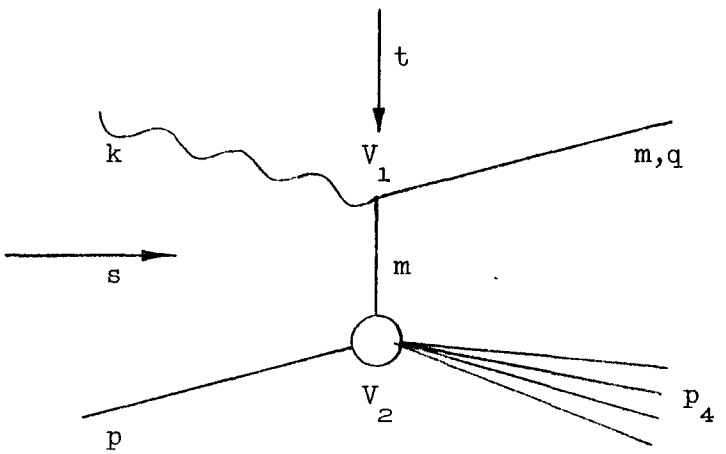

FIG. 2

In particular, we are interested in the cross section $\sigma(k, \theta, \omega)$ as a function of three laboratory variables, the incident photon energy k, and the angle θ and energy ω of the produced particle of mass m.

Despite the difficulties in generalizing from the elastic-scattering case we assume that the Drell cross section is modified as follows

$$\sigma(k, \theta, \omega) = R(k, \theta, \omega)\, \sigma_{\text{Drell}}(k, \theta, \omega) \tag{4}$$

One choice for R, based on an analogy with elastic scattering, is

$$R(k, \theta, \omega) = F(t)\left(\frac{s}{s_o}\right)^{\alpha(t)-\ell} \approx F(t)\, \frac{k}{m_N}^{\alpha(t)-\ell} \tag{5}$$

with $s_o = 2m_N^2$ where m_N is the nucleon mass. Our reason for choosing the exponent to be $\alpha - \ell$ is a guess. The factor $P_\ell(\cos \theta_t)$ in an amplitude arises in a perturbation theory from the vertex functions V_1 and V_2 of Fig. 1. Replacing P_ℓ by s^α in the amplitude, we obtain a factor $s^{2\alpha}$ in the cross section. The ratio of the cross section calculated with a Regge pole to the usual cross section then goes as $s^{2(\alpha-\ell)}$.

However, in a Drell process (Fig. 2), the contribution from the vertex V_2 is absorbed into an experimental total cross section. Therefore, we conjecture that $\sigma_{\text{Drell}}(k, \theta, \omega)$ already contains a factor s^{α}, and hence multiply it by $s^{\alpha-\ell}$. If this conjecture is wrong, it will be easy to modify the results simply by taking $\sigma/\sigma_{\text{Drell}} = R^2$ instead of R.

In order to get an estimate for R we need to make guesses about $F(t)$ and $\alpha(t)$. The best experimental information available about Regge trajectories concerns the so-called Pomeranchuk trajectory.[6] This trajectory appears to have a constant slope between $t = 0$ and $t = -1$ Gev^2. For $t < -1$ Gev^2, the trajectory is poorly determined, but $\alpha(t)$ appears to tend toward a constant. For want of better information, we assume that all trajectories have the same slope as the Pomeranchuk trajectory.[7] For $\alpha(t)$ we choose the following simple form, which is consistent with the experimental information about the Pomeranchuk trajectory:

$$\begin{aligned} \alpha(t) &= \ell + \xi(t - m^2), && t - m^2 > -1 \text{ Gev}^2 \\ &= \ell + \xi(t - m^2)/4 - \tfrac{3}{4}, && t - m^2 < -1 \text{ Gev}^2 \end{aligned} \qquad (6)$$

where $\xi = 1$ Gev^{-2}. With this choice, $\alpha - \ell$ is independent of spin.[8] We already have so much freedom in choosing the form of R and of $\alpha(t)$ that little is to be gained by also varying $F(t)$. We simply let $F(t) = 1$. To provide a test of Eq. (5) which does not depend on $F(t)$, one should make measurements at different energies and the same momentum transfer.

Numerical values for the R of Eq. (5) for photons of 25, 18.5, and 6 Gev incident on a nucleon target are shown in Table I. We have included a 6-Gev photon even though this energy is almost certainly too small for an asymptotic approximation to be valid. We have included forward angles for the K meson (but not the pion) even though the cross section for K production vanishes in the forward direction. This is so

---

[6] A. Diddens et al., Phys. Rev. Lett. 9, 111 (1962).

[7] For a summary of the situation with respect to Regge trajectories see S. D. Drell, Intl. Conf. on High Energy Physics, CERN, (1962).

[8] Without further justification, we ignore the spins of all particles in applying the formula.

TABLE I

Values of the ratio R of the conjectured cross section for ($\gamma + N \rightarrow$ particle + anything) to the corresponding Drell cross section according to Eq. (5) if $F(t) = 1$ and α is given by Eq. (6). Here k is the incident photon energy, and ω and θ are the energy and angle of the produced particle (all in the laboratory system).

k Gev	ω Gev	$m\theta/\omega$ radians*	R_π	R_K	R_ρ	$R_{\bar{N}}$
25	23	0	-	.4	.1	.04
		1/2	.9	.3	.08	.03
		3/4	.9	.3	.04	.02
		1	.9	.2	.03	.02
	18.5	0	-	.3	.08	.03
		1/2	.9	.3	.04	.02
		3/4	.9	.2	.03	.02
		1	.8	.1	.02	.01
18.5	17	0	-	.4	.2	.06
		1/2	.9	.4	.1	.04
		3/4	.9	.3	.06	.03
		1	.9	.2	.04	.02
	13.5	0	-	.4	.1	.04
		1/2	.9	.3	.06	.03
		3/4	.9	.2	.04	.02
		1	.9	.1	.03	.02
6	4.5	0	-	.5	.2	.1
		1/2	1	.4	.2	.1
		3/4	.9	.4	.1	.1
		1	.9	.3	.1	.1

*Note that θ is different for the different particles.

as to give an idea of the factor for a vector meson of mass ≈ 500 Mev if such a meson exists. Unfortunately, the expression of Eq. (5) is based on the assumption that $\cos\theta_t$ is large in a region where, as we have mentioned previously, it is not. Another choice, which does not have this deficiency, but is otherwise simply a guess, is

$$R = F(t)\left\{\frac{(1 + \omega^2\theta^2/m^2)k - \omega + m_N}{k - \omega + m_N}\right\}^{\alpha(t) - \ell} \qquad (7)$$

where $\omega \gtrsim k/2$ and $\theta \lesssim m/\omega$. The quantity in curly brackets has been chosen to have asymptotic properties which slightly resemble those of $\cos\theta_t$ in a production process with a two-body final state. Using this expression for R, again with $F(t) = 1$ and with $\alpha(t)$ given by Eq. (6), we obtain the results shown in Table II.

3. Conclusions

The numerical values of R, the ratio of the conjectured cross section to the cross section calculated by Drell, are based on too many unverified assumptions to be taken seriously. Two different assumptions about the behavior of Regge poles yield very different values for $R(k, \theta, \omega)$, both in average value and as a function of its arguments. Both of these assumptions lead to considerably larger cross sections than would the simplest guess,[9] $R = \left(s/s_o\right)^{2(\alpha-\ell)}$. One can easily obtain the values of R with this choice by squaring the numbers in Table I, but we believe this will seriously underestimate R. Likewise, if one accepts the argument that

$$\left[\left(1 + \omega^2\theta^2/m^2\right)\, k - \omega + m_N\right] \Big/ \left(k - \omega + m_N\right)$$

is a better approximation to $\cos\theta_t$ than s/s_o, but wishes to raise it to the power $2(\alpha - \ell)$, one should square the numbers in Table II.

It is important to remember that we have not discussed effects of diagrams not considered by Drell, e.g., diagrams in which one or more pions

[9] Drell, reference 7, has suggested looking for the factor $\left(s/s_o\right)^{2\alpha}$ in production reactions.

TABLE II

Values of R according to Eq. (7) if $F(t) = 1$ and α is given by Eq. (6). See caption for Table I.

k Gev	ω Gev	$m\theta/\omega$ radians	R_π	R_K	R_ρ	$R_{\bar{N}}$
25	23	0	-	1	1	1
		1/2	1	.7	.4	.3
		3/4	.9	.5	.2	.1
		1	.9	.3	.09	.06
	18.5	0	-	1	1	1
		1/2	1	.8	.6	.5
		1/4	1	.6	.3	.3
		1	.9	.4	.2	.1
18.5	17	0	-	1	1	1
		1/2	1	.7	.4	.3
		3/4	.9	.5	.2	.2
		1	.9	.3	.1	.07
	13.5	0	-	1	1	1
		1/2	1	.8	.6	.5
		3/4	1	.6	.3	.3
		1	.9	.4	.2	.1
6	4.5	0	-	1	1	1
		1/2	1	.8	.6	.6
		3/4	1	.6	.4	.4
		1	.9	.4	.3	.2

accompany the exchanged particle. The unknown contributions of such diagrams lead to additional uncertainties in the magnitudes of the cross sections.

Finally, we note that for many production processes a particle with the quantum numbers of the vacuum cannot be exchanged. The study of such processes can give information on Regge trajectories which is not masked by a dominant Pomeranchuk trajectory. Reactions in which only two particles come out and for which $|\cos \theta_t| \gg 1$ in part of the physical region will be simpler to interpret in this connection than a Drell process.

We should like to thank Dr. Sam Berman, Dr. Jon Matthews, and Dr. Pierre Noyes for valuable criticisms. However, they bear none of the responsibility for the speculations made here.

A PROPOSED METHOD TO SEARCH FOR INTERMEDIATE BOSONS AND HEAVY LEPTONS

by
M. Schwartz
August, 1962

The purpose of this note is to point out the possibility of constructing an experiment, with reasonable counting rates, which would be sensitive only to neutrinos from the decay of intermediate bosons and/or heavy leptons, provided they exist and have mass not much greater than that of the proton.

The experimental setup is exceedingly simple. The electron beam is allowed to hit a 45-foot-thick iron shielding wall, on the other end of which is a heavy detector (for example a 50-ton spark chamber; see Fig. 1).

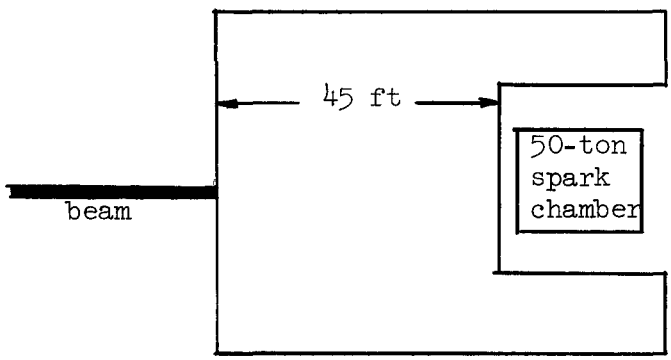

FIG. 1

We can estimate the flux of neutrinos as follows:

(a) Assume the primary intensity is 2×10^{14} electrons per second at 25 Bev. In a long target this should yield at some point $\approx 10^{14}$ gammas/sec in the energy range of 12.5 to 25 Bev.

(b) Using only the Bethe-Heitler formula and assuming that the cross section is not enhanced over what it would be for a fermion with no anomalous moment and the same mass, we expect the probability for

production of a boson pair to be

$$\approx \frac{1}{4} \times \frac{1}{(2 \times 10^3)^2} = 6 \times 10^{-8}$$

The factor 2×10^3 is the ratio of boson mass to electron mass. The factor $\frac{1}{4}$ is present because boson production would still be quite far from the asymptotic region. This means then a total of 6×10^6 boson pairs per second. In the 10-Bev interval from 5 to 15 Bev one might then expect a total of 10^7 bosons.

(c) The flux of neutrinos at a target 15 meters away, assuming that all bosons decay into neutrinos and leptons, is then

$$10^7 \times (1500)^{-2} \times 50 \approx 200 \ \nu/\text{sec-cm}^2$$

with an average energy of 5 Bev. This estimate seems fairly conservative and could easily be augmented by a substantial factor if the magnetic moment of the boson is higher than assumed above.

At any rate, one can ask what the event-rate will be using the above calculation. If the boson had a mass of 1 Bev, then the above neutrinos would make them with a cross section of 10^{-37} cm^2/nucleon, on the average. Given 5×10^7 gms of material the reaction rate would be 6×10^{-4}/sec, or about 2 per hour. Ordinary neutrino interactions should occur at a rate of 2 per day or better.

One of the more interesting possibilities that can be explored by this method is the question of the existence of leptons with mass higher than that of the muon. If such a lepton existed and had mass between the pion and the intermediate boson, it should decay into pion and neutrino in $\approx 10^{-10}$ seconds. If the neutrino coupled to this lepton were the same as that coupled to the muon, then it should be produced in presently planned neutrino experiments and would appear experimentally like the production of a charged pion without an accompanying muon. If the neutrino coupled to the heavy lepton were not the same as the muon's neutrino, then it could not be observed in presently planned experiments. In the experiment outlined above it could be detected through one of two different processes. In the first of these, the

boson decays into this lepton and its neutrino, and the latter is detected in the spark chamber through the appearance of pions. In the second process, the leptons themselves are produced in pairs, decay in $\approx 10^{-10}$ seconds into pion and neutrino, and these neutrinos are detected.

Should the lepton be heavier than the boson, but still not much heavier than the proton, it would be produced with abundances comparable to that estimated above for boson pairs. Each lepton would decay in $\approx 10^{-17}$ seconds into boson and neutrino, and these neutrinos could be detected. They would show up through the following sequence of events:

$$\nu_L + Z \rightarrow L^- + W^+ + Z$$

$$L^- \rightarrow W^- + \bar{\nu}_L$$

Namely, two bosons would appear to have been produced in the chamber.

Lastly, it should be pointed out that even though the above counting rates are not very large, there seems to be no real background source. Neutrinos from pion and K-meson decay in the energy region we are considering are very much suppressed by the shield. Neutrinos from muon decay also make no particular contribution. The only source of background would be cosmic rays, but at worse, if one is willing to throw out all single tracks aiming upward in the chamber, one could suppress all cosmic-ray background and still lose only half of the real events.

KINEMATIC CALCULATIONS TO DETERMINE YIELDS OF PARTICLES ARISING FROM THE DECAYS OF SHORT-LIVED INTERMEDIATE STATES

by

George Trilling
August, 1962

1. General Solution

Assume that we photo-produce the short-lived particle "a" (for example a ρ or a K^* meson) with a cross section given by

$$\frac{d^2\sigma}{dE_a d\Omega_a}$$

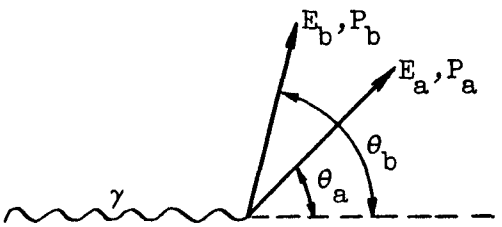

We now suppose that particle "a" undergoes a decay of the form $a \rightarrow b + c$. We ask for the yield of particle b,

$$\frac{d^2\sigma}{dE_b d\Omega_b}$$

We first define some additional quantities:

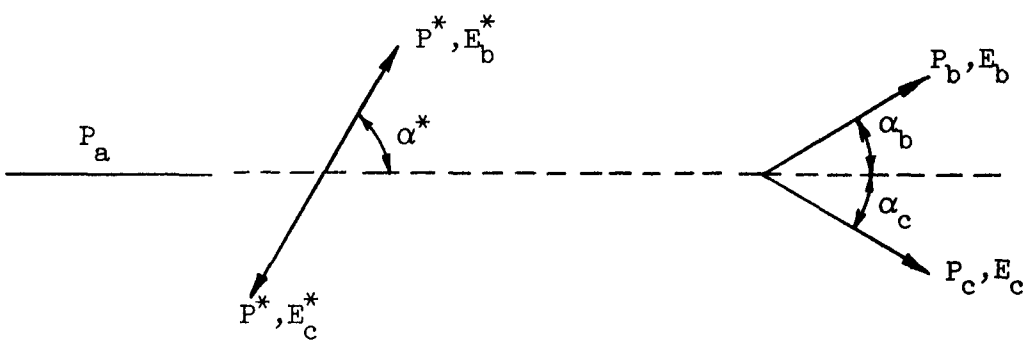

center-of-mass system laboratory system

These diagrams represent the vector relations in the decay of particle "a" both in its rest system and in the laboratory systems; and, given that P, E stand for momentum and total energy respectively, the notation is self-evident. We further define φ to be the angle between the production plane and the decay plane of particle "a".

The cross section for production of particle "a" with energy E_a, angle θ_a, and decay characterized by angles α^*, φ is given by

$$\frac{d^4\sigma}{dE_a d\Omega_a d\alpha^* d\varphi} = \frac{d^2\sigma}{dE_a d\Omega_a} \frac{\sin \alpha^*}{2\pi} \tag{1}$$

where φ ranges from 0 to π to cover once the complete range.

What we really need is

$$\frac{d^4\sigma}{dE_a d\Omega_a dE_b d\Omega_b}$$

and hence must make a transformation of variables:

$$E_a, \theta_a, \alpha^*, \varphi \rightarrow E_a, \theta_a, E_b, \theta_b$$

noting that

$$\frac{d^4\sigma}{dE_a d\Omega_a dE_b d\Omega_b} = \frac{d^4\sigma}{dE_a d\Omega_a d\alpha^* d\varphi} \frac{\partial(E_a,\theta_a,\alpha^*,\varphi)}{\partial(E_a,\theta_a,E_b,\theta_b)} \frac{1}{2\pi \sin \theta_b} \tag{2}$$

The appropriate relations between these variables are as follows:

$$E_b = \left(\frac{E_a}{m_a}\right) E_b^* + \left(\frac{P_a}{m_a}\right) P^* \cos \alpha^* \tag{3a}$$

$$\cos \theta_b = \cos \theta_a \cos \alpha_b - \sin \theta_a \sin \alpha_b \cos \varphi \tag{3b}$$

and

$$\tan \alpha_b = \frac{P^* \sin \alpha^*}{\left(\frac{E_a}{m_a}\right) P^* \cos \alpha^* + \left(\frac{P_a}{m_a}\right) E_b^*} \tag{3c}$$

We now evaluate the Jacobian:

$$\frac{\partial(E_a,\theta_a,\alpha^*,\varphi)}{\partial(E_a,\theta_a,E_b,\theta_b)} = \left[\frac{\partial(E_a,\theta_a,E_b,\theta_b)}{\partial(E_a,\theta_a,\alpha^*,\varphi)}\right]^{-1} = \left[\frac{\partial E_b}{\partial \alpha^*}\,\frac{\partial \theta_b}{\partial \varphi}\right]^{-1} \tag{4}$$

$$= \frac{m_a \sin \theta_b}{P_a P^* \sin \alpha^* \sin \alpha_b \sin \theta_a \sin \varphi}$$

Using (1), (2) and (4) we then have

$$\frac{d^4\sigma}{dE_a d\Omega_a dE_b d\Omega_b} = \left(\frac{d^2\sigma}{dE_a d\Omega_a}\right) \frac{m_a}{4\pi^2 P_a P^* \sin \alpha_b \sin \theta_a \sin \varphi} \tag{5}$$

and

$$\frac{d^2\sigma}{dE_b d\Omega_b} = \frac{m_a}{2\pi P^*} \iint \left(\frac{d^2\sigma}{dE_a d\Omega_a}\right) \frac{dE_a d\theta_a}{P_a \sin \alpha_b \sin \varphi} \tag{6}$$

We first briefly discuss the limits of integration.

Consider that E_b, θ_b are chosen, and the integration (6) over θ_a, E_a is to be performed. We select a particular E_a, and first integrate over θ_a. From (3a) and (3c) the quantity α_b is constant insofar as θ_a variations are concerned and depends only on E_a. From (3b) it is clear that the limits on θ_a are given by,

$$\theta_{a_{min}} = \left| \theta_b - \alpha_b \right|$$
$$\theta_{a_{max}} = \theta_b + \alpha_b \tag{7}$$

where θ_b is fixed a priori, and α_b is a function of E_a. After integration over θ_a, the integration over E_a proceeds between the following limits:

$$E_{a_{min}} = \frac{m_a}{m_b^2}\left(E_b^* E_b - P_b^* P_b\right)$$
$$E_{a_{max}} = \frac{m_a}{m_b^2}\left(E_b^* E_b + P_b^* P_b\right) \qquad (8)$$

In principle the numerical integration of (6) is straightforward, but in practice the fact that the integrand is singular at $\varphi = 0, \pi$ (i.e., at the two limits of θ_a) poses some difficulty. To remove this problem, we replace θ_a with a new variable u, defined as follows:

$$\int \frac{d\theta_a}{\sin \alpha_b \sin \varphi} = u \qquad (9)$$

From (3b),

$$\sin \varphi = \frac{\sqrt{(\sin \theta_a \sin \alpha_b)^2 - (\cos \theta_a \cos \alpha_b - \cos \theta_b)^2}}{\sin \alpha_b \sin \theta_a}$$

thus

$$u = \int \frac{d \cos \theta_a}{\sqrt{(\sin^2 \alpha_b - \cos^2 \theta_b) + 2 \cos \theta_a \cos \alpha_b \cos \theta_b - \cos^2 \theta_a}}$$

Furthermore note that if we keep E_a constant in the above integration, then by Eq. (3a) α^* is constant, and by Eq. (3c) α_b is constant. Thus all terms in the above integrand are constant except $\cos \theta_a$. We can rewrite

$$u = \int \frac{dx}{\sqrt{(x_{max} - x)(x - x_{min})}} \qquad (10)$$

where $x = \cos\theta_a$; $x_{max} = \cos\theta_{a_{min}} = \cos(\theta_b - \alpha_b)$; and $x_{min} = \cos\theta_{a_{max}}$

$= \cos(\theta_b + \alpha_b)$.

The integral (10) is elementary:

$$u = 2\tan^{-1}\sqrt{\frac{x - x_{min}}{x_{max} - x}} \tag{11}$$

Solving for $x = \cos\theta_a$ in terms of u,

$$\cos\theta_a = \sin^2\frac{u}{2}\cos(\alpha_b - \theta_b) + \cos^2\frac{u}{2}\cos(\alpha_b + \theta_b) \tag{12}$$

The angle θ_a covers its full range as u goes from 0 to π. We can now rewrite the integral (6) in the convenient form

$$\frac{d^2\sigma}{dE_b d\Omega_b} = \frac{m_a}{2\pi P^*}\int_{E_{a_{min}}}^{E_{a_{max}}}\int_0^{\pi}\frac{d^2\sigma}{dE_a d\Omega_a}\,du\,\frac{dE_a}{P_a} \tag{13}$$

Our integrand now has no singularity and is extremely convenient for numerical integration. Thus, for fixed E_b, θ_b we do the following:

(a) Select E_a.

(b) For this E_a, use Eqs. (3a) and (3c) to calculate α_b.

(c) Select values of u between 0 and π.

(d) For each u, use Eqs. (12) to calculate θ_a and hence

$$\frac{d^2\sigma}{dE_a d\Omega_a}$$

(e) Integrate over u.

(f) Integrate over E_a between $E_{a_{min}}$, $E_{a_{max}}$ as defined in Eq. (8).

It is perhaps amusing to note that the variable u which so greatly simplifies our computation has a very simple interpretation. From Eq. (12) one easily obtains the formula

$$\cos \theta_a = \cos \theta_b \cos \alpha_b - \sin \theta_b \sin \alpha_b \cos u \qquad (14)$$

Hence u is just the angle between the decay plane of particle "a" and the production plane of particle "b" (i.e., the plane defined by the photon and particle "b" directions).

2. Special Case

We now consider the special situation in which the production cross section of particle "a" is such that there is a one-to-one relation between θ_a and E_a (this would be true if particle "a" were produced in two-body final states by monoenergetic photons). Thus the cross section is simply defined by $d\sigma/dE_a$ and

$$\frac{d^2\sigma}{dE_a d\Omega_a} = \left(\frac{d\sigma}{dE_a}\right) \frac{\delta\left[\theta_a - \theta'_a(E_a)\right]}{2\pi \sin \theta'_a} \qquad (15)$$

where $\theta'_a(E_a)$ is the single angle of emission corresponding to energy E_a.

We now substitute into Eq. (13)

$$\frac{d^2\sigma}{dE_b d\Omega_b} = \frac{m_a}{4\pi^2 P^*} \int_{E_{a\,min}}^{E_{a\,max}} \left(\frac{d\sigma}{dE_a}\right)\left(\frac{du}{d\theta_a}\right)_{\theta_a=\theta'_a} \frac{dE_a}{P_a \sin \theta'_a}$$

Using (14),

$$\frac{du}{d\theta_a} = \frac{\sin \theta_a}{\sin \theta_b \sin \alpha_b \sin u} = \frac{\sin \theta_a}{\sqrt{(\sin \theta_b \sin \alpha_b)^2 - (\cos \theta_b \cos \alpha_b - \cos \theta_a)^2}}$$

Hence

$$\frac{d^2\sigma}{dE_b d\Omega_b} = \frac{m_a}{4\pi^2 P^*} \int_{E_{a_{min}}}^{E_{a_{max}}} \left(\frac{d\sigma}{dE_a}\right) \frac{dE_a}{P_a \sqrt{(\sin\theta_b \sin\alpha_b)^2 - (\cos\theta_b \cos\alpha_b - \cos\theta'_a)^2}} \tag{16}$$

where in the above integrand α_b is a function of E_a through Eqs. (3a) and (3c), and $\theta'_a = \theta'_a(E_a)$ is related to (E_a) through the production reaction of particle "a". In carrying out the integral (16), one must be careful to cover only whatever range of E_a (between $E_{a_{min}}$ and $E_{a_{max}}$) will lead to a positive term under the square root. At the limits of this variation (if these lie within $E_{a_{min}}$ and $E_{a_{max}}$) the integrand is again singular. No simplification such as was made before by use of a transformation of a dummy variable can be made until the explicit form of $\theta'_a(E_a)$ is written down. If such an explicit form is obtained, then the feasibility of conveniently removing the singularity depends upon being able to integrate in closed form,

$$W = \int \frac{dE_a}{P_a \sqrt{(\sin\theta_b \sin\alpha_b)^2 - (\cos\theta_b \cos\alpha_b - \cos\theta'_a)^2}}$$

and thus using W as a new dummy variable:

$$\frac{d^2\sigma}{dE_b d\Omega_b} = \frac{m_a}{4\pi^2 P^*} \int_{W_{min}}^{W_{max}} \left(\frac{d\sigma}{dE_a}\right) dW \tag{17}$$

3. Three-Body Decays

We now generalize Eq. (13) slightly to include the possibility that the particle "a" decays by a three-body mode into, say, particles "b", "c", and "d". Again let us ask for the cross section

$$\frac{d^2\sigma}{dE_b d\Omega_b}$$

This problem differs from that treated in Section 1 only in that P^* is no longer a constant but must be integrated over. In actual fact, even for the two-body decay of a short-lived resonance, the large width implies a distribution in P^* corresponding to a resonance shape for the mass of particle "a". In this sense the result to be obtained is also a more correct representation of the two-body decays.

Let the distribution of P^* be given by $F(P^*)dP^*$. Then we have, as the generalization of (13),

$$\frac{d^2\sigma}{dE_b d\Omega_b} = \frac{m_a}{2\pi} \int_0^{P^*_{max}} \frac{F(P^*)dP^*}{P^*} \int_{E_{a_{min}}}^{E_{a_{max}}} \frac{dE_a}{P_a} \int_0^{\pi} \left(\frac{d^2\sigma}{dE_a d\Omega_a}\right) du \qquad (18)$$

where the P^* dependence of the integrand is not only the explicit one appearing above but also through $E_{a_{max}}$, $E_{a_{min}}$ as shown by Eq. (8).

THE USE OF HYDROGEN BUBBLE CHAMBERS AT SLAC

by

George Trilling

August, 1962

I. GENERAL CONSIDERATIONS

If one assumes the validity of the Drell calculations, a hydrogen bubble chamber in a secondary-particle beam at SLAC may be a very valuable tool. It is likely that by 1966 or 1967 the energy region between 0 and 10 Bev will have been extensively explored by the large bubble chambers at Brookhaven and at CERN. It therefore seems reasonable to suppose that the secondary beams of interest obtained from the Monster will initially be in the 10-20 Bev range and eventually higher when 45 Bev operation is achieved.

In the considerations that follow, I shall assume (a) that production of various secondary particles of interest is sufficiently copious so that at pulsing rates of, say, one per second an adequate yield is available; and (b) that separation techniques will have been developed which yield reasonably pure beams of interesting particles.

The enormous contributions made up to now by hydrogen bubble chambers have been largely attributable to the possibility of analyzing individual events in all their detail, i.e., obtaining the energies, directions, and identities of all secondary particles. As the primary energy increases this becomes more difficult for the following reasons:

(a) The identities of particles become more difficult to determine. This is caused by two effects: (i) there are more particles and hence more hypotheses from which a correct choice must be made; (ii) the rest masses of the particles enter in the energy-conservation equation through the factor $P^2 + m^2 \approx P + m^2/2P$. As the momentum P increases, the total energy becomes insensitive to the mass. Furthermore, bubble density is not likely to be very useful at very high energies. These difficulties are solvable provided the precision of momentum and angular measurement in the chamber is sufficiently good. How good and whether such quality is achievable will be considered further in this report.

(b) The probability of producing one or more undetectable neutral secondaries (including neutrons, π^o, γ from Σ^o; but not including Λ^o or K^o, whose decays are detectable) increases with energy. In principle, if just one single neutral is produced there are enough constraints to permit complete analysis of the interaction; however, as will be shown later, the interactions with no unseen neutrals will by far be the easiest to analyze, and the feasibility of handling those with one neutral will depend greatly on the configuration of the specific interaction.

In order to alleviate somewhat the difficulty presented in (b), we propose to use an array of parallel converter plates at one end of the bubble chamber to permit detection and measurement of π^o secondaries. Because of the forward collimation at high energies, this array need only be at the beam-exit end of the chamber and still can intercept most of the π^o. The details and characteristics for such an array are considered in Appendices II and III.

In the discussion that follows we consider the required characteristics for a hydrogen bubble chamber to be used for the kinematic analysis of individual events. The formulae used for the computation of momentum and angular errors are discussed in Appendix I. Also, in part C of Appendix I, we list the parameters such as coordinate accuracy, magnetic field, etc., which we assume are physically realizable and which are used as the basis for all other calculations in this report.

II. DETERMINATION OF BUBBLE CHAMBER CHARACTERISTICS

A. Strange Particle Decay Mean Free Paths

The mean decay lengths for various particles for energies up to 30 Bev are listed in Table I. It is clear that if Λ, K^o, Σ and Ξ decays are to be observed with reasonable efficiency a decay distance of the order of at least 1 meter should be available. What additional distance must be allowed for accurate angle and momentum measurements on the particles will be considered further.

TABLE I

MEAN DECAY LENGTHS OF SOME STRANGE PARTICLES

Particle	Momentum 5 Bev/c	10 Bev/c	20 Bev/c	30 Bev/c
K_1^o	26 cm	52 cm	105 cm	157 cm
Λ^o	34 cm	67 cm	134 cm	202 cm
Σ^+	10 cm	20 cm	40 cm	60 cm
Σ^-	20 cm	40 cm	80 cm	120 cm
Ξ^-	15 cm	30 cm	59 cm	89 cm

B. Linear Momentum Balance for Interactions with Charged Secondaries

We wish to analyze events in which all secondaries are detected and measured. The question which arises is: How well can we tell that there are no undetected neutral secondaries? We rely for the answer upon linear momentum balance (energy balance also gives information, but since it depends on the assumed identities of the particles, we disregard it here).

Consider first longitudinal momentum balance. Assume that the momentum of the beam particles can be determined from the beam-transport characteristics and hence the only problem is the measurement of the secondaries.

Assume for simplicity that there are only charged secondaries, for which estimates of measurement uncertainties are given in Appendix I. Suppose that the chamber is large enough so that the charged secondaries have track lengths $\geq$ 1 meter. According to the error formulae, multiple-scattering dominates the momentum errors for particle energies $\leq$ 10 Bev, and hence we assume that the uncertainties in measured momentum are given by

$$\frac{\Delta P}{P} \approx \left(\frac{\Delta P}{P}\right)_{sc} = \frac{8 \times 10^{-3}}{\ell^{\frac{1}{2}}} \qquad \text{(Eq. 10b, Appendix I)}$$

Let us now be specific and assume that the initial momentum P is shared equally by n charged secondaries, each thus having a momentum $\approx P/n$. The total uncertainty in longitudinal momentum balance is

$$\Delta P \approx \sqrt{\Sigma(\Delta P_i)^2} = \frac{8 \times 10^{-3}}{\ell^{\frac{1}{2}}} \frac{P}{\sqrt{n}}$$

where uncertainties in the beam particle momentum have been neglected. Thus for P = 20 Bev/c, n = 4, and ℓ = 1 m, ΔP = $\pm$ 80 Mev/c. This represents a rather small uncertainty inasmuch as most of the secondaries in a 20-Bev interaction have energies of the order of several Bev.

We now consider transverse momentum balance, in which the situation is even more favorable. If we write down the relation satisfied in any one of the two directions transverse to the beam,

$$P_T \equiv \Sigma\, P_{Ti} \approx \Sigma\, P_i \theta_i = 0$$

and differentiate to obtain the total error,

$$\Delta P_T = \sqrt{\Sigma\, P_i^2 (\Delta\theta_i)^2 + \Sigma\, \theta_i^2 (\Delta P_i)^2}$$

now, roughly,

$$\theta_i = \frac{P_{Ti}}{P_i}$$

where P_{Ti} tends to average around 500 Mev/c independently of P_i. Thus the term

$$\theta_i \, \Delta P_i = P_{Ti} \frac{\Delta P_i}{P_i} \approx 500 \left(\frac{8 \times 10^{-3}}{\ell^{\frac{1}{2}}} \right) \approx 4 \text{ Mev/c}$$

for $\ell = 1$ meter. The interesting point here is that this error does not rise with increasing P_i (because of the constancy of P_{Ti}) as the longitudinal error does. The other term

$$P_i \, \Delta\theta_i \approx P_i (\Delta\theta_i)_{sc} \approx P_i \frac{2 \times 10^{-3} \, \ell^{\frac{1}{2}}}{P_i} = 2 \times 10^{-3} \, \ell^{\frac{1}{2}}$$

For $\ell = 1$ meter, this term ≈ 2 Mev/c. Thus for, say, four secondary particles, $\Delta P_T \approx 10$ Mev/c. Again, if we compare this to the average transverse momentum for a particle of ≈ 500 Mev/c, we note that there should be no problem in discriminating against events with undetected neutrals. We also note that for the transverse-momentum test we need no precise knowledge of the beam momentum.

C. Energy Balance

We now consider the following fundamental question. Assume that by momentum-balance arguments we have established that there are no undetected neutrals. Can we use energy balance to determine the identities of the

secondaries without having to have recourse to bubble density, which is not likely to be very helpful at the energies involved? In the limit of high energies, the energy-balance equation can be written in the form

$$P + \frac{m^2}{2P} + M = \Sigma\, P_i + \Sigma\, \frac{m_i^2}{2P_i}$$

where P and m are the beam particle momentum and mass, M is the nucleon mass, and P_i, m_i are the secondary-particle momentum and mass. Now in satisfying momentum balance we have constrained P, P_i to fit the equation

$$P = \Sigma\, P_i \cos\theta_i \approx \Sigma\, P_i - \Sigma\, P_i\, \frac{\theta_i^2}{2}$$

Combining this with the energy-balance equation, we obtain

$$M + \frac{m^2}{2P} = \Sigma\left(\frac{m_i^2}{2P_i} + P_i\, \frac{\theta_i^2}{2}\right)$$

Define

$$\Delta E \equiv \Delta\left[\Sigma\left(\frac{m_i^2}{2P_i} + \frac{P_i\theta_i^2}{2}\right) - \frac{m^2}{2P}\right]$$

as the uncertainty in energy balance caused by measurement errors.

$$(\Delta E)^2 = \Sigma\left[\Delta P_i\left(\frac{\theta_i^2}{2} - \frac{m_i^2}{2P_i^2}\right)\right]^2 + \Sigma\left(P_i\theta_i\Delta\theta_i\right)^2 + \left(\frac{m^2}{2P^2}\Delta P\right)^2$$

or

$$(\Delta E)^2 = \Sigma \left(\frac{\Delta P_i}{P_i}\right)^2 \left(\frac{P_{Ti}^2 - m_i^2}{2P_i}\right)^2 + \Sigma \left(P_{Ti}\Delta\theta_i\right)^2 + \left(\frac{m^2}{2P^2}\Delta P\right)^2$$

Let us again assume that the primary beam energy is well known and neglect the last term above. We consider the other terms. We also assume as before that the multiple-scattering errors dominate. The first term of interest is then

$$\Delta E_1 \equiv \sqrt{\Sigma \left(\frac{\Delta P_i}{P_i}\right)^2 \left(\frac{P_{Ti}^2 - m_i^2}{2P_i}\right)^2}$$

We take

$$\frac{\Delta P_i}{P_i} = 8 \times 10^{-3}\, \ell^{-\frac{1}{2}} \qquad \text{(Eq. 10b, Appendix I)}$$

$$P_i \approx \frac{P}{n} \qquad \text{(P = total momentum, and n = no. of particles)}$$

$$\left(P_{Ti}^2 - m_i^2\right)^2 \lesssim 1\ (\text{Bev})^2$$

Then

$$\Delta E_1 = \frac{8 \times 10^{-3}}{\ell^{\frac{1}{2}}} \frac{n^{3/2}}{2P}$$

If $\ell = 1$ m, P = 20 Bev/c, and n = 4, then

$$\Delta E_1 = 1.6 \text{ Mev}$$

The second term is the following:

$$\Delta E_2 = \sqrt{\Sigma \left(P_{Ti} \Delta\theta_i\right)^2}$$

Taking

$$\Delta\theta_i = 2 \times 10^{-3} \left(\ell^{\frac{1}{2}}/P_i\right) \qquad \text{(See Eq. 11b, Appendix I)}$$

we obtain

$$P_{Ti} \approx 0.5 \text{ Bev/c} \qquad P_i \approx P/n$$

$$\Delta E_2 = 2 \times 10^{-3} \ell^{\frac{1}{2}} (0.5) \frac{n^{3/2}}{P} = 10^{-3} \frac{\ell^{\frac{1}{2}} n^{3/2}}{P}$$

For the same parameters as above,

$$\Delta E_2 = 0.4 \text{ Mev}$$

Thus we estimate that a representative value of ΔE is about 2 Mev. We have to compare this with the effects of varying the identities of particles. Suppose for example that we wish to know if a certain $\pi^+ \pi^-$ pair could alternatively be a $K^+ K^-$ pair. Let us define $\Delta E'$ as the change in the quantity $\Sigma \left(m_i^2/2P_i\right)$ by virtue of changes in the assumed identities of the particles. Thus if we change a pair of $\pi^\pm$ to a pair

of $K^{\pm}$, we have

$$\Delta E' = \left(m_K^2 - m_\pi^2\right)\left[\frac{1}{2P_1} + \frac{1}{2P_2}\right]$$

where P_1, P_2 are the momenta of the two π or K particles. To be specific let $P_1 = P_2 = 5$ Bev/c; then

$$\Delta E' = \frac{\left(.5^2 - .14^2\right)}{5} = 0.046 \text{ Bev} = 46 \text{ Mev}$$

In comparison to this, the error of 2 Mev calculated above is very small. It thus appears that the identification of the secondaries is not a serious problem.

A variant of this sort of problem which is the one more commonly encountered in present lower energy experiments is the following. Because the momenta of two non-identical secondaries are nearly equal, there is no way of telling which is which. Thus suppose we have two secondaries of masses m_1, m_2 with momenta P_1, P_2 such that $P_1 - P_2$ is "small". Then the effect of interchanging the masses is

$$\Delta E'' = \frac{\left(m_1^2 - m_2^2\right)}{2}\left(\frac{1}{P_1} - \frac{1}{P_2}\right)$$

$$= \frac{m_1^2 - m_2^2}{2}\,\frac{P_2 - P_1}{P_1 P_2}$$

Take a specific example: $m_1 = M_K \approx 500$ Mev, $m_2 = m_\pi = 140$ Mev, $P_1 - P_2 = 4$ Bev/c; then

$$\Delta E'' = .007\left(P_2 - P_1\right)$$

Thus assuming that the ambiguity can be resolved if $\Delta E'' \approx 4$ Mev, we get as the least value of $P_2 - P_1$ for which a choice can be made about 600 Mev/c, i.e., the two momenta must not be within less than 15% of each other. This becomes still more favorable for lower momenta. The conclusion seems to be that in at least a substantial fraction of the events an unambiguous identification ought to be straightforward. It may seem surprising (it certainly was to me) that as one goes up to energies much higher than rest masses, kinematic fitting still permits unambiguous choices of hypotheses. The reason is that although the "signal" (i.e., in our previous calculations the quantities $\Delta E'$ and $\Delta E''$) indeed gets small as the energy increases, so does the "noise" ΔE, with the consequence that the signal-to-noise ratio does not change much with energy, for a fixed set of chamber parameters. On the other hand, we are here considering the design of a large chamber and hence are not necessarily subject to the present ambiguities in low- or intermediate-energy experiments with small chambers.

D. Interactions with Detectable Neutral Secondaries

In our previous considerations we have used error formulae appropriate to the measurement of charged tracks. We now consider what characteristics we need to handle satisfactorily interactions in which Λ^o or K^o particles or π^o mesons are emitted.

Consider first Λ^o and K^o particles, whose momentum errors we have already crudely estimated in formulae (14), Appendix I. The conclusions drawn from these estimates are that for visible lengths of secondary track of order 20 cm, the angular measurements coupled with the decay kinematics can yield very accurate K^o momenta ($\approx 2\%$ at 10 Bev/c) and somewhat less accurate Λ^o momenta ($\approx 9\%$ at 10 Bev/c). Since generally these errors do not cumulate (i.e., there is usually at most one Λ^o per interaction), and furthermore since one has relatively little worry about identification ambiguities, this kind of accuracy seems adequate. In other words, if we allow beyond the decay length of the V^o particle about 20 cm of secondary track, this would seem to provide adequate precision. If we wish to, we can always be a little selective and only use,

say, events with Λ^o decay lengths short enough to permit measurements on the secondaries of greater precision.

We now consider π^o meson emission and consider the design of a detector such as that described in Appendix III. The appropriate formulae, given in Appendices II and III, permit calculation of the properties of a suitable array of converter plates, given what precision is required for the π^o energy determination.

Simple calculations similar to those previously made in Section II.C show that as long as we are not dealing with many π^o, an energy accuracy of 6% is adequate to permit identification of the charged secondaries by energy conservation. This is somewhat poorer than the precision for charged tracks, but this is partly counterbalanced by (a) the unambiguity as to the identity of the π^o, and (b) the assumption that with this instrument one will concentrate on interactions with charged particles and detectable (i.e., Λ^o, K^o) neutral particles, with at most one, two or perhaps three π^o. If we then accept this 6% figure, and use equation (18) from Appendix II, with $\cos \theta^* = 0.5$ as a representative value, the required photon energy precision is about 17%. If we optimize for a photon energy of $\approx$ 2 Bev, and require four radiation lengths of converter ($\approx$ 95% efficiency per photon), then from equations (7) and (8) in Appendix III we obtain an array consisting of 18 plates, each 0.22 radiation lengths thick, separated by 9 cm gaps with a total length of about 1.7 meters.

E. Four-Constraint vs One-Constraint Fits

In low-energy bubble chamber work, the domain of interesting events is by no means confined just to those for which all secondaries are "visible". Indeed events with one neutral, "invisible" (i.e., not detectable by decay into charged secondaries) secondary such as one π^o have been of great interest; for instance the ω and η particles would never have been found if it were not for the study of such reactions. From a measurement-problem point of view, these events pose the problem that the momentum of the unseen neutral must be obtained by the momentum conservation law (rather than by direct measurement), and hence can be

subject to a rather large error. By contrast, in the events with no unseen secondaries, the momenta can all be directly measured, and then fitted, the conservation laws being used to reduce the errors in the poorest of the measurements. A second great simplification for such events is the quantization of hypotheses: the masses can only assume discretevalues, whereas with unseen neutrals the mass of the "neutral system" (i.e., all the unseen particles) can, if there is more than one neutral, have a continuum set of values. The problem of unambiguous interpretation becomes enormous, and it is for that reason that we have considered the use of a converter-plate array for detecting π^{o}. One cannot make any general rule that reactions with one unseen particle will or will not be unambiguously identifiable: this depends very much on the details of the particular event. Thus if one unseen neutral particle takes off a very large momentum, its identification will be easy because the fractional error in its momentum, as determined from momentum conservation, will be small; on the other hand, if it has low momentum, identification will be hard. A somewhat intermediate situation exists if the primary beam is a neutral beam, well determined in direction but poorly determined in momentum (three-constraint fit). If all secondaries are seen, there should not be great difficulty in identifying the reaction, although the removal of one constraint implies somewhat lower precision in the analysis. The detailed analysis of this question requires much more study.

F. Suggested Bubble Chamber Parameters

The considerations gone into in some detail in this report lead to the following general sort of bubble chamber design:

1. Length

Allowing about 1 meter for decay and about 25 cm more for measurement, and assuming that the average interaction takes place in the middle of the useful hydrogen volume, we obtain a length of 2.5 meters. To this we add about 2 meters of converter-plate array to make a total over-all length of 4.5 meters. A possible alternative might be to have the π^{o} array as part of a separate spark chamber: at this point I doubt if there would be great advantage in this, but it should be studied more carefully.

2. Width

From present CERN data on 16 Bev π interactions, we estimate a width and depth of about 1 meter would catch most of the π^{o} in the converter array, and would keep the energetic secondaries in the chamber to permit accurate momentum measurement.

3. Magnetic Field

From all we have said, it appears that if the sort of measurement accuracy postulated can be achieved, a conventional field of about 20 kgauss will be adequate. Since the length has been determined from decay mean free paths of strange particles, there would be no great gain (insofar as shortening the chamber is concerned) by using a high field from, say, a superconducting magnet. This is not true for the part of the chamber occupied by the converter array. The required length of this array for a given precision and conversion efficiency goes as $1/\sqrt{H}$. Thus a forty kilogauss field would permit a shortening of about 60 cm. Another point, however, requires mention here. A conventional magnet to provide a field of 20 kilogauss over a chamber such as the one discussed will require about 5 to 10 Mw (depending on details of design) of dc power. The operating cost for running such a chamber continuously is substantial. It may be that at the time of detailed design, the development of superconducting magnets will have reached a state of engineering practicality, in which case their usage should definitely be considered. Although their initial cost is high, they could lead to a large saving of operating cost over a period of several years.

III. CONCLUSIONS

From the analysis made in this report we now draw the following very preliminary conclusions.

If the intensities of secondary beams at high energies and the separator development lead to reasonable yields on the basis of continuous operation at the rate of about one pulse per second, a bubble chamber would seem to be a very useful tool. We have shown that a chamber about 5 meters long and 1 meter in each transverse dimension would be about right, provided great care were taken to insure the best possible conditions of performance insofar as the precision of coordinate measurement is concerned. For these dimensions, we have assumed that about 2 meters are used for an array of perhaps 20 plates, each about 1/5 radiation length thick to permit efficient detection of π^0 mesons and accurate determination of their directions and energies. We have seen furthermore that a conventional magnetic field would be adequate, but a superconducting magnet would permit some size reduction (although not a great deal because the decay lengths of strange particles principally determine the size), and possibly a substantial reduction of the operating power cost. The planning for such a chamber should include the assumption of essentially continuous operation, except for shutdowns and servicing periods. If such a chamber were indeed constructed, one would have to allocate to it on a permanent basis an adequate amount of beam-handling equipment, power, etc., which would then be totally unavailable to other experiments. The construction and operating cost of such equipment would have to be added to that of the bubble chamber itself to obtain a true picture of the total cost involved in this program. One can of course strongly question whether such an enormous investment ($\$1.5 \times 10^7$ for the chamber and magnet is a very rough guess) is worthwhile for a device which uses only about 1/360 of the accelerator time. The big questions here are: What fraction of the important physics can it do, and are there alternative techniques for doing the same thing? In particular one can consider an apparatus consisting of a hydrogen target and an array of very large magnetic spark chambers, which, at the very least, would have the advantage of operating on every pulse and hence would use magnets and power more efficiently. It is my own prejudice on

this that the ability to see the interaction point and its vicinity is an important and valuable feature of the bubble chamber approach and should not be given up too easily. Without this ability, a very much greater load is thrown on the precision-measurement capabilities of the detector. Futhermore the ability to select interesting events by scanning is strongly diminished, and the choice of interesting subgroups may require the measurement of all events, with consequent large expenditure of computer time and measuring-machine time.

We conclude by pointing out various directions in which more detailed studies of bubble chamber capabilities should be carried out to refine the rather rough considerations discussed in this report.

(1) One needs to know much better the measurement capabilities of large hydrogen chambers. Within less than a year both the Brookhaven and the British chamber will be operational, and will greatly supplement experience already gained with the Berkeley 72-inch chamber.

(2) The precision requirements for kinematic fitting have only been estimated roughly. This should be greatly improved by generating by Monte Carlo techniques, using all available information from CERN and Brookhaven on high-energy interactions, large numbers of events, putting in realistic measurement errors, and feeding them through fitting programs such as GUTS to determine more quantitatively the precision required for making unambiguous fits.

(3) It has been assumed that the chamber can pulse once per second. The Brookhaven chamber has been designed with that capability, and experience with it should show to what extent track quality is affected by such a pulsing rate. With such experience, it may be conceivable to design for more rapid rates, like perhaps four pulses per second. On the other hand, it may turn out that quality greatly deteriorates even at one pulse per second, in which case one would have to re-examine the yields.

(4) Calculations should be made to investigate in detail the possible usage of a superconducting magnet for the bubble chamber. Even for a conventional field ($\approx$ 20 kilogauss), the power saving over several years may make up for the high initial cost. Furthermore, if we have been over-optimistic in evaluating the precision capabilities of a very large

chamber, the use of a 40 or 50 kilogauss field from such a magnet could easily bring us back to our needed accuracy.

(5) Finally, I would suggest that running $\approx$ 20 Bev protons and π^- mesons from the A.G.S. into the large bubble chamber to see if detailed analyses such as we have discussed are indeed feasible would seem like a very useful experiment.

APPENDIX I

BUBBLE CHAMBER MEASUREMENT ACCURACY FORMULAE

A. Measurement Accuracy Neglecting Multiple Coulomb Scattering

Consider a track of length ℓ whose curvature and direction are determined by measurement of the coordinates y_1, y_2, y_3, z_1, z_3 shown in the sketches.

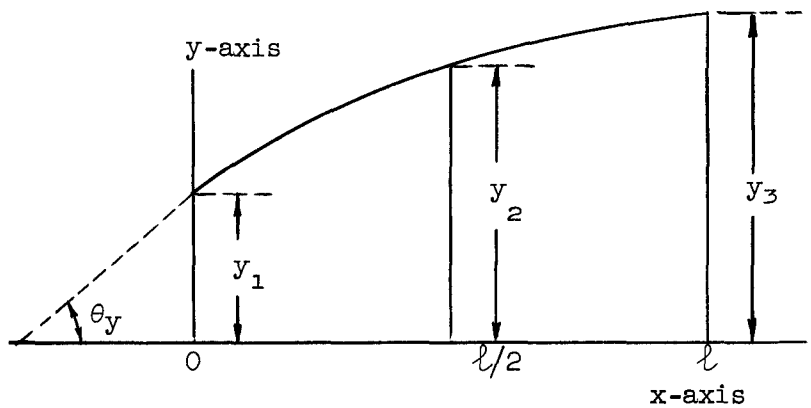

Projection of track on x-y plane

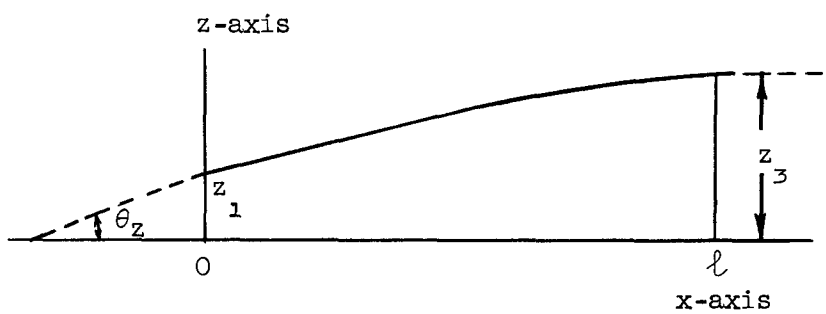

Projection of track on x-z plane

In order to make our analysis simple we make the following assumptions:

(1) The magnetic field H has no components in the x or y directions (the x-y plane is the plane of the window and of the film). It is simply a uniform field in the z-direction.

(2) The tracks are fairly much in the forward direction, and the angles θ_y and θ_z are small.

(3) The measurement errors (not including multiple Coulomb scattering) can be represented by errors of R.M.S. value δ in each of the coordinates y_1, y_2, y_3, and $S\delta$ in the coordinates z_1, z_3 where S is the stereo ratio determined by the lens geometry. This assumption is unquestionably a great simplification of the true situation, in which the coordinate errors depend upon such factors as position in the chamber, orientation of the track, etc. However, this model, though somewhat incorrect, permits rather simple calculations of expected precision.

With these assumptions in mind we can calculate various quantities of interest. The sagitta s is given by

$$s = \frac{y_1 + y_3}{2} - y_2$$

with error

$$\Delta s = \sqrt{1.5}\,\delta = 1.22\,\delta$$

The particle momentum P is given by

$$P = 3.75 \times 10^{-3} \frac{H\ell^2}{s} \qquad (1)$$

where P is in Bev/c, H is in kg, and ℓ and s are in meters. The corresponding error is

$$\frac{\Delta P}{P} = \frac{\Delta s}{s} = \frac{(325)P\delta}{H\ell^2} \qquad (2)$$

The angles θ_y and θ_z are given by

$$\theta_y = \frac{4y_2 - 3y_1 - y_3}{\ell} \tag{3a}$$

$$\theta_z = \frac{z_3 - z_1}{\ell} \tag{3b}$$

$$\Delta\theta_y = \sqrt{26}\,\frac{\delta}{\ell} = 5.1\,\frac{\delta}{\ell} \tag{4a}$$

$$\Delta\theta_z = \sqrt{2}\,S\,\frac{\delta}{\ell} = 1.4\,S\,\frac{\delta}{\ell} \tag{4b}$$

It is interesting to note that for stereo ratios of 4 or 5 (which are typical), $\Delta\theta_z$ is of the same order as $\Delta\theta_y$, although one might at first have expected a factor between them of the same magnitude as the stereo ratio. What makes up for the stereo ratio is the fact that the y-coordinate measurements have to yield <u>two</u> unknown parameters, namely θ_y and P, whereas the z-coordinate measurements yield just the one quantity θ_z.

B. <u>Multiple Scattering Errors</u>

Let the mean square projected scattering angle between tangents at the two ends of a track of length ℓ be given by

$$\langle \theta^2 \rangle = \eta^2 \ell$$

where the quantity η will be discussed below. It can then be shown that the mean square sagittal error due to multiple scattering is the

following:

$$< \Delta s^2 >_{sc} = \frac{\eta^2 \ell^3}{48} \tag{5}$$

Furthermore, the mean square angular errors are

$$< \Delta\theta_y^2 >_{sc} = \frac{\eta^2 \ell}{6} \tag{6a}$$

$$< \Delta\theta_z^2 >_{sc} = \frac{\eta^2 \ell}{3} \tag{6b}$$

It may appear paradoxical that the scattering angular errors seem to be anisotropic. In fact, the anisotropy comes from the effect of the magnetic field, which leads to very different formulae for θ_y and θ_z (namely 3a, 3b). The above scattering errors are based on the use of these formulae for the calculations.

We now consider the evaluation of η. From Barkas and Rosenfeld,

$$\sqrt{< \theta^2 >} = \frac{.015}{P\beta} (1 + \epsilon)\sqrt{\frac{\ell}{L_R}} \tag{7}$$

where L_R is the radiation length, and ϵ is a correction factor. For long tracks in liquid hydrogen we take $\epsilon = -0.14$ and $L_R = 9.9$ m. Consequently,

$$\eta = \frac{.015}{P\beta} \frac{(1 + \epsilon)}{\sqrt{L_R}} = \frac{4.1 \times 10^{-3}}{P\beta}$$

We now use this value of η to calculate the momentum and directional

uncertainties caused by multiple scattering.

For the momentum error we have

$$\left(\frac{\Delta P}{P}\right)_{sc} = \frac{0.16}{\beta H \ell^{\frac{1}{2}}} \tag{8}$$

and for the directional errors:

$$(\Delta\theta_y)_{sc} = 1.7 \times 10^{-3} \frac{\ell^{\frac{1}{2}}}{P\beta} \tag{9a}$$

$$(\Delta\theta_z)_{sc} = 2.3 \times 10^{-3} \frac{\ell^{\frac{1}{2}}}{P\beta} \tag{9b}$$

C. Specific Error Calculation

We now put down specific values for the parameters which enter into the above errors and which we assume are applicable to a practically realizable bubble chamber:

$$H = 20 \text{ Kilogauss}$$
$$\delta = 50\ \mu = 5 \times 10^{-5} \text{ m}$$
$$\beta = 1$$

Furthermore, for simplicity we choose a stereo ratio S such as to equalize θ_y and θ_z errors:

$$S = \frac{5.1}{1.4} = 3.6$$

and we represent the multiple scattering angular error either in the x-y or the x-z plane by the single expression

$$2 \times 10^{-3} \frac{\ell^{\frac{1}{2}}}{P\beta}$$

We now summarize the resulting error formulae:

momentum measurement error $$\left(\frac{\Delta P}{P}\right)_m = 8 \times 10^{-4} \frac{P}{\ell^2} \qquad (10a)$$

scattering error $$\left(\frac{\Delta P}{P}\right)_{sc} = \frac{8 \times 10^{-3}}{\ell^{\frac{1}{2}}} \qquad (10b)$$

angular measurement error $$(\Delta\theta)_m = \frac{2.5 \times 10^{-4}}{\ell} \text{ (radians)} \qquad (11a)$$

scattering error $$(\Delta\theta)_{sc} = 2 \times 10^{-3} \frac{\ell^{\frac{1}{2}}}{P} \qquad (11b)$$

D. Measurement Accuracy for Neutral Strange Particles

We wish to consider here how much length of track we need after decay of a neutral strange particle in order to measure its momentum with reasonable precision. For this purpose we consider decays with long decay lengths (if the decay length is short, then the situation is essentially the same as with charged tracks coming right from the production point) and assume that the direction of the V^o-particle is determined with negligible error (note that the absence of multiple scattering and curvature greatly reduces the errors below the levels discussed in A and B). We now consider two independent methods of obtaining the momentum: (a) the angles of the secondaries with respect to the V line of flight plus the known decay kinematics, (b) the vector sum of the measured secondary momenta. In principle the most precise approach would be one of fitting all the information by least-squares methods. We shall approximate this by simply combining the results of (a) and (b) properly weighted in relation to the errors.

(a) The appropriate notation for the decay in both the lab and the c.m. system are shown in the sketch.

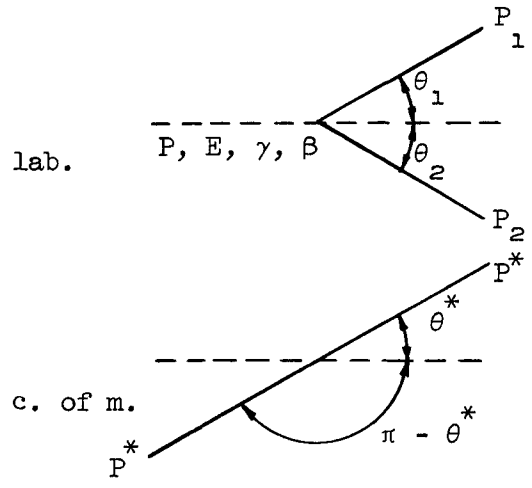

We first consider the problem: given θ_1, θ_2 with errors determined by the uncertainties in the directions of secondary particles 1 and 2, how accurately can we determine the momentum **P**?

By Lorentz transformation formulae,

$$\tan \theta_1 = \frac{\sin \theta^*}{\gamma(\cos \theta^* + \frac{\beta}{\beta_1^*})}$$

$$\tan \theta_2 = \frac{\sin \theta^*}{\gamma(-\cos \theta^* + \frac{\beta}{\beta_2^*})}$$

We now make the simplifying approximation that $\beta \approx 1$, $\theta_1 \approx \tan \theta_1$, $\theta_2 \approx \tan \theta_2$. Then we can solve the above equations to obtain

$$\cos \theta^* = \left(\frac{\theta_2}{\beta_2^*} - \frac{\theta_1}{\beta_1^*}\right) \frac{1}{(\theta_1 + \theta_2)}$$

$$P = \frac{M}{\theta_1} \left(\frac{\sin \theta^*}{\cos \theta^* + \frac{1}{\beta_1^*}}\right)$$

To simplify further consider $\theta^* \approx \pi/2$. In that limit

$$\frac{\Delta P}{P} \approx \frac{P}{M}(\beta_1^* + \beta_2^*)\left[\left(\frac{\beta_2^*}{\beta_1^*}\Delta\theta_1\right)^2 + \left(\frac{\beta_1^*}{\beta_2^*}\Delta\theta_2\right)^2\right]^{\frac{1}{2}} \tag{12}$$

We now apply this result to Λ^o and K^o. For Λ^o,

$$\left(\frac{\Delta P}{P}\right)_\Lambda \approx 7.2\ (\Delta\theta_p)P \tag{13a}$$

where $\Delta\theta_p$ is the proton angular error. For the K^o,

$$\left(\frac{\Delta P}{P}\right)_{K^o} = 1.7\ (\Delta\theta_\pi)P \tag{13b}$$

where $\Delta\theta_\pi$ is an average angular error for each of the π mesons.

Assuming that the measurement (and not the scattering) angular error is dominant, we substitute for $(\Delta\theta_p)$ and $(\Delta\theta_\pi) = 2.5 \times 10^{-4}/\ell$ and obtain:

$$\left(\frac{\Delta P}{P}\right)_\Lambda = \frac{1.8 \times 10^{-3}}{\ell} P \tag{14a}$$

$$\left(\frac{\Delta P}{P}\right)_K = 4.2 \times 10^{-4} \frac{P}{\ell} \tag{14b}$$

It is clear that for ℓ as low as 0.1 meter, the precision for K^o mesons is excellent, whereas that for Λ^o is about four times poorer.

(b) We consider momentum errors in simple vector-momentum addition. If ℓ is short enough that multiple scattering is not the limiting

error we have

$$\left(\frac{\Delta P}{P}\right)_{\Lambda \text{ or } K} = \frac{8 \times 10^{-4}}{\ell^2} P \qquad (15)$$

The errors from (a) and (b) are comparable for $\ell \approx 0.4$ m for Λ^o and $\ell \approx 2$ m for K^o. For lower ℓ values, method (a) always gives higher precision.

APPENDIX II

DETERMINATION OF THE DIRECTION AND ENERGY OF NEUTRAL PIONS FROM MEASUREMENTS OF THE ENERGIES OF THE DECAY PHOTONS

We consider the following problem: we have a π^o that decays into two photons which we detect and whose energies we measure. For given errors in the photon energy measurements, how accurately do we know the π^o energy and direction? We assume that the directions of the photons are known with high precision, and that only the energy uncertainties need be considered. If we use the known π^o decay kinematics, the problem is overconstrained and we can make a least-squares fit to obtain the most precise possible answer.

First we introduce appropriate symbols as follows:

β, P, E = velocity, momentum, total energy of incoming pion

θ = opening angle between the two photon directions

ξ = angle between π^o direction and line bisecting the angle θ

P_1, P_2 = momenta of the two photons

θ^* = angle between π^o direction and direction of photon #1 in the π^o rest system

P_{1m}, P_{2m} = measured momenta of the photons

ΔP_1, ΔP_2 = R.M.S. errors in the measured values of the photon momenta

m = π^o mass

Next we put down the following convenient relations for π^o decay kinematics:

$$\beta = \frac{\cos \theta/2}{\cos \xi} \tag{1}$$

$$\cos \theta^* = \frac{\sin \xi}{\sin \theta/2} \tag{2}$$

$$\cot \frac{\theta}{2} = \frac{P}{m} \sin \theta^* \tag{3}$$

$$P_1 = \frac{E}{2} + \frac{P}{2} \cos \theta^* \tag{4}$$

$$P_2 = \frac{E}{2} - \frac{P}{2} \cos \theta^* \tag{5}$$

Now we are given θ and P_{1m}, P_{2m} (the measured values of P_1 and P_2), and our task is to determine P and ξ (note that since we know the photon directions exactly, ξ just gives the direction of the π^o).

Now we can combine (1) and (2) with (4) and (5) to obtain relations for P_1 and P_2 which depend only on ξ, i.e., we can write $P_1(\xi)$ and $P_2(\xi)$ (taking θ to be a fixed parameter in our calculation). Then we define the following quantity L:

$$L = \frac{\left[P_{1m} - P_1(\xi)\right]^2}{2(\Delta P_1)^2} + \frac{\left[P_{2m} - P_2(\xi)\right]^2}{2(\Delta P_2)^2} \tag{6}$$

The best value of ξ is obtained by minimizing L, i.e., solving $\partial L/\partial \xi = 0$. The error in this value of ξ, $\Delta\xi$ can then be approximated by

$$\Delta\xi = \left(\frac{\partial^2 L}{\partial \xi^2}\right)^{-\frac{1}{2}} \tag{7}$$

We carry out these operations:

$$\frac{\partial L}{\partial \xi} = -\left[\frac{P_{1m} - P_1(\xi)}{(\Delta P_1)^2}\right]\frac{dP_1}{d\xi} - \left[\frac{P_{2m} - P_2(\xi)}{(\Delta P_2)^2}\right]\frac{dP_2}{d\xi} \tag{8}$$

$$\frac{\partial^2 L}{\partial \xi^2} = \frac{1}{(\Delta P_1)^2}\left(\frac{dP_1}{d\xi}\right)^2 + \frac{1}{(\Delta P_2)^2}\left(\frac{dP_2}{d\xi}\right)^2 \tag{9}$$

where, in (9), we have averaged to zero terms involving $\left[P_{1m} - P_1(\xi)\right]$, $\left[P_{2m} - P_2(\xi)\right]$.

It now remains to evaluate $dP_1/d\xi$, $dP_2/d\xi$. Using (2), (4) and (5),

$$\frac{dP_1}{d\xi} = \frac{P}{2}\frac{\cos\xi}{\sin\theta/2} + \left(\frac{P}{2E} + \frac{\sin\xi}{2\sin\theta/2}\right)\frac{dP}{d\xi} \tag{10}$$

$$\frac{dP_2}{d\xi} = -\frac{P}{2}\frac{\cos\xi}{\sin\theta/2} + \left(\frac{P}{2E} - \frac{\sin\xi}{2\sin\theta/2}\right)\frac{dP}{d\xi} \tag{11}$$

But

$$\frac{dP}{d\xi} = \frac{dP}{d\beta}\frac{d\beta}{d\xi} = m\,\gamma^3\,\beta\,\tan\xi$$

Furthermore, from (1) (2), and (3),

$$\tan\xi = \frac{\beta\cos\theta^*}{\cot\theta/2} = \frac{\cot\theta^*}{\gamma}$$

Thus

$$\frac{dP}{d\xi} = m\,\gamma^2\,\beta\cot\theta^* \tag{12}$$

Finally, from (10), (11) and (12), using (1), (2), (3)

$$\frac{dP_1}{d\xi} = \frac{m\gamma^2\beta}{2}\left[\sin\theta^* + (\beta + \cos\theta^*)\cot\theta^*\right] \tag{13}$$

$$\frac{dP_2}{d\xi} = \frac{m\gamma^2\beta}{2}\left[-\sin\theta^* + (\beta - \cos\theta^*)\cot\theta^*\right] \tag{14}$$

These can still further be simplified into the convenient forms

$$\frac{dP_1}{d\xi} = \frac{P\,P_1}{m\sin\theta^*} \tag{15}$$

$$\frac{dP_2}{d\xi} = \frac{-P\,P_2}{m\sin\theta^*} \tag{16}$$

From the above and (7), (9) we get our error in the π^o direction:

$$(\Delta\xi) = \frac{m\sin\theta^*}{P}\,\frac{1}{\sqrt{\left(\frac{P_1}{\Delta P_1}\right)^2 + \left(\frac{P_2}{\Delta P_2}\right)^2}} \tag{17}$$

The corresponding uncertainty in the π^o momentum is

$$(\Delta P) = \frac{dP}{d\xi}\Delta\xi = \frac{E\cos\theta^*}{\sqrt{\left(\frac{P_1}{\Delta P_1}\right)^2 + \left(\frac{P_2}{\Delta P_2}\right)^2}} \tag{18}$$

These are the results we wished to obtain. It is interesting to note that for $\cos \theta^*$ near zero the momentum uncertainty goes to zero. This is a consequence of the fact that in that circumstance the momentum depends almost exclusively on the opening angle θ, and very little on how the energy divides itself between the two photons. It is shown in the discussion on π^o detection by means of arrays of thin converters that the errors calculated by (17) and (18) are much less than those obtained if the π^o kinematic fitting is neglected.

APPENDIX III

THE DESIGN OF A PARALLEL PLATE ARRAY FOR STUDYING π^{o} SECONDARIES OF ENERGETIC INTERACTIONS

We discuss here some of the considerations affecting the design of an array of thin parallel converting plates placed at one end of a hydrogen bubble chamber for the purpose of detecting, and measuring the energy and direction π^{o} secondaries from interactions taking place upstream in the chamber.

A. General Considerations

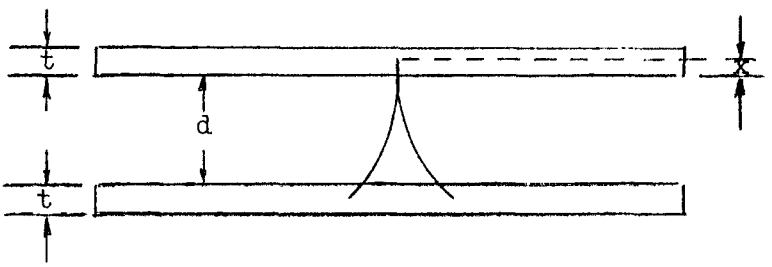

We assume that we have an array of plates, each of thickness t, separated surface-to-surface by a distance d. Suppose that a photon of momentum P converts at a distance x from the beginning of a gap ($x < t$) into a positron-electron pair in which the individual momenta are P_a and P_b. By measuring the curvatures of the tracks in the first gap, we determine experimentally P'_a, P'_b the momenta of the electrons in the gap. The total momentum of the photon is then given by

$$P = P'_a + P'_b + x\left(\frac{dP_a}{dx} + \frac{dP_b}{dx}\right) \tag{1}$$

The error in P is

$$(\Delta P)^2 = (\Delta P'_a)^2 + (\Delta P'_b)^2 + (\Delta x)^2\left(\frac{dP_a}{dx} + \frac{dP_b}{dx}\right)^2 + x^2\left[\left(\Delta\frac{dP_a}{dx}\right)^2 + \left(\Delta\frac{dP_b}{dx}\right)^2\right] \tag{2}$$

We consider each of these sources of error in turn.

(1) $\Delta P_a'$; $\Delta P_b'$ terms.

It has been shown in Appendix I that the momentum-measurement errors in a hydrogen chamber with 50μ coordinate accuracy and a field of 20 kg are

$$\frac{\Delta P_m}{P} = 8 \times 10^{-4} \frac{P}{d^2} \qquad \text{(for errors due to setting inaccuracy, turbulence, etc.)}$$

$$\frac{\Delta P_s}{P} = 8 \times 10^{-3} d^{-\frac{1}{2}} \qquad \text{(for multiple scattering in the hydrogen)}$$

where P is in Bev/c, and d is in meters.

These errors are equal when $P = 10d^{3/2}$ Bev/c. As we will see, $d \approx 0.1$ m will be reasonable, so that $P \approx 300$ Mev/c. Hence except for low momenta the setting error will usually dominate, and we will, for simplicity, neglect the scattering error. The total error from this source will then be

$$(\Delta P_1)^2 \equiv (\Delta P_a')^2 + (\Delta P_b')^2$$

$$= \left(\frac{8 \times 10^{-4} p^2}{d^2}\right)^2 \left[\lambda^4 + (1 - \lambda)^4\right]$$

where P is now the total photon momentum, $\lambda = P_a/P$, and $1 - \lambda = P_b/P$. If we make the approximation that λ is uniformly distributed, then the mean value of $\lambda^4 + (1 - \lambda)^4 = 0.4$, and the R.M.S. error becomes

$$\frac{\Delta P_1}{P} = 5 \times 10^{-4} \frac{P}{d^2} \qquad (3)$$

(2) $\Delta x \left(\frac{dP_a}{dx} + \frac{dP_b}{dx} \right)$ terms.

This error arises from our uncertainty as to precisely where, in the plate, the conversion of the photon occurred. If we assume that it occurred at the center of the plate, the maximum error in x is $t/2$, and the R.M.S. error is $t/2\sqrt{3} = 0.3\ t$.

If we now put

$$\frac{dP_a}{dx} = \frac{P_a}{L_R} \quad ; \quad \frac{dP_b}{dx} = \frac{P_b}{L_R}$$

where L_R is the radiation length of the plate material,

$$\frac{dP_a}{dx} + \frac{dP_b}{dx} = \frac{P_a + P_b}{L_R} = \frac{P}{L_R}$$

and the R.M.S. error from the uncertainty in x is

$$\frac{\Delta P_2}{P} = \frac{0.3t}{L_R} \tag{4}$$

(3) $x \left(\Delta \frac{dP_a}{dx} \right)$, $x \left(\Delta \frac{dP_b}{dx} \right)$ terms.

This error comes from the fluctuations in the radiative energy loss of the electron and positron as they come out of the plate. To avoid tedious calculations, we make the rough approximation that

$$\Delta \frac{dP_a}{dx} = \frac{dP_a}{dx} = \frac{P_a}{L_R} \quad ; \quad \Delta \frac{dP_b}{dx} = \frac{P_b}{L_R}$$

Thus the total squared error is

$$(\Delta P_3)^2 = \frac{x^2 p^2}{L_R^2} \left[\lambda^2 + (1 - \lambda)^2\right]$$

The mean value of x^2 is $t^2/3$, and of $\left[\lambda^2 + (1 - \lambda)^2\right]$ is 0.67. Thus the R.M.S. error is

$$\frac{\Delta P_3}{P_3} = \frac{0.5t}{L_R} \tag{5}$$

We now combine all these errors to obtain the total:

$$\frac{\Delta P}{P} = \sqrt{\left(\frac{0.6\ t}{L_R}\right)^2 + \left(\frac{0.0005\ P}{d^2}\right)^2} \tag{6}$$

B. Optimal Design Choices

We are now faced with the question of how to choose t and d to obtain a minimal error for a given volume of detector. Suppose that we require a given conversion efficiency which corresponds to, say, n radiation lengths of converter. The number of plates will be nL_R/t, and the length occupied by the array will be equal to $D = (nL_R/t)d$ (where we assume that $d \gg t$). Hence for a given volume of detector of fixed efficiency, the ratio $\sigma \equiv d/t$ is a constant. We now require that for given σ, the error $\Delta P/P$ be minimized.

We write the error in the form

$$\left(\frac{\Delta P}{P}\right)^2 = a^2 t^2 + \frac{b^2}{t^4} \quad ; \quad a = \frac{0.6}{L_R} \quad ; \quad b = \frac{0.0005\ P}{\sigma^2}$$

Minimizing, we get $t = 2^{1/6}\,(b/a)^{1/3}$ and

$$\left(\frac{\Delta P}{P}\right)^2 = 1.9\, a^{4/3}\, b^{2/3}$$

If we substitute n for a, b and express in terms of n, D defined above, we get the convenient relation

$$\frac{\Delta P}{P} = 7.7 \times 10^{-2}\, p^{1/3} \left(\frac{n}{D}\right)^{2/3} \qquad (7)$$

(P in Bev/c, and D in meters) for the accuracy of energy measurement of a photon of momentum P in an array of total length D, with n radiation lengths of converter. This formula can be applied to spark chambers or other systems with different spatial resolutions by noting that $\Delta P/P \approx \delta^{1/3}$, where δ is the coordinate-measurement error (and remembering that $\delta = 50\ \mu$ was used above). As an illustration of the above formula, assume that we wish to use $n = 4$ (4 radiation lengths $\approx 4 \times 7/9 = 3.1$ pair-conversion lengths corresponds to 95% efficiency). For a photon of 1 Bev with an array 2 meters long one can get about 12% in energy-measuring precision.

Once we have chosen appropriate P, n and D, the values of t and d can be obtained from the easily obtained formulae:

$$t = 2^{1/6}\left(\frac{b}{a}\right)^{1/3} = 0.101\, P^{1/3}\, \frac{n^{2/3}}{D^{2/3}}\, L_R \qquad (8)$$

$$d = \frac{Dt}{nL_R} = 0.101\, \frac{D^{1/3} P^{1/3}}{n^{1/3}}$$

Again, if a different spatial resolution is appropriate, both t and d vary as $\delta^{1/3}$. Taking once more our previous numerical example

of an array 2-meters long detecting 1 Bev photons, one calculates $t = 0.16\ L_R$ and $d = .08$ meters $= 8$ centimeters. We thus have a system with 25 plates each about 1/6 of a radiation length long.

C. π^o Momentum and Angular Resolution

We now consider a specific numerical example of a π^o meson of momentum 5 Bev/c decaying into two photons detected by the above 2-meter array. Assume that the π^o center of mass decay angle $\theta^* = 60^o$, so that $\cos\theta^* = 0.5$. The two photons then have energies 3.75 and 1.25 Bev. Now in calculating the expected errors, we must remember that equation (7) holds only for photons of the particular momentum for which the array has been optimized. Thus suppose that our array is optimized for 1 Bev photons, and that we require 95% conversion efficiency. Then, as shown before, we need 25 plates each .16 radiation length thick separated by 8 cm gaps. We use formula (6) to calculate the errors for the 3.75 and 1.25 Bev photons.

3.75 Bev photon: $$\frac{\Delta P_1}{P_1} = \sqrt{(0.096)^2 + (.29)^2} = 0.30$$

1.25 Bev photon: $$\frac{\Delta P_2}{P_2} = \sqrt{(.096)^2 + (.097)^2} = 0.136$$

We now use formulae (17) and (18) in Appendix II to calculate the π^o energy and directional errors:

$$\frac{\Delta P}{E} = \frac{\Delta P}{P} = \frac{\cos\theta^*}{\sqrt{\left(\frac{P_1}{\Delta P_1}\right)^2 + \left(\frac{P_2}{\Delta P_2}\right)^2}} = \frac{0.5}{8.1} = 0.06$$

$$\left(\text{i.e., } \frac{\Delta P}{P} = 6\%\right)$$

$$\Delta\xi = \frac{m}{P}\frac{\sin\theta^*}{\sqrt{\left(\frac{P_1}{\Delta P_1}\right)^2 + \left(\frac{P_2}{\Delta P_2}\right)^2}} = \frac{.135}{5}\frac{.866}{8.1} = .003 \text{ radians} = 0.17 \text{ degrees}$$

It may be noted that the advantage of using the π^o decay kinematics is evident: just by taking the vector sum of P_1 and P_2, the error in the π^o momentum would be about 23%, whereas by making use of the constraint, the error drops to about 6%.

D. Consideration of Various Possible Problems

1. Can electron pairs be related to their parent interactions?

The question we wish to consider is the following: Suppose that there are several interactions in the bubble chamber; can one properly associate the electron pairs with the interactions which produced them? In order to answer this, we must write down the uncertainties in the electron pair direction as determined from measurements on the electron and positron tracks.

First of all, the uncertainty in projected angle due to setting errors, turbulence in the hydrogen, etc., for a track has been shown to be

$$\delta\theta_m = \frac{2.5 \times 10^{-4}}{d} \text{ radians} \qquad \left[\text{Appendix I, formula (11a)}\right]$$

We assume the same formula holds for the directional uncertainty for the pair. We neglect multiple scattering in the hydrogen, but consider now the multiple scattering in the plate:

$$\delta\theta_s = \frac{.015}{P}\sqrt{\frac{x}{L_R}}$$

for each electron. Averaging over x, the R.M.S. error is

$$\delta\theta_s = \frac{.015}{P}\sqrt{\frac{t}{2L_R}} = \frac{.011}{P}\sqrt{\frac{t}{L_R}}$$

We now consider a typical situation: $d \approx 0.1$ m, $t \approx L_R/5$, $P \approx 2$ Bev/c for the pair, hence ≈ 1 Bev/c for each electron:

$$\delta\theta_m \approx \frac{2.5 \times 10^{-4}}{0.1} \approx 2.5 \times 10^{-3} \text{ rad.}$$

$$\delta\theta_s \approx \frac{.011}{1}\sqrt{\frac{1}{5}} \approx 5 \times 10^{-3} \text{ rad.}$$

There is one other major uncertainty in the measured photon direction, namely, the finite angle between the direction of the gamma ray and the directions of electron and positron. This angle is of order

$$\delta\theta_\gamma \approx \frac{m_e}{P} \ell n \left(\frac{P}{m_e}\right)$$

For $P = 1$ Bev/c,

$$\delta\theta_\gamma \approx 4 \times 10^{-3} \text{ radians}$$

Thus the total error is $\approx 7 \times 10^{-3}$ radians. If we assume, say, 2 meters between the interaction and the converter we find that the measured line of flight of the photon, when exprapolated back to the interaction should come within $2 \text{ m} \times 7 \times 10^{-3}$ rad. $= 1.4$ cm of the interaction point. For a chamber which is ≈ 1 meter wide, 1.4 cm is very small and should allow easy association of photon and origin.

2. <u>What spatial resolution is necessary to resolve the electron and positron tracks and thus permit independent measurement of their momenta?</u>

Let y be the displacement between the centers of the electron and positron tracks at a distance r from the upper plate. If P_a and P_b are the momenta

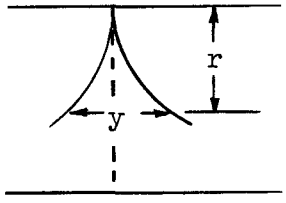

of the electron and positron,

$$y = 0.3\ r^2 \left(\frac{1}{P_a} + \frac{1}{P_b}\right)$$

where again we have assumed a magnetic field H of 20 kg. Thus, if P is the photon momentum, and $\lambda = P_a/P$,

$$y = 0.3\ r^2\ \frac{P}{P_a P_b} = \frac{0.3\ r^2}{P\lambda(1 - \lambda)}$$

The maximum value of $\lambda(1 - \lambda)$ is 0.25. Hence $y \geq 1.2\ r^2/P$. Thus at the center of the track $r = d/2$ and $y \geq 0.3\ d^2/P$. Typical values are $d = 0.1$ m, $P = 2$ Bev/c, hence $y \geq 1500\ \mu$. On the other hand, typical track diameters (obtained by full-size reprojection of apparent photographic track widths) are of the order of 300 - 500 μ. Thus with appropriate care, insofar as resolution is concerned, the individual tracks should be readily resolvable except right under the top plate.

SOME CONSIDERATIONS ON BUBBLE CHAMBER EXPERIMENTS WITH M

by

William Chinowsky

August, 1962

I. Introduction

It has been often pointed out that a bubble chamber operating with M could conveniently use one pulse in 360 and so might prove a convenient instrument for making experiments on interactions of secondary particles with protons. We will consider here some aspects of doing such experiments, touching upon such questions as beam intensity, chamber size, detection of secondary processes and also some consideration of possible hybrid devices. It is expected that most of the new and useful information will come from strong interactions of secondaries of high energy, say 10 Bev - 20 Bev. The reason is that the intensity is high, and that separation of particles can be more easily made at M than at AGS proton machines by using rf separators which take advantage of the "natural" bunching of the electron beam. These remarks, then, will be concerned with strongly interacting particles in the energy range 10 Bev - 20 Bev.

II. Beam Intensity

Particles of interest are $\pi^{\pm}$, $k^{\pm}$, $p^{\pm}$. Estimates of the yields of these particles at M have been made by Ballam and others on the basis of single particle exchange and are subject to some uncertainty. In particular, $\bar{p}$ yields are calculated with a proton pole and are probably unreliable. Consider first the pions and k's. The estimated yields per incident 25 Bev electron per Bev per sterad are, at different production angles and energies,

	10 Bev		15 Bev		20 Bev	
θ	π	k	π	k	π	k
$\frac{1}{2}^{o}$	3×10^{-4}	$.4\times10^{-5}$	3.5×10^{-4}	$.7\times10^{-5}$	1.1×10^{-4}	3.5×10^{-6}
1^{o}	4	1.3	2.5	2.0	.55	8.0
3^{o}	1	3.3	0.4	2.4	< 0.1	5.5
5^{o}	0.4	2.5	0.15	1.3	< 0.1	2.5

At an angle of $\frac{1}{2}^{o}$, the π/k ratio is ≈ 100, and the k meson contamination in a π beam is negligible; an unseparated beam would be used. With 30 μamp average electron beam intensity, in a π beam with momentum resolution $\Delta p/p = \pm 1\%$, the number of π's per sterad is, per pulse,

$$N/\text{sterad} \approx 2 \times 10^{-4} \times 5 \times 10^{11} \times 0.3 \approx 3 \times 10^{7}/\text{ sterad}$$

In a solid angle of $\approx 10^{-4}$, easily obtained with quadrupole lenses, many thousands of π's are available, and so pion exposures with a bubble chamber should be quite feasible.

Experiments with k mesons evidently require a separated beam, using rf separators to separate k's from π's. At 10, 15 and 20 Bev the maximum available intensities are $\approx 3 \times 10^{-5}$, 3×10^{-5}, 1×10^{-5} per steradian per incident 25-Bev electron per Bev. Again with 30 μamp and $\pm$ 1% momentum spread, we have, at

10 Bev, 3×10^{6} k's/ sterad
15 Bev, 4.5×10^{6} "
20 Bev, 2×10^{6} "

Experience with rf separators is quite limited, but it is expected that the solid angle accepted will be $\approx 2 \times 10^{-5}$ sterad. The drift spaces required to provide $\frac{1}{2}\lambda$ separation of π's and k's at the above energies are 46, 101 and 184 meters, respectively. In addition, $\approx$ 25 meters is required for the optical elements to transport the beam from the separator to the bubble chamber. The total length of the beam is then $\approx$ 70, 125, or 210 meters at the energies above. Mean decay distances of the k's are 72, 108, 144 meters, respectively, and are comparable to the required length of beam. If the beam is arranged to provide k's within the range 10 - 20 Bev with a fixed geometry, the length of the beam is 210 meters. The fractions of k's surviving this distance are .035, 0.14 and 0.23. The available separated beam intensities are then 2.1, 13 and 9 k's per pulse. These intensities are quite marginal for doing bubble chamber experiments. Maximum intensities, obtained by

matching the length of the beam to the momentum of the k's, are 22, 29 and 9 k's per pulse. These intensities are sufficient but not overwhelming.

It is clear that the intensity of antiprotons produced via ordinary pair production ($\approx 10^{-7}$/ electron/ sterad/ Bev) is much too small for worthwhile bubble chamber experiments if an rf separator were to be used. Yields calculated with a proton pole contribution are $\approx 10^{-4}$/electron/sterad/Bev at production angles $\theta \approx M/E$. This is comparable to the pion intensities and so would provide an over-abundance of antiprotons. In fact, the $\bar{p}/\pi$ ratio is > 1, and at some angles > 10, so that quite a pure antiproton beam would be available without any separation. It is difficult to evaluate the reliability of this calculation.

These rather pessimistic estimates of beam intensity per pulse should be tempered by some factors which could yield great increases. Among those known are the large production of k's from k* decay, production of antiproton pairs with a pion pole contribution, and the good possibility of operating rf separators in modes permitting larger size and greater solid angle acceptance. It is not clear yet that k meson and $\bar{p}$ intensities will be too low for bubble chambers.

III. Considerations of Size of Bubble Chamber

We presume that the bubble chamber will be used to study interactions with cross section ≥ 10 μ barn, so that in most cases many-body final states must be considered.

It may be presumed further that a large fraction of the total energy goes into neutral particles. Even if only one neutral particle is missing it is essentially impossible, at these energies, to determine kinematically the event without ambiguities of masses of the observed charged particles. We make now the fundamental statement that it is required to identify uniquely the reactions producing the observed events, i.e., to measure the momenta and masses of all particles involved. While it is true that in the past this has not been true for all classes of events in hydrogen bubble chambers, most of the useful

information has resulted from such uniquely determined classes of events. Particularly in events of high multiplicity many characteristics of the reactions are indeterminate if kinematical ambiguities cannot be resolved. It is proposed, then, that the chamber be such that neutral particles produced at any observed vertex be detected simultaneously with charged particles emerging from the interaction vertex.

We now consider the known neutral particles: K mesons, hyperons, pions, and neutrons. All but neutrons can be detected by their decay since their lifetimes are short. The requirement that V^o particles decay within the chamber volume already essentially determines the necessary chamber size. With incident momenta of 10-20 Bev/c there will result, in the interaction with protons, k^o and Λ^o in the forward direction, with comparable momenta. It is quite trivial then to decide on the length of the chamber. It need only be pointed out that the mean free paths for decays of V^o's are now in the range 60 cm - 120 cm. It is suggested that at least two mean free paths be available for decay, so that $\approx 85\%$ decay. It is not necessary to make very accurate momentum measurements of the decay products, so that perhaps 50 cm is needed to measure the tracks of the decay products. Thus, some 2-3 meters are required beyond the point of interaction. In addition a region of interaction of the incident particles of $\approx$ 1 meter is desired. It is not, of course, possible to determine quantatively the optimum size of chamber. It is even difficult to say, in complete generality, that identification of reactions is possible in any reasonable-size hydrogen bubble chamber. It can be said, however, that if the chamber is less than $\approx$ 3 meters long, it will not be possible to determine with accuracy the characteristics of strong interactions producing strange particles.

To make such arguments about transverse dimensions requires better knowledge of the dynamics of the reactions being studied. It may be sufficient to limit the transverse dimensions so that only tracks of particles produced at small angles to the incident beam can be measured. If it is required that V^o's produced at any angle in the center-of-mass

system have two mean free paths for decay, then the required distance perpendicular to the beam direction is $4P_{cm}/M \times c \times \tau$, where P_{cm} is the momentum in the center of mass, M is the mass of the particle, and τ is the lifetime. Center of mass momenta are $\approx$ 1.5 - 2.5 Bev/c, so required path length is $\approx$ 60 cm. A width and depth of chamber of approximately one meter is indicated, including $\approx$ 20 cm transverse dimensions occupied by the incident beam. These dimensions are impressively large, but it should be remembered that when the primary energy of the machine is increased to 45 Bev, the decay distances above are doubled. So V^o's produced by incident particles in the 20-40 Bev range will have only $\approx$ 65% decay probability.

An advantage to the large size is the possibility of measuring such interactions as Σ-p, Λ^o-p, etc. With an interaction mean free path of 8 meters in the hydrogen, some 10% of the hyperons interact in the chamber. Assume 20 incident beam particles, with hyperons produced in $\approx$ 5% of the interactions. With a one-meter interaction length and 1.5 mb for hyperon production there results one useful interaction of a hyperon in $\approx$ 150 pictures. This is quite a reasonable rate and probably the only practical technique for studying hyperon interactions.

In discussing uncertainties in event identification two basic assumptions are made, neither of which has been demonstrated. First, it is assumed that even in a chamber of the general size discussed above, distortions will not be significantly increased over those now present in, say, the 20-inch chamber of Shutt at Brookhaven, so that intrinsic inaccuracies in bubble location are comparable to those of the 20-inch chamber. Second, it is assumed that there will be no variation in bubble density along the track with the mass of the particle producing the track. This is an extrapolation of the observed $1/\beta^2$ dependence for nonrelativistic particles. Thus only consistency with the kinematics of the presumed reaction yielding the observed event can be used to identify the masses of the various reaction products. Greater accuracy in measurement is thus required. It is expected that both of these points will be subject to experimental study in the near future. Suitable modifications of the present discussion should be

made if either of the above assumptions proves untrue.

In what follows it will be indicated that if a chamber of the size required to provide adequate decay length for V^o particles is constructed, it will be of sufficient size to enable one to make measurements with the required accuracy. The discussion will be based somewhat on experience with a 2.0 Bev/c k^+ exposure made with the 20-inch chamber. Consider momentum errors first. The basic requirement is that sagittas of tracks be large compared with multiple-scattering errors. In liquid hydrogen, with magnetic field H, the ratio of the sagitta in the field to the average sagitta caused by multiple scattering, giving then the momentum uncertainty caused by multiple scattering, is

$$\frac{\Delta p}{p} = \frac{\rho_H}{\rho_{sc}} = \frac{1.2}{\beta H \sqrt{L}}$$

Where H is in kilogauss, and L is in cm. With $\beta = 1$ and $H = 20$ kilogauss,

$$\frac{\Delta p}{p} = .06/\sqrt{L.}$$

With a chamber size greater than $L \approx 150$ cm, there will result, on the average $R \approx .005$ as the fractional momentum uncertainty.

In addition to this "Coulomb" error δ_c there is the measurement error δ_m, so that the total error $\delta = \sqrt{\delta_m^2 + \delta_c^2}$. The measurement error may be crudely indicated from the sagitta error Δs, with $\Delta s \approx 2 \times$ [setting error in measuring the position of a bubble]. This latter quantity is ≈ 50 microns. The error in momentum is

$$\frac{\Delta p}{p} = \frac{27}{H} \frac{p}{L^2} \Delta s \approx \frac{27}{H} \frac{p}{L^2} \times 100 \times 10^{-4}.$$

With $H = 20$ kilogauss, for $\delta_c = \delta_m$,

$$\frac{\Delta p}{p} \approx 1.4 \times 100 \times 10^{-4} \quad \frac{p}{L^2} = .005$$

so that

$$\frac{p}{L^2} = .36$$

with p in Mev/c, and L in cm. Thus a 10 Bev/c track of 1.7 m length has a measurement error about equal to the Coulomb scattering error. Further increase in length brings only a slow increase in precision, since the scattering error dominates. The chamber considered above provides path lengths ≈ 200 cm and so is of adequate size to make momentum measurements with precision essentially limited by the Coulomb scattering.

Consider further a comparison with the 20-inch chamber of Shutt. With a <u>total</u> length of 3 meters, comparable measurement errors result for momenta $(300/50)^2 = 36$ times larger than those measured in the 20-inch chamber. Since experiments with incoming momenta of 2-3 Bev/c have been made with the 20-inch chamber, comparable precision would be obtained with incoming momenta of 70-200 Bev/c. In the 2.0 Bev/c k^+ experiment many kinematical ambiguities could not be resolved without bubble-density estimates. A decrease in errors of a factor two would have been sufficient to eliminate these ambiguities, and this would be obtained with the large chamber. Angle errors are essentially independent of momentum and are proportional to $1/L$. Thus absolute angle errors will be six times smaller. It appears then that a chamber 3 to 4 meters long should be more than sufficient to make complete event identification, based on these crude, overestimated error estimates.

These simple, qualitative remarks indicate that the primary determinant of size is the requirement that V particle decays be visible and measurable. Should this condition be relaxed, one might consider a smaller chamber (perhaps about 1 meter) with larger magnetic field.

IV. Detection of Neutral Pions

It is important, again in order to completely identify the event, that the bubble chamber system have γ-ray detection efficiency near 100%. Those events with only one π^o emerging are sufficiently determined from measurement of the angles of the γ-rays only. In such a case the event is triply over-determined: there are eight kinematical constraint equations and five missing variables. If more than one π^o is produced, momentum measurements of the photons are also necessary, especially since it will be difficult to associate pairs of γ-rays with the parent π^o. We consider first a series of lead plates at the downstream end of the chamber to convert γ-rays with high efficiency, but no momentum measurement. Such a system is necessary unless path lengths > 10 meters in liquid hydrogen are possible. We estimate the transverse dimension required when the first converter is 2 meters from the interaction vertex. For π^o center-of-mass production angle $\bar{\theta}$ and momentum $\bar{p}$, the π^o lab angle is

$$\tan\theta = \frac{\sin\bar{\theta}}{\gamma\left(\cos\bar{\theta} + \beta + \frac{1}{2}\beta\frac{m^2_{\pi^o}}{\bar{p}^2} + \ldots\right)}$$

where β is the velocity of the center of mass. For $\bar{\theta} = 90^o$ and incident particle momentum 15 Bev/c, and assuming $\bar{p} \gg m_{\pi^o}$, the lab angle $\theta = 18^o$; with $\bar{\theta} = 130^o$, $\theta = 65^o$. If high γ-ray detection efficiency is to be attained, one must detect γ-rays made at such large angles to the incident beam. It cannot in general be argued that π^o's will be preferentially produced, in the center of mass, at small angles to the incident particle. It need only be pointed out that those π^o's which result from decay of high-mass resonant states (N^*, Y^*, K^*, etc.) can be emitted at large angles to the direction of motion of the parent particle. Further, it may be presumed that a large fraction of N*, Y* will be produced in peripheral collisions and hence be emitted in the backward direction. This will further increase the probability of large angle π^o's. Restricting the solid angle subtended by the

converters is then likely to eliminate a large fraction of the interesting events. It is suggested that it is desirable to detect γ's at $\approx 65^{\circ}$ to the beam direction. If the plates are downstream of the bubble chamber, and are perpendicular to the beam direction, the plates must be ≈ 8 meters wide and deep. It seems rather more practical to put the converters along the sides of the chamber:

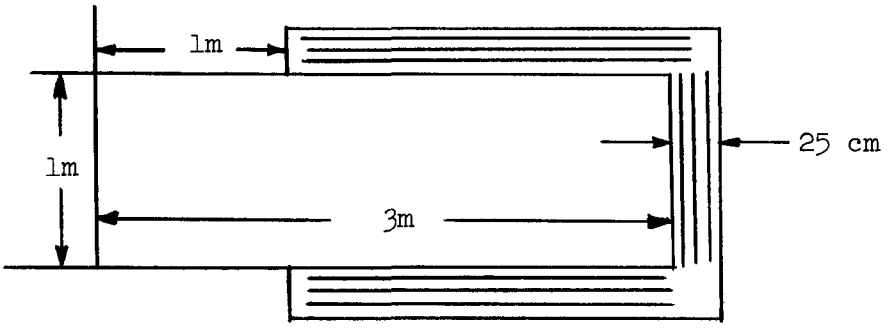

A depth of 8 meters seems impractical, so the depth should be chosen as large as possible, consistent with technical feasibility. For high conversion efficiency, perhaps 3 radiation lengths would suffice. A spacing of the plates of ≈ 2 cm should be sufficient to observe the converted pairs and determine the angle roughly. The accuracy needed in angle measurements is determined to a large extent by the background, i.e., it must be decided which γ's point to the interaction vertex. If we assume only a small γ-ray background, the 2 cm length is probably sufficient. For $\approx 1^{\circ}$ accuracy in measurement of the angle, the converters can be $\frac{1}{4}$ rad. length, so that ≈ 25 cm length perpendicular to the plane of the plates is needed. If it is required to measure the momenta of

the converted electron-positron pair, much longer distances are needed. A 5% momentum measurement, with 20 kilogauss, can be made on a track $\approx$ 7 cm long. Further, in this case one would want to restrict the plates to perhaps 1/10 rad. length or less, so that now the total length of the converter section is approximately 2 meters. Thus the chamber now has expanded to a length of some 5-6 meters, a width of 5 meters, and a depth of at least one meter but preferably larger.

We point out that only a small fraction of such a chamber, $\approx$ 1 meter by 20 cm, is used for interaction of the primary particles. It might be more feasible to replace that part of the system used for detection of V^o decays and conversion of γ-rays with spark chambers of equal size. Consider a system of pairs of .001-inch Al foils, spaced $\frac{1}{4}$ cm apart, arranged with 2 cm distance between pairs. In 2-meter flight paths, the total length of Al is

$$1 \times 10^{-3} \times 2.54 \times 2 \times 100 = 0.5 \text{ cm}$$

or about 0.05 radiation length; the number of radiation lengths of gas is negligible. This compares with $\approx$ 0.2 radiation lengths in liquid hydrogen. The accuracy in momentum measurement attainable (considering spark sizes approximately twice bubble sizes) with such a system is then within a factor of two of the bubble chamber and may in fact be quite comparable. A system of a "small" hydrogen bubble chamber, of the order of $1 \times \frac{1}{2} \times \frac{1}{2}$ meters, with spark chamber appendages of the sizes indicated above, all triggered once per second, is envisaged. Of course $\approx$ 20,000 gauss must still be provided in a volume of about $5 \times 5 \times 2$ meters if photon energies are to be measured. Such a system of large, low-density spark chambers is certainly technically feasible and probably capable of yielding the accuracy in measurement needed for kinematical determinations. It is not clear that such a gadget is more desirable on either technical or economic grounds. It has been suggested by Perl that the bubble chamber be replaced with a pot of liquid hydrogen, with the rather serious disadvantage that the primary interaction vertex

is invisible. The general size would be comparable and would also require magnetic field in a large volume. However, it could be triggered, presumably, 360 times per second.

V. Conclusions

These considerations are too unsophisticated to allow more than semi-quantitative conclusions. It does appear that a chamber of the general dimension of a few meters, rather than one meter, is needed to make good experiments with the high-energy secondary beams. With such uncertainties in beam intensity and bubble chamber characteristics it certainly cannot now be suggested that such a chamber be built. Hopefully within about a year many of these questions will be answered, and then one can start serious design of a monster chamber.

STRONG INTERACTION PHYSICS WITH SPARK CHAMBERS

by

M. L. Perl

August, 1962

1. Secondary $\pi^{\pm}$, $k^{\pm}$ and $\bar{p}$ beams

We consider two kinds of beams. The first kind we call an "unseparated beam," which means there is no physical mass separation although a Cerenkov counter may be used for mass identification; as a standard aperture for this beam we take 10^{-3} steradians and a momentum spread of $\pm$ 1/2%. The second kind of beam we call a "separated beam"; it uses radiofrequency separators whose aperture is taken as 2×10^{-5} steradians, and we assume a momentum spread of $\pm$ 1/2%. Furthermore we assume 10^{12} primary electrons per pulse, and 25 Bev primary electron energy.

No attempt is made to calculate the secondary electron background, because it depends very strongly on detailed beam design. However, we do allow for a variation in the angle of the central ray of the unseparated beam for π and k beams. In one form of the unseparated beam the central ray is at 0 degrees. However, if this gives too high an electron background an alternative of offsetting the central ray to 2×10^{-2} radians is provided, as shown in Fig. 1. For the eparated eam the central ray is always set at the angle of maximum production for the Drell process. Furthermore the radiofrequency separator is assumed to work perfectly, so that there are no other kinds of particles present.

This report was evolved over a period of two months, during which our estimates of the expected beam intensities fluctuated according to the sanguineness of the people we talked with. Therefore we have set down three sets of beam estimates. The optimistic estimates are taken from the calculations of Ballam in the 1960 Summer Study Report,* with some corrections furnished by him. The pessimistic estimates assume that everything is always harder to do by a factor of 10. The hyperoptimistic estimates are based on copious ρ and k^* production by the Drell process; there is no

*M Report No. 200, Stanford Linear Accelerator Center, Stanford University, Stanford, California (Summer, 1960).

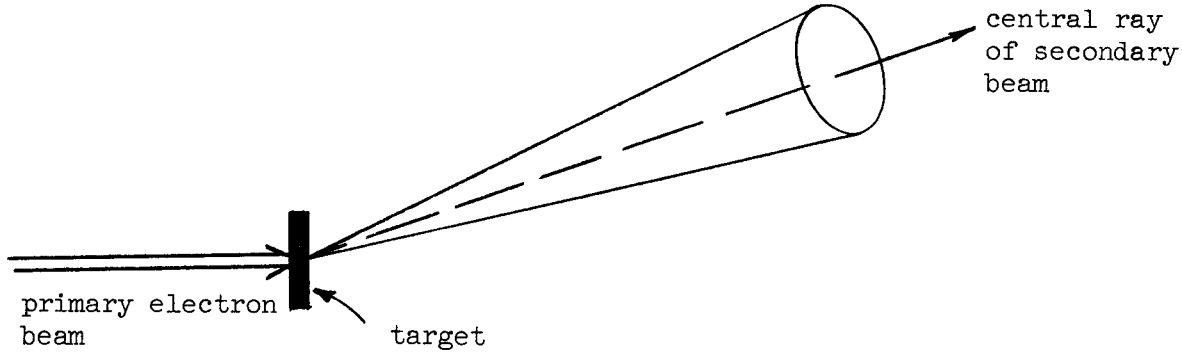

FIG. 1--Offset secondary beam.

separate hyperoptimistic estimate for $\bar{p}$ simply because the optimistic estimate already seems so amazing. The $\bar{p}$ pessimistic estimate is down by a factor of 20.

Table I gives three estimates in particles per pulse for 20-Bev particles produced by 10^{12} per pulse, 25-Bev electrons in a $\frac{1}{2}$-radiation-length target. Table II gives the same information for 10-Bev particles produced by 10^{12} per pulse, 25-Bev electrons in a $\frac{1}{2}$-radiation-length target.

2. Rate Limitations on Trigger Electronics and Spark Chambers

When a charged particle passes through a spark chamber it leaves a trail of free electrons and positive ions. When the high-voltage pulse is applied to the chamber these initial free electrons accelerate and initiate the spark. If any other charged particle goes through the chamber between the time of passage of the first particle and the end of the high-voltage pulse, then this second particle will also produce a pulse. Therefore this time interval between the passage of the initial particle and the end of the high voltage pulse is the time resolution of the spark chamber and assorted trigger electronics.

In this section we shall always assume that there is no background problem from stray charged particles or neutrons. That is, we assume the experiment can be adequately shielded.

J. Fischer and G. T. Zorn, in the Proceedings of the Eighth Scintillation Symposium, IRE Trans. on Nuclear Science, Vol. NS-9, No. 3, 261 (1962), have presented an excellent summary of the minimum time resolution that can be expected unless marvelously new ideas appear on how to speed up counter electronics, counter logic and conventional spark chambers. Table III is taken from their paper, in which they consider a very simple trigger system consisting of one Cerenkov and three scintillation counters, one coincidence circuit, and a single spark chamber of dimensions of the order of several feet.

In this system no cable delay occurs because the cables are all physically parallel to the direction of flight of the initial particle.

TABLE I

Number/Pulse of 20-Bev Secondaries

Principal Particle Desired	Beam Description	Estimate	$\mu^{\pm}$	$\pi^{\pm}$	$k^{\pm}$	$\bar{p}$
$\pi^{\pm}$ and $k^{\pm}$	unseparated beam, 10^{-3} sr, $\Delta p/p = \pm \frac{1}{2}\%$, 0° rad. central ray	hyperoptimistic	8,000	20,000	10,000	
		optimistic	8,000	14,000	500	
		pessimistic	800	1,400	50	
$\pi^{\pm}$ and $k^{\pm}$	unseparated beam, 10^{-3} sr, $\Delta p/p = \pm \frac{1}{2}\%$, 2×10^{-2} rad. central ray	hyperoptimistic	1,000	20,000	10,000	
		optimistic	1,000	4,400	600	
		pessimistic	100	440	60	
$k^{\pm}$ and $\bar{p}$	unseparated beam, 10^{-3}sr, $\Delta p/p = \pm \frac{1}{2}\%, M_{\bar{p}}/E = 4.7 \times 10^{-2}$ rad. central ray	hyperoptimistic	10	4,000	4,000	11,000
		optimistic	10	1,100	600	11,000
		pessimistic	1	110	60	500
$\pi^{\pm}$	separated beam, 2×10^{-5} sr, $\Delta p/p = \pm \frac{1}{2}\%, M_{\pi}/E = 7 \times 10^{-3}$ rad. central ray	hyperoptimistic	0	1,000	0	0
		optimistic	0	480	0	0
		pessimistic	0	50	0	0
$k^{\pm}$	separated beam, 2×10^{-5} sr, $\Delta p/p = \pm \frac{1}{2}\%, M_{k}/E = 2.5 \times 10^{-2}$ rad. central ray	hyperoptimistic	0	0	200 *	0
		optimistic	0	0	17	0
		pessimistic	0	0	2	0
$\bar{p}$	separated beam, 2×10^{-5} sr, $\Delta p/p = \pm \frac{1}{2}\%, M_{\bar{p}}/E = 4.7 \times 10^{-2}$ rad. central ray	hyperoptimistic	0	0	0	200
		optimistic	0	0	0	200
		pessimistic	0	0	0	10

*From an estimate by W. Chinowsky

TABLE II

Number/Pulse of 10-Bev Secondaries

Principal Particle Desired	Beam Description	Estimate	$\mu^{\pm}$	$\pi^{\pm}$	$k^{\pm}$	$\bar{p}$
$\pi^{\pm}$ and $k^{\pm}$	unseparated beam, 10^{-3} sr, $\Delta p/p = \pm \frac{1}{2}\%$, 0° rad. central ray	hyperoptimistic	29,000	37,000	10,000	
		optimistic	29,000	37,000	360	
		pessimistic	2,900	3,700	36	
$\pi^{\pm}$ and $k^{\pm}$	unseparated beam, 10^{-3} sr, $\Delta p/p = \pm \frac{1}{2}\%$, 4×10^{-2} rad. central ray	hyperoptimistic	7,000	20,000	10,000	
		optimistic	7,000	20,000	1,400	
		pessimistic	700	2,000	140	
$k^{\pm}$ and $\bar{p}$	unseparated beam, 10^{-3} sr, $\Delta p/p = \pm \frac{1}{2}\%$, $M_{\bar{p}}/E = .094$ rad. central ray	hyperoptimistic	10	9,000	9,000	25,000
		optimistic	10	9,000	1,500	25,000
		pessimistic	1	900	150	1,200
$\pi^{\pm}$	separated beam, 2×10^{-5} sr, $\Delta p/p = \pm \frac{1}{2}\%$, $M_{\pi}/E = .014$ rad. central ray	hyperoptimistic	0	2,000	0	0
		optimistic	0	2,000	0	0
		pessimistic	0	200	0	0
$k^{\pm}$	separated beam*, 2×10^{-5} sr, $\Delta p/p = \pm \frac{1}{2}\%$, $M_{k}/E = .049$ rad. central ray	hyperoptimistic	0	0	200	0
		optimistic	0	0	18	0
		pessimistic	0	0	2	0
$\bar{p}$	separated beam, 2×10^{-5} sr, $\Delta p/p = \pm \frac{1}{2}\%$, $M_{\bar{p}}/E = .094$ rad. central ray	hyperoptimistic	0	0	0	500
		optimistic	0	0	0	500
		pessimistic	0	0	0	25

*From an estimate by W. Chinowsky

TABLE III

From J. Fischer and G. T. Zorn

IRE Trans. on Nuc. Sci. NS-9, 3, 273 (1962)

Component	Minimum Delay in nanoseconds
Photomultiplier tube	12
Coincidence circuit	1
Avalanche trigger	3
H.V. amplifier tube and voltage rise time	6
Spark gap	7
Propagation of H.V. from gap to center of spark chamber of 2 feet	2
Spark formation time	2
TOTAL	33 nanoseconds

Now the usual trigger system will be more complex. For example, spark chambers may extend over 2 or 3 meters, sometimes for backward-traveling particles. Anti-coincidence counters may be placed 3 or 4 meters downstream. Coincidence circuits may be in triple cascades with a meter of cable between each of them. Just these three considerations add roughly (10 + 20 + 10) = 40 nanoseconds.

Therefore 80 to 100 nanoseconds is probably the minimum time resolution for a complex spark-chamber system. (Present systems vary from 200 to 500 nanoseconds in time resolution.) Thus if one is willing to have two particles or events in the spark chambers 10% of the time, and the machine pulse is 1 microsecond long, these systems can study only 1 to 3 particles per pulse. If one is willing to have an average of two particles or events in the chamber all of the time, then these rates increase to 10 to 30 particles per pulse. Some spark chambers are placed in the incident beam, if the beam is not sufficiently well collimated, in order to obtain the direction of the incident particles which initiate the events of interest. These in-beam spark chambers are the ones which will have the above rate

limitations; but they are also the ones that should have only one particle per pulse. Otherwise there may be confusion as to which incident particle caused the event.

Two obvious ways to allow a greater incident particle rate are (a) not to use the chamber in the incident beam; or (b) to select a specific experimental design in which it is permissible, yet still useful, for the in-beam spark chambers to have a large number (say 10 or 20) of incident particle tracks. To simplify things, we suppose there are no in-beam chambers, Fig. 9, and that the incident beam is interacting in a hydrogen target. Now there are two separate rate limitations. First, the chambers are now traversed only by particles from events. If f is the probability of a charged particle going through a chamber per incident beam particle, then f is given roughly by

$$f \approx \sigma \; L \; N \left[\frac{\Omega}{4\pi}\right] \; 4 \times 10^{-5}$$

where σ is the total cross section of the incident particles in mb, L is the length of the hydrogen target in cm, N is the multiplicity of charged-particle events, and Ω is the solid angle subtended by the chamber. As an example, take $\sigma = 30$ mb, $L = 50$ cm, $N = 4$, and $\Omega/4\pi = 0.1$. Then $f = .024$. This is an average sort of example. We can thus take as a good estimate that keeping the chambers out of the beam will improve the chamber-rate limitation by a factor of 50. Then allowing an average of one background track per chamber, in addition to the event which triggered the chambers, we have a maximum rate of 500 to 1500 incident particles per pulse.

Only in the case where the reaction one is studying needs small-solid-angle chambers can this rate be increased. Such an example is given in Section 4c, where a solid angle of $\Omega/4\pi = .01$ is used and the maximum rates are about 10,000 per pulse.

Once there are no spark chambers in the beam, the resolution time of the trigger electronics must be considered separately. Here again there are two possibilities. The first is that there are no triggering counters in the beam. Thus the incident-beam rate is limited by the singles rates

in the counters, the number of undesired events that produce coincidences through part of the logic but are later (in the logic sequence) removed by an anticoincidence or lack of a further required coincidence, and the number of desired events. However, the resolution time of the electronics is smaller than the resolution time of the chamber, and the solid angles will be about the same. Therefore the rate is limited by the chamber, as given in the previous paragraph.

The second possibility is that some part of the trigger electronics is in the beam. The most common reason for doing this is the use of a Cerenkov counter to select a particular mass. We consider a mixed beam of π and K mesons in which the π contamination is to be reduced, and we take the resolution time of the Cerenkov counter and associated counters and coincidence circuits as 2 nanoseconds. The maximum incident-beam rate of K's per pulse, N_K, depends upon the initial purity of the beam and the final required purity. If the initial fraction of π's is p and the final fraction is p' then

$$\text{initial number of } \pi\text{'s is } \frac{p}{1-p} N_K$$

$$\text{final number of } \pi\text{'s is } \frac{p'}{1-p'} N_K$$

and the Cerenkov counter is on for a fraction of the pulse $2 \times 10^{-3} N_K$ so that

$$\left(2 \times 10^{-3} N_K\right)\left(\frac{p}{1-p}\right) N_K = \left(\frac{p'}{1-p'}\right) N_K$$

or

$$N_K = 500 \left[\frac{p'(1-p)}{p(1-p')}\right]$$

The maximum rate is of course about 500. If $p = 0.5$, then a p' of .05 allows 26, and a p' of .01 allows 5. If the K-to-π ratio is already greater than 1, say $p = 0.2$, then a p' of .05 allows 104, whereas a p' of .01 allows 20. On the other hand, if the π's outnumber the K's, say $p = 0.8$, then a p' of .01 allows 6, and a p' of .01 allows 1. Thus in many cases a radiofrequency spectrometer is better than a Cerenkov counter.

Table IV sums up these considerations.

Comparison of Table IV with Tables I and II immediately makes clear that in most cases the entire "Unseparated Beams" for hyperoptimistic and optimistic estimates are not usable. On the other hand, the "Separated Beams" are usable for all estimates in most cases.

With these considerations in mind, we now consider how one would use a spark chamber to study $\pi^{\pm}$, $K^{\pm}$ and $\bar{p}$ interactions at M. At present, spark chambers have a dead time after they are pulsed of about 10 milliseconds. If pulsed again within this time, there are random sparks in the chamber in the region of the initial tracks. However, we expect that this dead time can be reduced to less than 3 milliseconds. Therefore, one event per pulse (at 360 pulses per second) could be exhibited. To record this event, one picture per pulse would be required.

For general use, we believe that photographing an event is to be much preferred to the use of television or sonic or digitized magnetic-core recording. Present television systems do not have the required linearity by a factor of at least four. Sonic recording and digitized magnetic-core recording have a long way to go before their reliability and precision can match photography. However, J. Tinlot has pointed out the greater cost of using film, and his objection will be discussed later. Returning to direct photography, the problem is to change the film for every pulse. Present fast cameras can move the film on a random signal in 20 to 30 msec. To decrease this time to the required 2.8 msec seems quite difficult if the film is to be started and stopped. One might consider running the film continuously. However, if the spark lasts 10 microseconds, the spark would smear on the film by an amount equal to 1/280 of the picture length, which for most purposes will destroy needed precision. Therefore, the difficult

TABLE IV

Counters		Chambers		Maximum Rates of Incident Particles Per Pulse
In Beam	Out of Beam	In Beam	Out of Beam	
Simple systems		Simple systems		30
Complex systems		Complex systems		10
Cerenkov with moderate rejection	Remainder of counters	None	Complex systems	100
None	All counters	None	Complex systems with 1.0 ster. per chamber	500
None	All counters	None	Simple systems with 1.0 ster. per chamber	1,500
None	All counters	None	Complex systems with 0.1 ster. per chamber	10,000

but certainly not impossible problem of changing film every pulse must be solved.

We assume that this problem will in fact be solved, and that spark chambers will be able to operate at M taking one picture per pulse. We point out again that, because of the dead time, this picture can contain only one triggering event, although accidental events may also be in the picture. Ideally, a spark chamber is to be operated with a perfect triggering system, so that every picture contains an event of interest, although in present spark-chamber experiments this ideal is not achieved. One's first idea is therefore to operate spark chambers at M in this way, using large fluxes of incident particles with as selective a triggering scheme as one can devise and taking one picture per pulse. The limitations on flux discussed in this section inhibit this idea, however, and in many cases it will only be possible to take one selectively triggered picture during a number of pulses. In Section 4 this question is discussed further, along with some typical experiments. While thinking about this problem, we realized that even for pessimistic beam estimates the separated beams were large enough to give one random kind of event per pulse, that is, to operate the spark chamber like a bubble chamber. This is the subject of the next section.

3. The Large Spark Chamber as a Substitute for a Large Hydrogen Bubble Chamber in a Separated Beam

Consider a very large liquid-hydrogen bubble chamber, say 3 meters long, operating at one pulse per second at M. More rapid operation of a very large hydrogen bubble chamber seems out of the question at present. Allow 20 tracks per picture from a separated beam and an interaction length of 1.5 m. The total cross section of $\pi^{\pm} + p$ is 30 mb. Using this cross section as representative, the average number of events per second in the chamber is

$$\left(20 \frac{\text{particles}}{\text{pulse}}\right)\left(1 \frac{\text{pulse}}{\text{second}}\right)(30 \text{ mb})\left(4 \times 10^{-5} \frac{\text{event}}{\text{particle, mb, cm of } < \mu_2}\right)(150 \text{ cm})$$

$$= 3.6 \text{ events/second}$$

These events are of course of all types; there is no selection in the bubble chamber.

Now consider a liquid-hydrogen target 50 cm long, surrounded by a large magnetic spark chamber in the same (20 particle per pulse) separated beam. Furthermore, let the spark chamber be triggered on any interaction, that is, wherever the incident particle interacts in the hydrogen target, the chambers are pulsed. Then the event rate is

$$\left(20 \frac{\text{particles}}{\text{pulse}}\right)\left(360 \frac{\text{pulses}}{\text{second}}\right)\left(30 \text{ mb}\right)\left(4 \times 10^{-5} \frac{\text{event}}{\text{particle, mb, cm of } < \mu_2}\right)(50 \text{ cm})$$

$$= 432 \text{ events/second}$$

The event rate is increased by a factor of 120! This factor stays the same even if the separated beam flux is smaller, because the spark chamber can use the same intensity beam as the bubble chamber.

One's first reaction may be that, although the event rate is much higher in the spark chamber, it is so inferior a measuring instrument compared to the bubble chamber that it is not useful to study unselective events in this way. On the contrary, however, we find for the high-energy events to be studied at M the large magnetic spark chamber is a better instrument than the large hydrogen bubble chamber.

This conclusion is based on the following advantages of the spark chamber.

(a) Momentum and angle can be measured more precisely in the spark chamber.

(b) It is easier to arrange for comprehensive $e^{\pm}$ and γ-ray detection.

(c) It is more flexible if certain types of events need additional instrumentation for analysis.

(d) In most cases there will be only one event instead of 3.6 events in the chamber, thus simplifying analysis.

(e) It is cheaper to build for the same volume and magnetic field.

(f) It has lower density, thus giving less background problems. For the helium-filled, aluminum-plate chamber we shall describe later, the average density is about 1/50 that of liquid hydrogen.

We shall now amplify points (a), (b), (c) and (e) above.

We consider first point a. From our report on the 3-Bev colliding-beam detection system,* we take the formula for the standard deviation σ_p in the measurement of the momentum p of a track as

$$\frac{\sigma_p}{p} = \frac{.27}{B}\sqrt{\frac{4.4}{v^2 L L_{rad}} + \frac{p^2 \sigma_M^2}{L^4}}$$

where the average track angle with the magnetic field is taken as 85°;

B is the magnetic field in kilogauss;

L is the track length in meters;

L_{rad} is the radiation length of the material in meters;

v is the velocity of the particle;

σ_M is the standard deviation in the measurement of the position of a spark or bubble in mm;

p is in Gev/c.

We take $v \approx 1$ for simplicity and the following values for comparing spark and bubble chambers.

Hydrogen bubble chamber: $L_{rad} = 11$ meters, $\sigma_M = .05$ mm

The σ_M value is that of the 20-inch chamber of Shutt, and is as small as can be obtained with present bubble-chamber techniques. It is doubtful if a very large bubble chamber can maintain this accuracy. In particular, the diffraction depth-of-field limitation on the minimum size of the bubble image will certainly increase σ_M. However, we shall continue to use this σ_M value so that there will be no chance of our underestimating the bubble-chamber accuracy.

The minimum σ_M for a spark chamber is of course not yet known. According to J. Cronin, who recently surveyed present spark-chamber techniques in his review articles [I.R.E. Trans. on Nuclear Science, NS-9, No. 3, 247 (1962); and International Conference on High Energy Instrumentation at CERN, 1962], $\sigma_M = 0.2$ mm has been attained in some chambers. This number is also

*Report H in this volume.

probably close to the limit for present techniques. We will add into this 0.2 mm the error due to diffraction depth-of-field broadening of the spark image for a 1-meter-deep chamber, as discussed in our report (SLAC-5H) on a colliding-beam detection system. This yields $\sigma_M = 0.22$ mm. We propose that the spark chamber be helium-filled at a pressure of one atmosphere and that it use very thin aluminum plates. A design that looks satisfactory is to use 30 plates, 1/2 mil thick, per meter. The radiation length of the helium is 1900 meters. The effect of the aluminum plates is to reduce this to a composite radiation length of 1050 meters. The best arrangement of the 30 plates per meter is not known at present. If wide-gap spacing gives the best σ_M, then the plates would be evenly spaced, thus giving 30 sparks per meter. If small spacing is used, then groups of three plates might be used, giving thus 20 sparks per meter. The values used for the spark chamber are therefore:

Helium-filled, thin-plate spark chamber:

$$L_{rad} = 1050 \text{ meters}, \quad \sigma_M = 0.22 \text{ mm}$$

Inserting these values in the $\sigma_{p/p}$ equation we find for the hydrogen bubble chamber

$$\frac{\sigma_p}{p} = \frac{1.7 \times 10^{-1}}{B} \left[\frac{1}{L} + 6.2 \times 10^{-3} \frac{p^2}{L^4} \right]^{\frac{1}{2}}$$

and for helium, thin-plate spark chamber

$$\frac{\sigma_p}{p} = \frac{1.7 \times 10^{-2}}{B} \left[\frac{1}{L} + 11.7 \frac{p^2}{L^4} \right]^{\frac{1}{2}}$$

When $11.7\ p^2/L^4$ is much smaller than $1/L$ we find

$$\frac{\sigma_p \text{ (spark chamber)}}{\sigma_p \text{ (bubble chamber)}} = 1/10$$

This is of course a consequence of the one-hundred-times-greater radiation length in the spark chamber. On the other hand, when $6.2 \times 10^{-3} p^2/L^4$ is much greater than $1/L$,

$$\frac{\sigma_p \text{ (spark chamber)}}{\sigma_p \text{ (bubble chamber)}} = \frac{1}{10}\left[\frac{11.7}{6.2 \times 10^{-3}}\right]^{\frac{1}{2}} = 4.3$$

The two instruments have equal $\sigma_{p/p}$ when

$$\left[\frac{1}{L} + 11.7\,\frac{p^2}{L^4}\right] = 100\left[\frac{1}{L} + 6.2 \times 10^{-3}\,\frac{p^2}{L^4}\right]$$

or when

$$p^2 = 9L^3$$

Thus for $L = 2$ meters, the spark chamber is better up to 8.5 Bev/c. For $L = 4$ meters, the spark chamber is better up to 24 Bev/c. The best way to make this comparison is to look at Fig. 2, where $\sigma_{p/p}$ is plotted in percent against the momentum p (in Bev/c) for $L = 1,2,4$, and 6 meters; and for a 17-kilogauss field.

The above comparison is based on a fixed number of measurements for the total path length of the particle, about 11. The rise in the spark chamber curves is caused by the increased importance of σ_M at large momentum. The size of the σ_M term can be decreased by taking more measurements. These additional measurements do not help the multiple scattering, however, and therefore will not help the bubble-chamber measurement since it is mostly limited by multiple scattering. Therefore, if we were willing to make more measurements in the spark chamber than in the bubble chamber, we could improve the spark chamber even further. We have not had time to analyze this curve carefully, but <u>very</u> roughly we find we can replace the

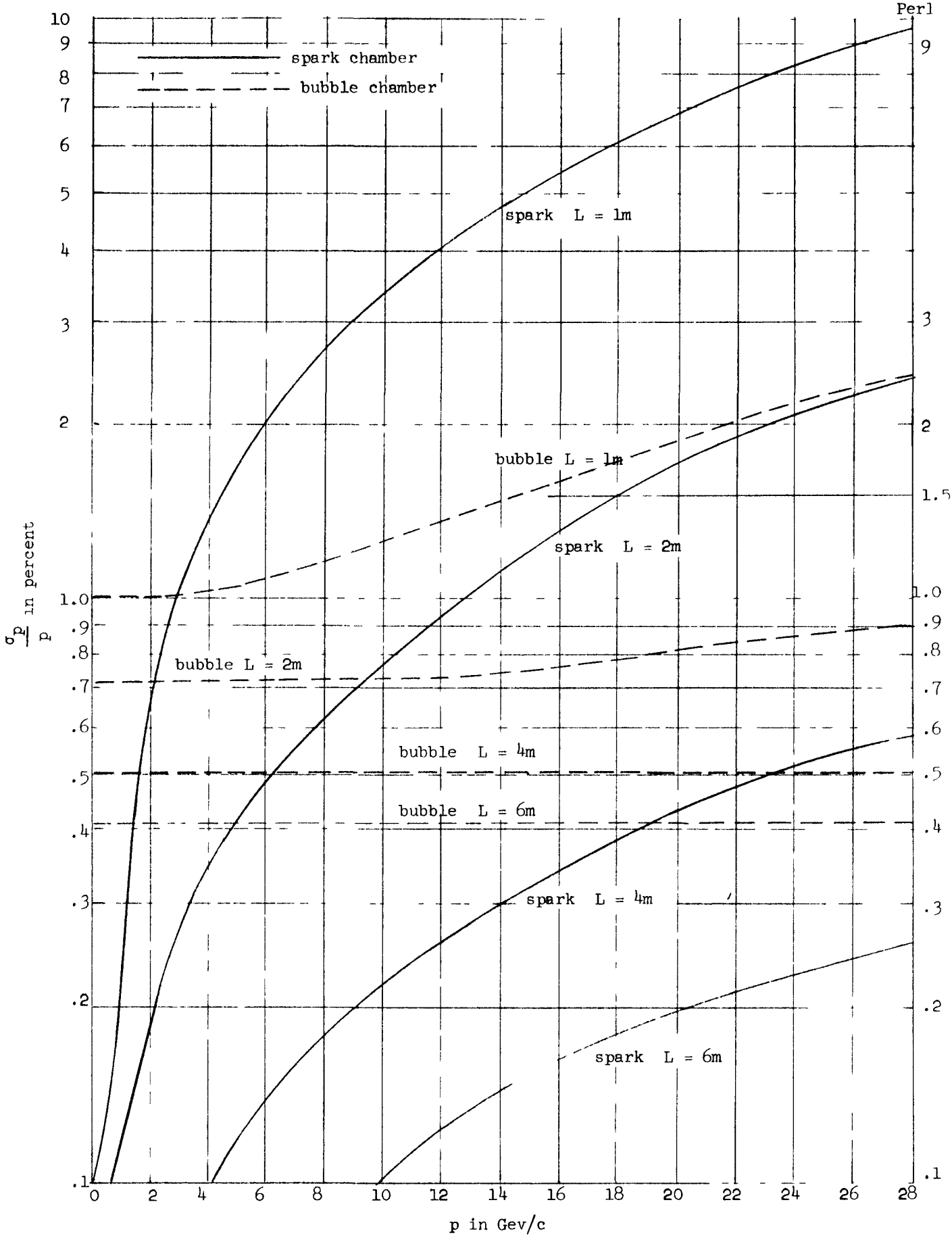
spark chamber
bubble chamber
spark L = 1m
bubble L = 1m
spark L = 2m
bubble L = 2m
bubble L = 4m
bubble L = 6m
spark L = 4m
spark L = 6m
$\frac{\sigma_p}{p}$ in percent
p in Gev/c

FIGURE 2

formula

$$\frac{\sigma_p}{p} = \frac{.27}{B}\left[\frac{4.4}{LL_{rad}} + \frac{p^2\sigma_M^2}{L^4}\right]^{\frac{1}{2}}$$

by

$$\frac{\sigma_p}{p} = \frac{.27}{B}\left[\frac{4.4}{LL_{rad}} + \frac{11p^2\sigma_M^2}{nL^5}\right]^{\frac{1}{2}}$$

where n is the number of measurements per meter.

For the spark chamber under consideration here, n can equal 20 or 30. Figure 3 uses this formula to compare the two kinds of chambers for $B = 17$ kilogauss and $L = 1,2$, and 4 meters. Here we see the type of spark chamber improvement which is probably possible for $n = 20$. The bubble chamber is also calculated for $n = 20$.

Closely connected with the precision of momentum determination in the identification of an event is the precision of angular measurement. However, for simplicity, we shall consider angular measurements without a magnetic field present. If there were no multiple scattering, and if n points per meter were measured along a track of length L meters, then the standard deviation in measurement of the angle of a track, σ_α, would be given by

$$\sigma_\alpha = \frac{\sigma_M}{L}\left[\frac{12}{Ln}\right]^{\frac{1}{2}} \times 10^{-3} \text{ radians}$$

where σ_M, as defined before, is in mm. When multiple scattering is included, the composite standard deviation is

$$\sigma_\alpha = \left[\frac{12\sigma_M^2}{nL^3} + \frac{81L}{p^2L_{rad}}\right]^{\frac{1}{2}} 10^{-3} \text{ radians}$$

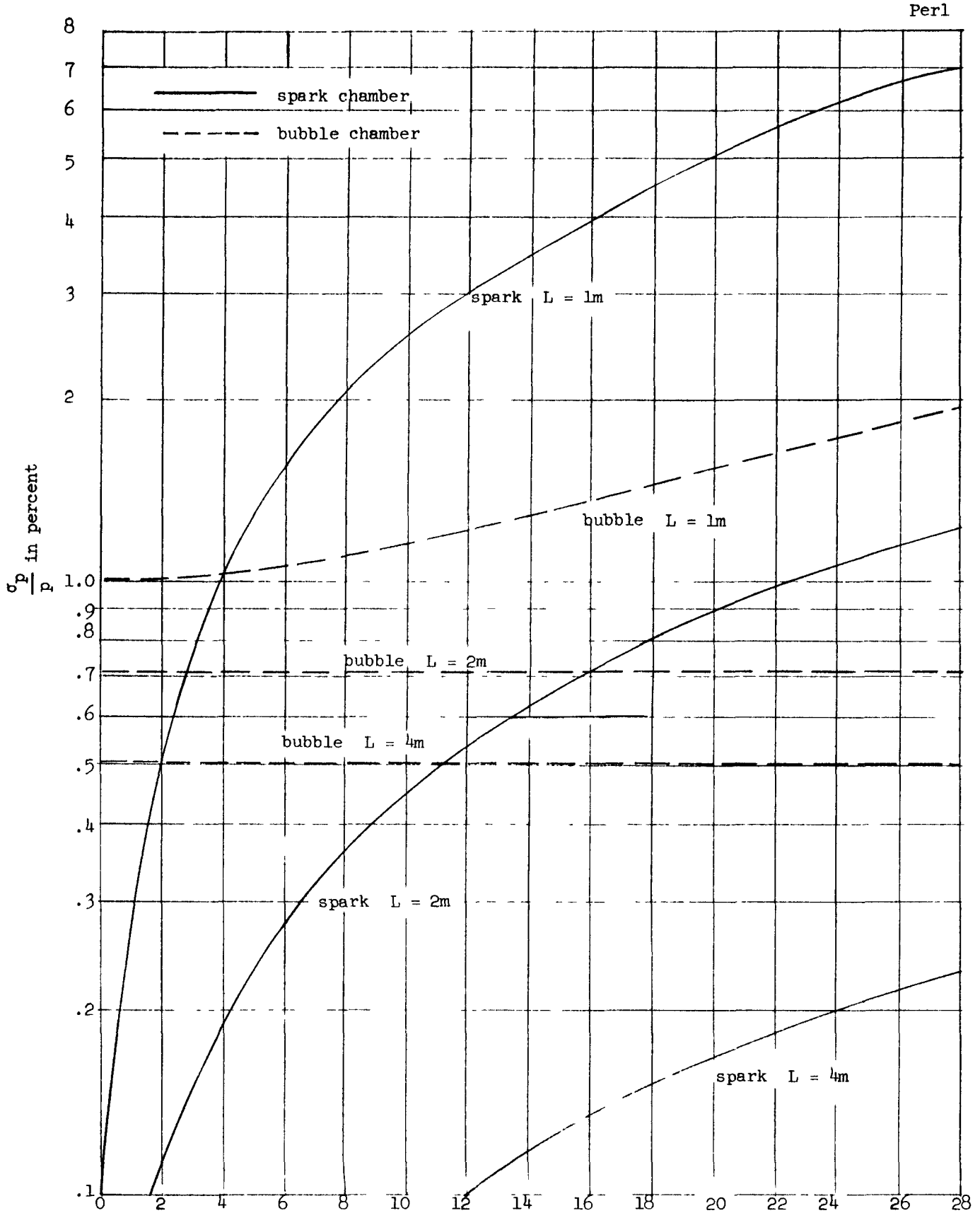
spark chamber
bubble chamber
spark L = 1m
bubble L = 1m
bubble L = 2m
bubble L = 4m
spark L = 2m
spark L = 4m
$\frac{\sigma_p}{p}$ in percent
p in Gev/c
8
7
6
5
4
3
2
1.0
.9
.8
.7
.6
.5
.4
.3
.2
.1
0
2
4
6
8
10
12
14
16
18
20
22
24
26
28

FIGURE 3

where p is in Bev/c, and we have taken $v \approx 1$. This formula and the ones that follow are the same as those used by R. W. Williams [Can. J. Phys. 37,] 1085 (1959) . Now σ_α is a minimum when $L = L_{min}$, where

$$L_{min} = \left[.67 \sigma_M p \sqrt{\frac{L_{rad}}{n}} \right]^{\frac{1}{2}}$$

For the spark chamber,

$$L_{min} = \frac{2.2 \sqrt{p}}{n^{\frac{1}{4}}}$$

For the bubble chamber,

$$L_{min} = \frac{.33 \sqrt{p}}{n^{\frac{1}{4}}}$$

In both cases we can take, if necessary, $n \approx 20$.

$$L_{min} \text{ spark chamber} \approx \sqrt{p} \text{ meters}$$

$$L_{min} \text{ bubble chamber} \approx .15 \sqrt{p} \text{ meters}$$

Therefore L_{min} is about 6 times smaller in the bubble chamber. However, at L_{min} the value of σ_α is different in the two cases because

$$\sigma_{\alpha_{min}} = \frac{9.4 \, \sigma_M^{\frac{1}{4}}}{p^{\frac{3}{4}} n^{\frac{1}{8}} \left(L_{rad} \right)^{\frac{3}{8}}}$$

Therefore if L_{min} is obtained in both cases (and n is the same in both cases),

$$\frac{\sigma_{\alpha_{min}}\text{(spark chamber)}}{\sigma_{\alpha_{min}}\text{(bubble chamber)}} = \left[\frac{\sigma_M(\text{spark})}{\sigma_M(\text{bubble})}\right]^{\frac{1}{4}} \left[\frac{L_{rad}(\text{bubble})}{L_{rad}(\text{spark})}\right]^{\frac{3}{8}} = 0.26$$

and the spark chamber angular measurement is <u>four</u> times better. Finally, in Fig. 4 the σ_α is compared for the two kinds of chambers for $p = 1$, 3 and 10 Bev/c for $n = 20$.

Next we consider point (b), namely, the case of γ-ray detection and $e^{\pm}$ identification. G. Trilling in his study of the use of a large hydrogen bubble chamber at M (SLAC-5-E) has shown the great importance of γ-ray detection in order to find π^o mesons and to obtain their kinetic parameters. He shows that large groups of events with missing mass cannot be identified without this π^o knowledge. He also develops formulas for the required number and thickness of high-Z plates to be placed in the hydrogen bubble chamber.

Following Trilling, the high-Z plates have thickness t (in radiation lengths), and these plates are separated by a distance d. In the bubble chamber this distance d is of course filled with liquid hydrogen, and the curvatures of the electron-positron pair in this gap give the γ-ray momentum. The analogous situation in the spark chamber is to fill the gap with several thin plates of the same type as are used in the main spark chamber. This is the situation we study here, for direct comparison with the bubble chamber.

The standard deviation in the momentum of a γ-ray converted to an electron-positron pair in the thick plate in either chamber is

$$\frac{\sigma_p}{p} = \left[\left(\frac{0.6t}{L_{rad}\text{ of plates}}\right)^2 + 0.4\left(\frac{0.27}{B}\right)^2 \times \left(\frac{4.4}{dL_{rad}\text{ of medium}} + \frac{p^2\sigma_M^2}{d^4}\right)\right]^{\frac{1}{2}}$$

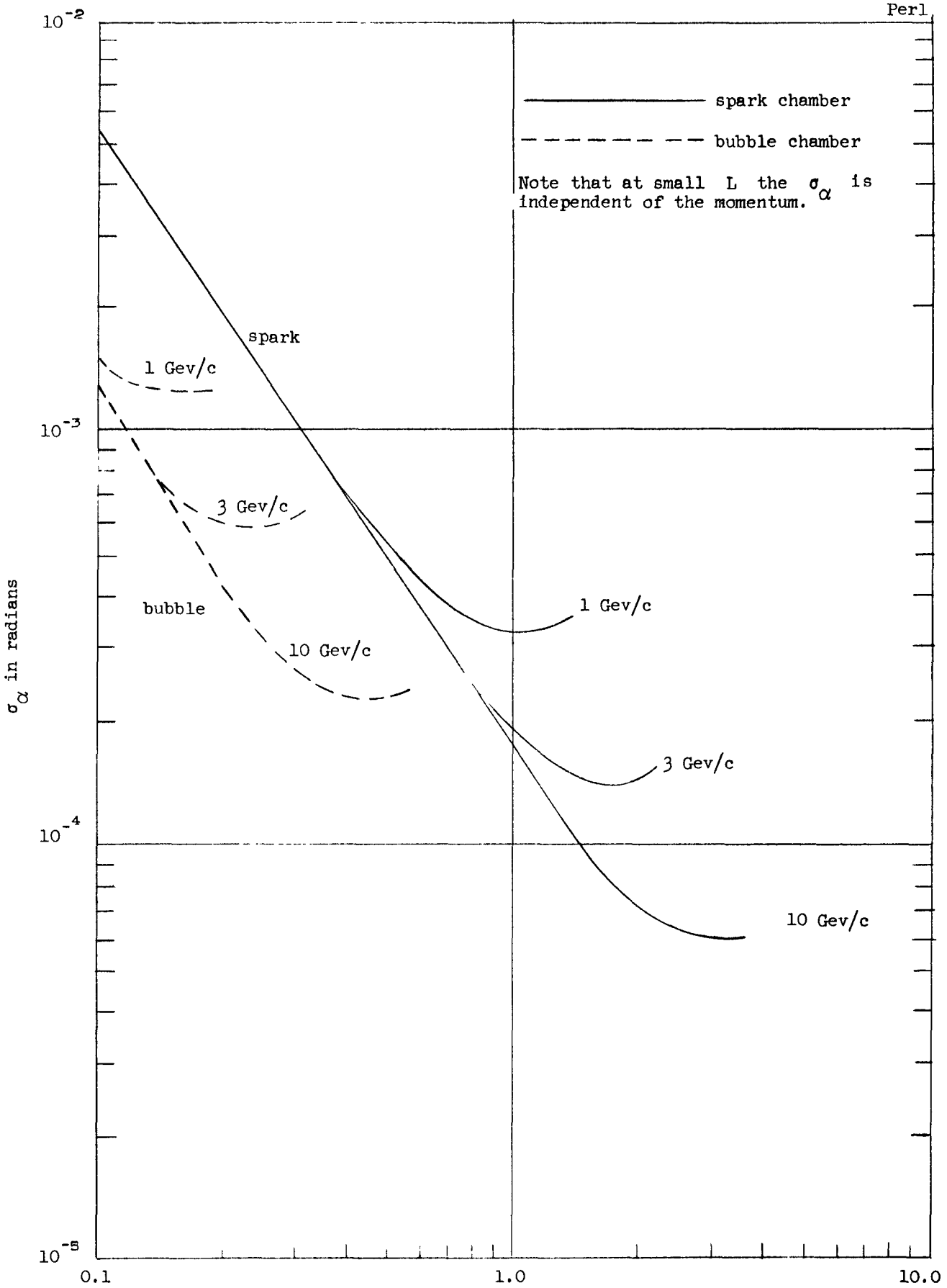
spark chamber
bubble chamber
Note that at small L the σ_α is independent of the momentum.
spark
1 Gev/c
3 Gev/c
bubble
10 Gev/c
1 Gev/c
3 Gev/c
10 Gev/c
10^{-2}
10^{-3}
10^{-4}
10^{-5}
σ_α in radians
0.1
1.0
10.0
L in meters

FIGURE 4

Since d will be a fraction of a meter, for the spark chamber the σ_M term will predominate over the multiple-scattering terms; for the bubble chamber, following Trilling, the σ_M term will also predominate. Therefore in both cases

$$\frac{\sigma_p}{p} = \left[\left(\frac{0.6t}{L_{rad\ plates}} \right)^2 + \left(\frac{0.17\sigma_M p}{Bd^2} \right)^2 \right]^{\frac{1}{2}}$$

If the total length of γ-detecting plates and gaps is D, and N radiation lengths are used, then

$$d = D \left[\frac{t/L_{rad}(\text{of plates})}{N} \right]$$

Trilling shows that the minimum $\sigma_{p/p}$ occurs when

$$t_{min} = (2)^{\frac{1}{6}} \left[\frac{0.17\sigma_M p}{B \left(\frac{D}{NL_{rad}} \right)^2 \left(\frac{0.6}{L_{rad}} \right)} \right]^{\frac{1}{3}}$$

or

$$t_{min} = L_{rad} \left[\frac{0.40\sigma_M p N^2}{BD^2} \right]^{\frac{1}{3}}$$

Finally, the minimum σ_p/p is given by

$$\left(\frac{\sigma_p}{p}\right)_{\text{minimum}} = 0.54 \left[\frac{\sigma_M p}{B}\right]^{\frac{1}{3}} \left[\frac{N}{D}\right]^{\frac{2}{3}}$$

For the same N and B in both kinds of chambers we obtain the same $\left(\sigma_p/p\right)_{\text{min}}$ when

$$\left(\frac{\sigma_M}{D^2}\right)_{\text{spark}} = \left(\frac{\sigma_M}{D^2}\right)_{\text{bubble}}$$

or

$$\frac{D(\text{spark})}{D(\text{bubble})} = \left(\frac{0.22}{0.05}\right)^{\frac{1}{2}} = 2.1$$

Therefore more space is required in the spark chamber for the same precision in γ-ray momentum measurement. Or if the same space is used,

$$\frac{\left(\sigma_p/p\right)_{\text{min}}(\text{spark})}{\left(\sigma_p/p\right)_{\text{min}}(\text{bubble})} = 1.6$$

We consider this requirement of more space, or the increased error, to be more than compensated for by the much greater ease of arranging the γ-conversion chambers in or around a large spark chamber. In particular, most of a large spark chamber can be surrounded by these γ-conversion chambers; whereas in a bubble chamber it is probably only feasible to put high-Z plates in the downstream end of the chamber. This larger-solid-angle coverage in the spark chamber also means that identification of electrons and positrons by showering in the γ-conversion plates will be used more often.

There is of course another way to build a γ-conversion chamber, which is to use a large number of thin but high-Z plates. This situation is then analogous to a high-Z material bubble chamber in a magnetic field. We have not had time to investigate this situation, but it should be studied.

Point (c), the greater flexibility of the spark chamber and the ability to incorporate additional instrumentation, becomes clear if one thinks of possibilities like differential Cerenkov counters placed downstream to determine the mass of the very fast and forward reaction products; or extra spark chambers being placed 5 or 10 meters downstream to measure some high momentum very well.

As an example of this last idea, consider the large spark chamber immersed in a relatively low magnetic field, say, 10 kilogauss. This would considerably decrease the magnet cost. But downstream of the main spark chamber let there be a high-magnetic-field evacuated region and then another spark chamber. Let the length of track in each spark chamber be L, and in the evacuated high-field region let it be L_B (Fig. 5). Then the standard deviation of the entering or exit angle is σ'_α, where

$$\sigma'_\alpha = \left[\frac{12\sigma_M^2}{nL^3} + \underbrace{\frac{81L}{p^2 L_{rad}}}_{\text{chambers}} + \underbrace{\frac{144t}{p^2 L_{rad}}}_{\text{end windows}} \right]^{\frac{1}{2}} 10^{-3} \text{ radians}$$

where t is the thickness of the vacuum end windows.

We take $\sigma_M = 0.22$ mm, $n = 20$ measurements/meter, $t = 5 \times 10^{-3}$ inches of mylar, L_{rad} of chamber = 1070 meters. This yields

$$\sigma'_\alpha = \left[\frac{0.029}{L^3} + \frac{0.076L + .037}{p^2} \right]^{\frac{1}{2}} 10^{-3} \text{ radians}$$

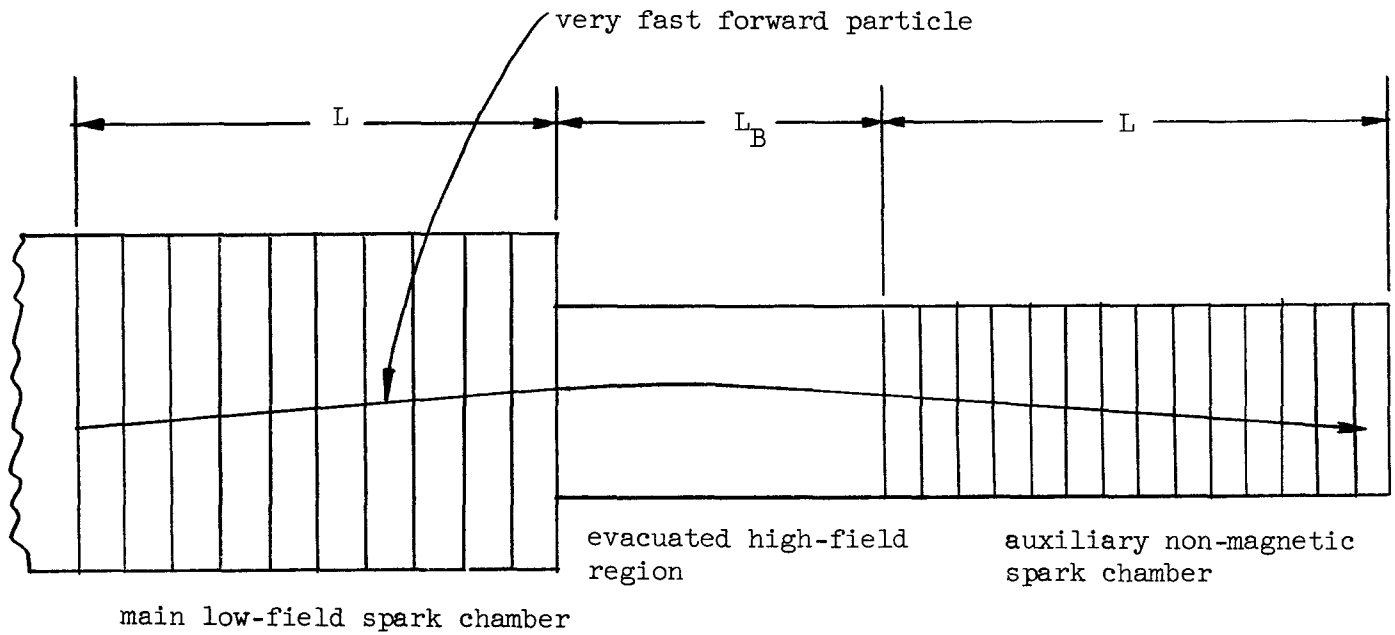
very fast forward particle
L
L_B
L
evacuated high-field region
auxiliary non-magnetic spark chamber
main low-field spark chamber

FIGURE 5

The particle makes an angle α' in the magnet, where

$$\alpha' = \frac{BL_B}{33.6p}$$

B is in kilogauss, L and L_B in meters, and p in Bev/c. Therefore

$$\frac{\sigma_p}{p} = \frac{4.7 \times 10^{-2}}{BL_B} \left[\frac{.029p^2}{L^3} + .076L + .037 \right]^{\frac{1}{2}}$$

We can easily obtain L = 2 meters and L_B = 1 meter; then

$$\frac{\sigma_p}{p} = \frac{2.0 \times 10^{-2}}{B} \left[1 + .018p^2 \right]^{\frac{1}{2}}$$

If B = 30 kilogauss,

$$\frac{\sigma_p}{p} = 0.7 \times 10^{-3} \left[1 + .018p^2 \right]^{\frac{1}{2}}$$

and for p = 24 Bev/c we still get

$$\frac{\sigma_p}{p} = 0.24 \text{ percent}$$

A similar precision was obtained with a 4-meter-long, 17-kilogauss spark chamber in Fig. 4, but this might be a cheaper way to get the same precision. We have not had time to study the best design, for the large spark chamber, for best momentum precision at fixed cost.

Although we have so far specified non-selective triggering, it is of

course possible to use partially selective triggering. Thus one can enhance the ratio of Λ^{o}-producing events by setting up triggering counters requiring a V in the chamber. Such triggering systems have already been used. It should also be noted that in the spark chamber the hydrogen target can be placed in the best position for event analysis. In a bubble chamber, events occurring too near the downstream end cannot be analyzed because of poor momentum measurements on the forward particles. In the spark chamber, the hydrogen target will usually be upstream, as shown in Fig. 6. But if certain experiments require a shift of the hydrogen target, this can be done.

Point (e) concerns the relative costs. If the same size and strength magnet is used for both kinds of chambers, the spark chamber will be cheaper, but the fractional saving may be only 0.2, especially if the costs of generating equipment are included. However, the possibility of using a more flexible magnetic-field arrangement exists for the spark chamber. Thus, the savings may be greater. Finally, the design and building of a large spark chamber is much simpler than a large hydrogen bubble chamber. A medium-size machine shop can make the chambers, and the pulsing electronics is also only a medium-size job. No special knowledge is required equivalent to the cryogenic knowledge and experience needed to design a large hydrogen bubble chamber. Of course the magnet is a major job for both chambers.

Figure 6 shows a 4-meter-long spark chamber based on the considerations we have discussed here. With this as an example we shall conclude this section with some of the disadvantages of the large spark chamber as compared to the large hydrogen bubble chamber.

(a) The interaction region is not seen. One important question is the error in the track angle caused by multiple scattering in the hydrogen target. The target in Fig. 6 is 50 cm long; the inner diameter is 4 cm; there is a 5 mil mylar inner jacket; there is a 1 cm thick "super insulation" between the jackets; and the outer jacket is 0.5 mm thick aluminum.

For a particle making an angle θ with the entering beam the maximum standard deviation caused by multiple scattering in the target is

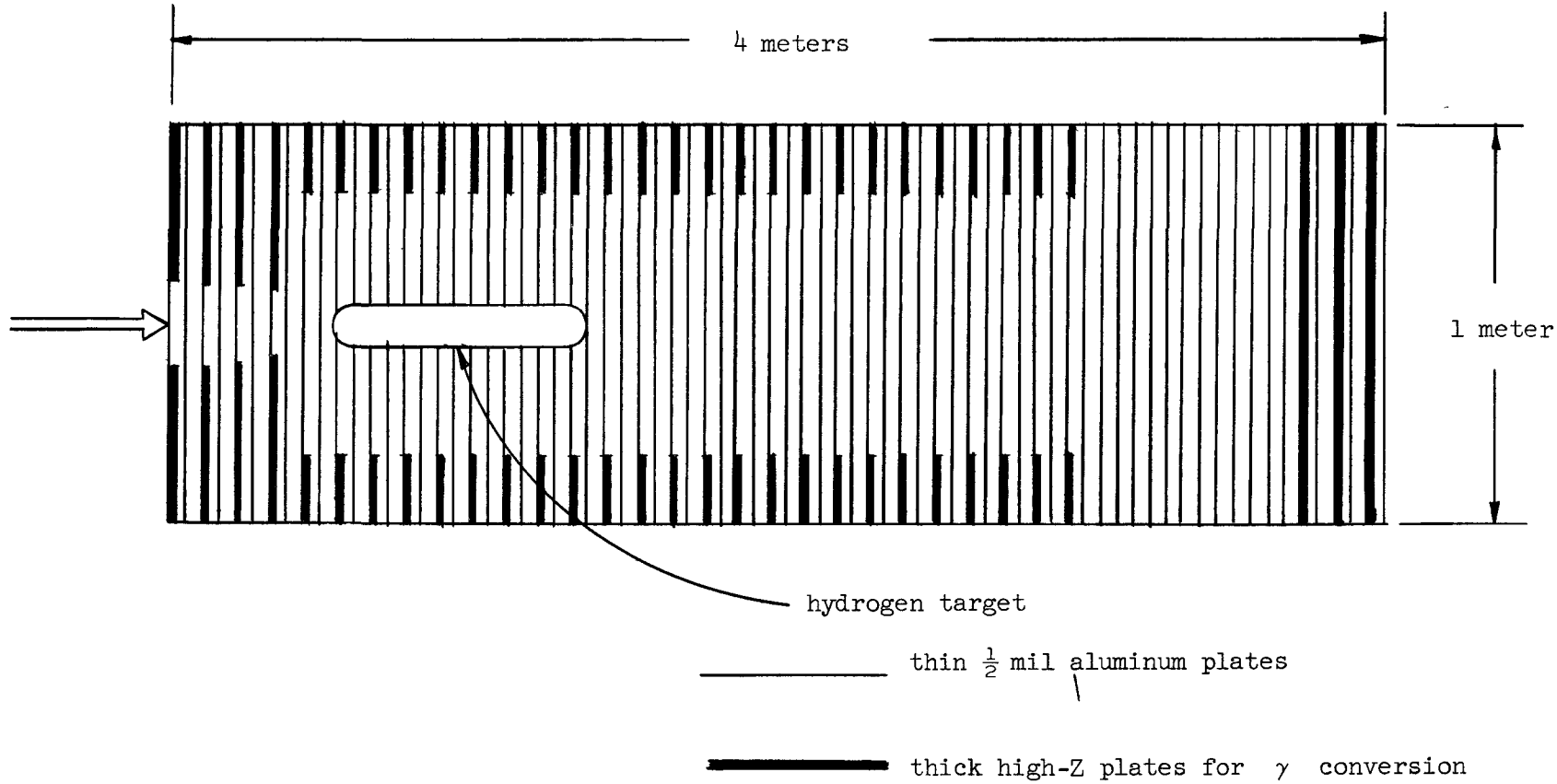

FIG. 6--Large spark chamber (magnet not shown; optics not shown).

$$\text{Maximum } \sigma_\theta \text{ (spark chamber target)} = \left\{ \begin{array}{l} \dfrac{1.1 \times 10^{-3}}{p\sqrt{\sin\theta}} \text{ rad for } \theta > \dfrac{1}{25} \text{ rad} \\ \\ \dfrac{2.6 \times 10^{-3}}{p} \text{ rad for } \theta < \dfrac{1}{25} \text{ rad} \end{array} \right\}$$

We wish to comapre this with the minimum σ_α in a hydrogen bubble chamber as calculated before:

$$\sigma_{\alpha_{\text{minimum}}} \text{ (bubble chamber)} = \frac{9.4\sigma_M^{\frac{1}{4}} \times 10^{-3}}{p^{\frac{3}{4}} n^{\frac{1}{8}} (L_{\text{rad}})^{\frac{3}{8}}} \text{ rad} = \frac{1.4 \times 10^{-3}}{p^{\frac{3}{4}}} \text{ rad}$$

for $n = 10$. The corresponding spark chamber quantity would be

$$\sigma'_\alpha \text{ (spark chamber)} = \left[\sigma^2_{\alpha_{\text{minimum}}} \text{ (spark chamber)} + \bar{\sigma}^2_\theta \text{ (spark chamber target)} \right]^{\frac{1}{2}}$$

where

$$\bar{\sigma}_\theta \text{ (spark chamber target)} = \text{maximum } \sigma_\theta \text{ (spark chamber target)}$$

and

$$\sigma_{\alpha_{\text{minimum}}} \text{ (spark chamber)} = \frac{0.30 \times 10^{-3}}{p^{\frac{3}{4}}} \text{ rad}$$

for $n = 10$.

Therefore for tracks starting in the target the ratio of the angular precisions is

$$\frac{\sigma'_\alpha \text{ (spark chamber)}}{\sigma_\alpha \text{ (bubble chamber)}} = \begin{cases} \left[\dfrac{0.16}{\sin\theta\sqrt{p}} + 0.06\right]^{\frac{1}{2}} & \text{for } \theta > \dfrac{1}{25} \text{ rad} \\ \left[\dfrac{0.9}{\sqrt{p}} + 0.06\right]^{\frac{1}{2}} & \text{for } \theta < \dfrac{1}{25} \text{ rad} \end{cases}$$

(These ratios are plotted in Fig. 7.) Therefore the loss of angular accuracy in the spark-chamber target is noticeable.

There will also be a loss of other kinds of information; for example, very slow recoil protons will not be seen, and the vertex of V particles which decay in the target will not be as well determined.

(b) The bubble chamber provides velocity information by ionization measurements. At present this can be done only very crudely in a spark chamber and no one knows how to improve this. These ionization measurements are therefore a clear bubble-chamber advantage.

(c) Another type of bubble-chamber advantage lies in range measurements. Range can be measured in a spark chamber by using many not-too-thin plates, but it is difficult to get precision equal to that of a hydrogen bubble chamber. It is hard to say how useful range measurements will be for 10- or 20-Bev events, but we suspect they will only be occasionally useful, no matter what kind of chamber is used.

(d) A final advantage of the bubble chamber is that secondary interactions can occur in the hydrogen and be studied. This can of course also be done in the spark chamber by using a second target, but it probably would not be done often. Table V summarizes the relative advantages of the two kinds of chambers.

For interactions at high energy there will be types of events that both kinds of chambers can handle, but there will be also types which are analyzable in one type of chamber but ambiguous in the other type. The selection of the best instrument therefore depends to some extent on

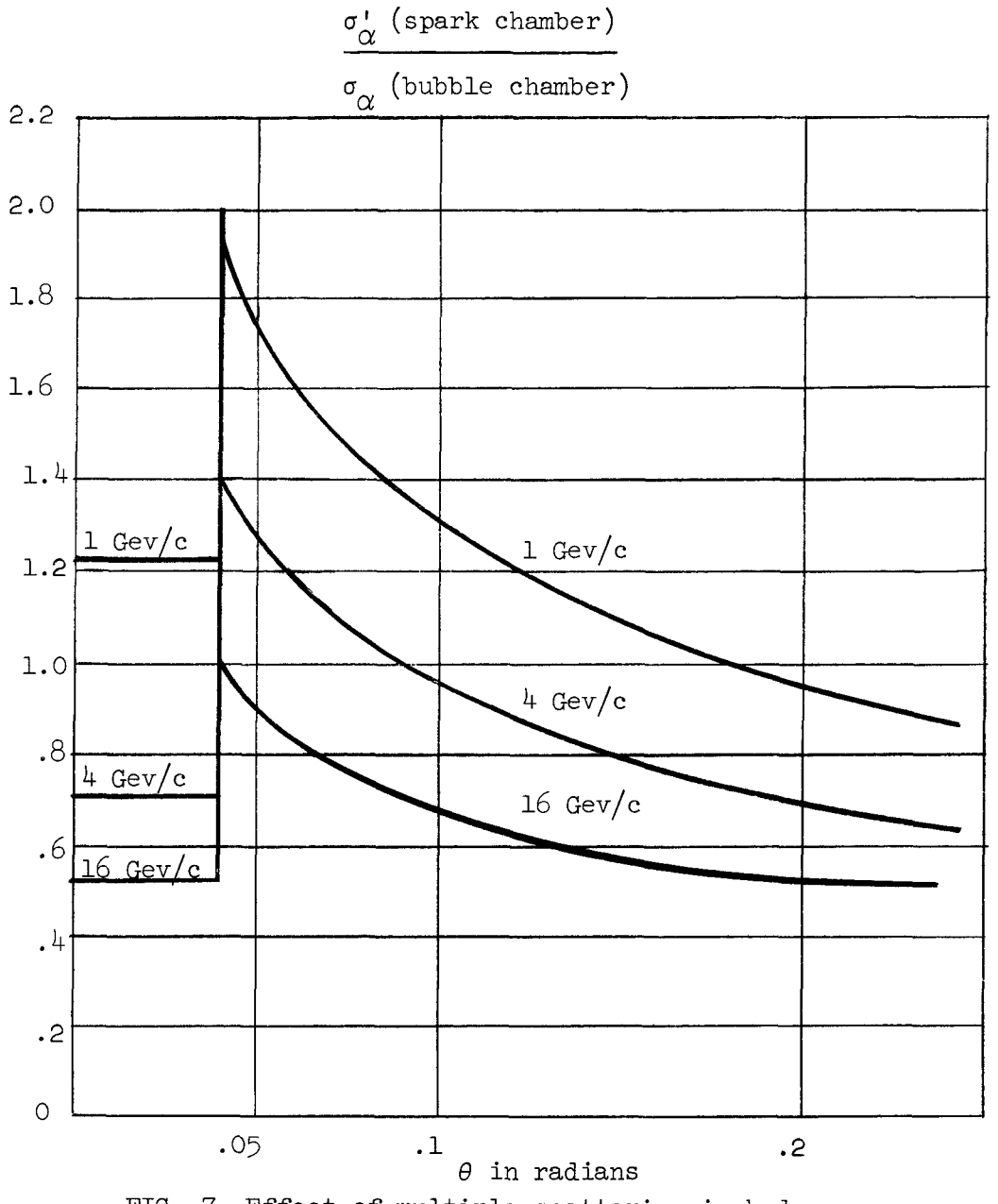

FIG. 7--Effect of multiple scattering in hydrogen target and target walls of spark chamber.

which kinds of events will be most interesting to study. We believe that the types requiring advantages 1,2, and 5 (in Table 5) of the spark chamber will be the most interesting types, and hence we favor the spark chamber.

TABLE V

Helium Spark Chamber with Thin Plates and Auxiliary High-Z Plates	Hydrogen Bubble Chamber with High-Z Plates
1. Several hundred times greater rate of recording events.	1. More information around interaction region.
2. Better momentum measurements.	2. Ionization measurements.
3. Better angular measurements for non-target particles. (Otherwise angular precision is roughly equal.)	3. Better range measurements.
4. More flexible.	4. More suitable for secondary interactions.
5. Easier to measure γ rays.	5. Several large chambers have been built and have proven very useful.
6. Cheaper.	
7. Simpler analysis.	

4. Selective Triggering of Spark Chambers

(a) Incident secondary beams limited by detection equipment

We now return to the conventional uses of the spark chamber. Referring to Table IV we see that when complex counter and spark-chamber systems are placed in the secondary beam only about 10 particles per pulse are allowed. This situation requires that one think more in terms of events per second rather than per pulse. Consider a 17 Bev/c π^- beam from M under these conditions, and a similar beam from the A.G.S. at Brookhaven. R. L. Cool [International Conference on High Energy Accelerators, Brookhaven (1961)] gives the rate for the A.G.S. as 10^{-3} (π^-/Bev, ster, proton) at 4.75° and for 30-Bev protons. Using 10^{11} protons and, as before, 10^{-3} ster. and $\pm \frac{1}{2}\%$ momentum resolution, this yields 17,000 π^- every two seconds or 8000 π^-/sec. The rate from M would be 3600 π^-/sec because of the detection-equipment limitation. Therefore, for these "in-beam" counter

and spark-chamber π experiments M has no advantage over the A.G.S. machines, and is probably harder to use and the electronics more costly and complicated. For K^+ the situation is somewhat the same. However for K^- and $\bar{p}$ the A.G.S. yield is down by factors of about 40 and 400, respectively, from the π yield. Therefore, although "in-beam" counter and spark chamber K^- and $\bar{p}$ experiments at M will not use the full intensity by any means, they will give data at 20 to 200 times the rate obtainable at the A.G.S. machines. Table I shows this to be the case even for the pessimistic "in-beam" estimates. Therefore, we expect that K^- and $\bar{p}$ "in-beam" spark-chamber experiments could be carried out advantageously at M. The equipment and electronics would not be very different from that now used, and there seems to be no need for further comment on how these experiments would be done except to point out that one cannot tell at this time whether electronically separated beams or physically separated beams would be used for these experiments.

(b) Incident secondary beams limited by a mass-separation requirement

Here we consider the case where the full intensity of M is used, but where physical mass separation is required and therefore the final secondary beam intensity is about 50 times smaller than in an unseparated beam. In this case, except for the pessimistic K^+ estimate, all other beams are greater than the A.G.S. beams. Thus even the pessimistic π^+ estimate for M is 18,000 per second compared to the aforementioned 8,000 per second. But the larger improvements occur in $K^\pm$ and $\bar{p}$. The $K^\pm$ rate is 40 times greater and the $\bar{p}$ rate is 4000 times greater if we use the optimistic estimates. Of course to make use of these greater rates, as compared to those given in the last section, the spark chambers must be out of the incident beam.

As an example of such an experiment we describe the study of peripheral interactions, as represented by the diagram of Fig. 8, in which the mass spectra of the two peripherally produced particles are studied along with their angular distributions. Figure 9 shows the experimental arrangement, in which all chambers and counters are outside the beam. The

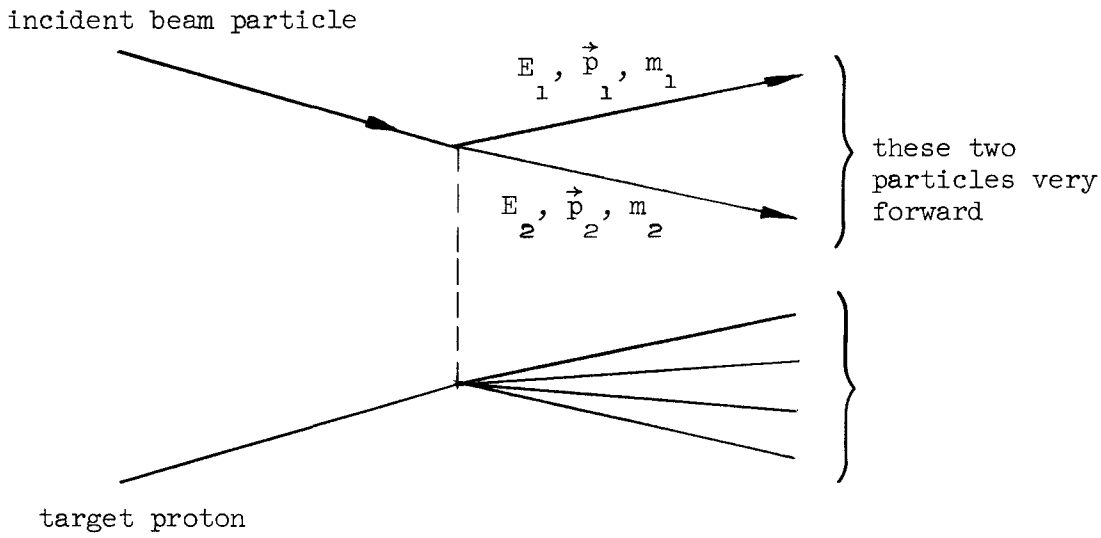
incident beam particle
$E_1, \vec{p}_1, m_1$
$E_2, \vec{p}_2, m_2$
these two particles very forward
target proton

FIGURE 8

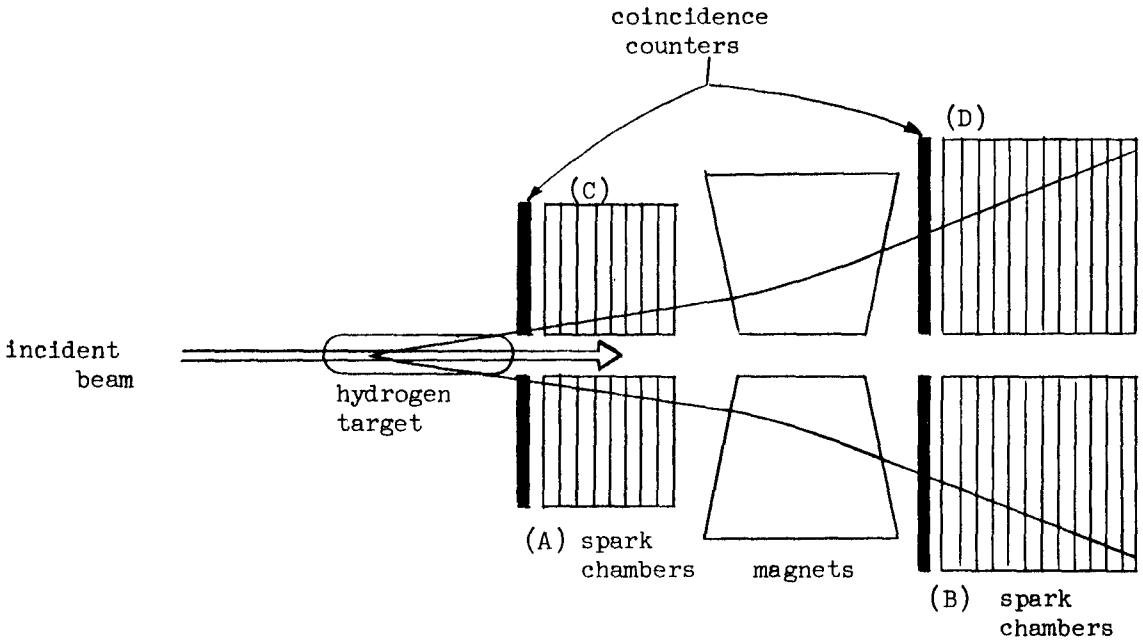

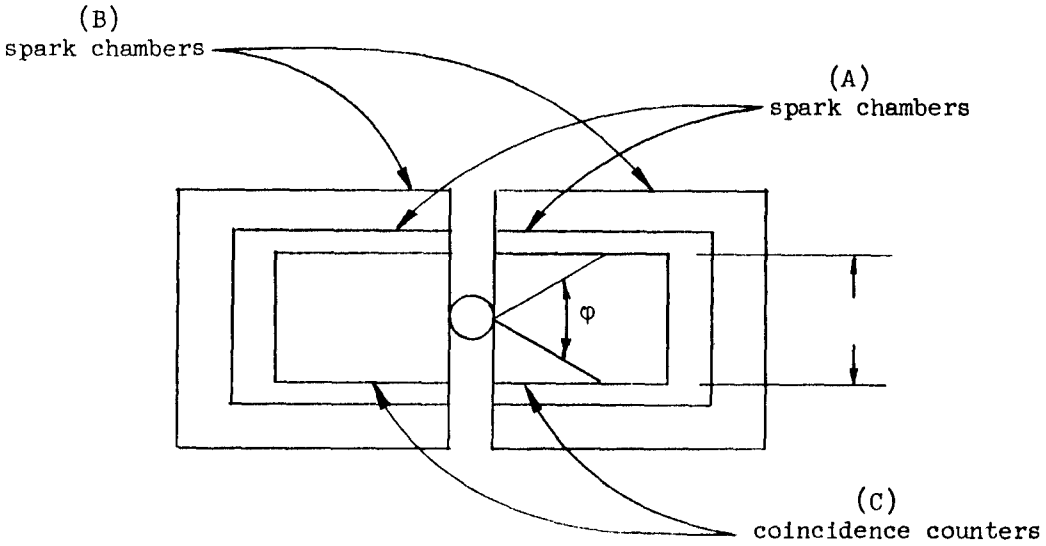

FIG. 9--View looking downstream (magnet not shown).

rest mass of the two-particle systems is given by

$$(M^*)^2 = m_1^2 + m_1^2 + E_1E_2 - 2\vec{P}_1 \cdot \vec{P}_2$$

From the previous spark-chamber calculations in this report, we feel confident that each momentum can be measured to at least 0.5% and the angles to 2×10^{-3} radians. If the total energy of the two particles is $E = E_1 + E_2$, then

$$\frac{\sigma_{M^*}}{M^*} \approx \left[\frac{E}{2M^*}\right]^2 \left[\theta\right] \left[1 + 3\theta^2\right]^{\frac{1}{2}} \left[2 \times 10^{-3}\right]$$

where θ (in radians) is the angle $\vec{p}_1$ and $\vec{p}_2$.

As an example, take $E = 20$ Bev, $M = 1$ Bev, and $\theta = 0.1$. Then

$$\frac{\sigma_{M^*}}{M^*} = .02$$

Note that although the beam collimation and momentum resolution is quite good, no use is made of these properties to determine M^*.

There are many such strong-interaction experiments in which no "in-beam" counters or spark chambers are required, and these can be done well at M. These are experiments in which the $\pm \frac{1}{2}\%$ momentum resolution and 2×10^{-5} ster solid-angle limitation are sufficiently precise. We note that the 2×10^{-5} ster means that the angular divergence of a beam particle is less than 2.5×10^{-3}, which is very small and is comparable with spark chamber angular precision. Therefore in most cases the insertion of spark chambers in the beam is only necessary for better momentum determination, but even that cannot be improved very much for large momenta. Thus the class of experiments which can be done without spark chambers or counters in the beam is very large.

(c) Spark-chamber use of the full secondary beam intensity at M

The great restriction on full use by spark chambers of the secondary, strongly interacting beams at M is that the beams very probably will not be sufficiently pure. As we have seen in Section 4.C, physical separation still gives very useful beams, but the beam is down by a factor of 50 from the full intensity obtainable if no physical separation is used. It is impossible now to estimate what the maximum intensity of the beams will be because both the magnitude and purity of the beams is unknown. If the contamination in a beam were small, then a small amount of physical or electronic separations might be sufficient, and there might not be the factor of 50 drop in intensity. Also, some experiments can use partially contaminated beams, such as the large-angle elastic scattering to be described later.

With these statements of ignorance in mind, we shall conclude this report with an example of how one might use beams of 1000 to 10,000 particles per pulse, if beams of this magnitude and sufficient purity can be produced. To examine the use of these high intensities we shall consider in some detail the measurement of elastic π - p scattering using spark chambers at 10 to 25 Bev. We first consider a detailed study of the diffraction peak. Of course there is no way to tell how one will interpret the diffraction peak five or ten years from now, but we shall use as a guide the present Regge theory and see how well one could measure the presently unknown parameters in that theory. According to the Regge theory the scattering amplitude in the diffraction peak can be written as

$$f_{\pi^+,p}(s,t) = \beta_v(t) \left(\frac{s}{s_o}\right)^{\alpha_v(t)^{-1}} + \beta_\rho(t) \left(\frac{s}{s_o}\right)^{\alpha_\rho(t)^{-1}}$$

$$f_{\pi^-,p}(s,t) = \beta_v(t) \left(\frac{s}{s_o}\right)^{\alpha_v(t)^{-1}} - \beta_\rho(t) \left(\frac{s}{s_o}\right)^{\alpha_\rho(t)^{-1}}$$

where v and ρ stand for the Pomeranchuk (or vacuum) and ρ-meson trajectories, respectively, t is the square of the four-momentum transfer,

s is the square of the total energy in the barycentric system, s_o is a constant, and the β's and α's are functions of t only. The ABC trajectory is neglected for simplicity.

At present we know that $\beta_v(0)$ is larger than $\beta_\rho(0)$, perhaps 10 or 20 times larger. Also we know $\alpha_v(0) \approx 1$ and $\alpha_\rho(0) \approx 0.5$. The problem is to evaluate these α's and β's over a range of t from $t = 0$ to the largest value at which this parameterization is still useful and meaningful. This might be $t = -50m_\pi^2$ or $t = -400m_\pi^2$. No one knows at present.

To study $\beta_\rho(t)$ and $\alpha_\rho(t)$, consider

$$\left(\frac{d\sigma}{d\Omega}\right)_{\pi^+ + p} - \left(\frac{d\sigma}{d\Omega}\right)_{\pi^- + p} = 4 \, \mathrm{Re} \left[\beta_v(t) \beta_\rho^*(t)\right] \left[\left(\frac{s}{s_o}\right)^{\alpha_v(t) + \alpha_\rho(t)}\right]^{-2}$$

To simplify the analysis we take β_v and β_ρ as real, and we suppose that we know β_v and α_v as functions of t from other experiments. Let the standard deviation in a differential cross section measurement divided by the differential cross section be denoted by Σ, and let

$$\Delta = \frac{\partial \left[\left(\frac{d\sigma}{d\Omega}\right)_{\pi^+ + p} - \left(\frac{d\sigma}{d\Omega}\right)_{\pi^- + p}\right]}{\left[\left(\frac{d\sigma}{d\Omega}\right)_{\pi^+ + p} + \left(\frac{d\sigma}{d\Omega}\right)_{\pi^- + p}\right]}$$

From present experimental data we believe Δ is probably less than 0.15 for the high energies being considered here. Then the standard deviations in $\alpha_\rho(t)$ and $\beta_\rho(t)$ are given by

$$\frac{\sigma_{\alpha_\rho(t)}}{\alpha_\rho(t)} = \frac{\sqrt{2\,\Sigma}}{\alpha_\rho(t) \, \ln\left(\frac{s}{s_o}\right) \Delta}$$

and

$$\frac{\sigma_{\beta_\rho}(t)}{\beta_\rho(t)} = \frac{\sqrt{2\,\Sigma}}{\Delta}$$

Now $\ln|s/s_o|$ increases with energy, but at 20 Bev it is still only about 4; $\alpha_\rho(t)$ is probably less than 1. Therefore, both $\sigma_{\alpha_\rho}/\alpha_\rho$ and $\sigma_{\beta_\rho}/\beta_\rho$ are about ten times greater than Σ, the fractional standard deviation in the differential cross sections. Both $\alpha_\rho(t)$ and $\beta_\rho(t)$ are probably smoothly varying functions, and their measurement at, say, ten different values of t in the diffraction peak would be sufficient. To know $\alpha_\rho(t)$ and $\beta_\rho(t)$ to, say, 10 percent, $d\sigma/d\Omega$ must be known to one percent in each of these t intervals. This requires 10,000 events per interval.

We propose to use a ± 0.25% momentum resolution, 10^{-4} ster, high intensity, secondary beam to allow highly efficient triggering of the spark chamber, so that almost every picture is of an elastic scattering. We do this by improving a triggering scheme we have already used for elastic scattering, which is similar to the inelastic experiment apparatus (Fig. 9). We trigger on coplanar events by decreasing the dimension (h) in Fig. 9 drastically. The coincidence counters then become coplanarity counters.

We also put extensive anticoincidence counters above and below the coplanarity plane. The coplanarity counters each subtend a φ angle of 2 degrees (Fig. 9). We also move the target more forward. From our present experiments we estimate that the fraction of inelastic events giving elastic-event-like triggers will be about .05 to .15 of all the triggers. Therefore 85 to 95% of the recorded events will be elastic. Measurement of the pictures will reduce the inelastic contamination to less than 1% because of the good angular measurements one can make in the chambers, and the narrow angle and momentum spread of the initial beam. The total elastic cross sections in the diffraction peak will be about 5 mb. If we use a 1-meter-long hydrogen target and want 1 event per pulse, the beam

required is given by

$$1 \frac{\text{event}}{\text{pulse}} = [5 \text{ mb}] \left[\frac{4 \times 10^{-4} \text{ events}}{\text{part., mb, cm of } LH_2}\right] [100 \text{ cm of } LH_2] \left[\frac{4^\circ}{360^\circ}\right] \left[N \frac{\text{part}}{\text{pulse}}\right]$$

or

$$N = 450 \text{ part./pulse}$$

The original $\pm \frac{1}{2}\%$, 10^{-3} ster beam would then have 9000 part./pulse.

We said we needed 10,000 events per interval and 10 intervals, or a total of 100,000 events. However the diffraction peak rises rapidly, and to get 10,000 events in an interval near the back takes much longer than to get the same number of events near the front. Therefore we shape the coplanarity counters so as to emphasize the larger angles by a factor of say 30. Then keeping the same beam we get roughly 10 events per second or 36,000 per hour. The 100,000 events thus take 3 hours, an experiment which at present would take weeks at existing machines. Furthermore the data is in very clear form, and the picture analysis can be done automatically with relatively simple analysis devices and programs. In a few days of running time a very comprehensive study of $\alpha_\rho(t)$ and $\beta_\rho(t)$ could be made, using different values of s to test the entire theory.

A very different situation occurs when large-angle elastic scattering is considered. Here the cross section is very small. There is no problem of large numbers of events, rather we are looking for a small number of elastic events in a large inelastic background. We want to measure the differential cross section at high energies and large angles where its value is certainly less than 10^{-30} cm^2/ster. and may be as low as 10^{-35} cm^2/ster. We shall not discuss here the reasons for studying these very small large-angle cross sections. S. Berman and myself expect to discuss the relative importance of strong interactions and electromagnetic interactions in these regions in another SLAC report.

Figure 10 shows the apparatus, which is like that of Fig. 9 except that larger coplanarity counters ($\varphi = 20^\circ$) are used and only one very wide magnet is used to measure the momentum of the pion scattered backward in

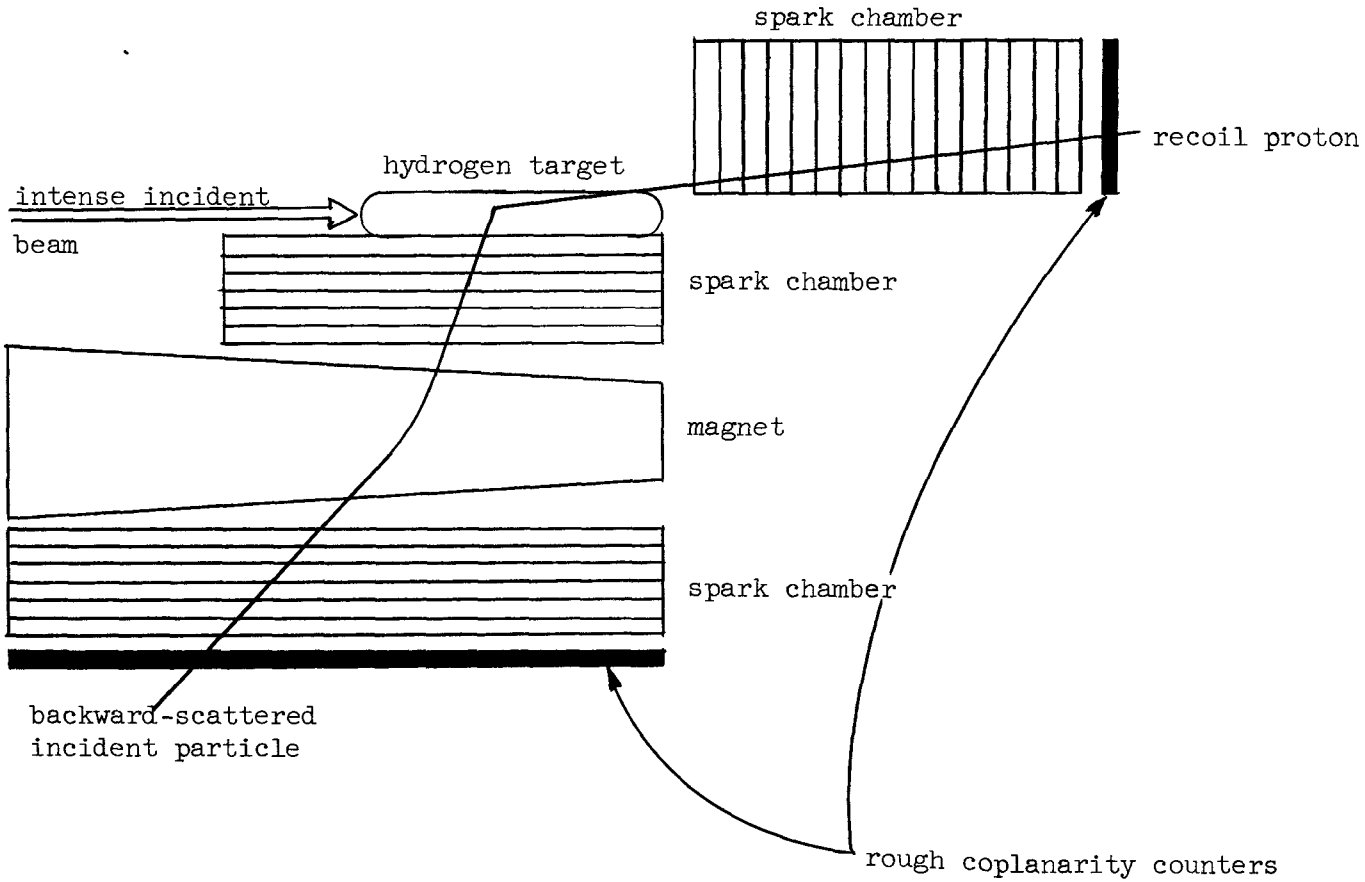
spark chamber
recoil proton
hydrogen target
intense incident
beam
spark chamber
magnet
spark chamber
backward-scattered
incident particle
rough coplanarity counters

FIGURE 10

the laboratory system. Suppose we would like 100 events per steradian throughout the backward scattering region. If $d\sigma/d\Omega$ is the cross section in mb/ster., then

$$100 = \left(\frac{d\sigma}{d\Omega}\right)\left(4 \times 10^{-4}\right)\left(100\right)\left(\frac{20}{360}\right)\left(N\right)\left(P\right)$$

where N is the particles per pulse required, and P is the number of pulses required.

Then

$$NP = \frac{(4.5 \times 10^4)}{(d\sigma/d\Omega)}$$

Therefore

$$NP = 4.5 \times 10^7 \qquad \text{for } \frac{d\sigma}{d\Omega} = 10^{-30}\ \frac{\text{mb}}{\text{ster.}}$$

$$NP = 4.5 \times 10^{12} \qquad \text{for } \frac{d\sigma}{d\Omega} = 10^{-35}\ \frac{\text{mb}}{\text{ster.}}$$

Now suppose we can get 10^4 particle per pulse. Then we require

for the $10^{-30}\ \frac{\text{cm}^2}{\text{ster}}$ cross section, 4.5×10^3 pulses or 13 seconds

for the $10^{-35}\ \frac{\text{cm}^2}{\text{ster}}$ cross section, 4.5×10^8 pulses or 15 days

Thus even the cross section of 10^{-35} cm^2/sec can be well measured in a few weeks. Remember that this is for a strongly interacting particle, and at present the smallest total cross sections measured for such particles are about 10^{-30} cm^2.

Finally, for such a measurement a very pure beam is not required.

The statistics only give 10% precision, and a 10% beam contaminators would not be annoying. Thus here is an example of how the full, secondary, strongly interacting beam at SLAC could be used with somewhat impure beams.

5. Data Analysis and Costs

We believe that this report shows a large number of uses for the spark chamber in secondary strongly interacting beams at M. We have not faced, however, the problems of how to analyze the great amount of data which spark chambers can produce at M, or how to reduce the analysis costs if present recording and analysis methods are used. An example of such costs was pointed out to us by J. Tinlot. Suppose the large, unselectively triggered spark chamber is built. It will probably require 3 cameras, each using 70 mm film with a 6-inch-long frame. If 200 events per second are recorded, this leads to about 1,000,000 feet per hour and 700,000 events per hour. The cost of film and film processing alone would be about $200,000 per hour. We do not know how to compute the analysis costs but they must be higher than the film costs.

In view of this kind of consideration, when we think of high-rate spark-chamber experiments at M (that is, experiments in which the picture rate is about 100 per second) we tend to visualize short runs of the order of a few days. That is, the limitation of several million pictures per experiment still remains. Thus the primary thing a spark chamber might accomplish at M in strong interactions is to enable an enormous number of experiments per year to be done, these experiments being done by many different people. It is true that by taking the same length of time for a run at M as is usual on present machines one can obtain 100 million pictures, but we do not know what one would do then.

SPARK CHAMBER DETECTION SYSTEM FOR 3-BEV STORAGE RING

by

Martin Perl
August 1962

I. INTRODUCTION

In this report we show that a large magnetic spark chamber is the best way, considering presently known detection devices, to study events from a 3-Bev electron-positron colliding-beam machine. Further, we show that most of the events can be analyzed sufficiently well with this chamber to make building the machine worthwhile provided that some of our estimates are confirmed by experimental tests. This conclusion is based, first, upon a study of the momentum, angle and energy precision attainable in a thin-plate magnetic spark chamber as compared with the precision required for general event identification; and, second, upon auxiliary means of particle identification by decay and interaction. Finally the weak points in the device are pointed out, and recommendations for further work are made.

This study is based upon the following assumed parameters for the colliding-beam machine:

(a) The current in each beam is 0.5 amps.

(b) The number of reactions per second R is given by

$$R = 1.75 \times 10^{30}\, \sigma(\text{mb})$$

(c) The region over which the beams intersect is less than 20 cm long.

(d) The outer diameter of the straight section enclosing the interaction region is less than 15 cm. The straight section is at least 4 m long.

(e) The beams can be maintained through a vertical magnetic field such that the product of the field and the length of immersed beam is less than 30,000 gauss meters.

(f) If the beam is immersed in the magnetic field of the detecting system, then the so-called straight section can be curved to fit the beam trajectory in this field.

(g) The standard deviation in the total energy of electron plus positron is 2.5×10^{-3} of the total energy.

(h) The standard deviation in the beam crossing angle is 10^{-3} radians.

(i) No angular restriction is set on three or more body events. Of course it will be impossible to analyze some of these events because some of the emergent particles are too close to the beam direction, but this will be a small fraction.

No attempt is made in the detecting systems discussed here to detect small-angle, two-body events. Small-angle $e^- + e^+$ scattering or small-angle 2γ production may be useful for measuring the interaction rate, but the physical interest in these small-angle events is small. Therefore, for two-body events, the study is restricted to events in which the emergent particles come out at greater than 10° to the beam direction, as shown in Fig. 1.

II. RATE OF EVENTS

The estimates of two-particle events are taken from the Proposal for Preparation for Operation and Research in the Stanford Linear Accelerator Center, and from N. Cabbibo and R. Gatto, Phys. Rev. 124, 1577 (1961). The estimates on three or more particle events were made by the author by guessing in various ways. For example, if $\sigma_{B\bar{B}}$ is the cross section for producing a baryon pair, $e^+ + e^- \rightarrow B^\pm + B^\mp$; then the cross section $\sigma_{B\bar{B}m\pi}$ for $e^+ + e^- \rightarrow B^\pm + B^\mp + m\pi$ (where $m\pi$ is 1, 2, 3 or so pions) will be between 0.1 $\sigma_{B\bar{B}}$ and $\sigma_{B\bar{B}}$ at a total energy of 6 Bev. But near threshold $\sigma_{B\bar{B}m\pi}$ is probably $\leqslant 0.1\ \sigma_{B\bar{B}}$.

Table 1 gives the rates of two-body events in number/minute at total energies of 2, 4, and 6 Bev based on condition 1(b) above and on the minimum angle criterion, 10°, of condition 1(i). Also the ratio of $\sigma(90^\circ)/\sigma(10^\circ)$ at 4 Bev is given as an indication of the anisotropy of the production. The proton-antiproton production depends on the electromagnetic form factors at time-like momentum transfers, which are unknown.

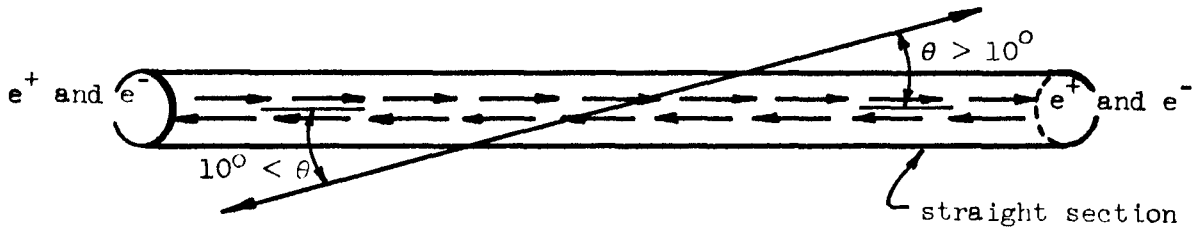

FIG. 1--Two-body event (in plane of event).

TABLE 1

EVENT	NUMBER/MINUTE							
	Total energy baryon	2 Bev		4 Bev		6 Bev		$\sigma(90^\circ)/\sigma(10^\circ)$ at 4 Bev
	Form factor choice	I	II	I	II	I	II	I II
$e^+ + e^-$		52.0		13.0		6.0		1.4×10^{-4}
$\mu^+ + \mu^-$		2.3		0.6		0.3		0.25
non-resonant $\pi^+ + \pi^-$		0.6		0.14		0.06		34.0
$K^+ + K^-$		.06		0.01		0.01		34.0
$p + \bar{p}$		8.5	1.1	7.8	0.6	5.7	0.2	1.3 3.2
$\Sigma^+ + \bar{\Sigma}^+$		0	0	15.0	1.2	12.0	0.4	
$\Xi^- + \bar{\Xi}^-$		0	0	7.8	0.6	5.7	0.2	
All charged two-body events except $e^+ + e^-$		11.5	4.1	31.4	3.0	23.8	1.2	
All charged two-body events		63.5	56.1	44.4	26.0	29.8	7.2	
$n + \bar{n}$		Not added in because it is too hard to detect						
$\Lambda^o + \bar{\Lambda}^o$ or $\bar{\Sigma}^o$		0	0	8.0	0.6	6.0	0.2	
$\Sigma^o + \bar{\Sigma}^o$ or Λ^o		0	0	8.0	0.6	6.0	0.2	
$\Xi^o + \bar{\Xi}^o$		0	0	4.0	0.3	3.0	0.1	
		6.5		1.8		0.7		0.18
$\pi^o + \pi^o$		0		0		0		
$K^o + \bar{K}^o$		0		0		0		
All neutral two-body events		6.5	6.5	21.8	3.3	15.7	1.2	
All two-body events listed above		70.0	62.0	66.0	30.0	45.0	8.4	
Resonant $\pi^+ + \pi^-$		30.0		7.0		3.0		

Two choices are used. In choice I, $F_1 = 1$ and $F_2 = 1.79$, while in choice II, $F_1 = 1$ and $F_2 = 0$. Choice II is used as a pessimistic estimate which gives a cross section decreasing much more sharply with increasing energy than occurs with choice I. The uncertainty in the form factors of the other baryons is so great that it is as reasonable to use the above values for all baryon pairs as it is to make separate calculations. The main object is to get extreme limits on the expected baryon production.

The resonant $\pi^+ + \pi^-$ events refer to the events in which the total energy is equal to a strong two-pion resonance energy, of which the only presently known example is the ρ.

Table 2 lists the rates for three or more body events. Here maximum and minimum estimates are given as a generalization of choice I and choice II. B stands for all baryons here.

TABLE 2

EVENT	NUMBER/MINUTE					
	Total energy	2 Bev		4 Bev		6 Bev	
	Estimate	Maximum	Minimum	Maximum	Minimum	Maximum	Minimum
$B + \bar{B} + m\pi$		0	0	50.0	0.5	40.0	0.15
$B + \bar{B} + m\pi + mK$		0	0	5.0	0.05	4.0	0.01
$m\pi$ non-resonant		8.0	0.8	50.0	5.0	40.0	4.0
$K^* + \overline{K^*}$ and other K resonant pairs		8.0	0.4	8.0	0.4	6.0	0.3
other $m\pi + mK$		0.8	0.1	5.0	0.5	4.0	0.4
$m\pi$ resonant pairs		30.0	0	7.0	0	3.0	0
$e^+ + e^- + m\gamma$		1.5	0.5	0.3	0.1	0.1	0.05
Total of three or more body events		48.0	2.0	125.0	6.5	97.0	5.0
Total of all events		148.0	64.0	198.0	37.0	145.0	13.0

From these tables the following conclusions are drawn for a total energy of 6 Bev.

(a) The $e^+ + e^-$ events will never constitute more than 1/2 of all events and may constitute less than 1/10 of all events.

(b) The three or more body events will constitute at least 1/4 of all events and may constitute more than 1/2 of all events.

(c) There is no preferred direction for outgoing particles subject to condition 1(i).

(d) The variety of types of events is great, and the only mode with a relatively high population is $e^+ + e^-$.

(e) The total rate of events will be between 2.4 and 0.21 per second at 6 Bev and between 3.3 and 0.61 per second at 4 Bev.

(f) If the colliding-beam machine is actually producing events one-fifth of the time, and if there is one picture per event, this leads to 1.4 million to 20 million pictures per year. Therefore the analyzing job is equivalent to that of a large hydrogen bubble chamber operating for several long runs per year.

III. KINDS OF DETECTION SYSTEMS AND REASONS FOR DESIRABILITY OF A MAGNETIC SPARK CHAMBER

From the previous section it can be seen that the problem is to study a great variety of events, many of which are of great physical interest. The individual rates are low but the total rate of all interesting events is reasonable if a high-duty-cycle detector is used. The following objectives for a detector are therefore proposed.

(a) The detector should be able to analyze three or more body events as well as two-body events. In particular, a counter-type detector which studies only events with two collinear charged particles is very wasteful. For example, it would miss all neutral hyperon-pair and resonant-pair (such as $K^* + \overline{K^*}$ events.

(b) To analyze a large variety of events and to avoid confusion between types of events, a maximum amount of momentum, angle, range and interaction information on each outgoing particle is required.

(c) To have a reasonable event rate and to obtain sufficient information on three or more body events, the detector must surround most of the interaction region. That is, a nearly 4π detector is required.

(d) The detector should be either continuously sensitive or presensitive and capable of being triggered. If it is of the latter type, the dead time should be less than 1/10 of a second.

(e) The event analysis must not be too difficult, because so many events must be analyzed.

(f) While not of primary importance, it would be desirable if the detector were capable of modification and extension in order to study particular classes of events with more care.

Objectives (a) and (b) argue strongly against a counter array, no matter how complex. Objective (d) eliminates the bubble chamber and expansion cloud chamber. If the total interesting event rate proved to be small, say a few per minute, then the expansion cloud chamber would be possible. However, it cannot provide as accurate momentum information as the magnetic spark chamber and therefore would still be eliminated. The diffusion cloud chamber and the scintillation chamber are both small devices at present and cannot satisfy objectives (b) and (c). If they could be made sufficiently large they could be used, but once again the magnetic spark chamber is better on the basis of objective (b). Finally, a large emulsion stack is eliminated by objectives (b) and (c).

The magnetic spark chamber satisfies all of the above objectives better than any other presently known device, and it is therefore the device most likely to succeed as a detector for the colliding-beam storage ring.

G. K. O'Neill has recently written a report on this same question of how to study the events from an $e^+ + e^-$ colliding beam. It is interesting to observe that, although he starts from much more limited objectives, namely the study of only two-body events, he reaches the same conclusion, namely, that a magnetic spark chamber should be used.

IV. GROSS DESCRIPTION OF THE MAGNETIC SPARK CHAMBER DETECTOR

To begin the analysis we consider the simplest kind of magnetic spark chamber, as shown in Fig. 2. The colliding beam goes through the vertical magnetic field, and the sensitive volume of the chamber is a vertical cylinder with a diameter equal to its height. Two sizes of chambers are considered:

(A) A very large low-field chamber of diameter 3 meters, height 3 meters, and a field of 10,000 gauss.

(B) A smaller high-field chamber of diameter 1 meter, height 1 meter, and a field of 30,000 gauss.

One sterioscopic view is always along the field direction, so that the magnetic curvature of the tracks is directly measured (Fig. 1). The other sterioscopic views depend on the more detailed chamber design to be discussed later, but they range between

(a) 90° stereo, which yields maximum angular precision but is not always possible; and

(b) small-angle (about 10°) stereo, which may increase the angular measurement error in depth by about 5 times.

Multiple scattering is one of the limitations on momentum measurements and must be minimized. Therefore the chamber is filled with helium at atmosphere pressure. Plates could be 1/2-mil aluminum foil. If large gap spacing (say 3 cm) were desired, then 30 plates per meter would be used. If small gap spacing (say 1 cm) were desired, then 30 plates per meter would still be used but arranged in groups of 3 to give 20 sparks per meter. This combination of helium and 30 thin plates per meter has a radiation length of 1070 meters.

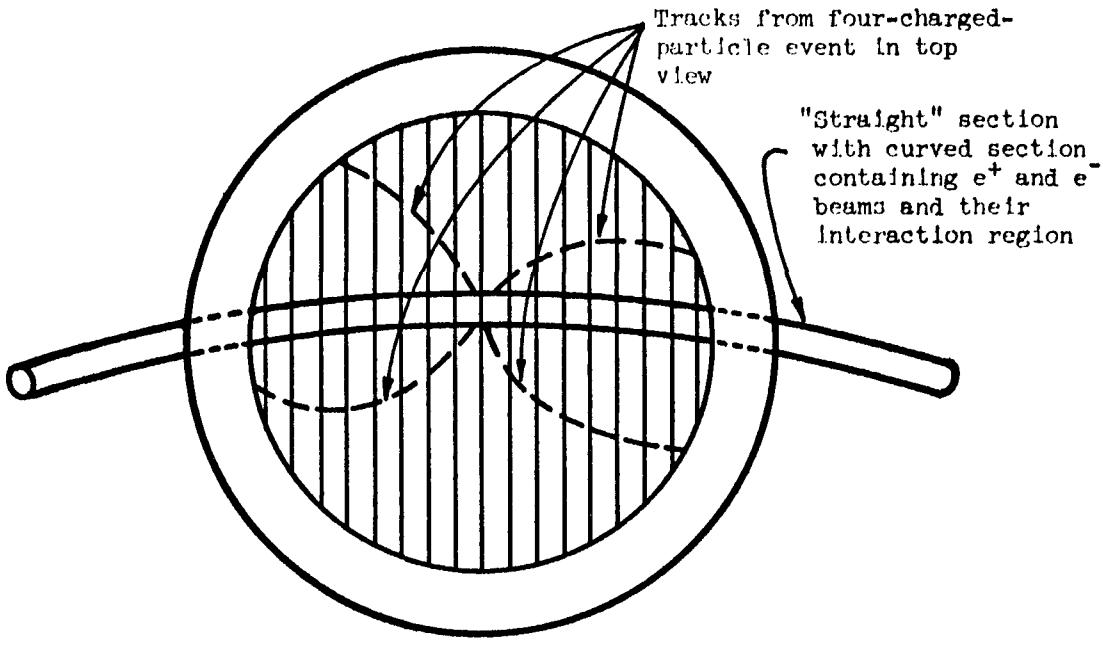

Top view of spark chamber

(one camera looks down onto this view)

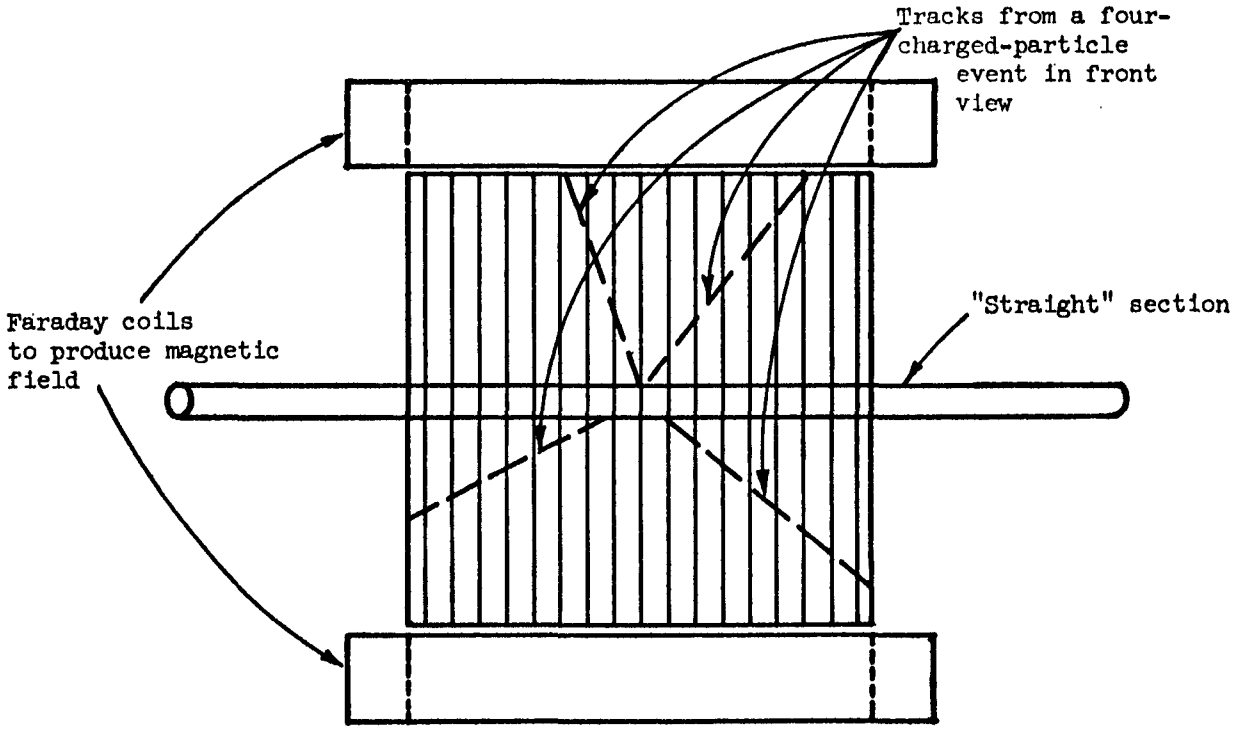

Front view of spark chamber

(one camera looks at this view)

V. ERRORS IN ENERGY, ANGLE AND MOMENTUM MEASUREMENTS

(a) The error in the total energy of the colliding particles is represented by its standard deviation σ_E, where

$$\frac{\sigma_E}{E} = 2.5 \times 10^{-3}$$

according to condition 1(f).

(b) In measuring the momentum and angle of a track in a magnetic spark chamber, two kinds of spark-position uncertainties arise. First the spark does not exactly center on the track. For tracks whose angles with the normal to the plates are large (above about 50°) the spark does not follow the track and there may be a curtain of sparks. We assume it will be possible to modify, improve, or arrange the spark chambers so that the standard deviation due to this effect σ_s is

$$\sigma_s = 0.2 \text{ mm}$$

for tracks making angles less than 30° to the normal to the plates; this is true in some presently existing chambers.

A second error is due to the diffraction broadening of the spark image in deep chambers. If h is the depth of the chamber and λ the wavelength of light, both in mm, then the standard deviation due to the uncertainty in finding the center of the diffraction-broadened spark is σ_D where

$$\sigma_D = 1/10 \sqrt{2.4\ \lambda h} \text{ mm}$$

This is assuming that the center can be read to 1/5 of the actual width of the spark image, and that the actual image width is 1/2 of the width calculated by setting the diffraction broadening equal to the depth of field broadening. These estimates are taken from bubble-chamber experience as described by H. Bradner, Ann. Rev. of Nuclear Science, 10, 109 (1960).

For chamber A $\sigma_D = 0.17$ mm
For chamber B $\sigma_D = 0.1$ mm

When σ_s and σ_D are combined into σ_M, where

$$\sigma_M = \sqrt{\sigma_s^2 + \sigma_D^2}$$

we obtain:

For chamber A $\sigma_M = 0.26$ mm
For chamber B $\sigma_M = 0.22$ mm

The uncertainty in the sagitta of a track due to multiple scattering is given by Bradner (ibid.) as

$$\delta = \frac{2.1\ L}{pv} \sqrt{\frac{L}{L_{rad}}} \quad \text{mm}$$

where L and L_{rad} are in meters and p is in Gev/c. The sagitta is given by

$$\Delta = \frac{L^2 10^3}{8\rho} \text{ mm} \quad \text{and} \quad \rho = \frac{p33.6}{B \sin\theta}$$

where ρ (in m) is the radius of curvature of the track, B is the magnetic field (in kilogauss), and θ is the angle between $\vec{B}$ and $\vec{p}$. Now as stated in Section II, there is no preferred direction for the track, and θ varies from 0° to 90°. We calculate therefore for $\bar{\Delta}$, where

$$\bar{\Delta} = \frac{L^2 10^3\ B\ \overline{\sin\theta}}{268\ p} = \frac{BL^2 10^3}{340\ p}$$

realizing that some Δ will be larger but that others will be very much smaller.

Finally we find σ_Δ, the over-all standard deviation in the sagitta:

$$\sigma_\Delta^2 = \delta^2 + K\sigma_M^2$$

Here k depends on how many sparks along the track are measured. If only three sparks are measured, $k = \frac{3}{2}$. Otherwise $k < \frac{3}{2}$. We take $k = 1$, but k can probably be reduced a little more. Then

$$\frac{\sigma_p}{p} = \frac{\sigma_\Delta}{\Delta} = \frac{0.340\ p}{BL^2}\sqrt{\frac{4.4\ L^3}{(pv)^2\ L_{rad}} + \sigma_M^2}$$

For simplicity we set $v \approx 1$, remembering that this underestimates the error in some cases. Inserting the values for B and L for chamber A and B, where $L \approx 1/2$ diameter, we find:

For chamber A $\quad \frac{\sigma_p}{p} = 1.8 \times 10^{-3}\ \sqrt{1 + 4.9\ p^2}$

For chamber B $\quad \frac{\sigma_p}{p} = 1.0 \times 10^{-3}\ \sqrt{1 + 94\ p^2}$

(c) Finally we consider the angular errors. Here again we take a length L of 1/2 diameter as a standard. We use σ_α as the standard deviation in the angular error. Then because for large p the error in curvature (momentum) measurement is due to σ_M mostly,

$$\sigma_\alpha \approx \frac{1}{L}\sqrt{2\left(\sigma_M\right)^2} \approx \sqrt{2}\left(\frac{\sigma_M}{L}\right)$$

For chamber A $\quad \sigma_\alpha = 2.4 \times 10^{-3}$ radians

For chamber B $\quad \sigma_\alpha = 6.2 \times 10^{-3}$ radians

This is true if there is no decrease in precision due to small angle stereo. As stated in 4(b), the error may be five times larger for a dip angle with 10° stereo.

Finally one should remember that if particles decay in the chamber, their track lengths will be smaller and the σ_p/p and σ_α errors will be larger than are given above.

VI. MOMENTUM AND ANGLE PRECISION REQUIREMENTS FOR EVENT IDENTIFICATION

The primary means of event identification is by momentum and angle measurement. The required precision is investigated by studying a number of special cases.

(a) In this simplest case only a charged particle and antiparticle of mass m are produced. If p_1 and p_2 are the measured momenta (ideally p_1 equals p_2) and E is the total energy then

$$\sqrt{p_1^2 + m^2} + \sqrt{p_2^2 + m^2} = E$$

The standard deviation in m is σ_m where

$$\sigma_m \approx \frac{E^2}{4m} \sqrt{\frac{1}{2}\left(\frac{\sigma_p}{p}\right)^2 + \left(\frac{\sigma_E}{E}\right)^2}$$

The error due to the uncertainty in the beam crossing angle does not enter here. Table III lists σ_m for the π, K, p, Σ and Ξ for $E = 2$, 4, and 6 Bev. Of course, the Σ and Ξ will mostly be recognized by their decay, but they are put in this table to give a feeling for the kind of mass discrimination which is available. σ_m is in Mev.

From this table it is clear that chamber A is required, and further calculations will be based on chamber A only. Chamber B can only be used if there is a substantial reduction in σ_M (at least a factor of 2).

It is clear that e, u, and π pairs cannot be separated by momentum. This has also been concluded by O'Neill.

TABLE III

σ_m (in Mev)

PARTICLE	MASS (Mev)	TOTAL ENERGY					
		2 Bev		4 Bev		6 Bev	
		Cham. A	Cham. B	Cham. A	Cham. B	Cham. A	Cham. B
π	140	27	52	>140	>140	>140	>140
K	494	9	15	51	113	160	380
p	940	5	8	27	60	84	200
Σ	1190			21	47	66	156
Ξ	1320			19	42	60	140

At 6 Bev the π mass is slightly more than two standard deviations from the K mass if a K mass is assumed. If the total energy were greater than 6 Bev, say 8 Bev, this difference decreases to a little more than one standard deviation. Therefore, for chamber A 6 Bev is about the maximum total energy at which the reaction $e^+ + e^- \rightarrow \pi^+ + \pi^-$ can be separated from $e^+ + e^- \rightarrow K^+ + K^-$.

Finally, chamber A, even at 6 Bev, separates pairs of π's, K's, p's, Σ's and Ξ's satisfactorily by momentum alone.

(b) Next we consider three-body events. Here we consider a special case in which a π is produced with another pair of particles. This other pair may be π's, K's, nucleons, or Σ's. Namely, we consider $e^+ + e^- \rightarrow \pi + x + \bar{x}$. Once again we neglect the fact that identification can be established in some cases by change or decay behavior in order to get a feeling for the effectiveness of pure momentum identification. Only the case of 6 Bev total energy is considered. The kinematics are presented in Figs. 3, 4 and 5, where the momentum of the antiparticle in the pair is fixed at 2.5, 2.0 and 1.5 Bev/c.

First it is seen that there are exact ambiguities when $P_\pi = P_x$. At these points momentum measurements cannot distinguish π from x. The ambiguity extends away from the $P_\pi = P_x$ point until the separation between the curves is several times larger than the uncertainty in the

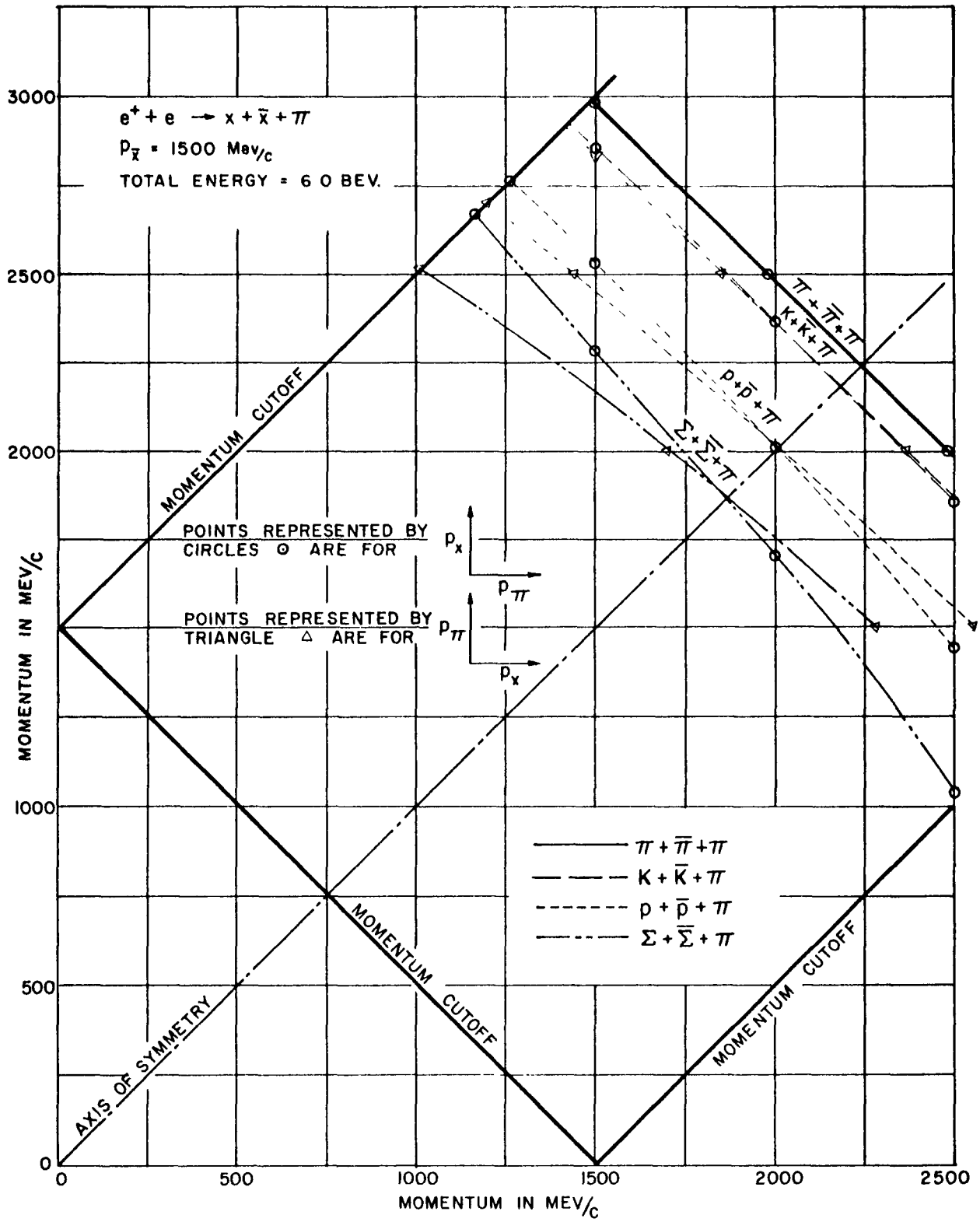
$e^+ + e \rightarrow x + \bar{x} + \pi$
$p_{\bar{x}}$ = 1500 Mev/c
TOTAL ENERGY = 6 0 BEV.
MOMENTUM CUTOFF
POINTS REPRESENTED BY CIRCLES ⊙ ARE FOR p_x p_π
POINTS REPRESENTED BY TRIANGLE △ ARE FOR p_π p_x
$\pi + \bar{\pi} + \pi$
$K + \bar{K} + \pi$
$p + \bar{p} + \pi$
$\Sigma + \bar{\Sigma} + \pi$
AXIS OF SYMMETRY
MOMENTUM CUTOFF
MOMENTUM CUTOFF
MOMENTUM IN MEV/c
MOMENTUM IN MEV/c
0
500
1000
1500
2000
2500
3000

FIG 3

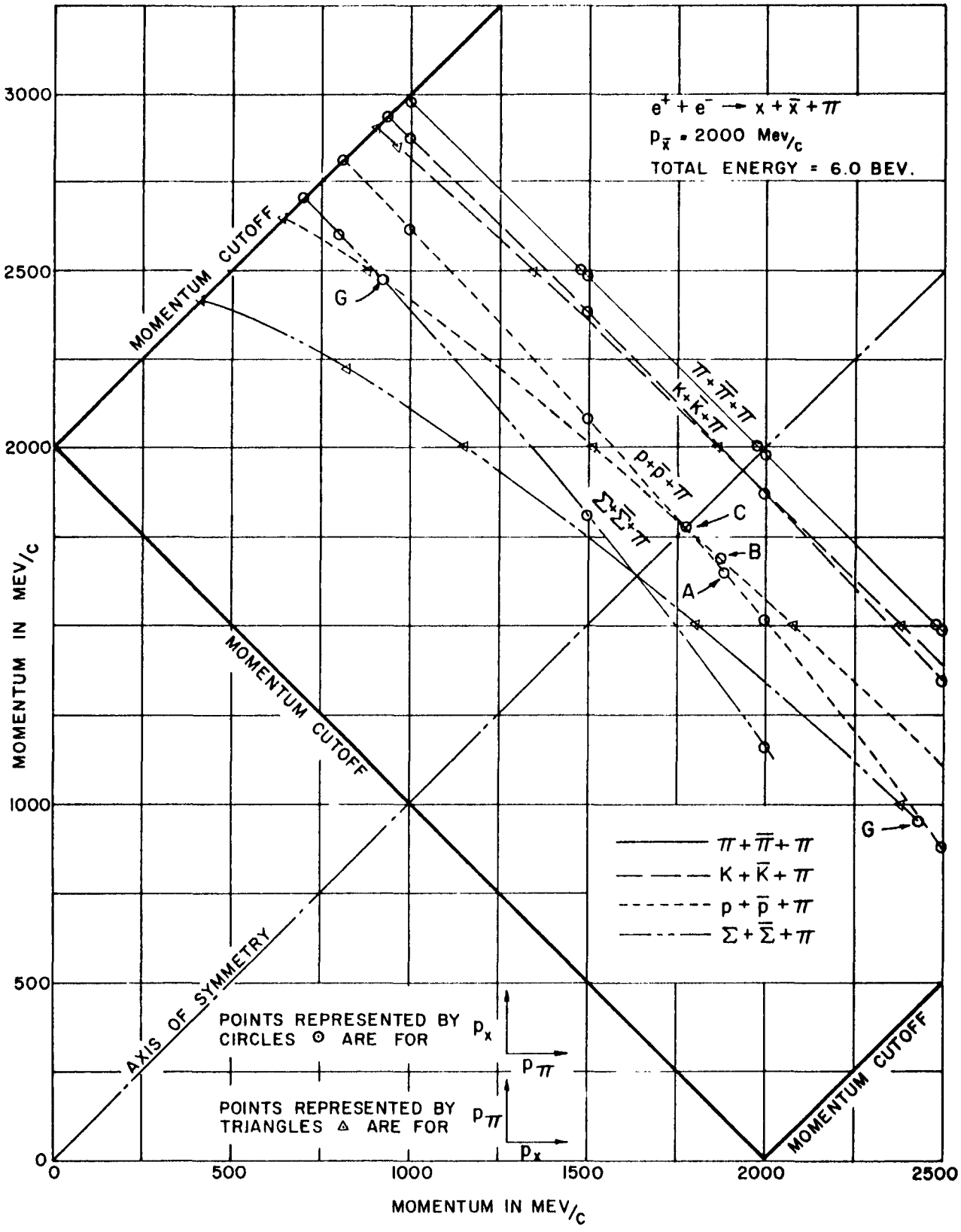
$e^+ + e^- \rightarrow x + \bar{x} + \pi$
$p_{\bar{x}}$ = 2000 Mev/c
TOTAL ENERGY = 6.0 BEV.
MOMENTUM CUTOFF
MOMENTUM CUTOFF
MOMENTUM CUTOFF
AXIS OF SYMMETRY
$\pi+\bar{\pi}+\pi$
$K+\bar{K}+\pi$
$p+\bar{p}+\pi$
$\Sigma+\bar{\Sigma}+\pi$
A
B
C
G
G
$\pi+\bar{\pi}+\pi$
$K+\bar{K}+\pi$
$p+\bar{p}+\pi$
$\Sigma+\bar{\Sigma}+\pi$
POINTS REPRESENTED BY CIRCLES ⊙ ARE FOR p_x p_π
POINTS REPRESENTED BY TRIANGLES △ ARE FOR p_π p_x
MOMENTUM IN MEV/c
MOMENTUM IN MEV/c
0
500
1000
1500
2000
2500
3000

FIG. 4

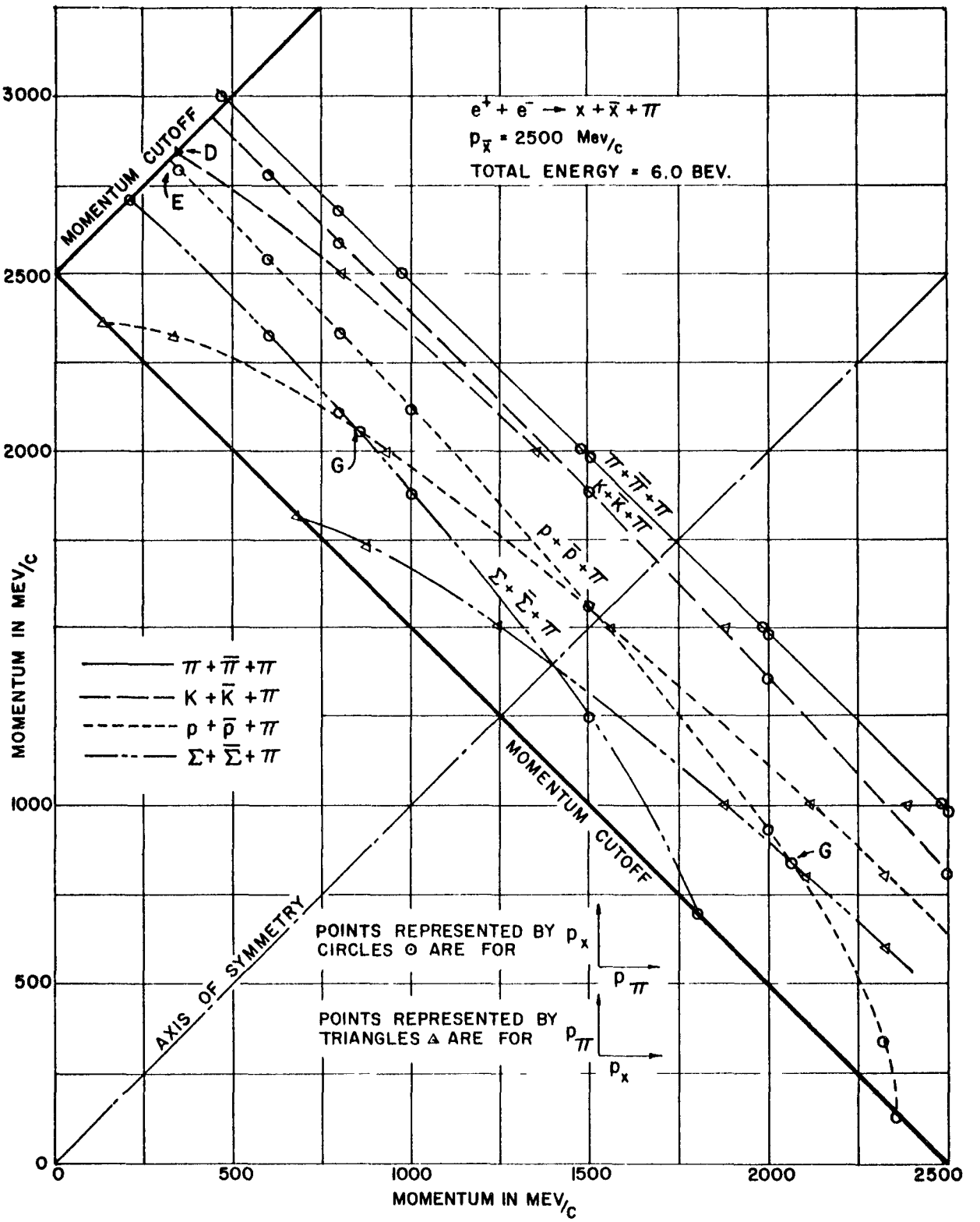
$e^+ + e^- \rightarrow x + \bar{x} + \pi$
$p_{\bar{x}}$ = 2500 Mev/c
TOTAL ENERGY = 6.0 BEV.
MOMENTUM CUTOFF
D
E
G
$\pi + \bar{\pi} + \pi$
$K + \bar{K} + \pi$
$p + \bar{p} + \pi$
$\Sigma + \bar{\Sigma} + \pi$
$\pi + \bar{\pi} + \pi$
$K + \bar{K} + \pi$
$p + \bar{p} + \pi$
$\Sigma + \bar{\Sigma} + \pi$
MOMENTUM CUTOFF
AXIS OF SYMMETRY
POINTS REPRESENTED BY CIRCLES ⊙ ARE FOR p_x p_{π}
POINTS REPRESENTED BY TRIANGLES △ ARE FOR p_{π} p_x
MOMENTUM IN MEV/c
MOMENTUM IN MEV/c
0
500
1000
1500
2000
2500
3000

FIG. 5

momentum measurements.

Consider the $e^+ + e^- \to \pi + p + \bar{p}$ case for $P_{\bar{p}} = 2.0$ Bev/c, Fig. 4. The exact ambiguity is at point C, where $P_\pi = P_p = 1.775$ Bev/c. At this point $\sigma_p/p \approx .007$ Bev/c. A separation of several times .007 Bev/c occurs between the $\pi + p$ curve CA and the $p + \pi$ curve CB at the points $A(P_\pi = 1.875, P_p = 1.650)$ and $B(P_p = 1.890, P_\pi = 1.675)$. Therefore the separation is possible except when $1.890 > P_p > 1.650$ and $1.675 < P_\pi < 1.875$, which is a relatively small region of ambiguity.

As in the two-body case, the πK separation is most difficult. Particularly when $P_{\bar{K}} = 1.5$ Bev/c, the other two momenta are high, and the πK is ambiguous over quite a large region.

Another kind of confusion is that between $\pi\pi\bar{\pi}$ and $\pi K\bar{K}$ due to errors in $P_{\bar{x}}$. Again from the kinematics curves this can be investigated, but not as directly. First imagine the curves shifted, in a direction parallel to the 45° line, because of the uncertainty in $P_{\bar{x}}$. For example, at $P_\pi = 2.0$ Bev/c the $P_\pi + P_\pi$ curve crosses the 45° line at $P_\pi = P_\pi = 1.990$ Bev/c, while at $P_{\bar{\pi}} = 2.5$ Bev/c, the crossing is at 1.740 Bev/c. Meanwhile the spacing of the $\pi + \pi + \bar{\pi}$ from the $\pi + K + \bar{K}$ curves is about .075 Bev/c for most of the curves and does not vary much. Since σ_p at 2.0 Bev/c is .008 there is no chance of confusion of these two cases. However for the $\pi + K + \bar{K}$ separation from $\pi + p + \bar{p}$, confusion occurs at the end points of the curves, like points D and E, Fig. 5. If $P_{\bar{x}}$ went as close to 3 Bev/c as possible, then D would get quite close to E and there might be confusion. The explanation of this is that as $P_{\bar{x}} \to 3$ Bev/c, at points D and E $P_\pi \to 0$, and this is similar to the two-body case, except that a π is produced at rest. However, for most of the region the separation of $p + \bar{p} + \pi$, $\pi + K + \bar{K}$ and $\pi + \pi + \bar{\pi}$ is sure and, in fact, is easier than the separation of $\pi + \bar{\pi}$ from $K + \bar{K}$ and $p + \bar{p}$. The reason for this is that the additional π takes up some momentum, the other two particles have smaller momentum, and the fractional error in the mass determination is smaller.

But there remains another ambiguity. There is a crossover of the $p + \bar{p} + \pi$ and $\Sigma + \bar{\Sigma} + \pi$ curves at the points G in Figs. 4 and 5.

At these points G the two types of events cannot be separated. However the region of ambiguity about the G points is small.

If the case $m + x + \bar{x}$ occurs where m is heavier than the π (this is not possible with the known particles), then the ambiguity regions shrink.

(c) Next we consider a special case of a four-body event. Suppose two pairs of particles are produced, $e^+ + e^- \rightarrow x_1 + \bar{x}_1 + \bar{x}_2 + x_2$, where x_1 has mass m_1, and x_2 has mass m_2. Also suppose x_1 and $\bar{x}_1$ each have momentum P_1 and x_2 and $\bar{x}_2$ each have momentum P_2.

This is admittedly a special case, but it has the flexibility of allowing P_1 or P_2 to become large, which is the condition for mass ambiguities to occur. Figure 6 shows the plots of P_1 versus P_2 for the mass combinations $2\pi + 2\pi$, $2\pi + 2K$, $2\pi + 2p$, $2\pi + 2\Sigma$, $2K + 2K$, $2K + 2p$, $2K + 2\Sigma$, and $2p + 2p$, at a total energy of 6 Bev.

Once again we see that exact ambiguities occur at various places. For example, $2K + 2K$ intersects $2\pi + 2\Sigma$ and $2\pi + 2p$. In general, if $m_1 > m_1'$ and $m_2 < m_2'$, then $2x_1 + 2x_2$ intersects $2x_1' + 2x_2'$. Around each point of exact ambiguity the short cross lines indicate the regions inside which the separations between the curves are less than three standard deviations σ_p in momentum. The uncertainty in total energy E is not taken into account here, but very roughly two of the σ_p are for direct momentum uncertainty, and the other σ_p is to take account of the E uncertainty.

A study of Fig. 6 shows that most of the time the events can be unambiguously identified. In fact, the increasing number of particles in general makes separation easier than in the two- or three-body case.

Of course the other type of ambiguity, that of telling which particle is which, once an event is identified, occurs at the point on the curves in Fig. 6 where $P_1 = P_2$. However, this kind of ambiguity is not very important because in the case of four bodies the probability is high that all four momenta will be different.

A further test is provided by the problem of determining a missing mass. Suppose the momentum of n particles is found not to balance. Further, take the most favorable case where all of the masses of the n particles

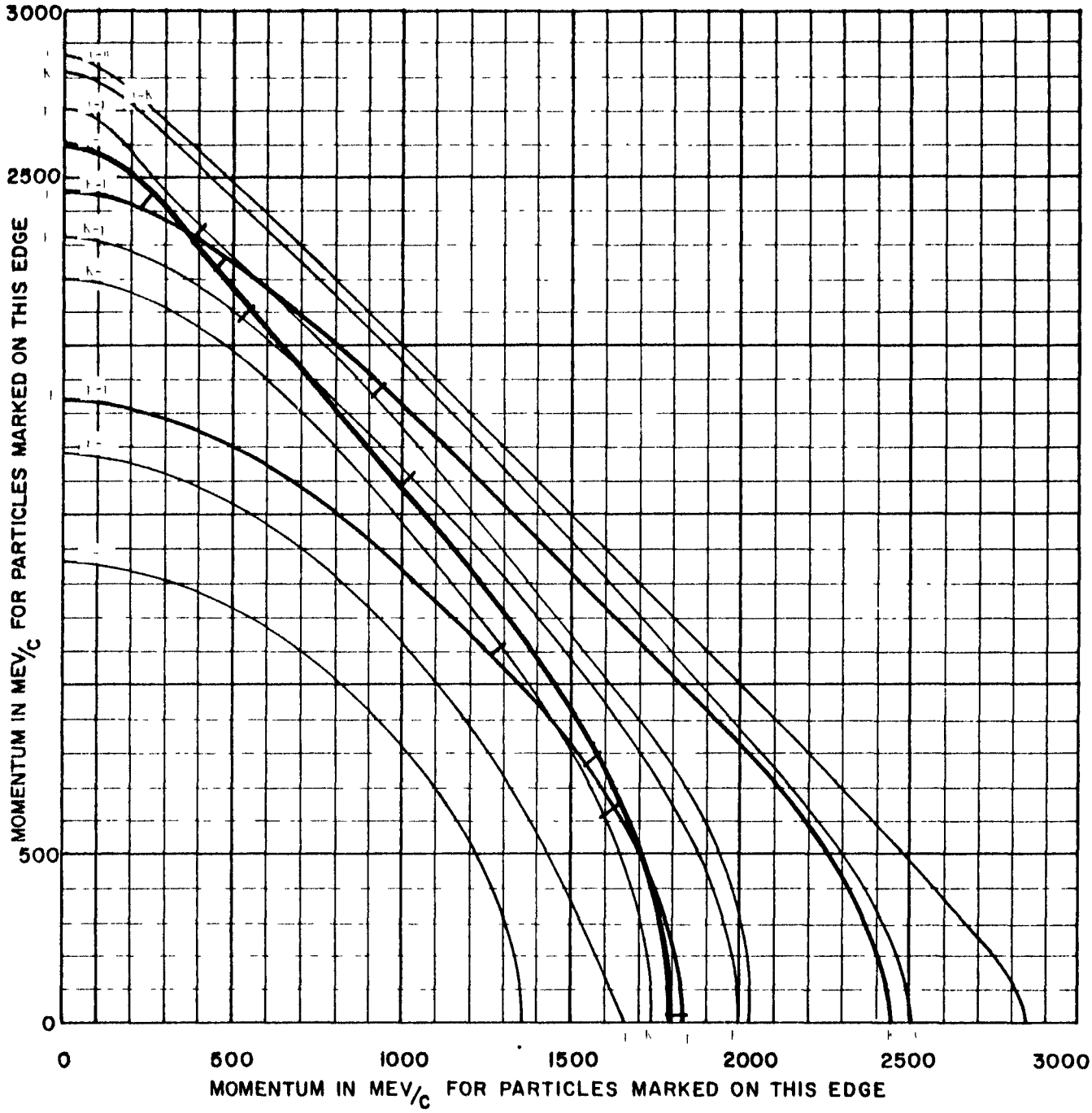
3000
2500
500
0
MOMENTUM IN MEV/c FOR PARTICLES MARKED ON THIS EDGE
0
500
1000
1500
2000
2500
3000
MOMENTUM IN MEV/c FOR PARTICLES MARKED ON THIS EDGE

FIG. 6

are known. If E is the total energy of the $e + e^+$ system, e is the total energy of the missing mass, $\vec{p}$ is the momentum of the missing mass, and m^* is the missing mass, then the maximum standard deviation in m^* (namely, σ_{m^*}) is given roughly by

$$\sigma_{m^*} \approx \frac{1}{m^*} \left| e^2 \sum_{i=1}^{n} \left(v_i \sigma_{p_i}\right)^2 + \left(\frac{pE}{2}\right)^2 \sigma_\theta^2 + e^2 \sigma_E^2 \right|^{\frac{1}{2}}$$

where σ_{p_i} is the standard deviation in the momentum p_i of the i^{th} particle, v_i is its velocity, and

$$m^{*2} = e^2 - p^2$$

To examine the relative size of the errors, let $E = 6$ Bev, $p = 1$ Bev/c, $m^* = 1$ Bev, $v_i = 1$, and use the approximate formula

$$\sigma_{p_i} = 4 \times 10^{-3} p_i$$

Then using

$$\sigma_E = 2.5 \times 10^{-3} E$$

and

$$\sigma_\theta = 10^{-3}$$

we find

$$e = 1.4 \text{ Bev}$$

$$\sigma_{m^*} = 10^{-3} \left[32 \sum_{n=1}^{n} (p_i)^2 + 9 + 450 \right]^{\frac{1}{2}} \text{ Bev}$$

The error due to σ_θ is negligible. We can therefore write a simpler general formula

$$\sigma_{m^*} = \frac{2.5\ e}{m^*} \left| 2.5\ n < v_i p_i >^2_{rms} + E^2 \right|^{\frac{1}{2}} \text{ Mev}$$

where e, m^*, and E are in Bev, p_i is in Bev/c, but σ_{m^*} is in Mev. Here $< v_i p_i >_{rms}$ is the root mean square average of $v_i p_i$ over the known particles, and n is the number of known particles.

As an example, set $E = 6$, $< v_i p_i >_{rms} = 1$, and $n = 4$. Then

$$\sigma_{m^*} = \frac{17\ e}{m^*} \text{ Mev}$$

Since

$$\frac{e}{m^*} > 1$$

then

$$\sigma_{m^*} > \left| 2.5\ E \right| \text{ Mev}$$

and it usually will be of the order of 20 or 30 Mev.

(d) Finally we consider the case of 2 or more charged particles of unknown mass and an unbalanced momentum leading to a missing mass. There is only a maximum mass limitation on the unknown charged particles if there is no non-momentum means of identification. Because most of the momentum will be of the order of 1 Bev/c or more, it is very likely that there will be no π - K separation and perhaps even no π - K - p separation. Therefore these events will not be identifiable unless the missing mass is detected. Thus the detection of neutral particles such as γ-rays, π^o, Λ^o and Σ^o is very important, which brings us to the subject of non-momentum means of identification.

VI. FURTHER MEANS OF PARTICLE IDENTIFICATION

(a) Decay

The identification of θ^o, Λ^o, and all Σ and Ξ particles can be made by their decay in the chamber. This will be of great help in the cases of π - K confusion discussed before and in baryon separation. Together with the momentum method of identification, events with these decays will be identified with great certainty. The fraction of 3 Bev/c θ^o, Λ^o, Σ, and Ξ particles that will decay inside the first meter of chamber is greater than .99. Furthermore, the low density of material in the chamber, 0.13 gr/cm^2 per meter of track length, leads to a very low probability for a chamber interaction which can be confused with a decay.

(b) Electron Showers and γ-Ray Conversion

The large number of purely electromagnetic final states, in particular $e^+ + e^-$ and $\gamma + \gamma$, require a positive identification of electrons and γ-rays. The chamber as so far described will not detect the $\gamma + \gamma$ event, and as we have seen electron-pair separation is usually not possible by momentum measurements. Also missing-mass measurements may easily miss low-energy γ-rays if there are heavy neutral particles produced. The π^o provides a similar problem. It will be very useful to detect one or preferably both γ-rays from the π^o.

The solution to this problem, also discussed by O'Neill, is to surround the magnetic thin-plate chamber by a thick-plate, high-Z chamber of several radiation lengths to produce showers from $e^{\pm}$ and showers or pairs from γ-rays. It is necessary to put these thick-plate chambers inside the coils to avoid electrons or γ-rays being absorbed by the coils before reaching the thick-plate chambers.

Because of our interest in three or more body events, it is necessary to surround most of the thin-plate chamber region by these chambers. Where the view is already blocked by the thin-plate chamber or coils, lead or iron plates may be used. One design, suggested by O'Neill, consists of 0.4 radiation-length-thick iron plates with 1 cm spacing. However, in contrast to O'Neill, we would use 5 radiation lengths, giving a thick-plate chamber 20 cm thick. For covering the openings through which the

chambers are photographed, conducting, transparent glass chambers may be considered as is shown in Fig. 7.

These glass-plate chambers would require extensive development and may distort the optics. The x-ray and therefore the π^{o} energy determination would be very poor, being determined to only a factor of 5 or so by the number of tracks in the shower.

An alternative type of $e^{\pm}$ shower and γ-ray conversion magnetic spark chamber would use thinner high-Z plates, separated by very thin low-Z plates, to measure the energy of pairs from x-rays. (This was suggested by the investigation of G. Trilling into the use of thin, high-Z plates in a hydrogen bubble chamber.)

For example iron plates 1/20 of a radiation length thick might be separated by 5 cm. In this 5 cm space would be four 1/2-mile-thick aluminum plates. In this 5 cm space a 10 kilogauss field would give a $\sigma_p \approx 0.12$ p, using the equations from Section V. The 1/2-radiation-length-thick plate would also cause an average loss per pair of 10%. Therefore the γ-ray energy determination would be to about 20%. Unfortunately, a 100-cm-thick chamber would be required to give one radiation length, and this chamber would still have to be backed up by a few one-radiation-length-thick plates to give sufficiently high $e^{\pm}$ shower and γ-ray conversion efficiency. We have not had time to investigate the best compromise between these two schemes.

Neither have we had time to investigate the exact efficiency and conversion behavior to be expected from a chamber five radiation lengths thick. In detail, the efficiency depends upon the plate thickness, because, for example, in a thick plate the initial electron may produce such a high-energy bremsstrahlung photon that the initial electron does not leave the plate. Then the photon would have to convert in another plate to start the shower. In the case of γ conversion, a Compton scatter of the initial γ in one plate and subsequent conversion in another plate would give an incorrect measure of the γ direction.

However, the electrons and γ-rays will almost always have high energies, above several hundred Mev. Therefore, we expect that the kind of difficulties mentioned above will be minor, that the $e^{\pm}$ shower and γ conversion

(Magnet coils not shown for simplicity)

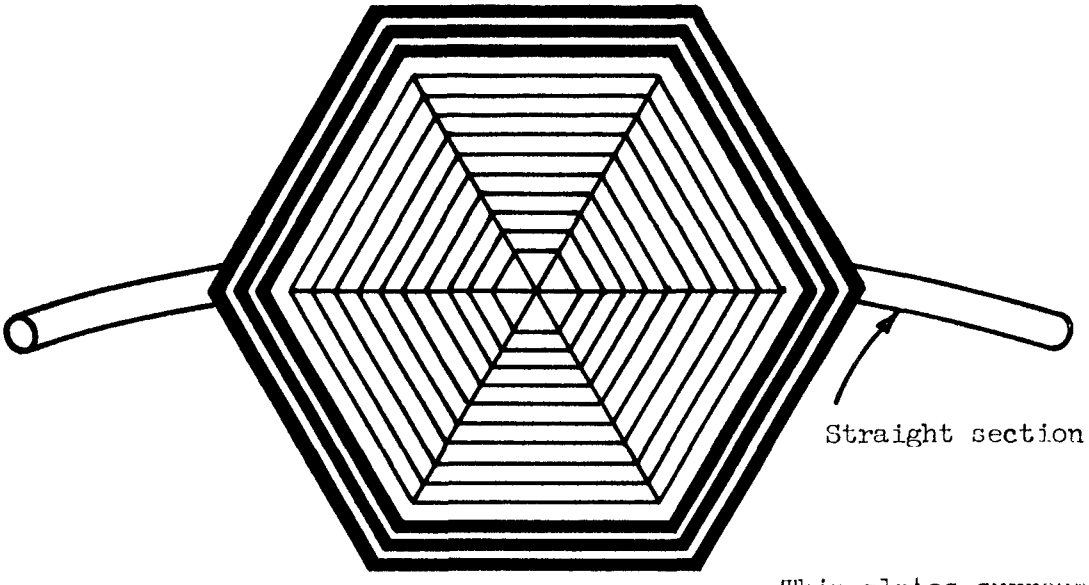

Top view

Thin plates surrounded by thick high-Z plates. These chambers are viewed only from the top. Small angle stereo is obtained by tilted mirrors at the chamber bottom.

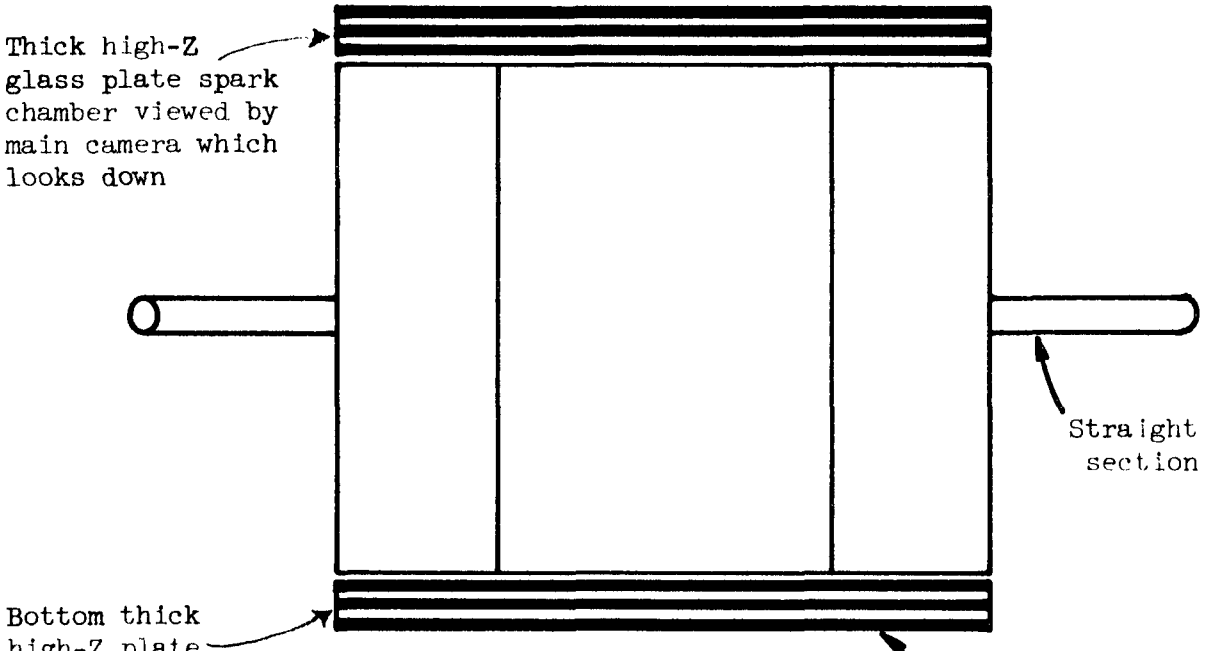

Front view

FIG. 7

efficiency will be above 99% and above 97% respectively (for 5 radiation lengths), and that the γ position will be given to within a plate width.

(c) μ - π Separation

One means suggested for this separation is by interaction. As discussed by O'Neill, the entire system of thin-plate and thick-plate chambers may be surrounded by several nuclear mean free paths of material in the form of more thick-plate chambers. These would stop the π's by interaction but not the μ's. This can be done below and around the sides of the chamber. The top must be left open for viewing. O'Neill suggests combining the thick-plate shower chambers and the thick-plate nuclear interaction chambers into single chambers containing 20 radiation lengths, 30 cm of iron. This is about 2.5 collision lengths, so that 92% of the π's would interact. However, the root-mean-square scattering angle for 1 Bev/c μ's would be about 4 degrees so that some μ's will scatter sufficiently and look like π's. Therefore we may expect that both π's and μ's will be contaminated by the other particle.

A somewhat simpler design is based on the consideration that μ production is very unlikely except in $e^+ + e^- \rightarrow \mu^+ + \mu^-$ events. Particularly in three or more body events where some strongly interacting particles are produced, it is very likely that all the particles are strongly interacting and no μ's will be produced. Therefore μ - π separation is only necessary in two-body final states, and there is no need to cover much of the solid angle by these heavy chambers. A ring of thick-plate chambers of relatively small depth would be used, as shown in Fig. 8. Only $\pi^+ + \pi^-$ or $\mu^+ + \mu^-$ events which go through this ring would be analyzed. The very different angular distribution of the μ pairs and π pairs (see Table I) will also aid in the separation.

Another means of separation using counters, but suitable for only $\mu^+ + \mu^-$ and $\pi^+ + \pi^-$ events is discussed in the next part of this section.

(d) Velocity Determination by Ionization

Bubble chambers make extensive use of ionization density at low energy and are beginning to use the relative rise in ionization density at very high energy to determine particle velocities. This, combined with momentum

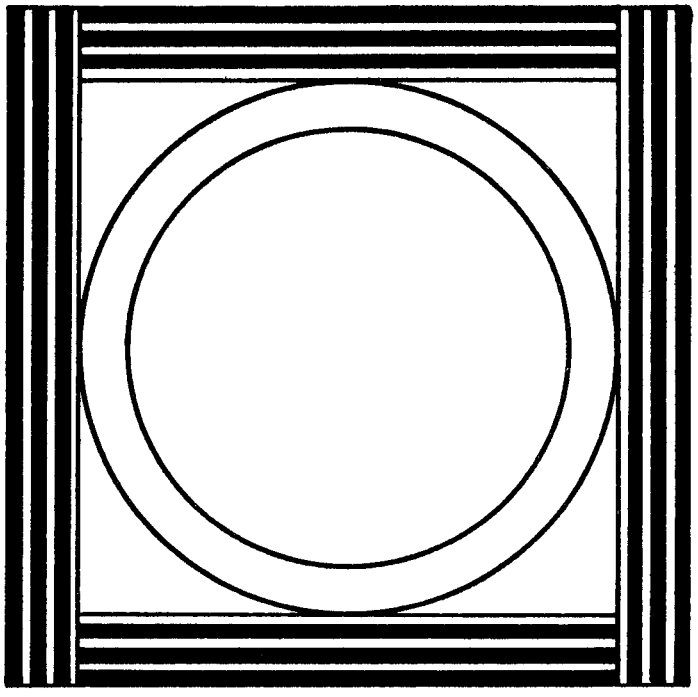

Top view

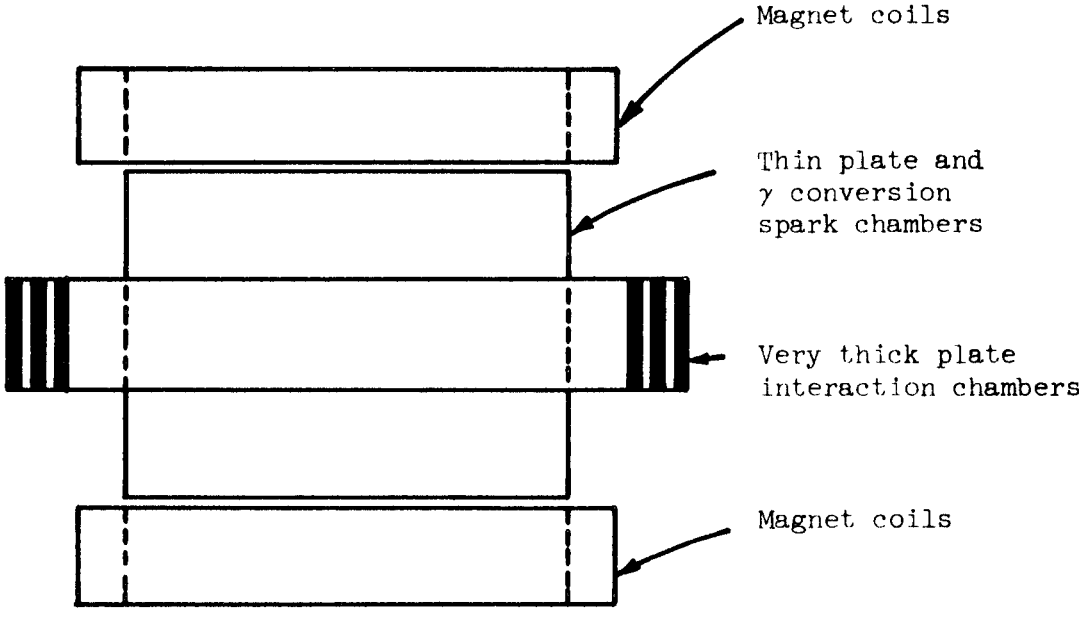

Front view

FIG. 8

measurements, aids mass identification. The ionization sensitivity of present spark chambers is very poor. It is limited to comparison of tracks in the same picture which have ionizations differing by factors like 2. We do not know if this can be improved sufficiently to be of use, considering the high energy of the events. In particular, even if the major thin-plate chambers cannot be improved, one might consider a shell of special ionization-sensitive chambers, if such chambers can be devised. But this is still only a speculation. Another speculation is that large scintillation chambers would have the desired ionization sensitivity, but no way is now known to make a sufficiently large shell of scintillation chambers.

(e) Use of dE/dx and Cerenkov Counters

Further speculation involves the use of a roughly spherical shell of scintillation counters to measure dE/dx. This shell would have a radius of about 2.5 m and be centered on the interaction region. Since it is unlikely that more than six charged particles leave the spark chamber region, a mosaic of say 50 counters would generally have only one particle per counter. The recording of the pulse height in each counter, combined with the particle direction information from the spark chambers, would give dE/dx and hence β.

Consider instead of scintillation counters that the mosaic consists of Cerenkov counters. Threshold or differential Cerenkov counters are of no use for three or more body events, since such counters indicate only that a particular velocity is above a certain threshold or in a certain band. The velocities of the particles from three or more body events will have all sorts of values and the information provided by the Cerenkov counters will be of little use. For two-body, charged, non-decaying final states, the threshold or differential Cerenkov counters could be used to make a single mass separation. The place to make this separation is between the $\mu^+ + \mu^-$ and the $\pi^+ + \pi^-$ events. The ring of interaction chambers in Fig. 8 would be replaced by a ring of Cerenkov counters. At 3 Bev per particle, $1-\beta$ is .00062 for the μ and .00109 for the π. Now the output signal from a threshold Cerenkov counter one-meter long, with a

15% efficient photomultiplier, would consist of n photo-electrons where

$$n = 4550 \left[1 - \frac{1}{\beta^2 n^2}\right]$$

and n is the refractive index. If the threshold velocity is β_t, then $n = 1/\beta_t$ and

$$n = 9000 \left[\beta - \beta_t\right]$$

Setting β_t at halfway between β_μ and β_π, so that μ's are detected and π's are not detected, gives for the μ signal

$$n = 4500 \left[\frac{\beta_\mu - \beta_\pi}{2}\right] = 2$$

which is of course much too small a signal to use. At 1.5 Bev per particle the value is about 10 and here the signal is usable. These calculations are confirmed by experience with threshold counters. The threshold counter separation method could be stretched to 2 Bev per particle by even thicker counters (about 2 meters thick), but it is impractical to get $\pi - \mu$ separation at 3 Bev per particle by this method. Even the 2 Bev counter is gigantic. It would consist of a horizontal, segmented, toroid of rectangular cross section, with 4 m inside diameter, 8 m outside diameter and 1 m high, covering about $\pi/2$ steradians. The entire outer circumference of the ring would contain photomultipliers. We believe the ring of thick-plate interaction spark chambers is preferable. The conventional differential Cerenkov counter would separate the μ's and π's, even at 3 Bev, but the angular acceptance of these devices is only 10^{-2} steradians. It is impractical to consider assembling enough of these complicated devices to subtend a reasonable solid angle at the interaction region.

At present the best hope for use of the Cerenkov principle is in the

recording of the Cerenkov light by an image-intensifying system as described by A. Roberts in the Proceedings of the International Conference on High Energy Instrumentation at Berkeley, 1960. This scheme has the advantage of recording all velocities and of having large angular acceptance. We do not have time to investigate in detail the use of this scheme in the colliding-beam detection system, but such an investigation should be made. At present the limitation to its use is the lack of cheap image-intensifier systems of large surface area. Channeled image intensifiers, now under development, may lead to such systems.

VII. ANALYSIS OF EVENTS, TRIGGERING AND BACKGROUND

In Section II (c) we estimated that 1.4 to 20 million single-event pictures would be produced per year. Most of these would have to be studied in order to find the interesting events. Somewhere around 1/2 of them will be completely measured and analyzed. This is an enormous analysis job and must be done automatically in large part. Fortunately, some of the events, such as the two-charged-body events, are susceptible to simple automatic analysis. This is not the place to go into the analysis question, but clearly the analysis system would be as extensive as that required for a large hydrogen bubble chamber. If the rate of background events from the machine and from cosmic rays is of the same size or larger than the rate of events from the $e^+ + e^-$ interaction, then the analysis job would be more expensive. Therefore it is necessary to use a triggering system which reduces the ratio of the background-event rate to the good-event rate. Reduction of this ratio to 1/4 or 1/2 is about all that is required, because further reduction will not save much analysis money.

The triggering systems would in general consist of two or more scintillation counters in coincidence, which surround the interaction region, and an anti-coincidence counter system to prevent cosmic-ray events. The simplest coincidence systems would consist of a split cylinder directly around the straight section enclosing the interaction region. However, this would miss some events like $\gamma + \gamma$ and $\Lambda^o + \overline{\Lambda^o}$ pairs which both decay outside these counters. On the other hand, placing the coincidence counter system

outside all of the spark chambers would pick up all events, but the counters would be very large and the cosmic ray background would be higher. Another consideration is the background events from e^+ or e^- interactions with the residual gas in the storage ring or with the walls of the ring. Again we have not had time to investigate how many of these events would look like good events and hence would trigger the chamber unless the triggering systems could discriminate against them. Therefore we do not have a definite trigger system to present at this time.

VIII. CONCLUSIONS, DEFECTS IN THE PRESENT SCHEME AND RECOMMENDATIONS FOR FURTHER WORK

(a) We conclude that a satisfactory spark-chamber detection system for the 6-Bev colliding-beam storage ring could be built with present knowledge and techniques, providing some of the further work suggested in this report substantiates our estimates and calculations. Many types of events could be identified with all of their generative parameters being established. Considering the possible knowledge to be obtained, the cost of the system seems acceptable.

(b) There are a number of defects in this detection scheme, as follows.

(1) In some three or more particle events, there will be difficulty in some momentum regions in separating charged π's from charged K's, or charged K's from protons; ambiguities of other types will also occur (Section VI).

(2) The separation of μ's from π's depends either on the π interaction in very thick plate chambers, or on an extensive set of Cerenkov counters, neither of which is an entirely satisfactory solution.

(3) The system does not detect neutrons or antineutrons or θ_2^0 mesons, which may create ambiguous situations if there is a larger missing mass. Similarly, an as yet unknown neutral particle, which did not decay inside the chamber, would be lost in this missing-mass confusion.

(4) No precise determinations of γ-ray energy can be made. Particularly if several π^0 mesons are produced, this will lead to ambiguous events.

(5) The immersion of the colliding beams in the magnetic field of the spark chamber as assumed throughout this paper may be more difficult than we expect. O'Neill has suggested an alternative scheme in which the beam is shielded from the magnetic fields of spark chambers on either side of the beam. Because of our emphsis on 3 or more body events, we are reluctant to go to such a scheme, which increases considerably the ambiguities in such events. Another scheme which consists of a magnetic field parallel to the colliding beams, with a magnetic shield around the colliding beam, seems to us to be of no advantage and to add considerable construction and viewing difficulties. Therefore while the immersion of the beam in the vertical magnetic field is a defect, it seems like a necessary one. We have not examined the possibility of shielding the beam from this magnetic field.

(c) Further work is required along the following lines.

(1) σ_M must be determined experimentally for the type of chambers to be used. In particular σ_M as a function of the angle between the track and the normal to the plates is required. The design of the complete system hinges on the behavior of σ_M versus this angle. If σ_M can be kept small as this angle goes to 90°, then 90° stereo can be used. Otherwise, small-angle stereo must be used with its attendant larger dip-angle errors (Fig. 7).

(2) Along with the measurement of σ_M should go attempts to reduce σ_M. One possible way to do this is faster pulse-rise times and shorter particle-to-pulse delay times. Another possible way is the use of a damped oscillating pulse as first suggested and studied by B. Zacharov at CERN. Also different gap spacings should be tried and slight adulterations of the helium with other gasses.

(3) A computer study generalizing Section VI of this report should be made with the experimentally determined σ_M. In particular we cannot determine at present if 6 Bev total energy is the limit for this detection system, or if at 8 or 10 Bev total energy most events could still be analyzed. The computer study would ensure that the total energy and the sensitivity of the detector are matched.

(4) Only after items (1) and (2) and possibly (3) above are concluded can a complete chamber and magnet design and cost estimate be made. Neater solutions to the placing and design of the thick-plate shower chambers should also be looked for and included in the design.

(5) A substitute for the very heavy chambers for μ identification should be searched for.

(6) Speculation on the use of dE/dx and Cerenkov counters and on spark-chamber ionization determination should be continued.

(7) The background from the machine and from cosmic rays should be studied in detail and then a good trigger system must be devised.

(8) The behavior of the $e^{\pm}$ shower and γ-ray conversion chambers should be studied in detail.

A STORAGE RING FOR 10-BEV MU MESONS

by
John Tinlot
August 1962

I. GENERAL

A. Introduction

It will be assumed in this report, as it was in the recent report of G. Masek [SLAC-5-J], that the mu meson will still be an interesting particle to study at the time of completion of the two-mile linear accelerator (1966-67). It seems likely that the situation then will be qualitatively similar to the present one, in that the mu-proton scattering data will be very inferior in statistical accuracy to the data obtainable in corresponding electron-scattering experiments. The interest in studying the mu-proton interaction will be in looking for possible deviations in the behavior of the mu relative to that of the electron. The study of nucleon structure and the investigation of possible breakdowns in quantum electrodynamics will always be done far more easily using electron beams.

The electron-proton and mu-proton scattering experiments at energies of several Bev or more have already been discussed in some detail by Cassels* and by Masek./ I shall list the principal points to which I shall refer in the description of the storage ring:

(1) The elastic-scattering events can be separated on kinematical grounds alone from inelastic events in which at least one pi is produced if the momentum resolution in the incident and scattered e (mu) beams is better than m_π/E (i.e., 1.5% for E = 10 Bev).

(2) The inelastic scattering is defined in terms of the two variable q^2 (square of momentum transfer) and $-q\cdot p$ (energy transfer in lab. system). At a fixed energy, a large part of the accessible area in

---

*M Report No. 200, "Some Aspects of Target Area Design for the Proposed Stanford Two-Mile Linear Electron Accelerator," by J. Ballam, et al., Stanford Linear Accelerator Center, Stanford University, Stanford, California, Summer 1960.

/Section J of this report.

$(q^2, -q\cdot p)$ space can be reached by covering the scattering angles from 10° to 30° lab.

(3) For very large momentum transfers ($q^2 > 200$ f^{-2}) the inelastic cross section may not be much larger than the elastic one. (I am ignoring the events in which gamma rays are emitted, assuming that this contribution can be included in a calculation of radiative corrections.) The expressions used by Cassels (electrons) and Masek (mu's) are somewhat different: Masek is much more optimistic; in his extrapolation, it appears that only 5% momentum resolution is needed to assure a tolerable inelastic background to the inelastic process at $q^2 \approx 400$ f^{-2}.

(4) The elastic differential cross sections for 10-Bev incident energy, and for q^2 between 100 and 400 f^{-2} may vary between 2×10^{-33} and 4×10^{-36} cm^2/ster. (See Table I.) Even with intensities of the order of 10^7/ second, and very large scattering targets, one expects in straightforward experimental geometry to deal with counting rates of a few an hour to a few per day.

It is interesting in connection with point 4 above to note that the experimental problem seems less forbidding if one can design experiments in which the effective solid angle is very large; in that case, one looks at increments in momentum transfer, rather than solid angle. Table I shows the cross section in units of cm^2/(Bev/c). Under the same assumptions as to form factor made above, these cross sections range between 3.9×10^{-34} and 3.1×10^{-35} cm^2. Note that the variation in this cross section is much less sensitive to q^2 than is the case for $d\sigma/d\Omega$.

B. Straight vs. Stored Beam

I shall take as a basis for comparison the parameters suggested by Masek. In brief, he produces a collimated 10-Bev mu beam with 5% momentum definition by filtering through concrete (or iron) and analyzing and focusing with a conventional magnetic lens system. The flux so obtained is about 3.5×10^6/sec; using a 2-meter hydrogen target, he thus obtains an effective hydrogen traversal (flux times surface density of the target) of about 5×10^7 g/cm^2-sec. With a solid angle of 2.8×10^{-2}ster, a counting rate of 1/hr corresponds to a detected cross section of 4.5×10^{-34} cm^2/ster.

Table I. Differential cross sections for mu-p elastic scattering, calculated from the modified Rosenbluth formula, assuming single-photon exchange.

σ_θ = cross section in $cm^2/ster$;

σ_q = cross section in $cm^2/(Bev/c)$.

The form factors in Column 6 are for use as a guide, since extrapolation to such high q^2 cannot be made now.

$q^2(f^{-2})$	$F_1^2 = F_2^2 = 1$		$F_1^2 = F_2^2 = F^2$ in Column 6		Assumed F^2
	σ_θ	σ_q	σ_θ	σ_q	
25		9.5×10^{-31}		3.2×10^{-32}	.034
45	5.0×10^{-30}		1.0×10^{-31}		.02
50		4.7×10^{-31}		8.9×10^{-33}	.019
67	2.5×10^{-30}		2.5×10^{-32}		.01
100	1.2×10^{-30}	2.4×10^{-31}	1.9×10^{-33}	3.9×10^{-34}	.0016
189	2.6×10^{-31}		2.6×10^{-34}		.001
200		1.2×10^{-31}		1.1×10^{-34}	.001
288	5.5×10^{-32}		5.5×10^{-35}		.001
300		0.64×10^{-31}		6.4×10^{-35}	.001
400	4.4×10^{-33}	0.31×10^{-31}	4.4×10^{-36}	3.1×10^{-35}	.001

I propose in this report to perform mu-proton scattering experiments at 10 Bev by using a recirculating beam of mu's trapped in a strong-focusing alternating-gradient storage ring. Thin hydrogen targets are placed in straight sections in the ring so that mu-proton interactions can take place over times of the order of the mean life of the mu's ($\approx$ 220 μsec in the lab frame). One begins counting $\approx$ 30 μsec after the injection of particles in the ring, so that π's and K's have decayed out almost completely. It will be shown that in this scheme one obtains about 3.7×10^8 g/cm^2-sec of effective hydrogen traversal. Since the irradiated target volume is very small, it should be possible to devise a detector geometry which subtends a large fraction of the total solid angle. If we assume that a solid angle of one-quarter of 4π will be included at a given value of q (as is done, for example, in current experiments at Berkeley and Brookhaven), one finds that a counting rate of 1/hr corresponds to a cross section of 5.0×10^{-36} cm^2. It thus appears that by this method one can cover quite adequately the range of momentum transfers listed in Table I. Since the inelastic cross sections are likely to be larger than the elastic ones, a good study of inelastic processes is also possible.

Even without having detailed specifications of the ring (such as momentum definition, angular definition, targeting, shielding, etc.) one can perceive a number of other advantages of the stored beam-system:

(a) The duty cycle is effectively about 100 times larger than one has in conventional experiments with the linear accelerator. The requirements on the scintillator geometry and electronic circuitry are therefore much relaxed, and it should be possible to use the spark-chamber arrays.

(b) The contamination of the mu beam by other particles is small and easily predictable. In 30 μsec pi's will have decayed over 21 mean lives, corresponding to an attenuation of 10^9. Thus one can completely neglect pi contamination. The same is true for K's. Thus after 30 μsec the negative circulating beam will contain only μ's, electrons and anti-protons; however, most of the electrons will have disappeared during the first few μsec of storage time because of their large

synchrotron radiation loss. The positive beam will also have a proton component; however, the proportion of anti-protons or protons probably will not be large enough to be troublesome.

(c) The background problem will in some ways be much less serious than in conventional experiments, since the only particles remaining near the detectors after 30 μsec are slow neutrons, and electrons from decay in flight of mu's. The mu's, which in the usual geometry are very difficult to collimate and contain, will here be well-localized, and their direction defined to a few milliradians.

Other agreeable features of the storage ring will become apparent during the following discussion.

C. Why is a Storage Ring so Advantageous When Used with the Linear Accelerator?

It would seem from the preceding points that the storage ring might be very advantageous for all mu-scattering experiments. The principal difficulty one meets in trying to use this scheme with proton accelerators is that one has great difficulty in introducing mu's into the ring with the required efficiency. At the Bevatron, the CERN PS and the Brookhaven AGS, mu's are produced only by decays of pi's and K's in flight. One can therefore form a linear mu beam, and then inject it into the ring. The problem of injecting and trapping such a beam is comparable to that of ejecting the proton beam from the accelerator; even though it probably can be done, the predicted intensity of trapped recirculating mu's is much too low to be useful. An alternative possibility is to produce the pi's in the ring, and to accept mu's from decays of trapped pi's. This again can be done only with very low efficiency, because the angles of production of pi's and decay of mu's are much larger than the limiting angles set by the allowable betatron oscillation amplitudes.

If one has electrons of energy greater than 10 Bev or so, mu pairs can be produced in appreciable numbers by purely electromagnetic interaction. Both the angular divergences of the high-energy bremsstrahlung photons and of the mu pairs are relatively small (of the order of tenths

of degrees or less). In addition, the electron beam from a linear accelerator occupies very small phase volume. It is therefore practical to produce mu's by directing the electron beam at a small high-Z target placed in the storage ring. Because the target cross section may be made much smaller than the area crossed by the beam as it undergoes betatron oscillations about the equilibrium, those mu's that are trapped will strike the production target again only infrequently. Even if mu's do strike the target, nothing much will happen to them. The principal difficulty appears to be to dissipate the heat generated in the target; because of its small dimensions, it would become impossibly hot. Several solutions seem practical, as will be shown later.

II. DESIGN OF THE STORAGE RING

A. General Considerations

As is usual in such problems, the desired characteristics of the ring conflict. As mentioned in Sec. I. A., one would like to have small momentum spread (less than 1.5% would be desirable at 10 Bev), small angular divergence, and small spatial spread (minimum phase space volume). For high trapping efficiency, one would like a large momentum acceptance and phase volume, particularly since multiple scattering in the production and interaction targets will spread the phase volume as the beam circulates. It is immediately evident that a weak-focusing magnet ring is out of the question, because of its small phase volume acceptance and poor momentum compaction. The FFAG system is almost ideal: An FFAG ring has large betatron frequencies and thus will accept particles making sizeable angles with the equilibrium orbit; and the high momentum compaction ($1/\alpha$ = 20 to 50) makes it possible to accept a satisfactorily large momentum band, and allows us to hold the beam as it loses momentum by repeated traversals of the hydrogen scattering target. Unfortunately the two usual types of FFAG rings are unsuitable. The radial AG, alternating-field ring has easily calculable properties and is known to have no appreciable non-linearities for large betatron amplitudes. The circumference factor, however, is very large; this results in a ring of

huge dimensions and high cost (for 10 Bev, the circumference is about 3000 feet!). The spiral-ridge FFAG ring has much smaller circumference factor, but has pronounced non-linear characteristics; it is also very difficult to construct the magnets, and almost impossible to have large enough straight, no-field sections in which to place the scattering targets and detectors.

It was finally decided that a "conventional" AGS type of ring could be used. This is not a fixed-frequency ring, and the equilibrium orbits of particles having momentum off the central momentum are complicated and rather unpleasant (see Fig. 3). However, on the basis of approximate orbit computations, it seems that a ring having properties close to that of the Cambridge Electron Accelerator would be suitable. It would accept a momentum band on "injection" of about ± 1.5%, and contain a total momentum spread of about 8.5%. (Note that in principle only the width at injection leads to an uncertainty in momentum of interacting mu's, since the momentum loss due to recirculation can be computed from a knowledge of the elapsed time after injection.) These seem like reasonable parameters, consistent with reasonable pole size, cost, and the demands of the scattering experiment. Fig. 1 shows a sketch of the ring, and Table II lists the desired characteristics. Fig. 2 shows a cross section of one magnet, indicating the excursions due to betatron oscillation, momentum spread at acceptance, and momentum loss from hydrogen traversal.

No mention has yet been made of the obvious possibility of introducing acceleration voltage to compensate for the ionization loss in the target; this can be done by means of high-frequency cavities, as in the CEA ring. It will be seen that this is perfectly possible. The advantage is that the magnet aperture can be reduced, and the orbits are prettier. On the other hand, the disadvantages are high cost, considerable loss in trapped efficiency, and loss from scattering on the production target. (The injection efficiency is lowered because not all mu's will fall into stable synchrotron phase and because the momentum acceptance of the rf system is smaller than that of the magnet.) In addition, the duty cycle is reduced by a sizeable factor because of rf bunching. However,

Fig. 1. Sketch of AG magnet. For optimum magnet efficiency, the magnets in quadrants A, B, C, and the half of quadrant D upstream from the production target may have H-yokes. The magnets in the downstream half of quadrant D should have C-yokes, with the open side out, to allow the forward electromagnetic cascade to escape to the dumping area.

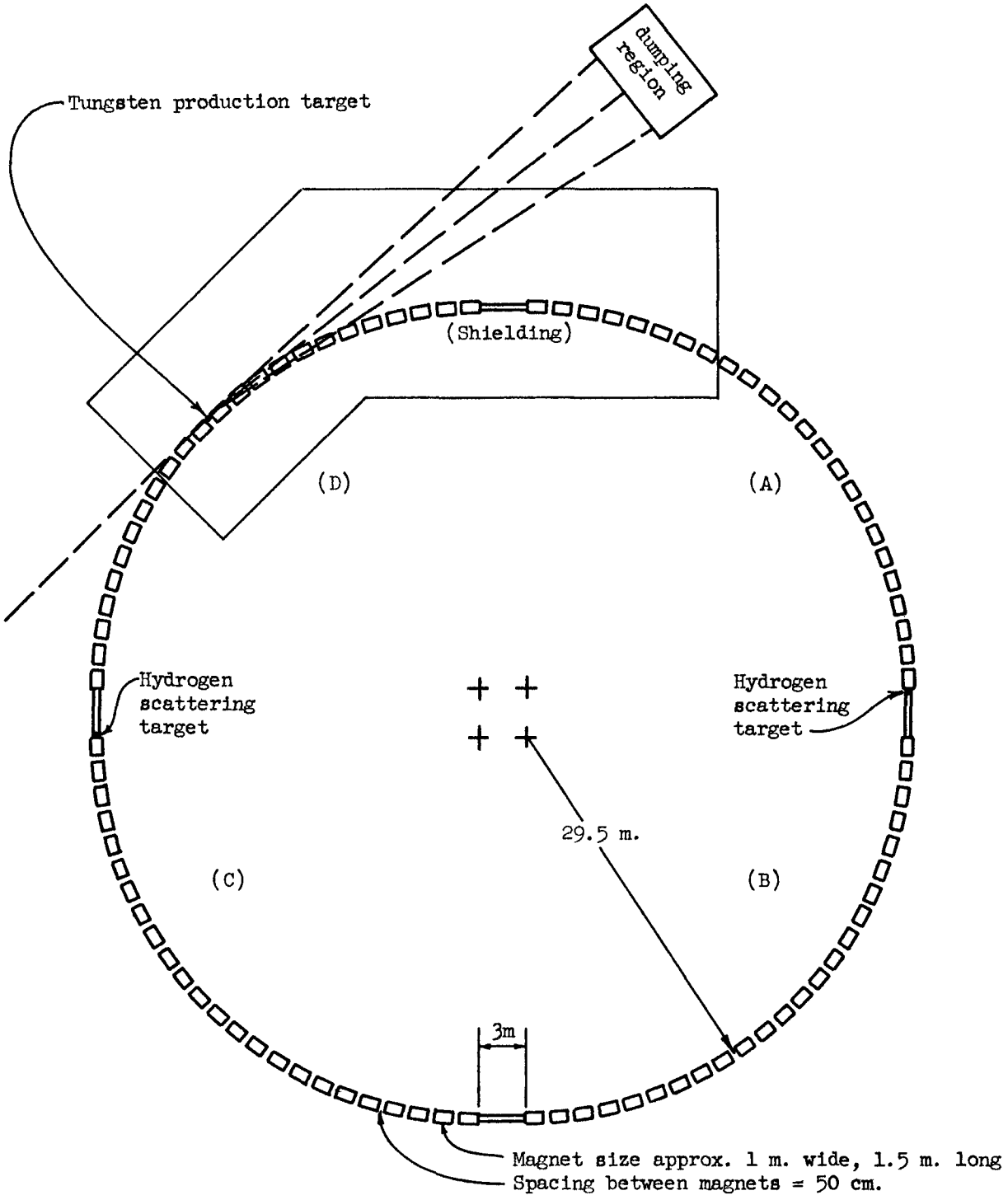

TABLE II

(a) Characteristics of the AG ring

N = number of magnets = 48

Order: Alternate focusing and defocusing

No-field section: Between magnets - 50 cm; Four straight sections - 3m

Gap field for central orbit: 15 kg

Minimum and maximum fields in gap: 10 kg and 20 kg

Gap (central orbit): 7.6 cm

Useful pole width: 16 cm

Frequency of revolution (central orbit): 1.6 Mc/s

Betatron frequencies: $\nu_T \approx \nu_z \approx 6.5$

Momentum compaction: $\alpha = 0.03$

Production target position: Center quadrant, 2 cm in from outer edge of useful field

(b) Injection conditions

E_o = energy for equilibrium orbit passing through production target; δE = deviation from E_o; δr = displacement of equilibrium orbit for energy $E_o - \delta E$; θ = maximum initial angle in horizontal plane, for given δE; P_o = approx. probability that particle will strike production target again before orbit shrinks in from ionization loss.

$\delta E/E_o$	δr(cm)	θ_o(mrad)	P
0.005	0.44	3.3	≈ 1
0	0	4.3	≈ 1
- 0.005	0.44	5.2	0.43
- 0.015	1.31	6.6	0.32
- 0.25	2.18	7.7	0.15

TABLE III

Probability per 25-Bev electron for producing a mu (either sign) at 0^o in a thick high-Z target ($t \gg 1$ r.l.).

E_μ	$d^2N_\mu/dE_\mu d\Omega$ (Bev^{-1}ster^{-1})
5	1.73×10^{-3}
10	2.21
15	1.98
20	1.10

Fig. 2. Profile of one magnet. Dimensions indicated are cm.

Key to labeling of various points across gap:

(0), (7). Limits of pole.

(1), (6). Limits of usable field; beyond these points fringe effects become excessive.

(5). Position of production target (center of quadrant; see Fig. 1).

(4). Position of equilibrium orbit at injection, in long straight section.

(3). Position of equilibrium orbit at which particles begin to be lost (in long straight section).

(2). Position of equilibrium orbit at which particles begin to be lost (in center of quadrant).

(C) Position of central orbit.

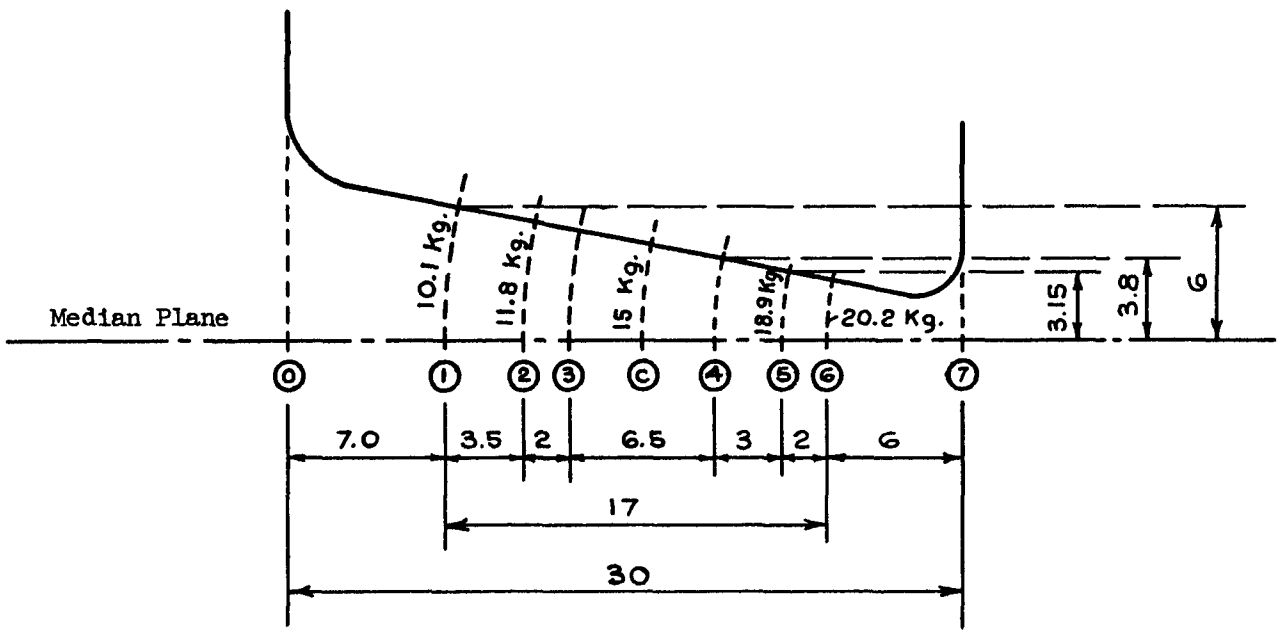

for completeness, the possibility of converting a "dissipative ring" into a "constant energy" ring will be discussed.

B. Dissipative Ring

(1) Mean Energy

Table III shows the computed differential yield of mu pairs produced by 25-Bev electrons. (This table should correspond to Fig. 5 of Ballam's report M-200-8*; however, there are appreciable unexplained discrepancies, particularly at 10 Bev.) The yield is almost constant with energy, principally because the angular spread decreases with increasing mu energy. Thus the choice of energy could be made from considerations of magnet cost, and of the possible interest in interactions at different energies. Although nothing leads us to believe that new phenomena will appear at high energies, it seems reasonable to plan to explore a new range of energy in planning such an experiment. 10 Bev is probably beyond the reach of the existing proton machines, and yet leads to a magnet ring size which is not impossibly expensive. Actually, 10 Bev is a rough lower limit for a storage ring using the principle of injection by pair production in the ring itself, since at lower mu energies the angular divergence and multiple scattering of mu's at production will greatly decrease the trapped mu flux.

(2) Magnetic Parameters

The mean field should be as high as possible in order to decrease the ring size, and to aid in getting rid of trapped electrons by means of synchrotron radiation. I chose 20 kg as the maximum practical field at the minimum gap; the central orbit lies at a field of about 15 kg in both the focusing and defocusing magnets. After trial computations and variations of parameters, I have concluded that the parameters of the CEA magnet are close to what one wants: $n \approx 90$, $\nu r = \nu z = 6.4$, $\alpha = 0.03$, $N = 48$. (For convenience the magnets would be constructed in sections 1/2 the length of a unit cell.) In order to have these values,

*In M Report No. 200, op cit.

it is necessary to preserve approximately the same ratio of straight sections to field sections. This means that 1/4 of the circumference is occupied by straight sections. This is very convenient, since it allows a spacing of about 50 cm between alternate magnets, plus four long straight sections of 3 meters each. Two diametrically opposite sections can be used for scattering stations. (One would be undesirable, since the orbit center would shift too much as the momentum decreased.) It should be emphasized that in the final design the exact betatron frequencies and the momentum compaction factor α may differ somewhat from the above values; the final choice involves a careful consideration of the best position of the production target, and an investigation of possible non-linear effects for off-central orbits.

Having chosen the n-value, and keeping in mind the fact that off-central orbits will be distorted, one chooses the total allowable momentum spread for stable orbits; 6 - 8% seems reasonable. Figure 3 gives an example of the appearance of the equilibrium orbit through 1/8 of a ring made up of 72 alternately focusing and defocusing magnets, with $n \approx 90$. The orbit shown is for a particle having 5% greater momentum than the central value. It is seen that the AG field causes this orbit to wander by about ± 1.2 cm from the mean radius. The usable horizontal aperture of the magnet is thus somewhat reduced. It is also probable that non-linear effects become important for smaller betatron amplitudes of oscillation relative to such distorted orbits than is the case for central momentum orbits (which would be circles in the absence of straight sections). The exact characteristics of off-central orbital motion should be investigated by digital computer methods.

(3) Production Target

The production target should be thick ($\gg \frac{1}{2}$ r.l.) along the beam direction, but small in cross section; the most convenient material is tungsten, since 2 r.l. is equivalent to only about 5 mm. The electron beam, because of its very small angular divergence, can be focused to perhaps 1 mm in diameter. Thus the target can have a cross sectional diameter of about 2 mm. The average full betatron oscillation amplitudes of trapped particles are about 1.25 cm vertically and 1.8 cm

Fig. 3. Approximate form of the equilibrium orbit through one octant of a strong focusing ring, starting from the center of one quadrant; the case considered is for a ring having 72 magnets 2 m. long, 50 cm spacing between magnets, and straight sections 3 m. long.

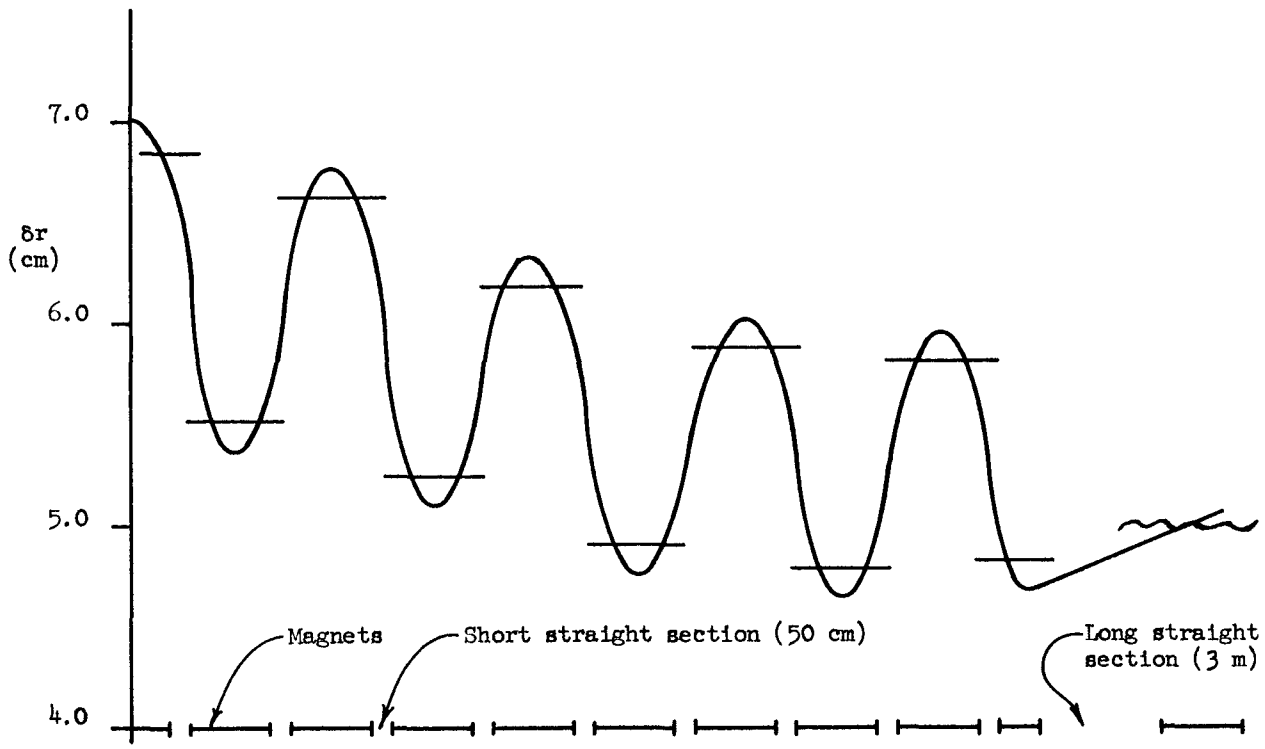

horizontally. The beam thus sweeps out an area of about 2.3 cm^2; the area of the tungsten target is .031 cm^2; thus the beam will not return to the target, on the average, until it has made 75 turns. In that time, the beam has lost momentum in the hydrogen target and shifted radially in by over 1.5 cm. Thus it will strike the target a second time no more than once before it is pulled in out of reach entirely. This question is discussed in more detail in Section II.B.6a.

(4) Energy Acceptance at Injection

The next question is the optimum placement of the production target. Suppose that at a given azimuth, the field in the gap is usable out to a radius R_1 (i.e., the n-value remains within the required limits, and azimuthal inhomogeneities are not excessive). If the targets were placed at that radius, only particles emitted at 0^o in the horizontal plane (i.e., tangent to the equilibrium orbit) would be trapped in the ring. In spite of the fact that they might be injected with appreciable vertical betatron oscillation amplitude, they would return to the production target point within a few turns (in fact, the average number of turns would be roughly equal to the ratio of betatron amplitude to target half-height). Any particles injected with a non-zero horizontal angle would eventually tend to oscillate to larger radius. Let us suppose, then, that the target is placed at radius $R_o = R_1 - a$, and that particles are produced with such energy E' that their equilibrium orbit (the orbit having zero betatron amplitude) has radial coordinate R'. Then particles may be trapped if their radial betatron oscillation amplitude b obeys the inequality.

$$\left|a\ \delta r\right| \geq b \geq \left|\ \delta r\ \right| \quad \text{where} \quad \delta r = R' - R_o, \text{ and } \delta r < \tfrac{1}{2}\, a$$

(Here, negative δr means the injected energy is less than E_o, the equilibrium energy at R_o.) Correspondingly, if the production target is considered to be a point source of particles, the initial radial betatron angle would be given by $\theta_r = (2\pi \left| b \right|)/\lambda_r$, where λ_r is the radial betatron wavelength (29 meters in the case considered here).

We see, then, that for each energy E' there is a range of acceptable radial betatron angles bounded by $(\theta_r)_{max} = (2\pi \left| a\ \delta r \right|)/\lambda_r$, where

$$\delta r/R_o = \alpha\ (E' - E_o)/E_o = \alpha\delta\ E/E_o$$

Table II lists $(\theta_r)_{max}$ and δr as a function of $\delta E/E_o$, for $a = 2$ cm.

Apparently, the only limit on the acceptable energy is that $E' \leq E_o + E_o a/2\alpha R_o$. However, an effective lower limit on the energy is imposed by two factors. First, if the betatron amplitude becomes too large, non-linear effects become important enough to produce destructive resonances, with consequent loss of the circulating beam; this limitation must be determined by second-order orbit computations. Second, the production of mu's by pair production follows the angular distribution.

$$F(\theta) \approx C/[\theta^2 + (\mu/E_\mu)^2]^2$$

i.e., it falls to $1/4$ of its maximum value for $\theta = \mu/E_\mu = 10$ mrad.

Thus, according to Table II, the injected intensity will be limited approximately to an energy band given by $0.005 > \delta E/E_o > -0.05$. The full width of the accepted energy distribution at half maximum corresponds approximately to $\delta E/E_o = 0.03$. This result seems compatible with the requirements on energy definition mentioned in Section I, although in some cases it may be desirable to reduce the accepted energy spread further by other means.

(5) Energy Loss in Hydrogen Targets and Target Thickness

According to the above paragraphs, the average value of $\delta E/E_o$ will be about -0.01, corresponding to $\delta r = -0.85$ cm. Because of the AG distortion of the off-central orbits, this will correspond to a radial shift in the region of the long straight sections by about 3.0 cm inward from R_o. [This is indicated by point (4) in Fig. 2.] As is seen in Fig. 2, there remains about 6.7 cm of radius through which the beam can shrink before it begins to be lost at the "inside" of the storage

ring. (The exact width of the poles is somewhat arbitrary, although because of the high field index n one cannot make the width much more than is indicated here.) Finally, then, 6.7 cm corresponds to an energy band of 7.5% or 750 Mev down from the mean injection energy of 10.4 Bev. Using this value, one computes the required thickness of hydrogen to cause the beam to lose this energy by ionization over a time T. The effective time for counting events is T - 30 μsec. Upon calculating the counting rate as a function of T for fixed total ionization loss, and given lab. mean life T_o, one finds that there is a broad maximum for $T \approx T_o$. We choose T = 230 μsec, corresponding to a total of 370 turns at 1.6 Mc/s. The required hydrogen thickness is then found to be $(141\ g/cm^2)/370 = 0.38\ g/cm^2$. If this is divided into two parts placed in diametrically opposite straight sections, each scattering target will have a thickness of $0.19\ g/cm^2 = 2.7$ cm of liquid hydrogen.

(6) Calculation of Effective Hydrogen Traversals

$$\text{Total hydrogen traversals} = (d^2N/dE_\mu\, d\Omega) \times \delta E_{acc} \times \Omega_{acc} \times x \times \eta \times N_e$$

where the quantities are defined as follows. The first factor is the differential μ production yield per electron, taken from Table III. This yield is computed for a "thick" target (>> 1/2 r.l.); $\delta E_{acc}/E_o = 0.03$, as explained in the previous section; Ω_{acc} is the effective solid angle for trapping mu's produced by pair production with an angular distribution

$$f(\theta) = C/[\theta^2 + (\mu/M)^2]^2$$

and it is defined by the maximum angles of betatron oscillation in both directions. The angles are assumed to be about 4.5 mrad for both radial and vertical oscillations. (The effective vertical aperture has been reduced from the gap of 6.3 cm shown in Fig. 2 by a factor 1.5, the AG "form factor," computed for the CEA ring.) This gives $\Omega_{acc} = 5.4 \times 10^{-5}$ ster.

η represents the loss of mu's by decay; it is the fraction of the injected flux which is effective in scattering from hydrogen between a time of 30 μsec and T after injection. For T = 230 μsec, $\eta = 0.48$.

x is the total thickness of hydrogen traversed from t = 0 to 230 μsec.

Finally, N_e is the flux of electrons striking the target per second, and is assumed to be 33 μamp, corresponding to 2×10^{14} electrons per second. Putting in these values, we then obtain a result of 4.0×10^8 g/cm^2-sec. [Note that the first three factors of the formula give the number of mu's trapped per incident electron per second $(= 3.57 \times 10^{-8})$. The number trapped per electron per pulse is 10^{-11}.]

The above number will be reduced somewhat by loss of μ's during recirculation. If the non-linear characteristics of the magnets are not troublesome, the principal causes of loss will be multiple scattering in the hydrogen targets and scattering of particles which strike the production target again. I have made an attempt to estimate this loss [see Sec. 8 (a) below] and find it to be probably less than 25%. Thus the net effective traversal is from here on assumed to be 3×10^8 g/cm^2-sec.

(7) Beam Contamination

As already mentioned, the fraction of pi's and K's remaining in the ring after 30 μsec is negligible. The number of electrons remaining is somewhat difficult to estimate. The number of trapped electrons is initially of the order of 10^5 as large as the number of trapped mu's. The synchrotron radiation for electrons is 50 Mev/turn ; thus 30 μsec = 48 turns = 2 Bev. The electrons remaining after 30 μsec will thus be on the extreme tail of the distribution in energy loss, and should be a tiny fraction of the initial trapped flux. I have not attempted to estimate the shape of this distribution. If the electron flux is still bothersome at 30 μsec, one can wait additional time before starting to count, with reasonably small loss of mu-scattering rate. In any case, one may be able to reject electron-scattering events, if they are not

too numerous, by filtering with an absorber in the detection apparatus.

The contamination from protons or anti-protons is likely to be small. One source of 10-Bev protons would be secondary interactions of pi's in the production target. The yield of pi's will be somewhat less than that of mu's, although both electromagnetic and "Drell-processed" pi's can be created. The cross section for pi's to transfer 10-Bev momentum to a proton is not known, but should be very small.

The number of protons (anti-protons) produced electromagnetically and accepted by the ring is no more than 10^{-4} the number of accepted mu's. However, the effective hydrogen thickness is at least two mean free paths for nuclear interaction, so that every proton (anti-proton) will produce an interaction in the hydrogen targets.

Such events can be rejected by requiring that at least one recoiling particle from the interaction have the penetration characteristic of mu mesons. The rate of nuclear interactions is only 0.2 per pulse, which is of no consequence in view of the large effective duty cycle.

(8) Radioactivity, General Heating, Shielding

The use of a storage ring with the primary electron beam as injector poses some rather unusual problems, but it appears that they are soluble with no great difficulty. Let us consider first the question of induced radioactivity in the components of the ring near the production target. The beam emerging from the 2 r.l. thick tungsten target will consist principally of electrons and photons, and their energy spectrum will be roughly of the form dk/k. About half of the beam energy will be in the form of photons which escape in the forward direction; one half of the charged component will be of the "wrong sign," i.e., will be dispersed by the magnet and deflected away. About 60% of the energy of the remainder will be contained in particles having momenta greater than 10 Bev/c, and these will also escape the ring, but with some deflection (and dispersion) away from the forward direction. Finally, then, about 15% of the incident beam energy will be contained in the flux of "right" sign charged particles with momentum under 10 Bev/c; most of these will spiral in and strike the material on the inside of the ring, near the production target. We may compare

this situation with that of the CERN or AGS synchrotrons, where perhaps 30% of the beam energy ends up in "right" sign charged particles which strike the ring components. In those cases, the average current is about 1/60 μamp, and the radioactivity in the components closest to the target falls to a tolerable value (1 r/hr at 10 cm) in a few days. As a general rule, one can consider electromagnetic radiation as 100 times less effective than protons in producing induced radioactivity. Thus the electron beam is roughly equivalent to 10^{12} protons (1/6 μamp) having energy spectrum approximately dk/k, with upper energy limit 10 Bev. Since the proton energy at the CERN and AGS synchrotrons is 30 Bev, it seems that the induced activity produced in the storage ring may not be much more than is found in the synchrotrons.

The heating of the ring components by the troublesome 15% of the incident beam is not negligible; if all the energy goes into heat, it is equivalent to the power dissipated by 5 μamp losing 3-4 Bev (15-20 kw). At least one half of this energy will escape in low-energy photons, but the remainder is still sufficient to require some water cooling in critical spots. Presumably, one would design the magnets so that the coils are exposed as little as possible, and most of the heating and radioactivity are produced in the iron yoke.

The problem of dumping the primary beam energy is complicated by the dispersion of the charged portion of the electromagnetic cascade which leaves the production target. However, the great majority of the energy will still be contained in particles emitted primarily forward.

As to shielding, it is evident that the section of the ring near the production target and downstream from it must be completely surrounded by a thick wall. From the considerations above, however, this does not seem too formidable a problem; it is much less severe, for example, than the problem faced by the designers of the MURA high intensity 10-Bev proton machine; in that case the circulating beam may be as high as 10^{15} protons per second, and the radiation emitted from an internal target and the material nearby would be 1000 times more intense than is produced in the mu storage ring.

Little or no shielding will be needed in the region of the interaction (hydrogen) targets, particularly if remote operation of the equipment is possible. This is because the only background radiation still present when the active counting interval begins consists of slow neutrons. Although these neutrons may create very high singles rates in scintillators, they are not likely to cause much trouble in the operation of Cerenkov counters or spark chambers.

(9) Miscellaneous Experimental Problems

(a) Multiple scattering loss

As discussed previously, and illustrated in Table III, the acceptable angles of betatron oscillation are 4.5 mrad vertically, and at least as much radially. The total amount of hydrogen traversed by a mu surviving 230 μsec is equivalent to about 2.5 radiation lengths, corresponding to a projected rms scattering angle of about 2 mrad. Taking the attenuation of mu's by decay into account, I estimate the loss by scattering in the hydrogen to be less than 10%. The tungsten production target produces scattering of about the same amount. The scattering of the mu's immediately after they are produced is completely negligible, since the angular divergence expected is much larger than the scattering angle. The loss from scattering of particles striking the production target again is more difficult to evaluate. I have considered orbits having 1/2 the maximum vertical betatron amplitude, and produced with various initial values of $\delta E/E_o$ and θ_o (see Table III). I assume that the probability of striking a given segment of the cross-sectional ellipse (defined by the maximum betatron excursions) is the same for all points in the ellipse; the probability of striking the target is then equal to the number of rotations times the ratio of target area to area of the ellipse. The effective number of rotations is such that the orbit has shrunk (from ionization loss in the hydrogen) so that the target no longer lies in the ellipse. This number is a function of the initial conditions. In this way, I have found that the probability is high for at least one strike if $\delta E/E_o > 0$. For $\delta E/E_o < 0$, the probability varies from a few percent to 50%, depending on the initial angle θ_o. The scattering

produced by one strike increases the phase volume by about 15%; thus the result is an almost negligible loss except for a few particles with very small vertical betatron amplitudes, and positive $\delta E/E_o$.

In sum, then, the combined loss from scattering in the tungsten and hydrogen is probably no more than 25%.

(b) Heating of production target

The average multiplicity of electrons in a 2 r.l. target is about 12, corresponding to an energy dissipation of about 20 joules per burst. Assuming the target is tungsten 5 mm long and 2 mm in diameter, the mass of the target is 3.6 g, and the temperature rise per burst is 40° C. Although tungsten may be heated to very high temperatures without damage, it is not possible to dissipate this energy by radiation alone. One solution is to mount a number of identical targets on a rotating wheel, and to cool them between irradiations. This solution appears easier than it first seems when one realizes that the target need not be in the vacuum chamber, but may be placed in an inert atmosphere and cooled by conduction, convection and radiation. The mu mesons will not be disturbed by the small mass of two thin windows and of the inert gas path near the target.

(c) Heating of hydrogen target

A very large flux of particles (principally electrons) will traverse the hydrogen in the first few microseconds after injection. Most of these, however, will have disappeared in 20 μsec, so that the heating corresponds to 10 watts or so, and a liquid loss of no more than 1 liter per hour.

(d) Vacuum

The path traveled by a mu living 230 μsec is about 70 km, which would correspond to about 10^4 g/cm^2 of air at atmospheric pressure. Thus, if the vacuum is 100 microns or so, the remaining air will be equivalent to only 1 g/cm^2, which is negligible compared to the effective hydrogen thickness. The storage ring will therefore work well with roughing pumps alone.

C. Constant Energy Ring

At first sight, the idea of providing energy to compensate for the ionization loss in the hydrogen targets is quite appealing. The advantages are that the energy spread is small and calculable, the equilibrium orbit is stationary and has a smooth shape, and the interaction volume in the hydrogen is even smaller than in the dissipative ring. The disadvantages are, however, quite formidable. Aside from those previously mentioned, it seems that the cost of the rf system may equal that of the magnet.

It may be worthwhile, however, to point out that, if it ever seems desirable, rf cavities may be added to the magnet described earlier.

The total peak accelerating voltage must be high, as is seen from the formula

$$\delta E/E_o = \left(\frac{2}{\pi} \frac{1}{h\alpha} \frac{eV}{E_o} \right)^{\frac{1}{2}}$$

which is obtained from Green and Courant (Handbuch der Physik, V. 44) and gives the synchrotron condition for the case of extreme relativistic energies. δE is the energy deviation; h is the rf harmonic number; α is the momentum compaction; eV is the electronic charge times the peak accelerating voltage, minus the energy loss per turn in the hydrogen; and E_o is the central energy. As an example, consider the accelerating system of CEA, which consists of 16 double cavities providing a total peak voltage of 6.4 Mv at about 475 Mc/s. This means $h = 250$, and $\delta E/E_o = 0.6\%$ (but the total accepted spread is twice this amount). Here I have taken the hydrogen target thickness to be the same as before, corresponding to about 2-Mev loss per turn. This could be doubled without decreasing the energy spread too much, but could only be increased further by adding more rf cavities.

One loses from the yield of events detected in the dissipative ring by the following factors:

2.5 for the accepted energy spread;

≈ 2 because not all particles injected fall into stable synchrotron phase;

2 because the radial betatron amplitude is limited by the cavity aperture.

An unknown additional factor is caused by repeated striking of the production target, leading to large phase volume. (In this case, the orbit does not shrink away from the production target, and the scattering is relatively more important because of the smaller acceptable betatron amplitudes.)

The conclusion is that the addition of rf cavities could only be justified if the energy definition of the beam is of over-riding importance.

D. Cost Estimates

The magnetic system proposed for the dissipative ring consists of 96 magnets with alternating gradient, providing a mean gap of 3 inches and a usable pole width of 6.5 inches (the actual pole width should probably be about 12 inches in order to avoid fringe-field distortions). The magnetic path is about 470 feet long, so that each magnet would be about 5 ft in length. The field at the 3-inch gap should be 15 kg, the peak field at minimum gap 20 kg, and the field at maximum gap 10 kg.

We can estimate the cost of such magnets using the rough rule of thumb of Leroy Schwarcz: \$6.00 per $in.^3$ of gap. The total volume of gap (including fringe-field allowance) is 2×10^5 $in.^3$; the cost would then be \$1.2 million.

The power requirement for reasonable magnet design would be of the order of 5 megawatts continuous, and the installed generating equipment (according to Schwarcz) would cost about \$750,000.

The vacuum chamber, vacuum system, hydrogen targets, production target, etc., are simple and their cost will be trivial compared to that of the magnets. The foundations and mounts for the magnets must be well made and accurate, but the problems of precision and stability

of positioning are not comparable to that required for pulsed synchrotrons.

The cost of the detection apparatus is not easy to guess without making a detailed study of the experimental program. However, in view of the small size of the target volume, and the good definition of energy and angle, it is probable that the detectors will be more compact than is the case in the geometry proposed by Masek. It may still be necessary, however, to measure the momentum of the recoil particles, and this will of course require good-sized magnets and spark-chamber arrays. As a guide, the last section of this report is devoted to a sample computation for two experiments to detect elastic and inelastic scattering at large momentum transfer.

III. DESIGN OF SAMPLE EXPERIMENTS

Suppose we want to measure the elastic-scattering cross section over as wide a range of momentum transfers as possible. Because of the expected low counting rates for $q^2 > 100\ f^{-2}$, it is desirable to try to measure the whole range at once. The simplest setup consists of a number of spark chambers completely surrounding the hydrogen scattering target, and of sufficient extent to see both recoil particles. Remember that the energy of the incident mu's is defined to approximately $\pm$ 1.5%, and the angle to about 5 mrad (0.25°). We can measure the directions of both of the recoil tracks to at least this accuracy using conventional spark-chamber techniques. The scattering event is therefore over-defined by one degree of freedom; this may be enough to reject more inelastic events on kinematical grounds, and, if Masek is correct, the inelastic contribution at large momentum transfers will be relatively unimportant.

Table IV shows the angles, recoil momenta, and the expected rate of events in counts per hour, assuming the entire 4π solid angle is subtended. Evidently, one must cover angles of emission of 6° to 53°; the smaller angles may be a little difficult because of the limited space in the straight sections. However, if the hydrogen target is

placed at the very beginning of the 3 m straight section, a 6° recoil will be displaced 30 cm at the end of the straight section. The irradiated cross section of the target is 12 cm wide by 5 cm high (approximately); the vacuum pipe in the straight section need not be much larger, and thus even a 6° recoil will leave the vacuum pipe in the straight section.

In order to guard against contributions from electron scattering and (in the case of μ^{+} beams) of proton-proton scattering it may be desirable to have thin-plate chambers to measure the direction, followed by absorbers and more spark chambers. The absorber should be in sections, the first thick enough to stop electrons, and the second, protons. The mu would be clearly identified by its ability to penetrate both absorbers.

Such an experiment would be very appealing because of its simplicity and high counting rate. Note that in the highest band of momentum transfers (q^2 = 300-365 f^{-2}), the yield of events is 5/hr, assuming that $F^2 = 10^{-3}$; in the region of $q^2 = 25\ f^{-2}$, one will get thousands of events per hour. This clearly will be a gain of about three orders of magnitude over the present state of the art. The experiment in this form will, of course, be practical only if the background of low-energy neutrons is tolerable, so that a fairly extensive scintillator array can be used to trigger the spark chambers.

The rates quoted in Table IV are computed for scattering in only one of the hydrogen target locations. Another setup could be operating simultaneously in the other station. As an example, Fig. 4 shows a possible setup in which one measures the recoil track directions, and, in addition, the momentum of the particle emitted at the larger angle. This might be useful in measuring the counting rate in inelastic channels. The solid angle is, of course, less than that of the first experiment above; even using magnets with large gaps (8 to 16 inches), one cannot subtend more than 10% of the total solid angle. The counting rates may be still quite sufficient to give interesting information. As in the first experiment, one would use a series of absorbers and spark chambers (before and after the magnets) to identify the recoiling

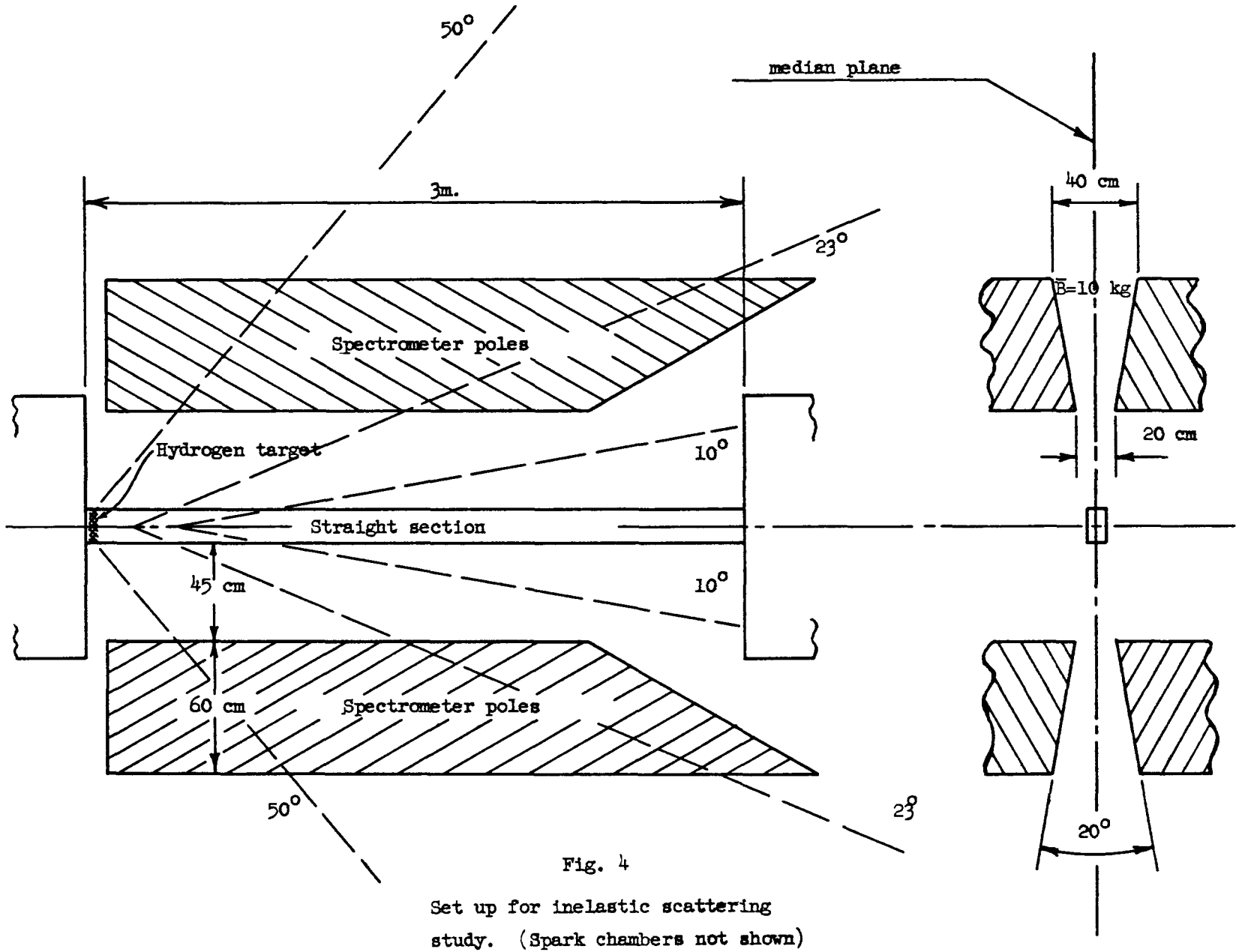

Fig. 4

Set up for inelastic scattering study. (Spark chambers not shown)

SLAC-5-I
Tinlot

particles. The exact dimensions of the magnets would depend on the desired accuracy of momentum measurement. For the dimensions shown in Fig. 4, the momentum of a 5-Bev particle could be measured to 5% if the angles before and after deflection are measured to 0.2°.

Table IV. Mu-p scattering kinematics at high momentum transfers; counting rate yield computed assuming 1.5×10^{8} g/cm^2-sec effective hydrogen traversal, and taking cross sections in column 5 of Table I; the detector solid angle is assumed to be 4π.

q(Bev/c)	$q^2(f^{-2})$	Mu angle	Proton angle	Mu momentum (Bev/c)	Proton momentum (Bev/c)
1.0	25	6°	55.6°	9.45	1.19
1.63	67	10	48.7	8.75	2.02
2.03	102	13	43.4	8.15	2.67
2.75	189	20	27.7	6.27	4.62
3.0	225	23	24.1	5.57	5.33
3.39	288	30	22.6	4.73	6.18
3.80	362	42	15.2	3.11	7.96
4.0	400	53	10.3	2.00	8.94

Range of $q^2(f^{-2})$	Counting Rate (per hour)
25-50	$\approx$ 3000
50-100	$\approx$ 1000
100-200	50
200-300	17
300-400	5

In conclusion of this report, I should say that the storage ring seems to be a very useful device for investigating the mu-proton interaction at very high momentum transfers. Although many of the assumptions made here are somewhat shaky, it is likely that the general result is correct: That one can study the elastic cross section as long as the form factor stays of the order of 10^{-3} or larger, and that one can also profitably investigate the inelastic processes with not too elaborate detection equipment. As has already been said, the experiments one can do in this way are not suitable for verifying the validity of the Rosenbluth form of the cross section, since the energy of the incident beam is fixed. One can make measurements with both signs of mu's, however, and remove the cross term in the cross section arising from interference between one- and two-photon exchange. If it ever seems very desirable to design experiments at much higher energies, it is perfectly possible to increase the number of magnets in the ring, using the same magnetic parameters. The effective hydrogen traversals will remain about the same. Such an extension is then just a matter of cost.

μ-BEAMS WITH M AND THEIR APPLICATION TO μ-p ELASTIC SCATTERING EXPERIMENTS

by

George Masek

August, 1962

1. Introduction

The high yields of muons calculated by Ballam[1] indicate that "M" might be an excellent machine for high-energy muon experiments. This report looks into the use of these beams in muon elastic scattering and discusses the implications of these experiments for end station design.

The general conclusion of this report regarding μ-p scattering is that the large fluxes available would indeed be useable in practical experiments and that a 5% experiment can probably be done up to $q^2 \approx 200\ f^{-2}$.

2. The Muon Beam and Comparisons with other High-Energy Machines

In most applications, the muon beam will need to be purified of pions. In elastic muon scattering at high muon energies, the competition with pion elastic scattering is possibly* not too severe (see Fig. 3); however, one needs to reduce the total interaction rate to a low enough level so that the triggering electronics, etc., is not saturated. If one assumes that the total inelastic pion yield falls into a forward cone including the scattering detectors, and requires that the detectors see less than one count per pulse (see Section 4), then the ratio of pions to muons in the beam should be less than $\approx 10^{-6}$. This is a pessimistic estimate, and it may be that a considerably higher ratio could be tolerated. [This situation is quite different than that which exists at lower energy muon scattering, where the ratio of elastic pion to elastic muon scattering is quite large (10^4 - 10^5, see Fig. 3), and for this reason one needs to reduce the incident pions to about 10^{-5} to 10^{-6} of the muons.] Thus

---

[1] M Report No. 200, Stanford Linear Accelerator Center, Stanford University, Stanford, California, Summer 1960.

*It should be pointed out that at the time of this report, the three basic cross sections that are needed (elastic and inelastic muon scattering and the pion elastic scattering at high energies and at high momentum transfers) are unknown; although the best estimates of these are used, they may be off by an order of magnitude or more.

there is a need to reduce the pion fluxes produced at the target. At these high energies (10 to 20 Bev), physical separation can best be achieved by the use of absorbers of several m.f.p. for pions. The principal effects of this absorber on the muon beam (aside from reducing the pion flux) will be to reduce and spread the energy, increase the lateral spread, and increase the angular divergence. Figure 1 shows these effects for two absorbing materials, iron and concrete. Concrete appears to be superior to iron in most respects, i.e., for a given pion attenuation, the beam divergence $< \theta >$ and energy loss are considerably smaller, while the lateral spread $< y >$, although slightly larger because of the longer distance involved, is almost the same. These curves were calculated using the approximate multiple-scattering relations given in Rossi (pp. 68-72), and the following values of λ_π (m.f.p. for pion attenuation) were extrapolated from Tinlot's measured values up to 9 Bev.

$$\lambda_\pi(\text{concrete}) \approx 1.85 \text{ ft} \qquad (E_\pi \approx 20 \text{ Bev})$$

$$\lambda_\pi(\text{iron}) \approx 0.85 \text{ ft} \qquad (E_\pi \approx 20 \text{ Bev})$$

In the comparisons which follow, we assume that we use sufficient concrete absorber to give the beams a ratio of $N_\pi/N_\mu \approx 10^{-10}$, even though in making beam estimates for the scattering experiment with M we will use somewhat less.

We now wish to obtain the muon fluxes from M and compare these with other high-energy machines under similar conditions. We first calculate the total yields (Table 1) $\left| dN_\mu/dP \left| \text{Bev/c}^{-1} \text{ sec}^{-1} \right| \right|$ and the yields per unit area $\left| d^2E_\mu/dP_\mu dA \left| \text{Bev/c}^{-1} \text{ sec}^{-1} \text{ cm}^{-2} \right| \right.$ that would be obtained at the end of the absorber mentioned above, but not taking into account the effect of the absorber in spreading the beam. Finally, the effect of the absorber is put in $\left| d^2N_\mu/dP_\mu dA \left| \text{Bev/c}^{-1} \text{ sec}^{-1} \text{ cm}^{-2} \right| \right|$ for concrete. For the M machine, Ballam gives $dN_\mu/dE_\mu d\Omega$ for $\theta \sim \theta_o = \mu/E_\mu$, folded into the bremsstrahlung spectrum for $\frac{1}{2}$ radiation length of Be. The

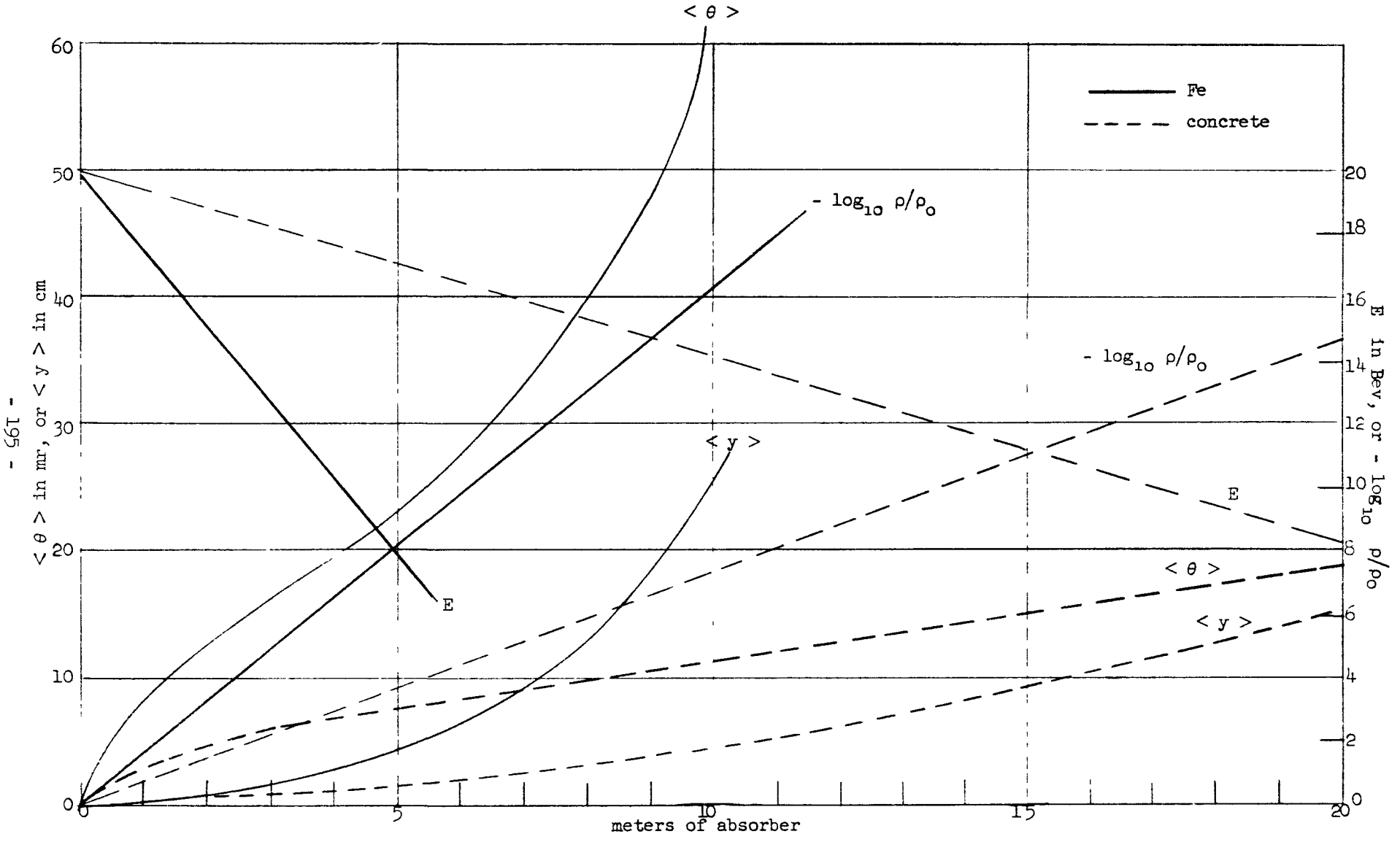

FIG. 1--Absorber properties. The energy E, the rms multiple-scattering angle $< \theta >$, the rms lateral beam spread $< y >$, and the ratio of pions transmitted ρ to those incident ρ_o are shown as a function of absorber thickness for both concrete and iron.

SLAC-5-J
Masek

pair-production cross section can be written in the form

$$\frac{d^2N_\mu}{d\Omega dE_\mu} = \frac{4\sigma_o\left(E_\mu\right)}{\left[1 + \left(\theta/\theta_o\right)^2\right]^2} \tag{1}$$

where

$$\sigma_o\left(E_\mu\right) \equiv \left.\frac{d^2N_\mu}{d\Omega dE_\mu}\right|_{\theta=\theta_o} \tag{2}$$

Then

$$\left.\frac{dN_\mu}{dE_\mu}\right|_{\theta_M} = 8\pi\sigma_o \int_o^{\theta_M} \frac{\theta\, d\theta}{\left[1 + \left(\theta/\theta_o\right)^2\right]^2} = 4\pi\sigma_o \left[\frac{\theta_M^2}{1 + \left(\theta_M\, \theta_o\right)^2}\right] \tag{3}$$

and

$$\left.\frac{dN_\mu}{dE_\mu}\right|_{max} = 4\pi\sigma_o\theta_o^2 \tag{4}$$

The muon fluxes are now calculated using the values of σ_o from the Ballam curves (one could actually gain a factor of about 2 by using more radiation lengths than Ballam has used), and using an average electron beam intensity of 30 μa. Putting these into Eq. (4) gives dN/dP_μ of Table 1. The $d^2N/dP_\mu dA$ (without concrete) is obtained by assuming the beam is spread uniformly over an area $\pi\left(\theta_o \ell\right)^2$ where ℓ = 50 feet. Finally, $d^2N/dP_\mu dA$ after the concrete is calculated assuming the area of beam is spread out additionally by the multiple scattering (see Fig. 1).

TABLE 1

Machine	P_μ Bev/c	$\frac{dN}{dP_\mu}$ Bev/c^{-1} sec^{-1}	$\frac{d^2N}{dP_\mu dA}$ Bev/c^{-1} sec^{-2} cm^{-2}	$\frac{N_\pi}{N_\mu}$	for $\frac{N_\pi}{N_\mu} = 10^{-10}$ equiv. concrete (meters)	$y = y_{ms} + y_{div.}$ (cm)	$\frac{d^2N}{dP_\mu dA}$ Bev/c^{-1} sec^{-1} cm^{-2} after concrete
M†	2	4.6×10^8	2.2×10^4				
	5	2.0×10^8	7.4×10^4				
	10	2.0×10^8	2.7×10^5			9 + 10	1.5×10^4
	15	3.2×10^7	9.4×10^4			7 + 8	8.0×10^3
	20	7.6×10^6	4.0×10^4				
				1	13.5		
AGS*	2	1.2×10^7	2.1×10^3				
	5	1.2×10^6	7.2×10^2			9 + 16	2.8×10^1
	10	5.5×10^4	7.2×10^1			7 + 14	2.1
	15	3.0×10^3	5.6				
				20	15		
ZGS*	2	4.6×10^8	8.4×10^4				
	5	15.0×10^6	9.8×10^3				
	10	11.0×10^4	13.0×10^1				
				20			
Bevatron	2	$.5 \times 10^6$	1.2×10^4	10			

* Assumes 4.75° production angle for π's. If one assumes, instead, 0°, these numbers will be increased by factors of the order of 10.

† These numbers are based on Ballam's report in M-200; they are larger than Tinlot's values by a factor of 2 at 15 Bev.

To obtain the AGS comparison flux, we assume the beam is formed from the pion decays in flight and is contained in a system of quadrupoles. Further, when the beam leaves the last quadrupole, it must travel a distance equivalent to the above absorber (50 ft). We also assume the following:

(i) The pion flux given by Cool et al. (Phys. Rev. Lett. 7, 101) at 4.5° and a proton energy of 30 Bev fits very closely the following relation:*

$$\frac{d^2N_\pi}{d\Omega dP_\pi} = 3.3\, e^{-P_\pi/2.1} \left(\text{Bev/c}^{-1}\ \text{proton}^{-1}\ \text{sr}^{-1}\right) \tag{5}$$

The muon flux is then

$$\frac{d^2N_\mu}{dx dP_\mu} = \int_{P_\mu}^{\alpha P_\mu} \left(\frac{d^2N_\pi}{d\Omega dP_\pi}\right) \Delta\Omega_\pi \frac{e^{-x/\lambda_\pi}}{\lambda_\pi} \frac{dP_\pi}{P_\pi - 1/\alpha P_\pi} \tag{6}$$

where λ_π is the mean pion decay length, $\alpha = 1.85$, and x is the distance along the decay path. This is approximately (when $x \ll \ell_\pi$)

$$\frac{d^2N_\mu}{dx dP_\mu} = (.19) \frac{\Delta\Omega_\pi}{P_\mu} e^{-P_\mu/2.1} \left(\text{Bev/c}^{-1}\ \text{meter}^{-1}\ \text{proton}^{-1}\right) \tag{7}$$

(ii) Set $\Delta\Omega_\pi = 2 \times 10^{-4}$ (from Tinlot), x (pion decay path) = 35 meters, and a loss of 2 in quadrupoles.

---

*A better comparison might be to use 0° production angle, which will soon be available with the external proton beam. This will give factors of about $\times$ 10 over most of the energies considered, and perhaps $\times$ 100 at 15 Bev.

(iii) When the beam leaves the quadrupole system it will have a divergence

$$\theta_{div.} \approx \frac{m_\pi}{m_\mu} \frac{P^*_\mu}{P_\mu} \approx .042/P_\mu$$

where the asterisk denotes the average transverse momentum.

(iv) The proton beam intensity will be 10^{11} per sec.

With these assumptions we obtain

$$\frac{dN_\mu}{dP_\mu} \approx (2 \times 10^7) \frac{e^{-P_\mu/2.1}}{P_\mu} \left(\text{Bev/c}^{-1}\,\text{sec}^{-1}\right) \tag{8}$$

These are the numbers given under the AGS heading in Table 1. The beam spread is obtained from

$$y = \tfrac{1}{2} \text{ quad. aperture} + \theta_{div.}(50 \text{ ft})$$

and the flux/cm^2 is obtained from this.

The ZGS yields are estimated by assuming the following expression for scaling the pion yields:*

$$\frac{d^2N_\pi}{d\Omega dE_\pi} = \frac{n}{d\pi P_o^2 T} E_\pi^2 e^{-E_\pi\left(1/T + \theta/P_o\right)} \equiv N\left(E_p\right) \tag{9}$$

where $n = 1.28\, E_p^{\frac{1}{4}}$, $T = .293\, E_p^{\frac{3}{4}}$, $P_o = 0.18$, E_p is the primary proton energy, and θ is the angle of pion emission.

Assuming we hold θ and E_π the same,

$$\frac{N\left(E_{p1}\right)}{N\left(E_{p2}\right)} = \left(\frac{E_{p1}}{E_{p2}}\right)^{\frac{3}{4}} \exp - \frac{E_\pi}{.293}\left(\frac{1}{E_{p1}^{\frac{3}{4}}} - \frac{1}{E_{p2}^{\frac{3}{4}}}\right) \tag{10}$$

*See Masek, UCID-1440.

Using this to scale from Cool et al. $\left(E_{p1} = 30 \text{ Bev}\right)$ to the ZGS $\left(E_{p2} = 12.5 \text{ Bev}\right)$, we obtain

$$\frac{d^2N_\pi}{d\Omega dP_\pi} = 6.5\, e^{-P_\pi/1.4} \left(\text{Bev/c}^{-1}\ \text{sr}^{-1}\ \text{proton}^{-1}\right) \tag{11}$$

and for the μ's derived from this beam by decay in flight,

$$\frac{dN_\mu}{dP_\mu} = 0.21\, \frac{\Delta\Omega_\pi}{P_\mu}\, \frac{e^{-P_\mu/1.4}}{P_\mu} \left(\text{Bev/c}^{-1}\ \text{proton}^{-1}\right) \tag{12}$$

We now make the same assumptions that we made for the AGS, except that we put the proton flux at 2×10^{12} sec^{-1}, then:

$$\frac{dN_\mu}{dP_\mu} = 15 \times 10^8\, \frac{e^{-P_\mu/1.4}}{P_\mu} \left(\text{Bev/c}^{-1}\ \text{sec}^{-1}\right) \tag{13}$$

This is shown in Table 1 under ZGS.

The Bevatron heading of Table 1 gives the estimate to be expected after the Bevatron conversion. The estimate is made by increasing the muon beam recently obtained there by a factor of 50.

Table 1 also gives the ratio of π's to μ's in the beam before the concrete, and hence indicates what initial pion beam intensity must be assumed for calculating the attenuation needed. The equivalent concrete is then the amount of concrete needed to give $N_\pi/N_\mu = 10^{10}$ after the absorber. Finally, the mean beam spread and the flux per unit area are given after the concrete. The ZGS and Bevatron numbers are not given; the ZGS would scale like the AGS and the Bevatron beam does not use concrete to separate its pions.

The following are the more important conclusions from Table 1.

(i) At low energies (2-5 Bev) the yields from M are comparable to other machines.

(ii) At very high energies (15-20 Bev) the M muon yields are about 10^3 to 10^4 times higher than the other machines.

(iii) The concrete absorber used to filter the pions (to obtain $N_\pi/N_\mu \approx 10^{-10}$) reduces the flux per unit area by a factor of 4 to 10.

The question of whether or not these large muon fluxes can be used in a practical experiment must now be answered.

3. Kinematics and Discussion of Background Cross Sections

Before attempting a specific design for a μ-P experiment, we will need some information concerning the kinematics of the process and a discussion of some of the possible background cross sections. Figure 2 shows the muon scattering angle and the proton recoil angle as a function of momentum transfer. A complete program of muon scattering would attempt to measure the cross sections for various momentum transfers and various muon energies and would thus require measurements over wide ranges of muon and proton recoil angles. This report looks at only one such measurement (E_μ = 10 Bev, q = 2.9 Bev/c, $\theta_\mu = \theta_p = 22^\circ$). This is probably not the most difficult measurement in such a program; however, it looks at a very high momentum transfer, and many of the problems are probably representative of those that would be encountered in other measurements. It might be a good first experiment in such a program.

We first look at the question of defining elastic scattering, i.e., separating the elastic muon scattering from kinematically similar inelastic processes, in particular

$$\mu^\pm + p \rightarrow \mu^\pm + n + \pi^+ \qquad (14)$$

When the pion from this reaction is produced in the same direction and with the same velocity as the recoil nucleon, the outgoing muon's energy will be maximum and hence closest to the elastic scattering energy with the same scattering angle. We can write the elastic scattering outgoing energy E_2 in terms of the incident energy E_1 and the scattering

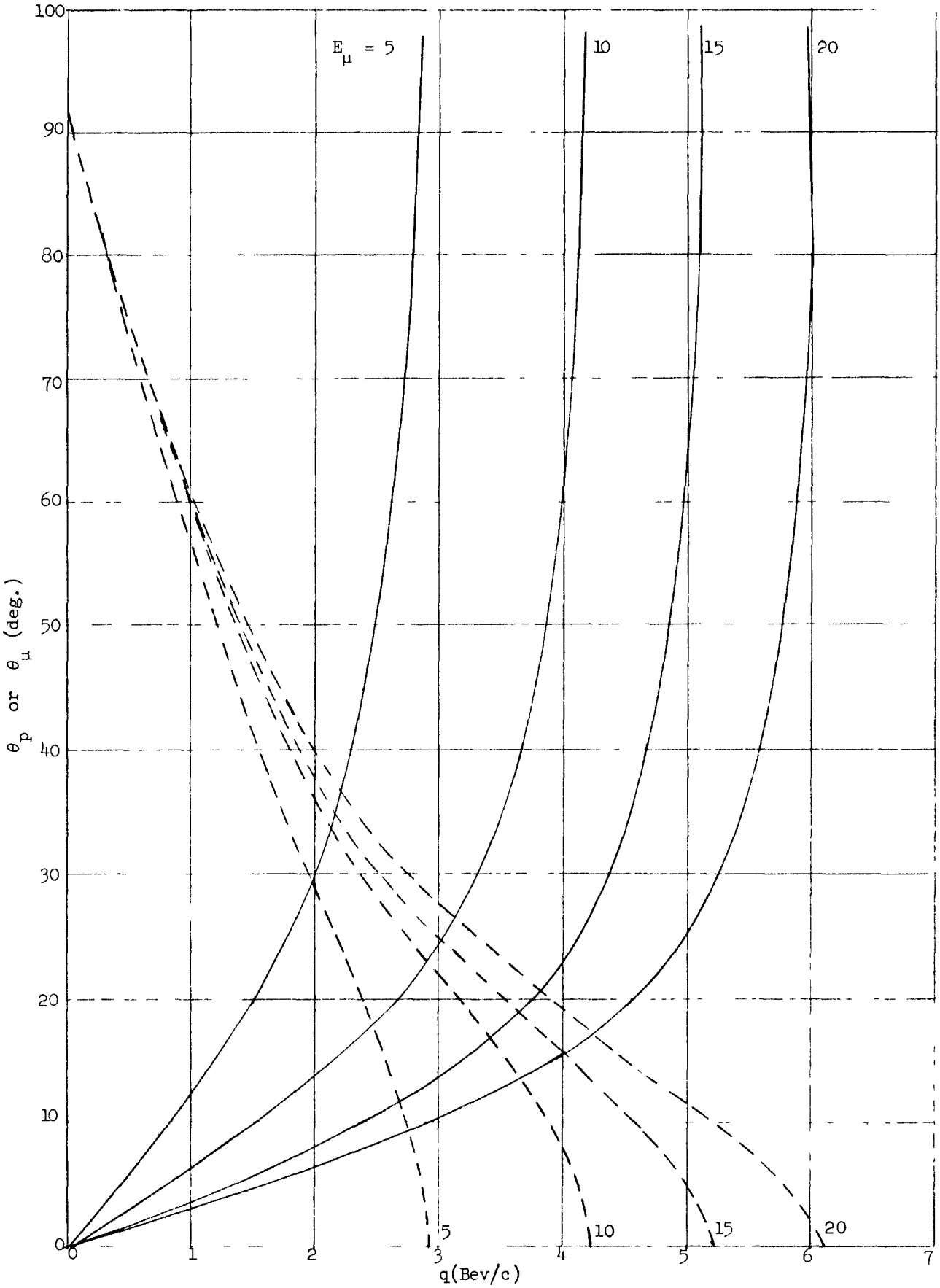

FIG. 2--μ-p kinematics. The muon scattering angle θ_μ and proton recoil angle θ_p are given as a function of the momentum transfer q.

angle θ_μ,

$$E_2 = \frac{\mu^2 + ME_1}{E_1\left(1 - \beta_1 \beta_2 \cos\theta_\mu\right) + M} \tag{15}$$

Here and subsequently the subscripts 1, 2, 3 denote the incident muon, the scattered muon, and the recoil proton; E, P, and β refer to the energy momentum, and velocity (in units of the velocity of light). The difference between (15) and the inelastic case with maximum energy (assuming $\beta_1 \approx \beta_2 \approx 1$ and neglecting π^2 and μ^2 with respect to $2\pi M$) is

$$\Delta E \approx \frac{\pi M}{E_1 (1 - \cos\theta) + M} \tag{16}$$

and

$$\frac{\Delta E}{E_2} \approx \frac{\pi}{E_1} \tag{17}$$

For $E_1 = 10$ Bev this gives $\Delta E/E_2 \approx 1.4 \times 10^{-2}$, and this sets the order of magnitude of the resolution necessary to separate elastic from inelastic μ's. Next we need to inquire into how accurately the other kinematical parameters need be determined. We may use as the variables P_1, P_2, and P_3 (the recoil proton momentum), and θ_μ, and θ_p (the opening angle $\theta_p + \theta_\mu$ may also be used, but it is particularly insensitive in the regions discussed here). Energy and momentum conservation give 3 equations for these 5 variables, hence specification of any two determines the others and defines the elastic scattering. However, to separate the 3-body inelastic process requires another parameter (three altogether) and we must inquire into the accuracy needed on these three parameters. We assume that one parameter is always P_2 and that we can specify it to the accuracy given by Eq. (17) above. We compute the relevant partials from the elastic kinematics which are evaluated for the experimental

conditions stated above. The differential values of the respective variables are also given for the condition $\Delta E_2/E_2 = 1.4 \times 10^{-2}$.

$$\left.\frac{1}{E_2}\frac{\partial E_2}{\partial \theta_\mu}\right|_{E_1} = \frac{-E_1 \sin\theta_\mu}{E_1(1-\cos\theta_\mu)+M} = 2.55 \quad \left(\Delta\theta_\mu \approx 0.55\right) \tag{18}$$

$$\left.\frac{1}{E_2}\frac{\partial E_2}{\partial \theta_p}\right|_{E_1} = \frac{M \cot\theta_p}{E_1\left(\sin^2\theta_p + 2M/E_1\right)} = 2.90 \quad \left(\Delta\theta_p \approx 0.48 \times 10^{-2}\right) \tag{19}$$

$$\left.\frac{E_1}{E_2}\frac{\partial E_2}{\partial E_1}\right|_{\theta_\mu} = \frac{M}{E_1\left(1-\cos\theta_\mu\right)+M} = 0.65 \quad \left(\Delta E_1/E_1 \approx 2.2 \times 10^{-2}\right) \tag{20}$$

$$\left.\frac{P_2}{P_3}\frac{\partial P_2}{\partial P_3}\right|_{E_1} = \beta_3\left(\frac{P_2}{P_3}\right) = 0.99 \quad \left(\Delta P_3/P_3 \approx 4 \times 10^{-2}\right) \tag{21}$$

(In all of the foregoing we have assumed that $P_1 \approx E_1$, $P_2 \approx E_2$, and $\theta \gg 1/\gamma_1$. Hence, for example, if we fix θ_μ to 5 mr, the incoming energy to 2%, and the outgoing muon energy to 1.5%, we can distinguish elastic from inelastic purely kinematically.

Next, let us see if it is necessary to define the kinematics this accurately, i.e., we look at the cross section for the inelastic process for those cases where the kinematics are similar to those of the elastic scattering. Chilton (private communication) has calculated the following inelastic cross sections for muons on protons:

(22)

$$\frac{d^2\sigma}{d\Omega_2 dE_2} = \frac{\alpha}{4\pi^2}\,\frac{E_1 - E_2}{E_1^2\left(1 - \beta_1\beta_2\cos\theta\right)}\,\sigma_\gamma\left(E_1 - E_2\right)\,F_{in.}^2(q) \equiv \frac{\sigma_i}{\Delta E_2}$$

This is essentially a Weizsacker-Williams approximation and holds for small q^2 and large energy loss. However, it still gives the correct order of magnitude in the regions of the proposed experiment. Here $\sigma_\gamma\left(E_1 - E_2\right)$ will be taken as the total photo-pion cross section and will be approximated as 2×10^{-28} cm^2. $F^2_{in.}(q)$ will be assumed equal to $F^2_{el}(q)$, when one demands that the proton carry away almost all of the momentum transferred (this will be fixed by the experiment). Then the ratio of the elastic (σ_e) to the inelastic (σ_i) can be written:

$$\frac{\sigma_e}{\sigma_i} \approx \left(4.4 \times 10^{-28}\left[\text{Bev-cm}^2\right]\right) \frac{E_1}{\left(E_1 - E_2\right)^2} \frac{1}{\sigma_\gamma(\Omega)} \left(\frac{\Delta E_2}{E_2}\right)^{-1} \qquad (23)$$

Putting in the above experimental conditions and requiring that $\sigma_e/\sigma_i \approx 10$,

$$\Delta E_2 / E_2 \approx 0.11$$

which is considerably larger than the kinematical limits. This estimate should, of course, not be taken too seriously, since neither σ_γ (which is really a function of q also) and $F^2_{in.}(q)$ are known. Also, if resonances occurred in σ_γ they might give trouble. If one were aware of the resonances, it might be possible to design the experiment to avoid them. However, this does show that the inelastic scattering does not seem to present a large experimental problem, and that it may be possible to relax the requirements set by the purely kinematic limits.

We now look at the question of pion contamination in the muon beam. As stated earlier, we have assumed that large absorbers are placed in the beam; the question now arises as to how much absorption is necessary to prevent elastic pion scattering from dominating the experiment. We reproduce in Fig. 3 the recent results of Perl et al. on elastic pion scattering at high energies (up to 5 Bev), and high q(up to 2 Bev/c). In addition we show recent p-p cross sections and the elastic μ-p cross sections for comparison. The μ-p cross sections are taken from the

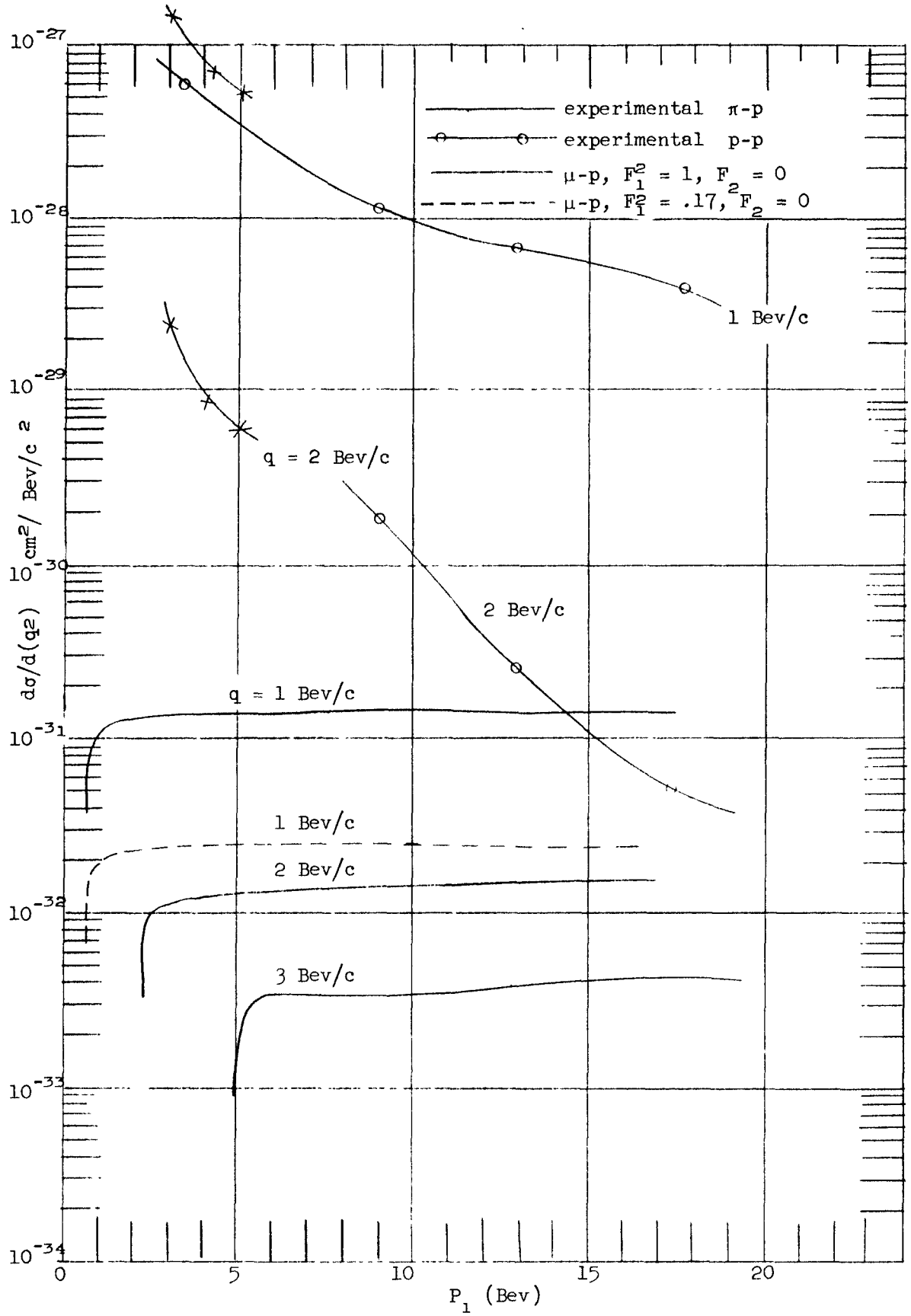

FIG. 3--Comparison of elastic scattering cross section. Experimental π-p, and p-p cross sections and theoretical μ-p cross sections are shown as a function of incident particle momentum for various momentum transfers q.

approximate relation

$$\frac{d\sigma}{d(q^2)} = \frac{4\pi^2 r_o^2 m_e^2}{q^4}\left(\frac{E_2}{E_1}\right)\left[1 + \frac{E_2}{E_1}\left(\frac{E_1}{E_2} - 1\right)^2\right] F_1^2(q^2) \qquad (24)$$

where r_o is the classical electron radius, m_e is the electron mass, and where we have set $F_2 = 0$. The above is insensitive to E_1 and depends primarily on q^2. The qualitative behavior of the cross sections is that π-p and p-p drop rapidly with increasing energy while the μ-p cross section stays up. Hence, for example, at 15 Bev and $q = 3$ Bev/c it may be that $\sigma_{\pi\text{-}p}/\sigma_{\mu\text{-}p} \approx 1$ with $F_1 = 1$ and $F_2 = 0$. Thus even if the form factor reduces the cross section by 10^{-3}, the elastic-scattered pions do not represent a difficult problem since attenuation of 10^3 or 10^4 are quite easy. However, as mentioned in Section 1, greater attenuation than this will be needed to reduce the total interaction rate due to pion inelastic processes.

4. Design of the Experiment

The following observations govern the design of the experiment:

(1) The large muon flux and short machine duty cycle (giving of the order of 10^5 muons per μsec) make it impossible to examine the incident beam with any type of counter or visual techniques.

(2) The usual experimental technique used in electron scattering (which also can never "look" at the incident beam but in which this beam is precisely defined physically) cannot be employed here without prohibitive loss in yield. This is because the muon beam is not defined well physically (its cross section, divergence, and energy are all poorly defined in comparison to the electron beam), and also because one would like to take advantage of large targets, which one cannot do with electrons because of the radiative effects.

(3) The requirements on the accuracy of measurement of momenta and angles, although probably not as severe as the kinematic limit, are still formidable and would probably rule out most forms of hodoscopes.

(4) Because the muons do not interact strongly (and we assume that sufficient pion attenuation has been used so that there are very few pion interactions), we assume coincidence-counter techniques can be employed. (This point is discussed in somewhat greater detail later.) Once again, this cannot always be done with electron beams because of the large number of secondaries created by the photoproduction processes (also because the beam intensities are larger by 10^4 to 10^5).

We now look into the possibility of using spark chambers in conjunction with wide-aperture magnets, which appear to accommodate the aforementioned observations. They allow one to observe large targets and still give excellent resolution. The principal difficulty will involve reducing the background tracks in the spark chambers to several per picture. The machine's short duty cycle combined with the spark chamber's long resolving time (about 0.2 μsec at best) makes this a difficult problem, but as we will see later it appears to be soluble with these weakly interacting beams.

We will choose as our principal kinematical observables the three momenta P_1, P_2 and P_3, and although θ_μ and θ_p will also be measured, their accuracy will be limited because we will choose to make the cross section of the beam and target as large as possible. (As mentioned before, the opening angle is very insensitive to the scattering process.) Hence, we will physically define the muon beam by a system of magnetic slits, bending magnets, and quadrupoles* (see Fig. 4). The muons will then be directed into a large (6 ft long, 10 inch diameter) liquid hydrogen target. The scattered muons and recoil protons will first pass through lead absorbers, followed by small clearing magnets (see Fig. 5). This is to elimate knock-on electrons and protons originating from the target. Then the scattering products pass through a system of counter-triggered spark chambers and bending magnets which will measure their momenta.

The Beam

We will analyze a beam formed in the manner shown in Fig. 4. The flux from the target is momentum analyzed and focused into the "absorber channel" by Q_{1A} - M_1 - Q_{1B}. The channel allows physical separation

*The physical definition is not only needed to define the incident momentum P_1 but also to keep muons that are not directed at the target out of the spark chambers.

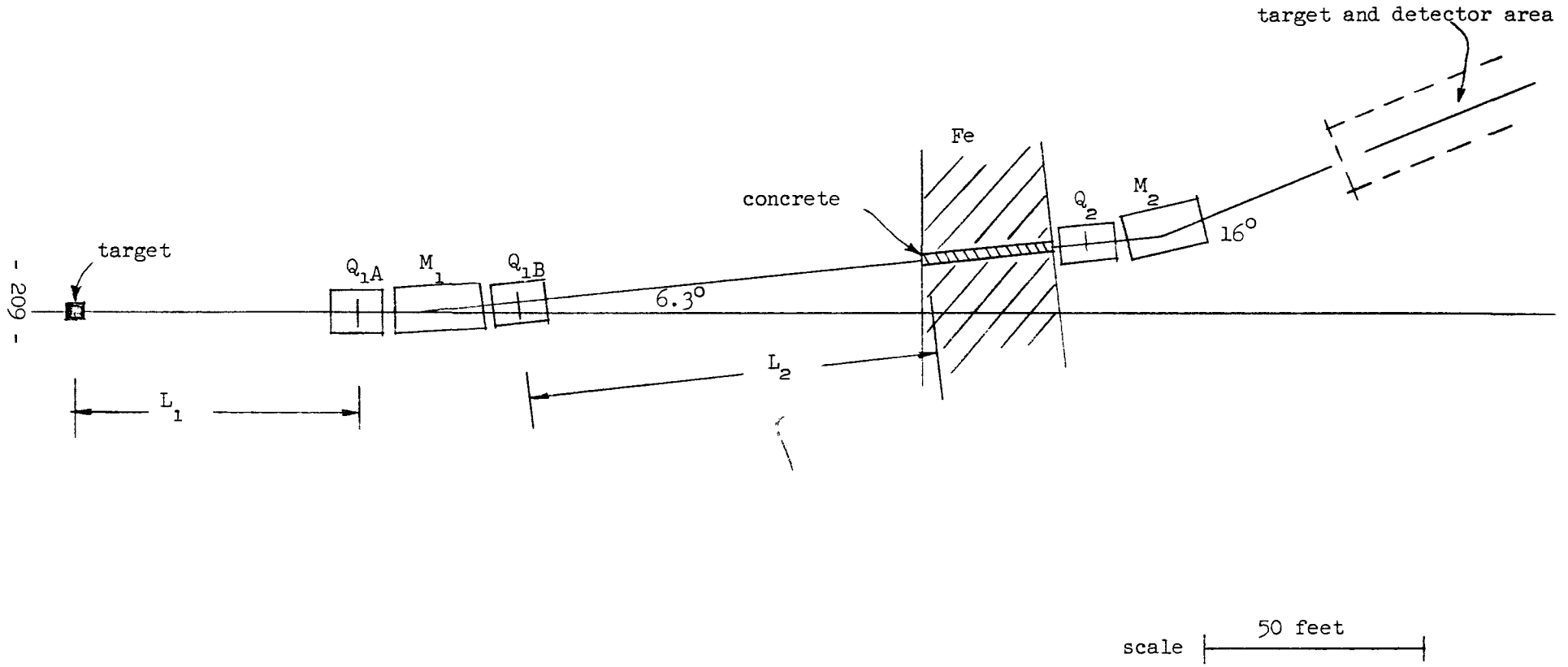

FIG. 4--Beam layout for proposed μ beam.

SLAC-5-J
Masek

of those muons which will form the beam from those outside the channel which will be totally absorbed. M_2 and Q_2 momentum-analyze the beam again and direct it onto the scattering target. The concrete absorber after the channel is 9.1 meters, which should give a pion attenuation of $\approx 10^7$, and the energy loss will be ≈ 5 Bev (also, $< y >_{ms} \approx 7$ cm, $< \theta >_{ms} \approx 15$ mr, and $\theta_o \approx 7$ mr). We first set

$$\frac{a_1}{2L_1} = \frac{\mu}{E_\mu} \tag{25}$$

where a_1 is the effective aperture of Q_1, and L_1 is the distance from the target to Q_1. This will accept 50% of the μ's of energy E_μ produced at the target. We will allow some magnification in the system for we will not lose appreciable intensity as long as the image at the absorber channel is small compared to $2 < y >_{ms}$. Thus if the initial electron beam size $\approx \frac{1}{2}$ cm and we make $L_2 = 2L_1$, then the image will be ≈ 1 cm, which is to be compared with 14 cm for $2 < y >_{ms}$. Treating Q_1 as a thin lens, and choosing a focal length of 40 feet, we then get $L_1 = 60$ feet, $L_2 = 120$ feet, and $a = 10$ inches. The angle of bend will be determined from

$$\delta = L_2 \theta (\Delta p/p) \tag{26}$$

where δ is the spatial spread for a momentum spread Δp at a distance L_2 from M_1. If one requires that $\delta \approx 2 \times$ image size (to obtain momentum separation) and $\Delta p/p \approx .05$, then $\theta = 6.3^\circ$. This quadruple-magnet system is somewhat smaller than that described by Penner in M-200-10. If $dB/dR \approx 3 \times 10^3$ gauss/inch, then the quadruples would be about 12 feet long. The magnet would have a 10-inch gap and would be ≈ 20 feet long. A rough estimate of the cost of Q_1 and M_1 would be \$175,000.

The $M_2 - Q_2$ system is needed to reject those muons of the wrong momenta which have scattered into the absorber channel. The number of muons

accepted by Q_2 will be

$$N_\mu\Big|_{E_\mu=10\ \text{Bev}} \approx \frac{1}{2}\,\frac{\left|a_2/2\right|^2}{\langle y\rangle^2}\,\left|\Delta p\right|\frac{dN}{dP_\mu}\Big|_{E_\mu=15\ \text{Bev}} \tag{27}$$

where $\Delta p = (.05)(15) = .75$ Bev; a_2 is the aperture of Q_2 which we will take to be 0.8 inches; $\langle y\rangle \approx \mu\ell/2E_\mu + \langle y\rangle_{ms} \approx 10$ cm [ℓ is the thickness of the absorber, and the $\frac{1}{2}$ appears because $L_2 = 2L_1$]; and $dN/P_\mu|E_\mu = 15$ Bev is taken from Table 1. The $\frac{1}{2}$ appears because of the loss in Q_1 - M_1 system. Then at Q_2

$$N_\mu\Big|_{E_\mu=10\ \text{Bev}} = 3.2 \times 10^7\ (.75)(.5) = 1.2 \times 10^7\ \text{sec}^{-1} \tag{28}$$

since $\langle\theta\rangle_{ms}$ is somewhat larger than the natural beam divergence from the target. We will assume that the muons incident on Q_2 are spread uniformly over the aperture of Q_2, and have a uniform distribution in angles up to $\langle\theta\rangle_{ms}$. Then we may say the beam will be smallest at a distance from Q_2 equal to the focal length of Q_2, and will have a radius $\approx \langle\theta\rangle_{ms} F$, where F is the focal length of Q_2. If we choose F to be 30 feet, then $\langle\theta\rangle_{ms} F \approx 5.5$ inches, and thus a 10-inch-diameter liquid hydrogen target will contain about 70% of the beam. In addition, there will be a loss of about a factor of two due to the dispersion introduced by M_2. The bend at M_2 will need to be about 16°, using the requirement of Eq. (26). We then get for the muons on the target

$$N_\mu\Big|^{\text{Target}}_{E_\mu=10\ \text{Bev}} = 1.2 \times 10^7\ (.7)(.5) = 4.2 \times 10^6\ \text{sec}^{-1} \tag{29}$$

and for a 6-foot liquid hydrogen target we get

$$N_\mu N_\rho = 4.2 \times 10^6 (12.7) = 5.3 \times 10^7 \text{ gm cm}^{-2} \text{ sec}^{-1} \qquad (30)$$

The total cost of the magnets and quadrupoles (including the detectors) is estimated to be about $400,000.

Scattering Detector

The scattering detector consists of two spectrometers, each being a bending magnet with associated spark chambers which measure the incident and outgoing trajectories of the particles passing through the magnets (see Fig. 5). We wish to optimize the solid angle accepted by these magnets for a given momentum resolution $\delta P_\mu / P_\mu$, maximum average field $\bar{B}$, a minimum spark chamber track width dx, and magnetic field volume V_m. (We assume that the cost of such a magnet would be proportional to the volume of magnetic field. This certainly oversimplifies the problem, since the cost of a magnet depends upon the ratio of width to height as well, and in fact the power supply for the magnet may be the determining factor.) If ℓ_m is the length of the magnet and ℓ_c is the distance between spark chambers, then the solid angle accepted by the magnet from the first spark chamber can be written

$$\Delta\Omega \approx \frac{\ell_c^3 V_m \alpha}{\left(\ell_c^2 + d\ell_c + \frac{1}{2\alpha}\right)^2} \qquad (31)$$

where d is the distance from the target to the first spark chamber, and

$$\alpha = \frac{\bar{B}\, \delta P_\mu / P_\mu}{4\, dx\, (B\rho)} \qquad (32)$$

Optimizing $\Delta\Omega$ with respect to ℓ_c gives

$$\ell_c = d/2 + \sqrt{d^2/4 + 3/2\, \alpha} \qquad (33)$$

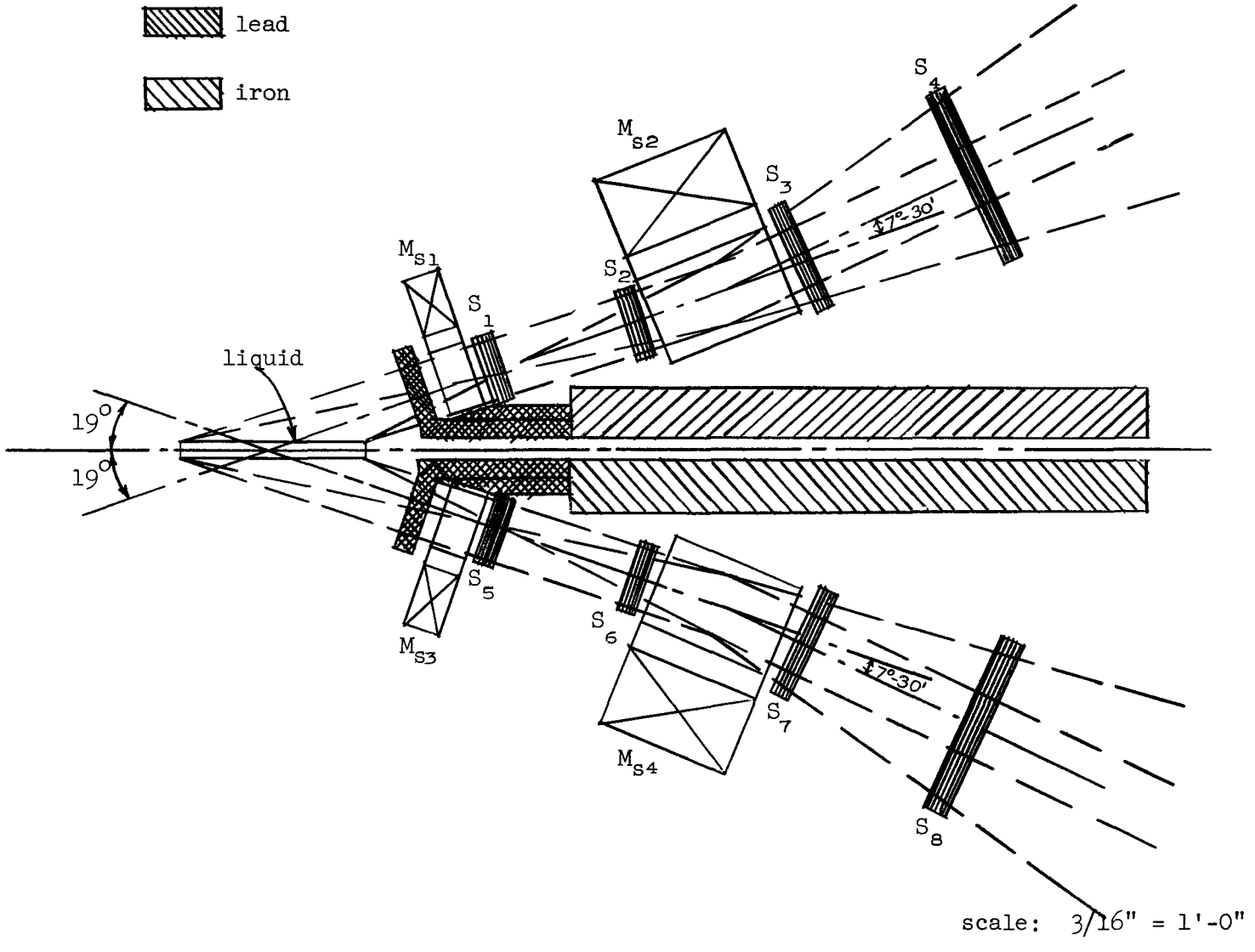

FIG. 5--Experimental layout for proposed μ-p scattering detector. This is an elevation view. The magnets M_{S2} and M_{S4} would actually be rotated 90% about their beam lines to reduce the acceptance angles θ_μ and θ_p.

SIAC-5-J
Masek

and

$$\ell_m = \left(\ell_c \alpha\right)^{-1} \tag{34}$$

Taking $dx = .04$ in., $\delta P_\mu / P_\mu = .03$, $P_\mu = 8.1$ Bev/c (scattered momentum, P_2), $\bar{B} = 20$ kg, and $d = 30$ in., we get $\alpha = .36 \times 10^{-3}$ in.$^{-2}$, $\ell_c \approx 80$ in., and $\ell_m \approx 40$ in. These are the dimensions of the detector which appear in Fig. 5, except that clearances have been added to separate the spark chambers from the magnets. If one assumes a magnet aperture of 12×24 inches, Eq. (27) gives a solid angle acceptance of $\Delta\Omega \approx 2.8 \times 10^{-2}$ sr. The yield for the experiment is then computed from

$$Y = \left(\frac{d\sigma}{d\Omega}\right) \Delta\Omega \, N_\mu N_p \, (3600) \text{ hr}^{-1} \tag{35}$$

The yield is given in the following table for $d\sigma/d\Omega$ given in Fig. 6 and with two sets of form factors, $F_1 = F_2 = 1$ and $F_1^2 = 10^{-3}$, $F_2 = 0$, which represents the best guess from present experimental extrapolations. Also given are yields expected for $E_\mu = 5$ Bev, and $q = 1.1$ Bev/c $\left[\theta_\mu = 13.8^\circ, \theta_p = 52^\circ\right]$. This is the region of q now being explored by electron scattering.

E_μ (Bev)	θ_μ	q^2	Yield (point charge)	Best F_1^2	Yield with best F_1^2 ($F_2 = 0$)
5	13.8°	30 f^{-2}	1.7×10^4 per hour	.16	2.7×10^3 per hour
10	22°	220 f^{-2}	6.5×10^2 per hour	10^{-3}	6.5×10^{-1} per hour

The 5-Bev experiment is a little different from the 10 Bev (e.g., a shorter target would have to be used to allow detection of θ_p, and appropriate

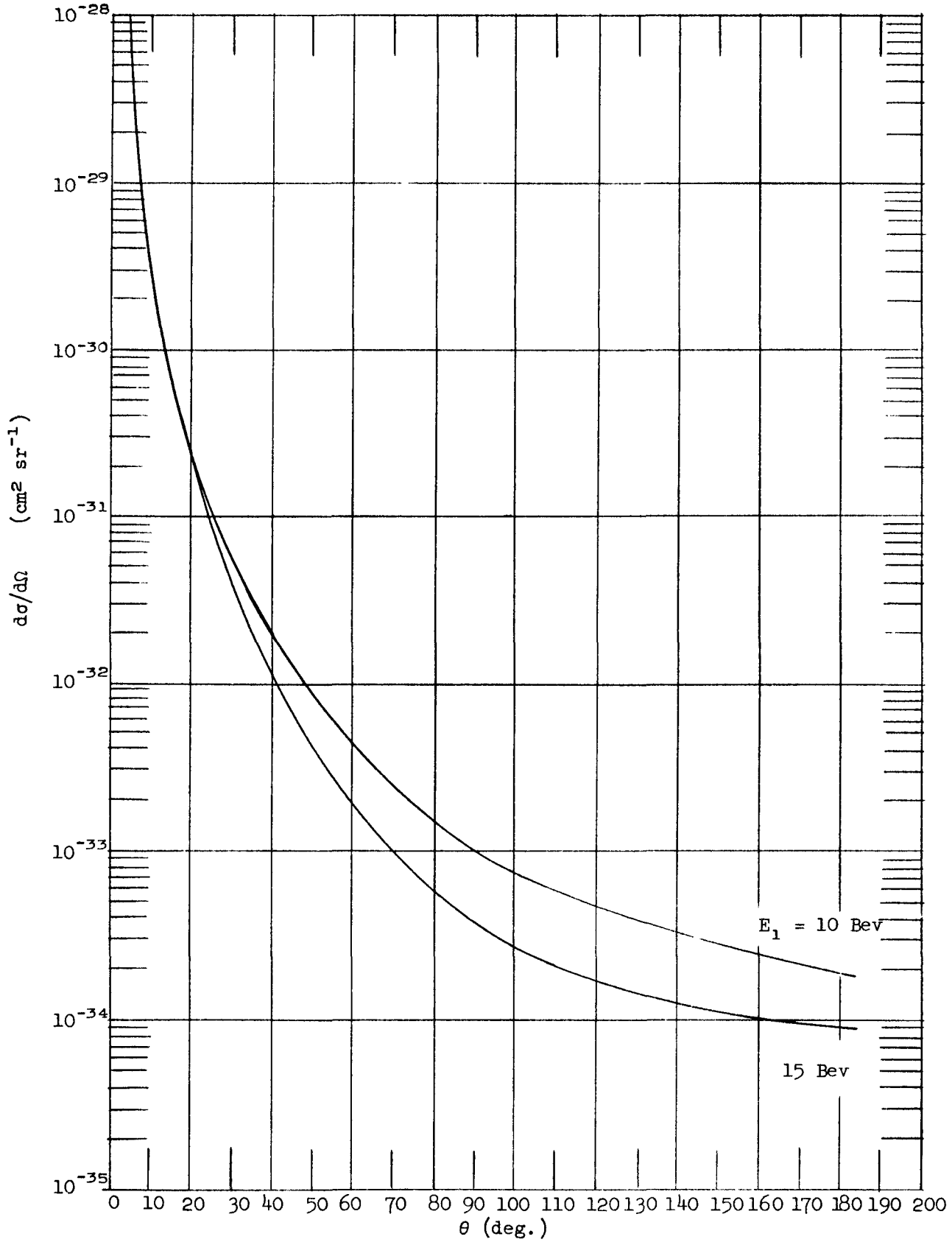

FIG. 6--μ-p elastic scattering cross sections without form factors (i.e., for point charge).

changes have been made in the table. The dq/q accepted in both cases (5 and 10 Bev) is about 15%, where the detector magnets are assumed to be aligned so that the 12-inch dimension defines θ_2, the angle of the scattered muon. Thus, it appears that a 5% experiment could probably be done up to $q^2 \approx 200\ f^{-2}$ (assuming the form factor is not much smaller than .03); the yield in the region around $q^2 \approx 25\ f^{-2}$ seems sufficient to allow fairly accurate comparison experiments with the electron scattering.

Knock-on Electrons

One possible source of background trouble might be knock-on electrons. In the design we have attempted to eliminate any unwanted muons from the target region; in fact, to further facilitate this it would seem advisable that the M_{s1}, M_{s2}, M_{s3} and M_{s4} be located in the vertical plane, as shown in Figs. 4 and 5. However, we still have $\approx 10^7$ muons per second or $\approx 3 \times 10^4$ per μsec passing into the target. For the conditions considered in this experiment the knock-on probability can be written as

$$\Phi_{coll.}\ dx\ d\Omega \approx \frac{0.3\ Z}{A}\ \frac{\sin^2\theta}{2M}\ d\Omega\ dx \qquad (36)$$

which at 19° and in 14 g/cm² of liquid hydrogen gives

$$\Phi_{coll.}\ d\Omega = .05\ d\Omega \qquad (37)$$

Also, the energy of the knock-on is related to its angle by

$$E_{elec} \approx 2\ m_e\ \cot^2\theta_e$$

which for 19° gives

$$E_{elec} \approx 8\ \text{Mev}$$

The first such chamber subtends a solid angle of approximately 0.1 sr,

and might have a resolving time of 0.2 μsec. Therefore,

$$N_{elec} = (0.1)(.05)(3 \times 10^4)(0.2) = 3 \times 10^1 \quad \text{per } 0.2 \ \mu\text{sec.} \qquad (38)$$

Thus, in order to resolve the muon and proton tracks in the spark chambers, the magnets M_{s1} and M_{s3} have been placed in front of the first spark chambers to sweep these electrons out. In addition, γ-rays originating from knock-ons in the target might also give pairs in the spark chambers. Thus 25 radiation lengths of lead have been placed in front of these first magnets, which would make the effects of 10 - 50 Mev γ's negligible. This precaution might not be necessary since the target is only 0.25 radiation lengths; however, there may be many electrons and γ's accompanying the beam from M_2 and Q_2.

5. End Station Considerations and Compatibility with Neutrino Experiments

It would be extremely desirable to be able to conduct such muon experiments simultaneously with neutrino experiments. The above experiment was a general design, and we did not attempt to fit it into any particular proposed experimental end station. In this section we attempt to modify the experiment to see if the proposed neutrino experiments and the above muon experiments could be carried out in the "straight-ahead end station" of the M machine, and hence what recommendation can be made regarding this area.

If running time were assigned to muon experiments and neutrino experiments on the basis of expected yields and current interest, it might be expected that neutrino experiments would have 5 to 10 times the running time. Therefore, any system which allows the two to run compatibly may involve a decrease in muon flux of the order of 5 to 10. On the other hand, the muon experiment must not greatly interfer with the neutrino experiments, e.g., we will assume that no more than a 10% loss in neutrino flux is permitted.

In order to establish some method of comparison, we need a sample neutrino experiment. There have been no specific designs so we will use

a combination of Panofsky's calculations in M-200-17 and the current experiment at the AGS. Some pertinent parameters of the AGS experiment are:

Total shielding system: 22 feet of Fe plus 14 feet of concrete
Side shielding: $\approx 1/3$ of upstream
Decay path: $\approx$ 120 feet
Detector area: 8×8 feet

Panofsky gives an absorber thickness for M of $\approx$ 15 m, and also a decay length of $\approx$ 15 m. Since the mean neutrino angle is m_π/P_π, and we may assume a detector somewhat in excess of (15 m) m_π/P_π, where P_π is a yield-weighted average momentum, we will assume a decay path of about 30 m (similar to AGS) and a detector of about twice the area of AGS, 12×12 ft. We also assume that we will need about 7 ft of side shielding from the muon beam. In order that the muon beam clear this lateral distance at the neutrino detector, it will need to be deflected about 15° (see Fig. 7). After deflection, the muon beam will pass through 5 meters of Fe (see Fig. 1), and then up a diverging channel in iron. This channel would be about 3-in. diameter at the upstream end, and would diverge with a few times the mean muon beam divergence [which for 15 Bev muons after 5 meters of iron is $\approx$ 20 mr (see Fig. 1)]. The primary question is whether such a channel would introduce objectional background in the neutrino area. From Fig. 7, the end of the muon channel is about the same distance from the electron beam line as the edge of the neutrino detector; therefore, for muons to enter the neutrino detector they must lose negligible energy and scatter through 15°. For 15-Bev muons elastic scattering at 15°, the outgoing muon has lost 1/3 of its energy. It would, therefore, have to travel approximately 1/3 the absorber thickness up the muon "open" channel. This is clearly impossible if it is to get into the neutrino area. Further, one can estimate how much available path length x in iron must be presented to the muon beam in order that we get 1 muon per square foot per pulse in the neutrino detector. For this we use the fluxes in Table 1 and the elastic-scattering cross section with a form factor of about 10^{-1}. We also assume that the momentum bite available is determined by the

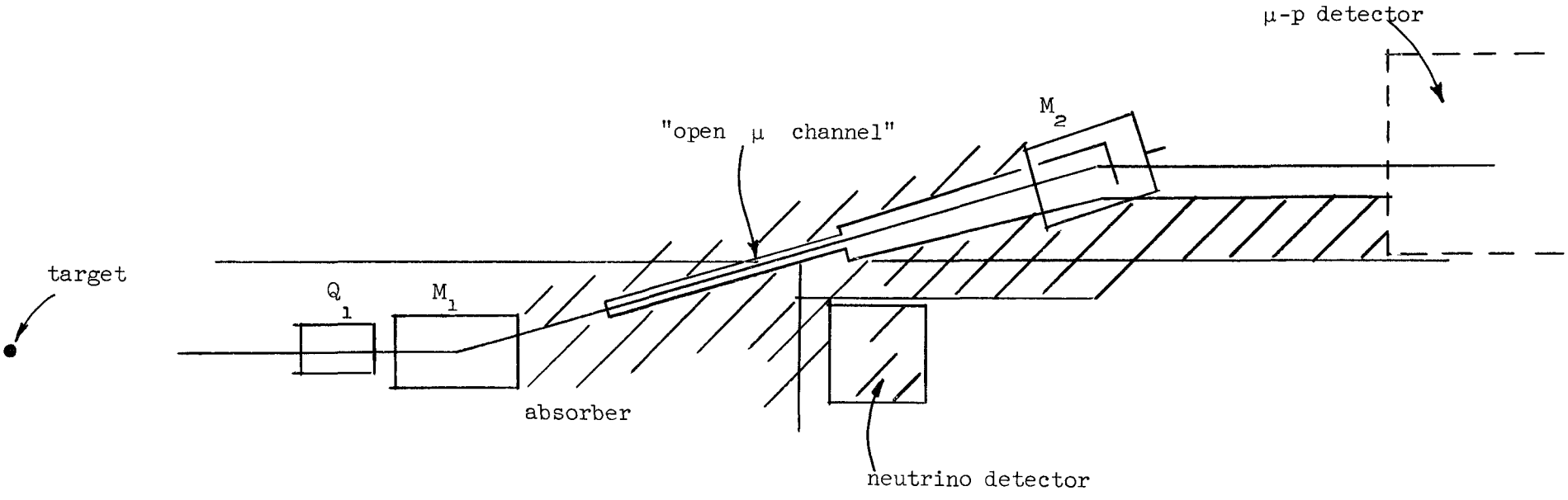

FIG. 7--Possible orientation of neutrino experiment and μ-p experiment so that both could be run simultaneously.

SLAC-5-J
Masek

aperture of the muon channel. Then we get $\times 10^4$ cm. Thus, even if the muons could get through the iron (which appears unlikely), the numbers that could get there would be negligible. These are certainly rather crude order-of-magnitude estimates; e.g., we have not looked at inelastic processes and one should analyze such an "open channel" in greater detail. However, before such analysis is done, more definite neutrino plans must be made.

The question of the neutrino flux reduction is answered by how much space is needed for the 15° bending magnet in front of the shielding. For 15 Bev/c and a field of 20 kg, it takes a magnet length of about 20 ft. Our assumed decay path was about 120 feet; therefore, assuming the yield is proportional to the decay path, we would lose about 20% of the neutrino flux. Once again, this must wait on more detailed estimates of the neutrino experiment. The muon flux reduction (compared to the experiment described by Fig. 4), is principally due to the changes in optics, and introduces loss in intensity of about a factor of 4.

6. Conclusions

It appears possible to design a muon beam which would yield usable fluxes of $\approx 5 \times 10^6$ muons/sec, with a $\Delta p/p \approx .05$, and spread over an area of ≈ 500 cm^2. Such a beam could be used to give an interaction rate of $\approx 5 \times 10^7$ gm/sec for a 6-foot liquid hydrogen target, and by employing spark-chamber magnet spectrometers to measure the momenta of the scattered muon and recoil proton it appears possible to measure the elastic μ-p cross section to 5% at $q^2 \approx 200$ f^{-2}. Further, μ-p experiments to compare with present electron-scattering experiments at $q^2 \approx 30$ f^{-2} appear to be possible with quite high precision. Such experiments could be compatible (i.e., run simultaneously) with neutrino experiments with negligible loss in neutrino flux, but with perhaps a loss of a factor of 4 in muon flux. The latter must wait until more definite designs of neutrino experiments are proposed.

The principal conclusions regarding end station design are: (1) If neutrino experiments are done in the straight-ahead section, and muons are to be run simultaneously, it will be necessary to provide room on either side of the neutrino experiment (see Fig. 7). (2) Since this

is extremely early to make detailed experimental designs, the most expedient course would be to leave the straight-ahead area open for future development and planning but provide enough space to accommodate such experiments (i.e., 50 feet to either side of the straight-ahead beam line, and 200 feet beyond the neutrino absorber).

MASS ANALYSIS AT HIGH ENERGY

by

J. J. Murray

August, 1962

I. INTRODUCTION

In all probability there will be applications for mass analyzed particle beams at energies as high as one cares to contemplate. Present methods of mass separation have their limitations, however, and it is these limitations and how they relate to the environment expected at SLAC which we shall discuss here.

Mass separation may involve either electromagnetic interactions or nuclear interactions. In the latter case particular particles are selected preferentially by taking advantage of favorable features of the kinematics of their nuclear interactions with other particles, e.g., neutral K meson beams from associated production of K's by π's or from K charge exchange scattering.[1] Such techniques will no doubt prove to be useful but each case is a subject unto itself requiring detailed consideration. This will not be undertaken here; rather the discussion will be confined to methods involving electromagnetic interactions.

Electromagnetic mass separation may be achieved in three basically different ways: momentum analysis plus velocity analysis by

1) degradation in matter,
2) electrostatic deflection, or
3) phased radiofrequency deflections or acceleration depending on time of flight.

Mass separation was first achieved, in high energy physics, by the degradation method; this method, however, was quickly superseded, at moderate energies, by the more effective electrostatic separation. At very high energies it has been proposed[2] to revive the degradation method, taking

---

[1]G. Goldhaber, S. Goldhaber and B. Peter, "Separation of High Energy Particles by Means of Strong Interaction Processes," CERN NP/364/nc/61-3, 27 January, 1961.

[2]S. Marcowitz and L. Ratner, "Separation Scheme for High Energy Particles by Differential Energy Loss and Momentum Analysis," Rev. of Sci. Inst. 33, 552, May 1962.

advantage of the relativistic rise in ionization loss. Attractive as is this technique in its simplicity, more experience will be required to evaluate its effectiveness.

II. ELECTROSTATIC SEPARATION

Electrostatic separation is the most fully developed method at the present time. Unfortunately, however, it may be almost unequivocally ruled out as a useful method above $\gamma \approx 20$ for the heavier particle of a separated pair of particles. This assertion is based on the following practical consideration. The relative angular deflection of particles of the same momentum and of different mass in an electrostatic field E with length L along the particle trajectory is given relativistically by

$$\Delta\theta = \left(\frac{EL}{pc}\right)\frac{1}{2\gamma^2} \tag{1}$$

where γ relates to the particle with largest mass and pc is momentum in energy units. The first factor in Eq. (1) is approximately the total deflection of either particle; the second factor is the useful fraction of the total deflection. The latter may be regarded as a measure of the precision required in spatial uniformity and stability of the deflecting field for effective separation. Values of $1/2\gamma^2$ less than about 10^{-3} are surely unreasonable from this practical point of view. Hence the limit $\gamma \approx 20$, a limitation which cannot be relieved by higher electric fields or longer separators.

It is doubtful, however, that even this relatively low basic limit can be achieved for K mesons at predicted SLAC production intensities because of limited acceptance which decreases rapidly with momentum. We discuss the scaling with momentum of an electrostatically separated beam on the basis of the following assumptions:

1) That there is an "ideal" optical configuration, fixed except for a scale factor common to all drift spaces including separator length, and

2) That the relative separation, η, in phase space is fixed.

The first assumption can be fulfilled with a given set of quadrupole and bending magnets if the scale factor is proportional to or increases more rapidly than momentum. The second assumption is evidently necessary as $\eta \to 1$ and amounts to the assumption that the smallest practical value of η is constant. It is also tacitly assumed that separators are used optimally, that is with a parallel beam in the plane of separation.

Let the scale factor be γ^n, with n to be determined. Then $\Delta\theta$, given by Eq. (1), is proportional to γ^{n-3}; other scaling relationships are as follows.

$$\eta = \text{constant} = \frac{\Delta\theta f_v}{h_v} \propto \gamma^{2n-3} \quad \text{or} \quad h_v \propto \gamma^{2n-3}$$

where f_v is the focal length in the separator in the vertical plane (plane of separation) and h_v is the vertical target height. Vertical acceptance is given by

$$A_v = \frac{g}{\eta}\Delta\theta = \theta_v h_v \propto \gamma^{n-3} \quad \text{or} \quad \theta_v \propto \gamma^{-n}$$

where g is the plate separation and θ_v is the vertical acceptance angle. (Incidentally, $g\Delta\theta$ is proportional to total potential; the actual gap and electric field are irrelevant, as far as acceptance is concerned, for a fixed total potential.) The horizontal acceptance angle is

$$\theta_H \propto \gamma^{-n}$$

and the acceptable horizontal target width and/or percent momentum bite is fixed. The solid angle accepted at the target is

$$\Omega = \theta_v \theta_H \propto \gamma^{-2n} \qquad (n \geq 1)$$

In scaling, one is also interested in the optical precision required.

The tolerable percent aberration in each lens of focal length f is proportional to $f\Delta\theta$ which in turn is $\propto \gamma^{2n-3}$.

A final point of interest is the behavior of background. In a two-stage system at high momenta the principal background is caused by Coulomb scattering in the mass slits and, if pions are rejected, by μ's from π decays within the system. It can be shown that with V-shaped mass slits, tapered to conform to the vertical convergence and divergence of the beam at the focus, the intensity of Coulomb-scattered background on the central axis of the beam is given approximately by

$$\frac{dN}{d\Omega} = \int_{p-\Delta p}^{p} (d^2N/d\Omega dp)dp = \frac{1}{12\pi}\,\theta_v\,\frac{w^2}{y}\int_{\xi_{min}}^{\infty}\frac{e^{-\xi^2/2}}{\sqrt{2\pi}}\,d\xi \qquad (2)$$

where $d^2N/d\Omega dp$ is the number of scattered particles per unit solid angle per unit momentum interval per incident particle incident on the slit at a distance y in radiation lengths projected in the vertical plane from the apex of the slit. The argument of the error integral is given by

$$\xi_{min} = \frac{\sqrt{6wy}}{t^{3/2}}$$

where t is the distance in radiation lengths required to degrade the particle from p to $p - \Delta p$ and $w = 2p\beta/21$, with $p\beta$ in Mev/c. Typically at high momenta $\xi_{min} \lesssim 1$, so that the integral may vary relatively little, the main momentum dependence of the scattered background at high momenta coming from the leading factor in Eq. (2). At low momenta, incidentally, and especially for large η, the integral dominates Eq. (2) and slit-scattered background decreases rapidly. Since $y \propto \eta h_v$ and neglecting the integral we have

$$N \propto \Omega\,\theta_v\,\frac{w^2}{y} \propto \gamma^{5(1-n)}$$

Background from $\pi - \mu$ decay is easily shown to be proportional to γ^{n-2}.

The various scaling proportionalities obtained above are given in Table I for several values of n.

Table I - Scaling Proportionalities for Various Quantities Involved in Electrostatic Separation

n	Target Size h (and y)	Bgnd From Scattering in Resolving Slit - N	μ Bgnd	Max. Allowable Optical Aberration	Ω at Target
2	γ	$\rightarrow \gamma^{-5}$	Constant	γ	γ^{-4}
3/2	Constant	$\rightarrow \gamma^{-5/2}$	$\gamma^{-1/2}$	Constant	γ^{-3}
1	γ^{-1}	$\rightarrow$ Constant	γ^{-1}	γ^{-1}	γ^{-2}

(n = exponent in scaling parameter γ^n for drift spaces and separator length. Optical configuration fixed.)

The value $n = 1$ is the best choice from the standpoint of solid angle accepted at the target, but its slit-scattered background could become a problem. There would also be some minimum practical target size and/or optical aberration which would ultimately prevent scaling to higher momenta with $n = 1$. For $n = 3/2$ all quantities scale acceptably but with Ω proportional to γ^{-3}. There would appear to be no reason for scaling with $n > 3/2$.

Figure 2 gives the separated K yields for $n = 1$ and $n = 3/2$ with Ω normalized to the value 0.1 msr at 3 Bev/c (a practical value actually achieved with 8-inch-diameter 32-inch-long quadrupole magnets). The separated K yields shown in Fig. 2 are for 10^{12} primary electrons and 1% momentum bite (based on the expected K yield of SLAC[3] as shown in Fig. 1) but do not include decay losses. For $n = 1$, decay loss would be constant and for a target-to-experiment distance of 200 feet at 3 Bev/c

[3] J. Ballam, "Computation of Secondary-Particle Yields from High Energy Electron Accelerator," Hansen Laboratories Report No. M-200-8, Revision A, 1960 (unpublished).

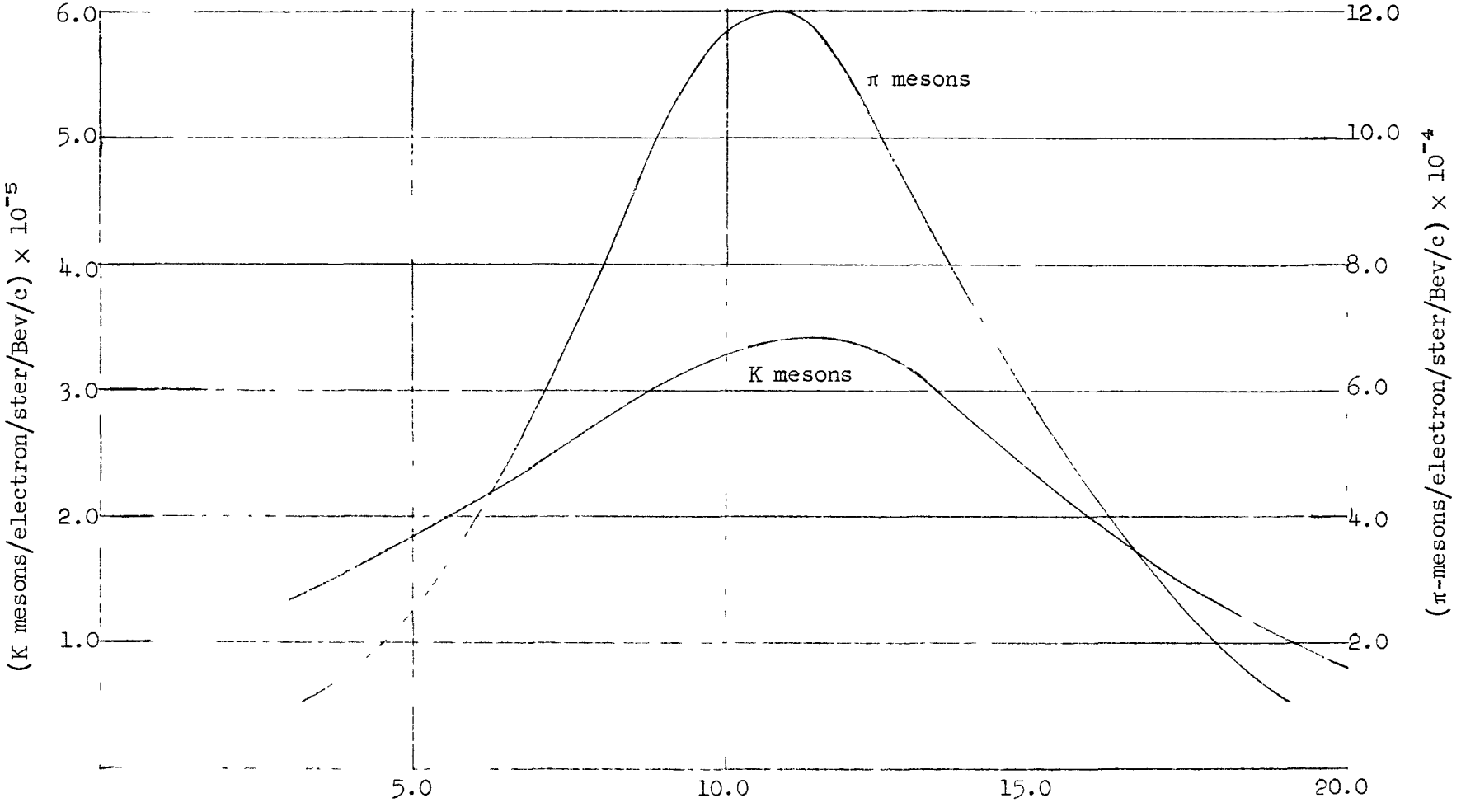

FIG. 1-- π and K yields expected at SLAC for 25 Bev electrons.

Target: 1/2 radiation length H_2

Production Angle: $\theta_\pi = 1^\circ$

$\theta_K = 1^\circ$ at 20 Bev/c, 5° at 5 Bev/c

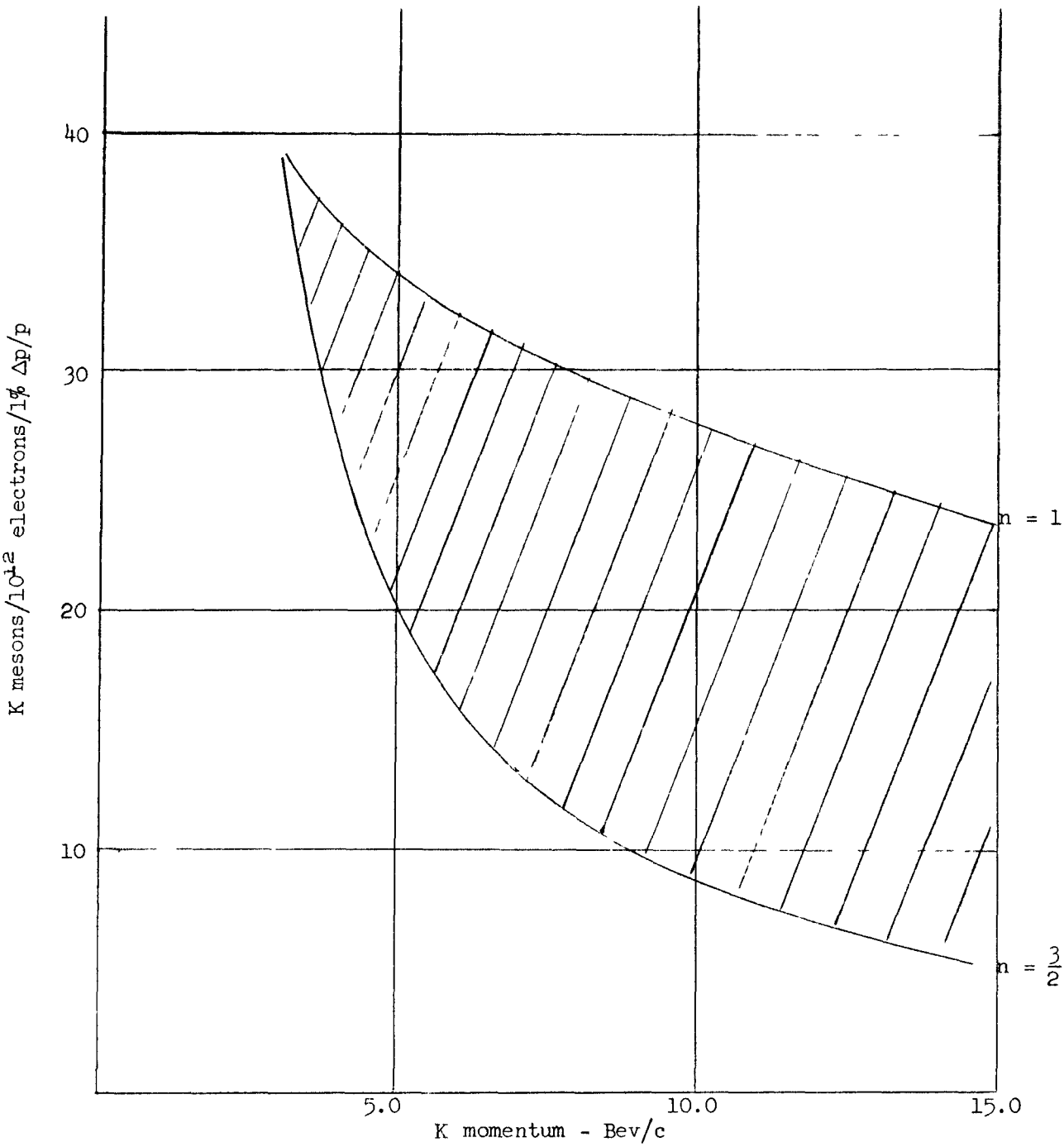

Fig. 2--Separated K yield with electrostatic separation (decay losses not included).
n = exponent in scaling parameter γ^n for drift spaces and separator length.
See Fig. 1 for assumed K production yield.

(a practical length for a two stage beam), decay loss would reduce the separated K yield by a factor of about 15. For the same loss at 3 Bev/c but scaling with $n = 3/2$, the decay loss would be $(15)^{(p/3)1/2}$ at higher momenta, p.

One would expect the separated K yields actually obtained to lie somewhere within the shaded region of Fig. 2. Including decay loss, then, only a few K's per 10^{12} electrons per 1% $\Delta p/p$ can be expected at best, probably less than one at above 5 Bev/c. One may conclude tentatively that electrostatic separation is not likely to be a useful technique at SLAC.

III. RF SEPARATION

SLAC will be ideally suited for application of rf separation because of inherent bunching of the primary beam. This will allow the simplest possible beam configurations and the highest transmission efficiency. RF separation involving time of flight is expected to be effective well above the basic limit of electrostatic separation. However, there exists an analogous limit which depends on deflector phase stability.

The maximum relative deflection in an rf system is given by

$$\Delta\theta = \frac{EL}{pc} 2 \sin \frac{\tau}{2} \qquad (3)$$

where L is the total length of deflector, E the effective deflecting field, and pc is momentum in energy units. $\tau = \Phi/2\gamma^2$ is the relative phase shift of the separated pair of particles over the available flight path, ℓ, and $\Phi = 2\pi \frac{\ell}{\lambda}$ is approximately the total phase shift of either particle. λ is the radiofrequency free space wavelength. If $\Delta\Phi$ and $\Delta\psi$ are independent spurious fluctuations in Φ and in ψ (ψ is the deflector phase angle), we must have both

$$\frac{\Delta\Phi}{\Phi} < \frac{1}{2\gamma^2} \quad \text{and} \quad \frac{\Delta\psi}{\Phi} < \frac{1}{2\gamma^2}$$

for effective separation. Spurious deviations in Φ will result from (1) velocity spread with finite momentum bite, and (2) departures from isochronism associated with finite acceptance and the process of momentum analysis; spurious deviations in ψ will result from (3) finite bunch length and (4) deflector phasing instability.

Velocity spread with finite momentum bite (1) is unimportant for usual momentum spreads since $d\beta/\beta = 1/2\gamma^2 \frac{dp}{p}$ implying $\Delta p/p < \frac{1}{2}$ for $\Delta\beta/\beta < 1/2\gamma^2$.

Departure from isochronism (2) also is unimportant as far as the effects of finite acceptance are concerned. For example, finite acceptance gives a contribution

$$\frac{\Delta\Phi}{\Phi} = \frac{\Delta\ell}{\ell} \approx \theta^2$$

where ℓ is the drift length and θ the half angle of acceptance. θ might typically be 10^{-2} radians at say 4 Bev/c and proportional to $1/\gamma$ so that for K's, $\theta^2 \approx 10^{-2}(1/2\gamma^2)$ is negligible. Single deflection involved in momentum analysis on the other hand will give $\Delta\ell$ approximately equal to the bending angle times the aperture at the point of bending. For example, if at 10 Bev/c we have a bending angle of 1/15 radian and a fixed 15 cm aperture, $\Delta\ell = 1$ cm and may be assumed to vary in proportion to $1/\gamma$. If, as might be reasonable for K-pion separation, we have $\tau = \pi$ at 10 Bev/c and allow τ to decrease no more rapidly than $1/\gamma$, the effect of $\Delta\ell$ above 10 Bev/c becomes smaller or at worst remains constant. For a 10-cm radiofrequency wavelength, λ, we would have in the worst case $2\pi \frac{\Delta\ell}{\tau\lambda} = 1/5$ or $\Delta\Phi/\Phi = 1/5\ (1/2\gamma^2)$, possibly too large to be acceptable. At lower momenta, with τ equal to an odd multiple of π, the effect becomes relatively worse. It may therefore be mandatory that momentum analysis within the drift space of an rf-separated beam be performed achromatically. An achromatic system is also approximately isochronous and under comparable conditions would be expected to contribute to $\Delta\ell$ an order of magnitude less than estimated above.

Finite bunch length (3) could be important for small τ in a single

deflector system. With two deflectors, however, the relative deflection, $\Delta\theta$, may be made approximately independent of initial phase of the particles over the small phase interval within a bunch so that finite bunch length need not be a limitation.

Deflector phase instability (4) is another matter. The contribution to $\Delta\psi/\Phi$ from this source may be expected to contain momentum-independent factors and therefore to limit γ. Stability of phase is difficult to evaluate a priori but $\Delta\psi/\Phi \lesssim \frac{1}{2}\,10^{-4}$ does not seem unreasonable. In that event the basic limit for rf separation would be $\gamma \approx 100$, a limit considerably higher than the analogous electrostatic limit and adequate for K separation up to maximum SLAC energy.

Whether or not such a basic limit can be reached depends on intensity considerations which may be discussed with the aid of scaling relationships as follows. The solid angle accepted at the target may be limited by either the beam transport system or the rf deflector. The maximum solid angle accepted by an efficient beam transport system will not differ radically from

$$\Omega_{max} = \tfrac{1}{2}\left(\frac{d}{\Lambda}\right)^2 \quad ; \quad \Lambda = \frac{2p}{H'\ell_e} \tag{4}$$

where d, H' and ℓ_e are respectively the effective aperture, maximum field gradient and effective length of the quadrupole magnets. (For convenience rectangular apertures are assumed throughout.) Λ is the large scale wavelength of trajectories in a strong focusing channel. $p/H'\ell_e$ is approximately equal to the minimum focal length of individual quadrupole magnets. The factor of 1/2 in Ω_{max} is empirical. On the other hand the maximum acceptance of an rf deflector is

$$A_{max} = \frac{1}{3}\,\frac{ED^3}{pc}\,\sin\frac{\tau}{2} \tag{5}$$

corresponding to an optimum deflector length

$$L_{opt} = \left(\frac{Dpc}{6E \sin \tau/2}\right)^{\frac{1}{2}} \qquad (6)$$

where D is the full aperture of the deflector. This "optimum" length maximizes the rectangular phase space in the plane of deflection inscribed within the phase boundaries at the center of the deflector (assuming both that a relative separation of two exists between the phase spaces of wanted and unwanted particles and that unwanted particles may be allowed to strike the deflector). See the sketch below.

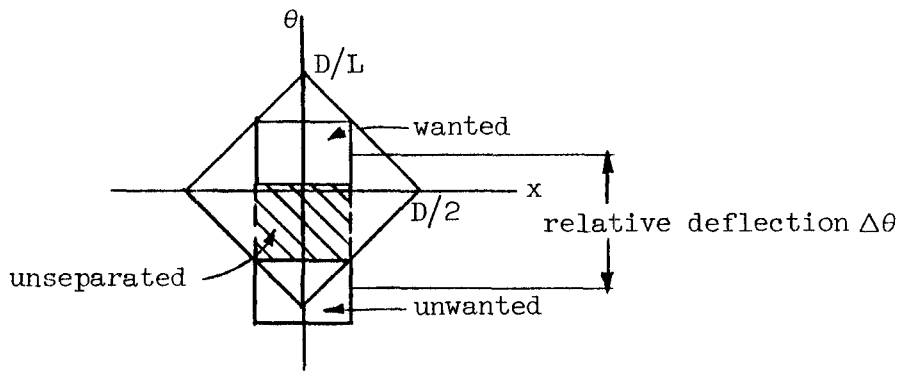

Optimum acceptance in the other plane is 9/4 times the optimum acceptance in the plane of separation. If h is the effective linear dimension of a square target, the acceptance of the beam transport system and the acceptance of the deflector are matched when

$$\Omega_{max} h^2 = A_{max}$$

with a magnification $M \approx D/h$ between target and deflector.

There will be a minimum useful target size h (or equivalently a practical magnification) so that below a certain momentum, with $\sin \tau/2 = 1$,

A_{max} will limit and

$$\Omega = \frac{A_{max}}{h^2} \propto 1/p$$

$$< \Omega_{max}$$

Above this transition momentum p_1, the beam transport system limit,

$$\Omega = \Omega_{max} \propto 1/p^2$$

and maximum deflector acceptance is not necessarily required. Up to a certain momentum, p_2, τ may be made equal to an odd multiple of π with $|\sin \tau/2| = 1$. In the region $p_1 < p < p_2$ a deflector of fixed length and field is sufficient to separate the maximum phase space delivered by the beam transport system. Alternatively, if deflector acceptance were optimized in this region larger targets could be used, with $h \propto p$.

Above p_2, $\sin \tau/2$ must decrease or else the beam transport length, mainly drift space, must increase approximately in proportion to p^2 which would require additional beam handling equipment in order to maintain $\Omega = \Omega_{max}$. If on the other hand the beam transport length is increased only in proportion to momentum and if $\sin \tau/2$ is allowed to decrease (with $\tau \propto 1/p$), then when $\sin \tau/2 \approx \tau/2$ is a good approximation, the deflector length required to maintain separation also increases in proportion to p. This is the same as optimum scaling for L when $\sin \tau/2 \propto 1/p$ so that a beam transport deflector match with $\Omega = \Omega_{max}$ would be preserved indefinitely for a fixed target size. As previously noted, however, above a certain momentum, when τ becomes comparable to a bunch length, two deflectors would be required.

The scaling procedures outlined above are illustrated qualitatively in the following sketch

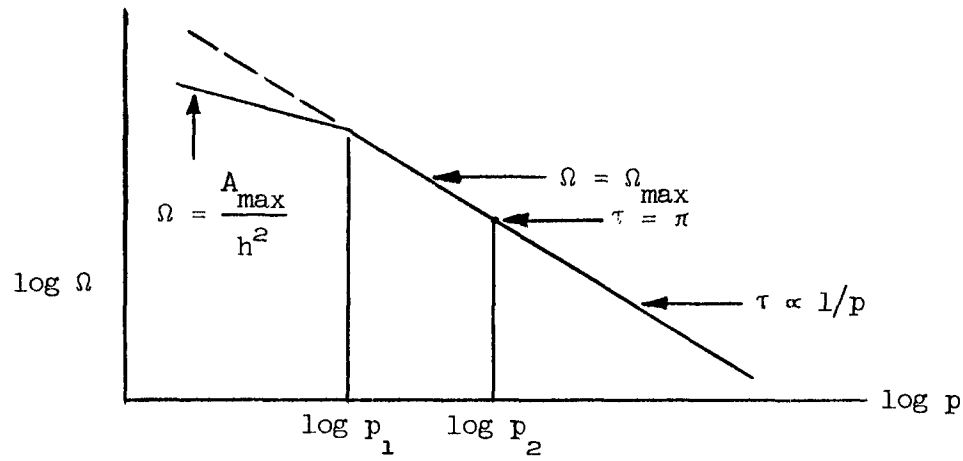

It is below p_1 that separation by linear acceleration[4] rather than by transverse deflection could be advantageous in the respect that the maximum beam transport-limited solid angle could be utilized.

Possible values of p_1 and p_2 are illustrated in the following example:

$d = 6$ in.
$H' = 2$ kg/in. } 8-inch-bore × 32-inch-long quads
$\ell_e = 40$ in.
$h = \frac{1}{2}$ in. } $M = 4$
$D = 2$ in.
$E = 2$ Mev/ft
$\lambda = 10$ cm

$$p_1 = (3/8)\,\frac{d^2H'^2\ell_e^2h^2}{ED^3} = 10 \text{ Bev/c}$$

[4]J. J. Murray, "Mass Separation by Means of Microwave Linear Acceleration in Secondary Beams," UCLRL - 10279, June 18, 1962.

$$p_2 = \frac{5\pi(mc)^2}{\lambda H' \ell_e} \approx 15 \text{ Bev/c for } K, 60 \text{ Bev/c for } \bar{p}$$

The value of p_2 above is based on the assumption that the minimum distance between target and deflector is determined by the beam transport system and for $M = 4$ is $5/4\ \Lambda = 5\pi p/H'\ell_e$; then $\gamma_2^2 = 5/4\ \Lambda^2/\lambda$. For a bunch length of 1/6 radian the maximum momentum at which a single deflector will suffice (with beam length scaled in proportion to momentum) is about 10 times p_2 or too high to be of significance at SLAC.

In the numerical example above $\Omega_{max} = 0.2$ msr at $p_1 = 10$ Bev/c. Realistically this should be reduced by a circular factor $(\pi/4)^2$ applying as well to A_{max}. The corresponding rf-separated K yields are given in Fig. 3 for 10^{12} primary electrons and 1% momentum bite, based as before on the expected K production given in Fig. 1 and with decay loss not included.

Above $p_1 \approx 10$ Bev/c the decay loss factor should be approximately constant. Overall beam length can best be estimated at $p_2 = 15$ Bev/c where the drift length is $5/4\ \Lambda \approx \lambda\gamma_2^2 = 310$ feet (more exactly 340 feet). About one additional wavelength $\Lambda = 260$ feet would be needed for mass resolution and post-momentum analysis giving an overall length, target-to-experiment, of about 600 feet at 15 Bev/c which would scale in proportion to momentum for all momenta. The corresponding decay loss factor for K mesons would be about 1/5, a considerable improvement over the decay loss factor in typical two stage electrostatically separated beams.

As far as background is concerned there does not appear to be any particularly bothersome source. In fact, μ background will tend to be suppressed because the relatively large separating deflections will sweep the μ cone out of the acceptance aperture for a large fraction of the π decays. By the same token, slit-scattered background, which is bothersome at high momentum with electrostatic separation, will be suppressed because of the relatively large absolute displacement of rejected beam at the resolving slit. Single stage systems with adequate post-momentum analysis will probably give acceptable background rejection.

It would seem safe to conclude that rf separation will be a useful technique up to (and even above) maximum SLAC energies.

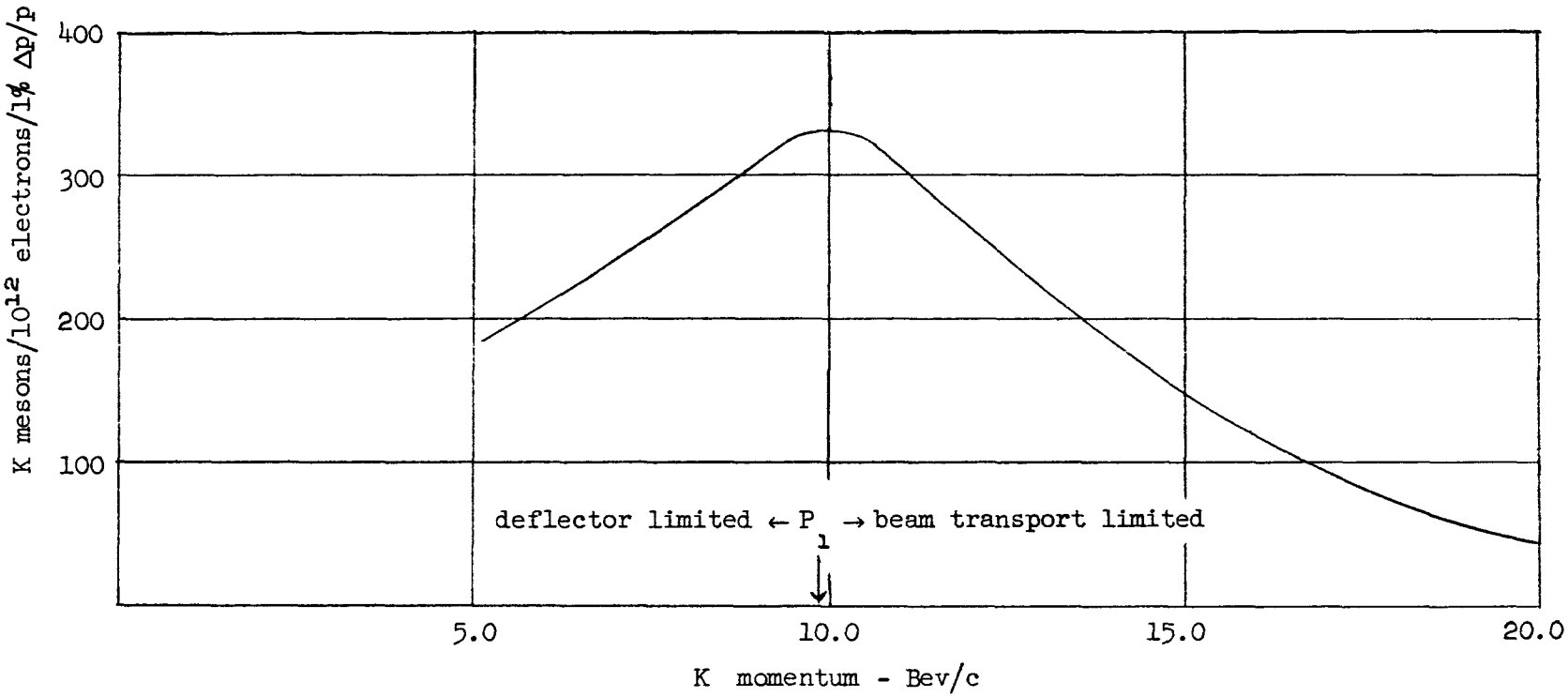

FIG. 3--Separated K yield with rf separation (decay loss not included); factor ≈ 1/5

See Fig. 1 for assumed K production yield
Ω = 0.1 msr at target at 10 Bev/c